

Investigating Extended Linker Analogues of Risperidone for Treatment of Multiple Sclerosis

By

Thomas Bird

A thesis submitted to Victoria University of Wellington in
partial fulfilment of the requirements for the degree of Master
of Drug Discovery and Development by thesis.



School of Chemical and Physical Sciences

2020

Abstract

Risperidone is a second-generation antipsychotic used to treat psychiatric disorders such as schizophrenia, bipolar disorder and autism. It targets dopamine D₂ and serotonin 5-HT_{2A} receptors and has immunomodulatory properties. Multiple sclerosis is a chronic inflammatory disease that affects over 2 million people worldwide and currently has no cure. Recent research at Victoria University of Wellington has shown that risperidone is able to reduce disease severity in mouse models of multiple sclerosis. Further research has demonstrated that truncated and unsaturated analogues of risperidone have varying immunomodulatory effects in immune cells.

The current research describes the synthesis and preliminary *in vitro* testing of four extended-linker analogues of risperidone. Structure-activity relationship studies with neurotropic drugs have shown that altering the length of the alkyl chain found in many of these compounds can have significant effects on receptor binding profiles. Synthesis and cytokine production assays of these analogues begin to provide further insight into how risperidone exerts its immunomodulatory effects and may contribute to the development of new treatments for multiple sclerosis.

“Completed it mate.”

Jay Cartwright

Acknowledgments

Firstly, I would like to thank Associate Professor Joanne Harvey. Your encouragement, constant positivity and incredible enthusiasm for all things chemistry has made this project what it is. I could not have asked for a better supervisor this year.

Ben and Jordan, you have been my big brothers this year in more ways than one. Ben, without the crazy amount of work you did in Honours I would not be here. Your methods actually work the first time! What a revolutionary idea. Jordan, I think I lucked out being in the fume hood beside you with your massive organic chemistry knowledge. Thank you for telling me it all for free. Thanks to both of you for giving me stick all year long, making me be a better chemist and a better person I hope. I look up to the both of you immensely. Laundry.

Ethan, thank you for putting up with my constant stream of questions all year. Your help with NMR has been brilliant, but more importantly, your sarcasm throughout the years has been a pleasure. Sarah, thank you for being the friendly face that helped in the beginning when I had no clue what I was doing. You helped me settle into the group so quickly. Tao, your hard work and dedication to your PhD has been an inspiration while writing this. I hope to see you back soon celebrating a successful defence. Matt, thank you for singing Stormzy every day, making crazy crystals and just being a ridiculously happy guy to be around. Hayden, thank you for asking mate. Sophie, thank you for waking me up every day. Katie, thank you for your positivity, your encouragement and your Scouse accent. I cannot thank you enough for reading through my drafts that should never have seen the light of day. But more importantly, thank you for the constant barrage of Inbetweeners quotes that manage to suit every situation.

A massive thank you to Dr. Helen Woolner for showing a chemist how to be a biologist. You have been a great teacher and made the whole process a lot less daunting. Also, to Associate Professor Paul Teesdale-Spittle for your helpful suggestions drawing from your vast biology and chemistry knowledge. Thank you to Ian for your help all year with NMR and solving the many technical issues I had.

I would also like to thank my grandparents for their support, encouragement and interest in everything I have done over the years, in and out of university. Lastly, I would like to thank my mum. Mum you have done so much for me over my life and the past few years especially, I will never be able to thank you enough. Thank you for letting me attempt to teach you everything I have learnt, you deserve a degree from it too. This thesis is for you, I hope it makes you proud.

Table of Contents

Abstract.....	i
Acknowledgments	iii
List of Figures.....	viii
List of Schemes.....	xi
List of Tables	xiii
List of Abbreviations	xiv
1 Introduction.....	1
1.1 Risperidone.....	1
1.1.1 Background.....	1
1.1.2 Pharmacokinetics and Receptor Affinities	4
1.1.3 Side Effects.....	5
1.2 Multiple Sclerosis and Cytokines.....	6
1.2.1 Multiple Sclerosis	6
1.2.2 Current Treatments	6
1.2.3 Cytokines and Multiple Sclerosis	7
1.3 Risperidone, Inflammation and Cytokines.....	9
1.4 Alkyl Spacer Effects in Drug Molecules.....	10
1.5 Previous Studies at Victoria University of Wellington.....	12
1.5.1 Risperidone Reduces Disease Severity in EAE.....	12
1.5.2 Immunomodulatory Activity of Risperidone Analogues.....	13
1.6 Project Aims.....	15

1.6.1 Synthetic Chemistry	15
1.6.2 <i>In Vitro</i> Assays	19
2 Synthesis of Risperidone Analogues.....	21
2.1 Retrosynthesis	21
2.2 Synthesis of the Benzisoxazole Fragment.....	22
2.2.1 Isonipecotic Acid Acetylation	22
2.2.2 Friedel-Crafts Acylation of 10	23
2.2.3 Oxime Formation.....	25
2.2.4 Benzisoxazole Ring Closing.....	27
2.3 Synthesis of Extended Linker Pyridopyrimidones.....	30
2.3.1 Preparation of the Three-Carbon Alkylated Ethyl Acetoacetate	31
2.3.2 Preparation of the Four-Carbon Alkylated Ethyl Acetoacetate.....	35
2.3.3 Condensation of 17 and 18 with 2-aminopyridine	39
2.3.4 Pd/C Catalysed Hydrogenation of Pyridopyrimidones 19 and 20	44
2.4 Debenzylation Attempts.....	50
2.4.1 DDQ-mediated Deprotection Attempts	50
2.4.2 TiCl ₄ -mediated Deprotection Attempts	51
2.5 Completion of the Synthesis of 8 , 9 , 28 and 29	55
2.5.1 Synthesis of Four-Carbon Saturated Analogue 9	56
2.5.2 Synthesis of Analogues 8 , 28 and 29	61
3 <i>In Vitro</i> Assays.....	66
3.1 MTT and ELISA Assay Results.....	66

3.1.1 MTT Assay Results	66
3.1.2 IL-12 ELISA Results	68
3.1.3 IL-10 ELISA Results	69
3.2 Discussion	69
4 Summary and Future Work	76
4.1 Summary	76
4.2 Future Work	78
5 Experimental	81
5.1 Synthetic Chemistry Experimental.....	81
5.1.1 General Methods.....	81
5.1.2 Procedures and Experimental Data.....	82
5.2 <i>In Vitro</i> Assay Experimental	103
5.2.1 Cell Culture and <i>In Vitro</i> Experiments	103
5.2.1.1 Quantification of Analogues	103
5.2.1.2 Compounds for <i>In Vitro</i> Use.....	103
5.2.1.3 Culture and Maintenance of RAW 264.7 Macrophage Cell Line	104
5.2.1.4 MTT Reduction Assay	104
5.2.2 Cytokine Assays	104
5.2.2.1 General ELISA Protocol	104
6 Appendix.....	106
6.1 NMR Spectra.....	106
6.2 Buffers and Solutions	162

6.3 ELISA Reagents and Concentrations	163
7 References	165

List of Figures

Figure 1. Risperidone and structurally related atypical antipsychotics.	2
Figure 2. Top left, top down view of risperidone (yellow) bound in the pocket created by transmembrane helices III, V and VI (not shown). Top right, risperidone bound to D ₂ receptor. Bottom, risperidone orientation when unbound vs bound to D ₂ receptor. Bottom right, overlaid unbound (green) and bound (yellow). Adapted from Wang <i>et al.</i> <i>Structure of the D₂ dopamine receptor bound to the atypical antipsychotic drug risperidone.</i> <i>Nature</i> 555 , 269. ¹⁰	3
Figure 3. Left, 3-dimensional structure of risperidone bound to 5-HT _{2A} receptor. Right, interactions between risperidone and 5-HT _{2A} . Adapted from Kimura <i>et al.</i> <i>Structures of the 5-HT_{2A} receptor in complex with the antipsychotics risperidone and zotepine.</i> <i>Nature Structural & Molecular Biology</i> 26 , 121. ¹¹	4
Figure 4. Oxindoles targeting 5-HT ₇ synthesised by Volk <i>et al.</i> ⁹⁰	11
Figure 5. Quinoline- and isoquinoline-sulfonamides synthesised by Zajdel <i>et al.</i> ⁹²	11
Figure 6. Arylpiperazines synthesised by Bojarski <i>et al.</i> ⁹³	12
Figure 7. Piperazines synthesised by Smid <i>et al.</i> ⁹⁴	12
Figure 8. Risperidone analogues synthesised by VUW researchers. ⁹⁷	14
Figure 9. Three- and four-carbon linker analogues of risperidone.	15
Figure 10. Possible nitrogen rotamers of 10	23
Figure 11. Comparison of ¹ H NMR spectra of <i>N</i> -acetylated acid 10 and Friedel-Crafts product 12	24
Figure 12. Splitting of ¹³ C peaks caused by fluorine coupling to neighbouring carbons in product 12	25
Figure 13. Comparison of ¹³ C NMR spectra of alcohol 13 and iodide 15 . Highlighted in green are the terminal carbon shifts.	34
Figure 14. Comparison of ¹³ C NMR spectra of iodide 15 and alkylated product 17 . Highlighted in green are shifts indicative of ketone (left) and ester (right) functionalities.....	35
Figure 15. Key COSY and HMBC correlations of 18	39
Figure 16. Comparison of ¹ H NMR spectra of 2-aminopyridine condensation crude reaction mixture (top) and purified (bottom) 19 . Pyridine ring shifts are highlighted in green	42
Figure 17. Numbered carbon environments for pyridopyrimidone 20	44
Figure 18. Comparison of ¹³ C shifts of C-6 and C-8 in 19 (top) and 21 (bottom).....	46
Figure 19. Comparison of ¹³ C shifts of C-6 and C-8 in 19 and 21	46

Figure 20. Possible resonance structures of 19 .	47
Figure 21. Photo (left) and schematic (right) of apparatus used for second hydrogenation attempt.	48
Figure 22. Comparison of ^1H NMR spectra of 19 (top), tetrahydropyridopyrimidone 21 (middle) and deprotected tetrahydropyridopyrimidone 23 (bottom). Highlighted are unsaturated pyridine shifts (green) and benzylic shifts (yellow).	48
Figure 23. Stacked ^1H NMR of protected alcohol 19 (top) and unknown DDQ-mediated deprotection product (bottom).	51
Figure 24. Stacked ^1H NMR spectra of one fraction of chromatographed TiCl_4 reaction product (top) and combined fractions of TiCl_4 reaction product (bottom).	52
Figure 25. The four proposed risperidone analogues.	54
Figure 26. Triplicate TLC analysis (acetone + 0.5% triethylamine) of crude reaction mixture pre-workup for Appel reaction on 24 . Stained with ceric ammonium molybdate. 254 nm UV active spots are outlined in red.	57
Figure 27. Quadruplicate TLC analysis (acetone + 0.5% triethylamine) of the crude reaction mixture of the coupling reaction towards 9 . Stained with ceric ammonium molybdate. 254 nm UV active spots are outlined in red.	58
Figure 28. Stacked ^1H NMR spectra of benzisoxazole 3 (top) and crude condensation product 9 (bottom), focussed on shifts representative of positions C-8' and C-10'.	59
Figure 29. Expansion of HMBC spectrum of 9 with the key correlation circled.	60
Figure 30. Comparison of ^1H NMR spectra of analogue 9 in D_2O (top) and CDCl_3 (bottom).	61
Figure 31. Stacked ^1H NMR spectra of benzisoxazole 3 (top), iodide 25 (middle) and analogue 8 (bottom). Residual PPh_3O is highlighted in red.	62
Figure 32. RAW264.7 cell viability measured by MTT assay. Presented as a percentage of vehicle control. RAW 264.7 cells were plated at 50,000 cells/well, primed with $\text{IFN-}\gamma$ (20 U/mL), and stimulated with LPS for 24 hours in increasing concentrations of analogues 8 , 9 , 28 , 29 and risperidone at 1% DMSO. Shown are means and SEM of triplicate wells from one experiment.	67
Figure 33. IL-12 in the supernatant measured by ELISA.	68
Figure 34. IL-10 in the supernatant measured by ELISA.	69
Figure 35. Acarbose binding site alignments in 4- α -glucanotransferase and glucoamylase. Binding sites are highlighted in red and ligands are presented in orange. Adapted from Haupt	

<i>et al. Drug Promiscuity in PDB: Protein Binding Site Similarity Is Key. PLOS ONE</i> 2013 , 8 (6), e65894. ¹⁴¹	70
Figure 36. Overlay of 9 (green) and risperidone (red), demonstrating their proposed positions in relation to a tryptophan residue (yellow) in the D ₂ receptor.....	73
Figure 37. Proposed deep-pocket ligand-protein interactions of 8 (top) and risperidone (bottom).....	74
Figure 38. Proposed shallow-pocket ligand-protein interactions of 8 (left) and risperidone (right).	75
Figure 39. Proposed five- and six-carbon linker analogues of risperidone.	79
Figure 40. Proposed rigidified analogues of 8	80

List of Schemes

Scheme 1. Proposed synthesis of benzisoxazole 3	16
Scheme 2. Proposed synthesis of extended linker coupled pyridopyrimidones 19 and 20	17
Scheme 3. Outcome of Durrant's Pd-catalysed hydrogenation reactions. ⁹⁸	18
Scheme 4. Proposed DDQ-mediated deprotection of 21 and 22	18
Scheme 5. Proposed synthesis of analogues 8 and 9	19
Scheme 6. Retrosynthesis of extended linker analogues of risperidone.	21
Scheme 7. Synthetic route to yield benzisoxazole 3	22
Scheme 8. Acetylation of isonipecotic acid.	23
Scheme 9. Friedel-Crafts acylation of 10	24
Scheme 10. Synthesis of <i>Z</i> -oxime 4	26
Scheme 11. Proposed mechanism of oxime formation.	27
Scheme 12. Proposed mechanism of oxime isomeric conversion.....	27
Scheme 13. Synthesis of benzisoxazole 3	27
Scheme 14. Proposed mechanism of benzisoxazole formation.....	28
Scheme 15. Proposed synthetic route tetrahydropyridopyrimidones 23 and 24	31
Scheme 16. Benzyl protection of 1,3-propanediol.	32
Scheme 17. Proposed mechanism of Ag ₂ O mediated 1,3-propanediol.....	32
Scheme 18. Appel reaction of 13	32
Scheme 19. Proposed Appel reaction mechanism.....	33
Scheme 20. Alkylation reaction of 15 with ethyl acetoacetate to give 17	34
Scheme 21. Benzyl protection of 4-chlorobutanol.	36
Scheme 22. Proposed mechanism of benzyl protection of 4-chlorobutanol.	36
Scheme 23. Finkelstein reaction of 14	36
Scheme 24. Alkylation reaction of ethyl acetoacetate to give 18	37
Scheme 25. Condensation of 2-aminopyridine with 17 and 18	40
Scheme 26. Possible mechanisms of the condensation of 17 and 18 with 2-aminopyridine. .	41
Scheme 27. Hydrogenation of 19 and 20	45
Scheme 28. Mechanism of palladium catalysed hydrogenative <i>O</i> -debenzylation.	49
Scheme 29. Proposed mechanism of TiCl ₄ -mediated deprotection.	53
Scheme 30. TiCl ₄ -mediated benzyl-deprotection of pyridopyrimidones 19 , 20 , 21 and 22 . ..	54
Scheme 31. Proposed synthesis of analogues 8 , 9 , 28 and 29 via Appel reactions yielding iodides 25 , 26 , 31 and 32	55

Scheme 32. Synthesis of analogue 9	56
Scheme 33. Synthesis of analogues 8 and 29	62
Scheme 34. Possible products of an alcohol (27) and iodide (31) mixture in the final condensation reaction.....	63
Scheme 35. Synthesis of analogue 28	64
Scheme 36. Synthesis of analogues 8 , 9 , 28 and 29	65
Scheme 37. Overall synthetic route for risperidone analogues 8 , 9 , 28 and 29	77

List of Tables

Table 1. Cytokines and their related pathways.	7
Table 2. Tabulated NMR spectroscopic data (500 MHz, CDCl ₃) for benzisoxazole 3	29
Table 3. Tabulated NMR spectroscopic data (500 MHz, CDCl ₃) for alkylation product 18 ..	38
Table 4. Reaction conditions investigated by Durrant toward the condensation of 17 and 2-aminopyridine to form 19 . ⁹⁸	40
Table 5. Tabulated NMR spectroscopic data (500 MHz, CDCl ₃) for pyridopyrimidone 19 ..	43
Table 6. Comparison of terminal triplet shifts and <i>J</i> -couplings of Appel starting materials and products.....	64
Table 7. NMR parameters and settings for quantification experiments.....	103

List of Abbreviations

α1	Alpha-1
δ	NMR chemical shift (ppm)
^{13}C NMR	Carbon nuclear magnetic resonance
^1H NMR	Proton nuclear magnetic resonance
5HT	5-Hydroxytryptamine
ABCB1	ATP-binding cassette sub-family B member 1
Ac₂O	Acetic anhydride
AcOH	Acetic acid
Ar	Aromatic
Asp	Aspartic Acid
atm.	Atmosphere
BG-12	Dimethyl fumarate
BMMΦ	Bone marrow derived macrophages
Bn	Benzyl
CNS	Central nervous system
COSY	Correlation spectroscopy
CTCM	Complete T-cell media
CYP2D6	Cytochrome P450 2D6
CYP3A4	Cytochrome P450 3A4
d	Doublet
D2	Dopamine-2
dd	Doublet of doublets
ddd	Doublet of doublet of doublets
DDQ	2,3-Dichloro-5,6-dicyano-1,4-benzoquinone
dH₂O	Distilled water
DMF	Dimethylformamide
DMSO	Dimethyl sulfoxide
dPBS	Dulbecco's phosphate-buffered saline
dtd	doublet of triplet of doublets
EAE	Experimental autoimmune encephalomyelitis
ELISA	Enzyme-Linked Immunosorbent Assay

EPS	Extrapyrarnidal Symptoms
eq.	Equivalents
Et₂O	Diethyl ether
EtOAc	Ethyl acetate
EtOH	Ethanol
FCS	Fetal calf serum
GHB	Gamma-hydroxybutyrate
HEPES	4-(2-hydroxyethyl)-1-piperazineethanesulfonic acid
HMBC	Heteronuclear multi-bond correlation
HRMS	High resolution mass spectrometry
HSQC	heteronuclear single quantum correlation
Hz	Hertz
IFN-γ	Interferon-gamma
IL-	Interleukin
IR	Infrared
K₂CO₃	Potassium carbonate
kg	Kilogram
K_i	Inhibitory constant
LPS	Lipopolysaccharide
m	Multiplet
<i>m/z</i>	Mass to charge ratio
MAPK	Mitogen-activated protein kinase
MBn	para-Methylbenzyl
MCP-1	Monocyte chemo-attractant protein 1
MeOH	Methanol
mg	Milligram
MgSO₄	Magnesium sulfate
MHz	Megahertz
MS	Multiple sclerosis
MTT	3-(4,5-Dimethylthiazol-2-yl)-2,5-diphenyl-2H-tetrazol-3-ium
mult.	Multiplicity
NAAA	<i>N</i> -acylethanolamine acid amidase
NF-κB	Nuclear factor kappa-light-chain-enhancer of activated B cells

NMR	Nuclear magnetic resonance
Nrf2	Nuclear factor erythroid 2-related factor 2
OD	Optical density
Pd/C	Palladium on carbon
Ph	Phenyl
Phe	Phenylalanine
PMB	para-Methoxylbenzyl
ppm	Parts per million
<i>p</i>-TsOH	para-Toluenesulfonic acid
qd	quartet of doublets
R_f	Retention factor
RT	Room temperature
SA-HRP	Streptavidin-horseradish peroxidase
t	triplet
TfOH	Triflic acid
TGF-β	Transforming growth factor- β
Thr	Threonine
TLC	Thin layer chromatography
TMB	Tetramethyl benzidine
TNF-α	Tumour necrosis factor- α
Trp	Tryptophan
U	Units
UV	Ultraviolet
VUW	Victoria University of Wellington
w/w	weight per weight

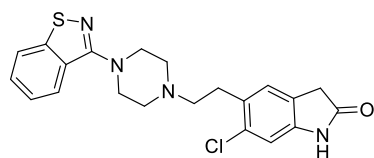
1 Introduction

1.1 Risperidone

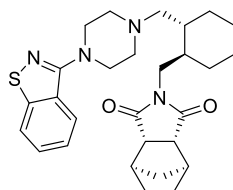
1.1.1 Background

Risperidone is an atypical antipsychotic drug, originally developed by Janssen Pharmaceuticals in 1986 as a treatment for psychiatric disorders associated with schizophrenia.¹ Its use has since expanded to the management of bipolar disorder² and irritability associated with autism.³ As an atypical or second-generation antipsychotic, risperidone improved on the first generation of antipsychotics by reducing adverse effects associated with treatment, particularly extrapyramidal symptoms (EPS) like dyskinesia, akathisia, dystonia and parkinsonism.⁴ First generation antipsychotics, such as Haloperidol, competitively block post synaptic type-2 dopamine (D₂) receptors, resulting in their anti-hallucinogenic and anti-delusionary effects.⁵ However, this strong antagonism of the D₂ receptor combined with a narrow therapeutic window was found to be the cause of EPS associated with treatment.⁶ Second generation antipsychotics target a wider range of receptors including D₁-D₅ receptors, type-2 serotonin (5HT₂) receptors and α_1 adrenergic receptors with varying affinities. This broader range of receptor affinities as well as a greater 5-HT₂/D₂ binding ratio is thought to be the reason for the reduction in EPS associated with risperidone treatment.⁷

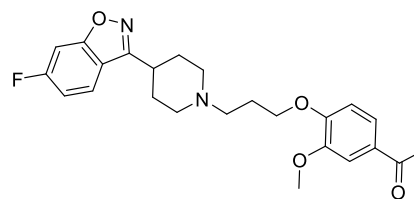
Structurally risperidone consists of a fluorinated benzisoxazole linked to a pyridopyrimidone moiety by a piperidine ring and a two-carbon alkyl spacer. Risperidone shares some structural features with other atypical antipsychotics (**Figure 1**).⁸ Paliperidone, a metabolite of risperidone, has a high structural similarity to its parent molecule, the difference being a 9-hydroxy moiety. This has also been developed by Janssen as a schizophrenia treatment.⁹ In other antipsychotics, benzisoxazole or benzisothiazole structures are commonly linked to another moiety by a piperidine or piperazine ring. Alkyl spacers of varying lengths are frequently used to link these rings to another bulky group which have a large range of structural variance.



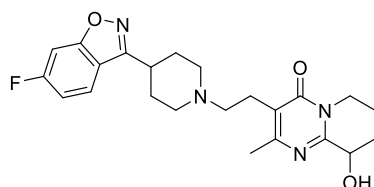
Ziprasidone



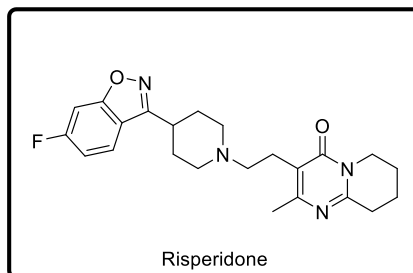
Lurasidone



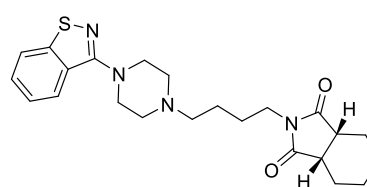
Iloperidone



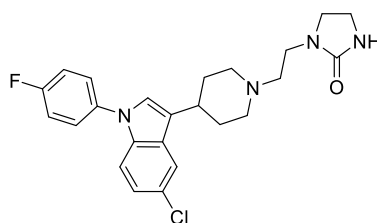
Paliperidone



Risperidone



Perospirine



Sertindole

Figure 1. Risperidone and structurally related atypical antipsychotics.

Recently the crystal structures of risperidone bound to the D₂ and 5-HT_{2A} receptors have been elucidated.¹⁰⁻¹¹ When bound to the D₂ receptor, the benzisoxazole moiety of risperidone sits in a deep hydrophobic binding pocket created by the side chains of transmembrane helices III, V and VI (**Figure 2**). Of particular importance for binding are residues Thr119, Phe198, Phe382 and Trp386. When these residues were replaced individually by alanine, at least a ten-fold reduction in binding affinity was observed. Another hydrophobic pocket is found to enclose the pyridopyrimidone ring nearer to the entrance of the pocket. A salt bridge is also found to form between Asp114 and the nitrogen of the piperidine ring, further stabilising binding. The orientation of the pyridopyrimidone moiety in its unbound state significantly changes when bound to the D₂ receptor in order to make a hydrophobic contact with Trp100.

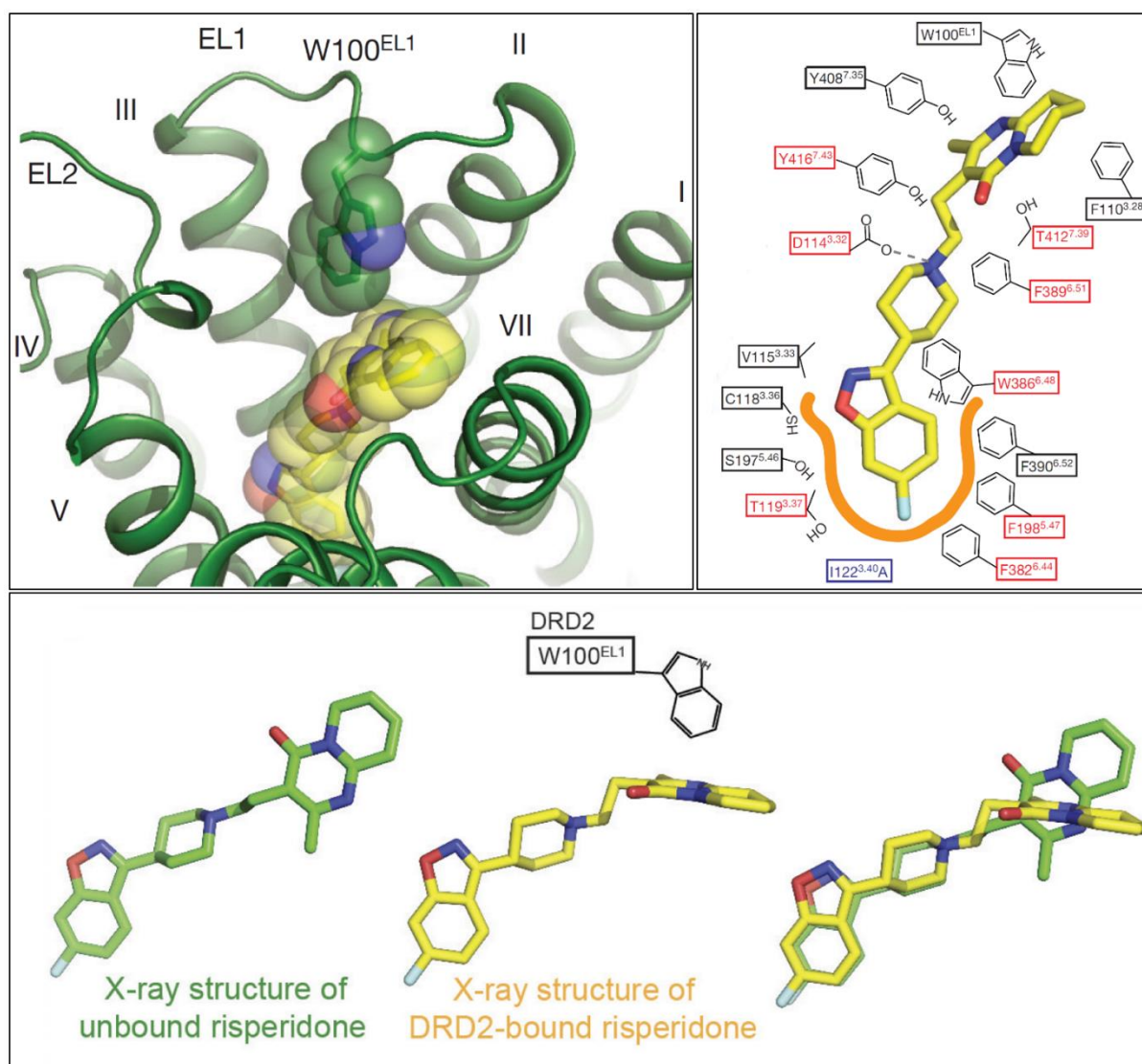


Figure 2. Top left, top down view of risperidone (yellow) bound in the pocket created by transmembrane helices III, V and VI (not shown). Top right, risperidone bound to D₂ receptor. Bottom, risperidone orientation when unbound vs bound to D₂ receptor. Bottom right, overlaid unbound (green) and bound (yellow). Adapted from Wang *et al.* *Structure of the D₂ dopamine receptor bound to the atypical antipsychotic drug risperidone.* *Nature* **555**, 269.¹⁰

Similar interactions are found when risperidone is bound to the 5-HT_{2A} receptor due to the conservation of many residues between the two aminergic receptors.¹² This is indicated by the residues highlighted in green in **Figure 3**. As with the D₂ receptor, alanine mutagenesis of interacting residues in the benzisoxazole binding pocket results in a significantly reduced binding affinity, noted by residues in red. Mutation of Trp336 in particular caused a 1000-fold

reduction in risperidone binding affinity. A salt bridge is also observed between an Asp residue and the piperidine ring. This is expected as it is a conserved residue among aminergic receptors.¹²

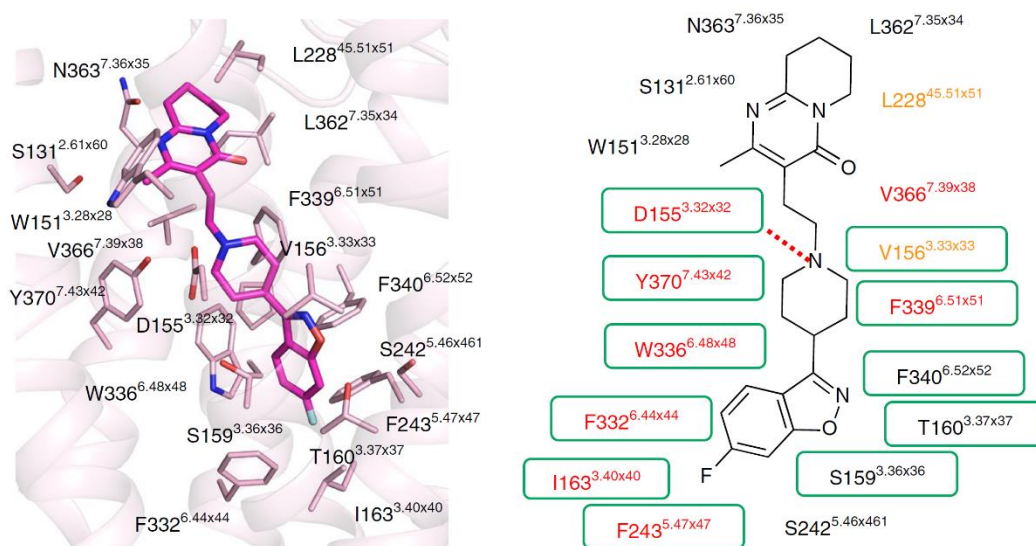


Figure 3. Left, 3-dimensional structure of risperidone bound to 5-HT_{2A} receptor. Right, interactions between risperidone and 5-HT_{2A}. Adapted from Kimura *et al. Structures of the 5-HT_{2A} receptor in complex with the antipsychotics risperidone and zotepine. Nature Structural & Molecular Biology* **26**, 121.¹¹

1.1.2 Pharmacokinetics and Receptor Affinities

Risperidone is most commonly taken orally as a tablet with dosages ranging from 0.5 to 6 mg/day for schizophrenia patients.¹³ It is also provided as a depot injection, a slow-release, long-lasting form of administration.¹⁴ Following oral administration, bioavailability is approximately 68% and maximal plasma concentrations are achieved after approximately 1 hour.^{3, 15} Plasma protein binding of risperidone to albumin and α -acid glycoprotein is 90%.³ Risperidone is primarily metabolised in the liver by CYP2D6, and to a lesser extent CYP3A4, to give 9-hydroxyrisperidone (Paliperidone), an active metabolite.¹⁶⁻¹⁷ 9-Hydroxyrisperidone has a slightly reduced maximum plasma protein binding of 77%.³ Risperidone has a mean half-life of approximately 3 hours while 9-hydroxyrisperidone has a substantially longer mean half-

life of 24 hours.¹⁵ Efflux from cells is mediated by the ABCB1 transporter¹⁸ and excretion of risperidone and its metabolites is primarily in the urine.³

Risperidone demonstrates very strong antagonistic affinity for 5-HT_{2A} receptors ($K_i < 1$ nM *in vitro*) and a strong affinity for D₂ and α_1 receptors ($K_i < 10$ nM *in vitro*).¹⁹⁻²⁰ Antagonistic activity has also been observed for dopamine type-1, 3, 4 (D₁, D₃, D₄), serotonin type 1A, 1C, 7 (5-HT_{1A}, 5-HT_{1C}, 5-HT₇), α_2 adrenergic and H₁ histaminergic receptors both *in vivo* and *in vitro*.²¹⁻²² Risperidone has also been shown act as an inverse agonist towards D₂, 5-HT_{2A}, 5-HT_{2C} and H₁ receptors.²³⁻²⁴

Binding to D₂ and D₃ receptors in the limbic and cortical regions of the brain is thought to be the source of risperidone's therapeutic effects while binding to D₂ receptors in the striatum may be the cause of motor side effects.²⁵ Studies in schizophrenic patients show that a 1 mg/day oral dose results in a maximum D₂ receptor occupancy of 50%²⁶ while larger doses of 3 and 6 mg/day result in 72% and 82% D₂ receptor occupancy respectively.²⁷ 5-HT_{2A} receptor occupancy was found to be greater, with 3 and 6 mg/day dosing regimens resulting in 83% and 95% receptor occupancy, respectively.²⁷

Atypical antipsychotics in general have a greater 5-HT_{2A}/D₂ binding ratio compared to first generation antipsychotics.²⁸ Risperidone has a high 5-HT_{2A}/D₂ ratio of 21, while only ziprasidone (31) and clozapine (45) are higher.²⁹ In contrast, the majority of first generation antipsychotics have a 5-HT_{2A}/D₂ binding ratio less than one. Greater 5-HT_{2A} antagonism has been associated with an atypical drug profile and is required for treatment of the negative symptoms of schizophrenia.²² Nonetheless, D₂ antagonism is required for antipsychotic activity and is responsible for treatment of the positive symptoms of schizophrenia. It has been hypothesised that strong antagonism of 5-HT_{2A} receptors alongside weaker antagonism of D₂ receptors observed with atypical antipsychotics is responsible for the reduced incidence of EPS.

1.1.3 Side Effects

Risperidone produces a range of side effects when used in the treatment of schizophrenia. The most commonly observed major side effects in clinical trials and Phase IV monitoring were EPS-related events including tremor, dyskinesia and hyperkinesia.³⁰⁻³¹ These side effects are also common in patients being treated for bipolar mania.³² A common relationship observed with antipsychotics is as D₂ receptor occupancy increases, so does the likelihood of EPS. This

correlation is particularly strong when D₂ receptor occupancy increases past 80%.³³ This increase in EPS occurs most commonly in patients taking larger doses of risperidone (6 mg/day) despite the near complete 5-HT_{2A} receptor occupancy associated with treatment.³⁴

Minor side effects frequently reported include sleepiness and moderate weight gain.³⁵ Risperidone is a strong binder of 5-HT_{2A} and H₁ and antagonism of these receptors has been associated with deep sleep and sedation respectively.³⁶ Weight gain is also associated with H₁ antagonism as well as 5-HT_{2C} binding.³⁶ Risperidone-associated weight gain has also been correlated with altered levels of inflammatory factors when used in the treatment of schizophrenia.³⁷

1.2 Multiple Sclerosis and Cytokines

1.2.1 Multiple Sclerosis

Multiple sclerosis (MS) is the most common chronic inflammatory, demyelinating and neurodegenerative disease in people under 40 with over 2.2 million cases reported worldwide in 2016.³⁸⁻³⁹ It is an autoimmune disease caused by demyelinating lesions that accumulate along the spinal cord and in the brain. This damage is caused by immune system attack on the myelin sheath surrounding neurons. As over 200 alleles are associated with this multifactorial disease it is not a simple condition.⁴⁰ Demyelination causes relapses, reversible periods of neurological deficits that affects a person's movement and bladder and bowel function and can last for days or weeks. The disease can be classified as relapsing, characterised by relapses at irregular intervals with complete or incomplete recovery.⁴¹ In a minority of cases disease is progressive.⁴¹ This is characterised by symptoms worsening over time with acute periods of relapse, sometimes without full clinical recovery.

1.2.2 Current Treatments

Current treatments, such as Natalizumab and BG-12, aim to reduce the rate of these relapses and the growth of new lesions. Natalizumab works by reducing T-cell trafficking to the central nervous system, one of the possible causes of inflammation.⁴² However, after public release it was found to increase the chances of patients developing progressive multifocal

leukoencephalopathy and now carries a black box warning.⁴³⁻⁴⁴ BG-12 reduces the rate of disease progression by activating the Nrf2 antioxidant response pathway,⁴⁵ as well as potentially suppressing pro-inflammatory cytokine production or associated downstream pathways.⁴⁶ It is currently used to treat relapsing forms of MS. Vitamin D has even been suggested to lower the risk of MS although there is some disagreement over its efficacy.⁴⁷⁻⁵⁰

1.2.3 Cytokines and Multiple Sclerosis

Cytokines are a broad category of small proteins important for cell signalling. They are unable to cross lipid bilayers so rely on interactions with cell surface receptors to initiate intracellular signalling cascades. They are predominantly produced by T helper cells and macrophages.⁵¹ Many cytokines are associated with pro- and anti-inflammatory pathways, or both, as listed in **Table 1**. T helper cells produce interleukin (IL)-2, IL-4, IL-5, IL-10, IL-13, tumour necrosis factor- α (TNF- α), IFN- γ and transforming growth factor- β (TGF- β).⁵²⁻⁵³ As well as some of the previously mentioned cytokines, macrophages also produce IL-1 β , IL-6 and IL-23.⁵⁴

Table 1. Cytokines and their related pathways.

Associated Pathways	Cytokine	Refs.
Pro-inflammatory	TNF- α , IFN- γ , IL-1 β , IL-2, IL-6, IL-12 IL-15, IL-17, IL-18	51, 55-58
Anti-inflammatory	TGF- β , IFN- α , IL-2, IL-4, IL-6, IL-10, IL-11, IL-13	51, 55, 58-59

Uncontrolled production and secretion of pro-inflammatory cytokines has been widely observed in cases of MS and is suspected to be one of the causes of inflammation associated with the disease. In particular, dysregulation of IFN- γ , TNF- α , IL-12 and IL-6 has been demonstrated to be important in the progression and severity of disease. To study these effects, experimental autoimmune encephalomyelitis (EAE) is often used as an animal model for MS.⁶⁰ EAE is commonly used in mice or rats where the condition is artificially induced by immunisation with myelin-derived antigens.⁶¹

IFN- γ can be considered a pro-inflammatory cytokine because of its regulatory activity towards TNF- α and nitric oxide. IFN- γ expression has been shown to begin at the onset of central nervous system (CNS) inflammation, increase at the peak of disease in EAE and subside during remission.⁶² Overexpression of IFN- γ results in demyelination throughout the CNS.⁶³ Surprisingly, IFN- γ knockout mice were also found to be susceptible to EAE induction.⁶⁴ These knockout mice exhibited large amounts of CNS inflammation and a further progressed form of EAE. This led to the suggestion that IFN- γ is not vital for induction or continuation of EAE. In humans, increased levels of IFN- γ have been observed in patients with progressive forms of MS.⁶⁵ This dysregulation of IFN- γ production is suspected to be important in the transition of MS from a relapsing to a progressive form of the disease.

TNF- α is a pro-inflammatory cytokine produced by immune cells as well as astrocytes and neurons. Artificially increased TNF- α levels in mice results in a prolonged disease period for EAE and more severe infiltration of the spinal cord by immune cells.⁶⁶ Injection with anti-TNF- α antibodies prior to TNF- α treatment resulted in a dose-dependent reduction in disease severity suggesting a direct correlation between TNF- α levels and EAE severity. In transgenic mice, induced TNF- α expression resulted in a chronic inflammatory, demyelinating disease in 100% of subjects.⁶⁷ Extensive T-cell infiltration was observed particularly in the meninges of the brain and the parenchyma of the CNS. Again, this was preventable by introduction of TNF- α antibodies. In humans, MS lesions have been associated with significantly increased levels of TNF- α which is expressed by macrophages and microglia found in chronic lesions.⁶⁸⁻⁶⁹ High cerebrospinal fluid levels of TNF- α have also been associated with severity and progression of MS, particularly in patients with a chronic progressive form of the disease.⁷⁰

IL-12 is involved in the differentiation and proliferation of T cells and produced primarily by monocytes and dendritic cells. In rat models that had recovered from induced EAE, administration of IL-12 was able to induce a relapse in disease.⁷¹ This was observed as an increase in CNS lesions, which coincided with increased macrophages peripheral to the surrounding blood vessels. Nitric oxide synthase, catalyst of nitric oxide production, was also upregulated in macrophages. Increased levels of nitric oxide and its metabolites have since been associated with progression of MS.⁷² In humans, IL-12 is found to be upregulated in the lesions and not in other areas of the brain of MS patients.⁷³ Inhibitors of IL-12 production are now used for treatment of relapsing forms of MS.⁷⁴⁻⁷⁵

IL-6 can act as a pro- and anti-inflammatory cytokine whose production in monocytes and macrophages is stimulated by IL-1.⁷⁶ Upregulation of IL-6 in the CNS coincides with the induction phase of EAE in murine and rat models.⁷⁷⁻⁷⁸ Elevated plasma levels of IL-6 have also been observed in MS patients.⁷⁹ In the brain of MS patients, IL-6 levels are found to be elevated.⁸⁰⁻⁸¹ This is localised to macrophages and astrocytes found within lesions. Schönrock *et al.*⁸⁰ noted that the number of IL-6 expressing cells was greatest in inactive demyelinated lesions with large numbers of oligodendrocytes, suggesting that IL-6 may also play a role in remyelination.

1.3 Risperidone, Inflammation and Cytokines

Multiple studies show that some of the psychosis related symptoms observed in schizophrenia cases develop from neuroinflammation and immune system dysregulation. Risperidone treatment has been shown to have anti-inflammatory effects by modulation of cytokine profiles and cellular immune responses.

Atypical antipsychotics including risperidone have been shown to suppress production of proinflammatory cytokines while also upregulating production of the anti-inflammatory cytokine IL-10 in LPS-treated mice.⁸² Further research in rats shows risperidone also decreases LPS-induced production of pro-inflammatory cytokines IL-1 β and TNF- α , as well as MAPK and NF- κ B.⁸³ Risperidone treatment also restored activity of anti-inflammatory pathways usually suppressed by LPS treatment.

A small-scale study in schizophrenia patients treated with risperidone showed changes in cytokine levels after 3 months of treatment.⁸⁴ Most notably, IL-10 levels increased while IFN- γ levels decreased. As IL-10 is a suppressor of IFN- γ , this was an unsurprising connection, but it is unclear if IFN- γ suppression was directly caused by the upregulation of IL-10 or other unspecified mechanisms. These modifications in cytokine levels were also seen in non-responders to risperidone treatment, indicating the effect was unlikely to be entirely related to a specific psychopathological state.

Cytokine levels were also found to be altered in children with autism who were prescribed risperidone to manage irritability associated with their condition.⁸⁵ Changes in plasma pro-inflammatory cytokine levels were more pronounced in responders to treatment vs non-responders. This indicates a relationship between a patient's psychopathological state and the

effect risperidone treatment has on their cytokine levels. This is contrary to the study previously described in schizophrenia patients.⁸⁴

In patients with first episode paranoid schizophrenia, serum levels of IL-2, IL-6, IL-18 and TNF- α were found to be significantly reduced after 1 to 6 months, demonstrating an immunosuppressive effect in schizophrenia patients involving pro- and anti-inflammatory cytokines.⁸⁶ Another study showed an initial anti-inflammatory effect where levels of IL-1 β , IL-6, and TNF- α decreased in the first month but reverted to baseline levels at the end of a 6-month risperidone treatment period.³⁷ However, baseline levels of these pro-inflammatory cytokines were greater in schizophrenia patients vs the control group. Juncal-Ruiz *et al.*⁸⁷ suggested that the difference in baseline levels of these cytokines may be as a result of prior exposure to antipsychotic drugs because their study showed no difference in baseline levels of IL-1 β , IL-6 and TNF- α between healthy volunteers and drug naïve schizophrenia patients.

Risperidone has been shown to inhibit the IFN- γ induced production of nitric oxide and pro-inflammatory cytokines in microglia.⁸⁸ Haloperidol showed a much lesser inhibition of these pathways, leading to the suggestion that risperidone's wider aminergic receptor binding profile could be responsible for its improved inhibitory activity.

1.4 Alkyl Spacer Effects in Drug Molecules

A common structural motif in drug molecules, particularly those targeting the dopamine and serotonin receptors, is an extended alkyl spacer connecting two different moieties. Often in the development of a drug, structure-activity relationship studies will modify the length of alkyl spacers as this can drastically alter receptor binding profiles. This can be as a result of the increased flexibility afforded by a longer chain.

For example the *N*-acylethanolamine acid amidase (NAAA) inhibitory potency of pyrrolidine amide derivatives synthesised by Zhou *et al.*⁸⁹ increased with chain length and flexibility. However, the increased length also reduced their selectivity for NAAA when compared to analogues with more restricted linkers.⁸⁹

More specifically in neurotropic drugs targeting the various dopamine and serotonin receptors, the distance between two different moieties, linked by an alkyl chain and often with a nitrogen-containing 6-membered ring, has been shown to have large effects on receptor binding profiles.

Multiple studies investigating the structure-activity relationships of compounds targeting 5-HT₇ have found that longer alkyl linkers correlate to an improved binding affinity for 5-HT₇. Development of selectivity over other serotonin and dopaminergic receptors has also been possible from the introduction of these modifications. Volk *et al.*⁹⁰ found that a four-carbon alkyl spacer was optimal for 5-HT₇ binding with minimal off target binding to 5-HT_{1A} (**Figure 4**). Three- and five-carbon spacers were also investigated but exhibited strong off-target binding and reduced 5-HT₇ binding respectively. The efficacy of the four-carbon compound was confirmed *in vivo*. This was also consistent with prior work on structurally similar compounds where a four-carbon alkyl spacer was found to be superior in terms of 5-HT₇ affinity and specificity.⁹¹ Further study of 5-HT_{2A}, 5-HT₆ and 5-HT₇ antagonists showed a four-carbon alkyl spacer to provide an improved binding affinity for these receptors compared to a three-carbon spacer compound (**Figure 5**).⁹² Interestingly, introducing a semi-rigid four-alkylene spacer into the compound further improved the molecule's binding affinity for 5-HT₇. This is likely because adding rigidity to the molecule will lock it into a more bioactive conformation. Upon interaction with 5-HT₇, less conformational rearrangement is then required for it to bind.

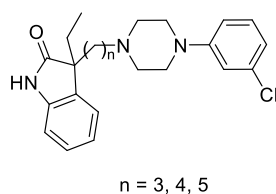


Figure 4. Oxindoles targeting 5-HT₇ synthesised by Volk *et al.*⁹⁰

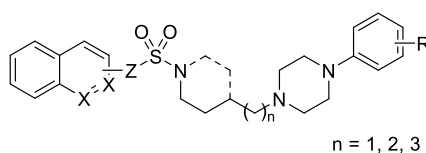


Figure 5. Quinoline- and isoquinoline-sulfonamides synthesised by Zajdel *et al.*⁹²

The flexibility afforded by an extended alkyl linker when compared to more conformationally restricted linkers has also been investigated. Bojarski *et al.*⁹³ found a tetramethylene linker to

be optimal for 5-HT₇ binding and specificity when compared to more conformationally restricted linkers such as alkenes and cyclohexanes (**Figure 6**).

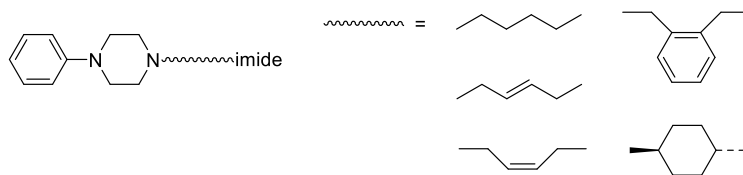


Figure 6. Arylpiperazines synthesised by Bojarski *et al.*⁹³

Smid *et al.*⁹⁴ investigated the effects of altering the alkyl linker length while optimising a molecule for D₂ receptor binding (**Figure 7**). Compounds were tested for D₂ receptor binding and serotonin reuptake inhibition *in vitro* and *in vivo*. *In vitro* experiments show the three-carbon compound to have a superior binding profile for the D₂ and serotonin reuptake inhibition. The four- and five-carbon variants had a slightly increased binding affinity for D₂ but also significantly reduced serotonin reuptake inhibitory activity.

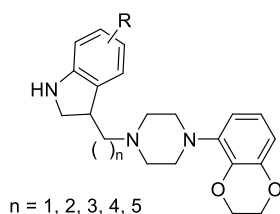


Figure 7. Piperazines synthesised by Smid *et al.*⁹⁴

1.5 Previous Studies at Victoria University of Wellington

1.5.1 Risperidone Reduces Disease Severity in EAE

Researchers at VUW examined the effects of risperidone treatment on EAE on mice.⁹⁵ Following induction of EAE, mice were treated with risperidone orally at either 1 or 3 mg/kg/day via their drinking water. No obvious adverse effects were observed except for moderate weight gain as previously reported.

Severity of disease was found to be reduced in a dose-dependent manner as measured by a reduction in the size and number of spinal cord lesions, which decreased with treatment compared to control.⁹⁵ However, the incidence of disease was similar between treated and untreated subjects.

Risperidone treatment altered the production of specific cytokines measured in the peripheral lymphoid organs.⁹⁵ Significantly decreased levels of IL-2, IL-4, IL-13 and IL-17a were observed while IFN- γ production was unaffected, indicating that risperidone modulates antigen-specific T-cell responses.

In vitro testing with IFN- γ -primed bone marrow derived macrophages (BMM Φ) showed that risperidone altered their ability to bias naïve T-cells.⁹⁵ Risperidone had a direct immunomodulatory effect on BMM Φ . A reduction in pro-inflammatory cytokine levels and an altered ability for BMM Φ to bias naïve T-cells was observed. Little effect was observed on activation of macrophages *in vivo* during EAE. Risperidone reduced the activation of microglia and macrophages in the CNS.

Use of D₁ and D₂ antagonists did not cause inhibition of pro-inflammatory cytokines.⁹⁵ This lead the authors to suggest that risperidone's immunomodulatory activity is achieved through a unique and yet to be described mechanism, independent of D₁ and D₂ antagonism. As the concentration of doses administered were physiologically comparable to those used for schizophrenia treatment, it was suggested that they could have a therapeutic use for inflammatory diseases like MS. The safety, toxicity and side effects of risperidone are well understood which would also make further investigation in humans more straight forward. Risperidone and clozapine have since been used in Phase Ib/IIa trials to assess the possibility of their being repurposed to treat MS.⁹⁶

1.5.2 Immunomodulatory Activity of Risperidone Analogues in Macrophages

To further investigate the immunomodulatory activity of risperidone, VUW researchers synthesised truncated analogues of risperidone and used them in structure-activity relationship studies.⁹⁷ Their aim was to discern what components of the molecule were responsible for the immunomodulatory effects of risperidone.

Analogues investigated were the truncated benzisoxazole (**3**) and the ring-open variant oxime (**4**), unsaturated pyridopyrimidone (**2**) and truncated pyridopyrimidone analogues (**5,6,7**) (**Figure 8**).⁹⁷ These were synthesised using known methodologies and their ability to modify the production of pro-inflammatory cytokines IL-6, IL-12, TNF- α and monocyte chemo-attractant protein 1 (MCP-1) in primed macrophages was assessed. Their activity was compared to unmodified risperidone (**1**). Cytokine assays showed that only the unsaturated risperidone (**2**) and ring closed benzisoxazole (**3**) modified cytokine levels in RAW 264.7 macrophages and BMM Φ .

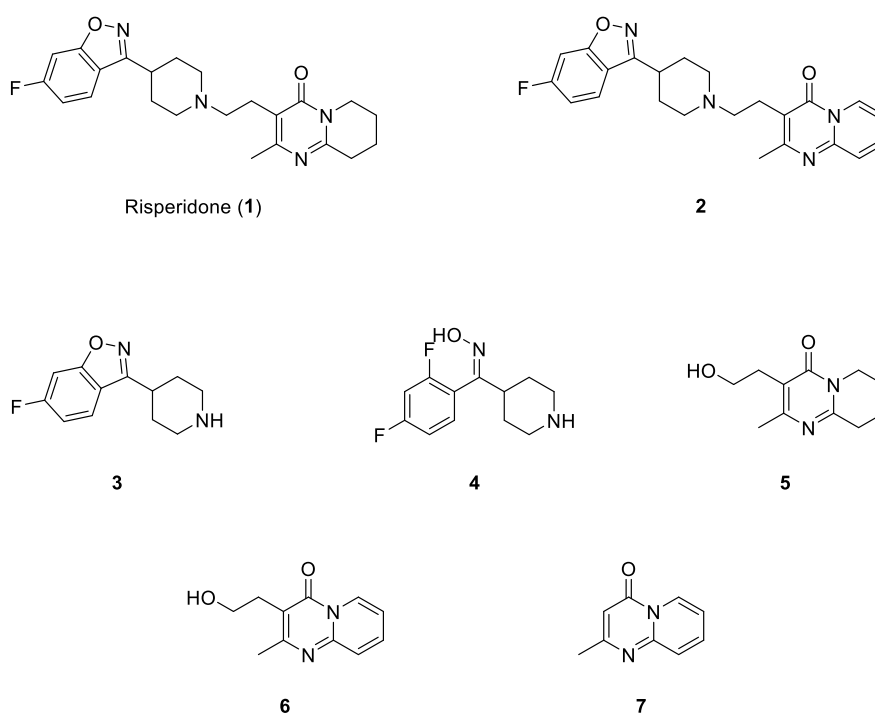


Figure 8. Risperidone analogues synthesised by VUW researchers.⁹⁷

Risperidone was shown to upregulate production of IL-10 and suppress production of IL-12 and MCP-1.⁹⁷ The unsaturated analogue **2** reduced production of IL-12 and MCP-1 to a lesser extent and had no measurable effect on IL-10 production. The truncated benzisoxazole **3** was more effective at suppressing production of IL-12 and MCP-1 compared to **2** but also showed no effect on IL-10 production. MTT assays showed that the unsaturated analogue **2** was less toxic than risperidone, with no change in macrophage cell viability at concentrations of up to 100 μ M. At similar concentrations, risperidone treated cell viability was approximately 30%

less than control. The truncated benzisoxazole **3** was more toxic than risperidone in macrophages, particularly at lower concentrations (20 μ M). This increase in toxicity observed with **3** and the subsequent reduction in cell number may be the cause of the reduction in cytokine production. As the oxime **4** did not have any effect on cell viability or cytokine production, it is likely the benzisoxazole moiety is required for immunomodulatory activity. The truncated pyridopyrimidone analogues (**5,6,7**) had no observable effect on cytokine production or macrophage viability, however the pyridopyrimidone moiety appears to be important for immunomodulatory activity as demonstrated by risperidone **1** and the unsaturated analogue **2** compared to the truncated benzisoxazole **3**.

1.6 Project Aims

The aim of this project is to synthesis two extended linker analogues of risperidone (**Figure 9**). Analogues **8** and **9** have three- and four-carbon alkyl spacers, respectively. RAW 264.7 cells will then be treated with analogues **8** and **9** and the cytotoxicity and pro-and anti-inflammatory cytokine production associated with treatment will be assessed. This will allow for the mechanism of action responsible for the anti-inflammatory activity of risperidone to be explored.

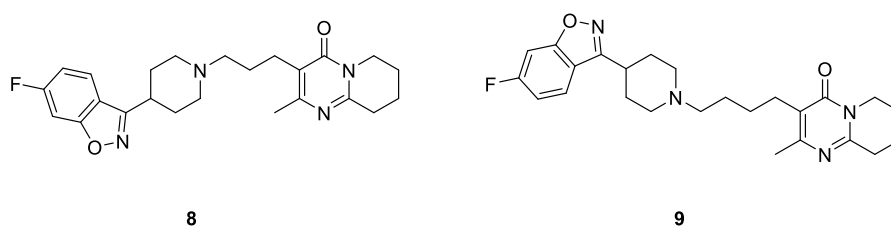


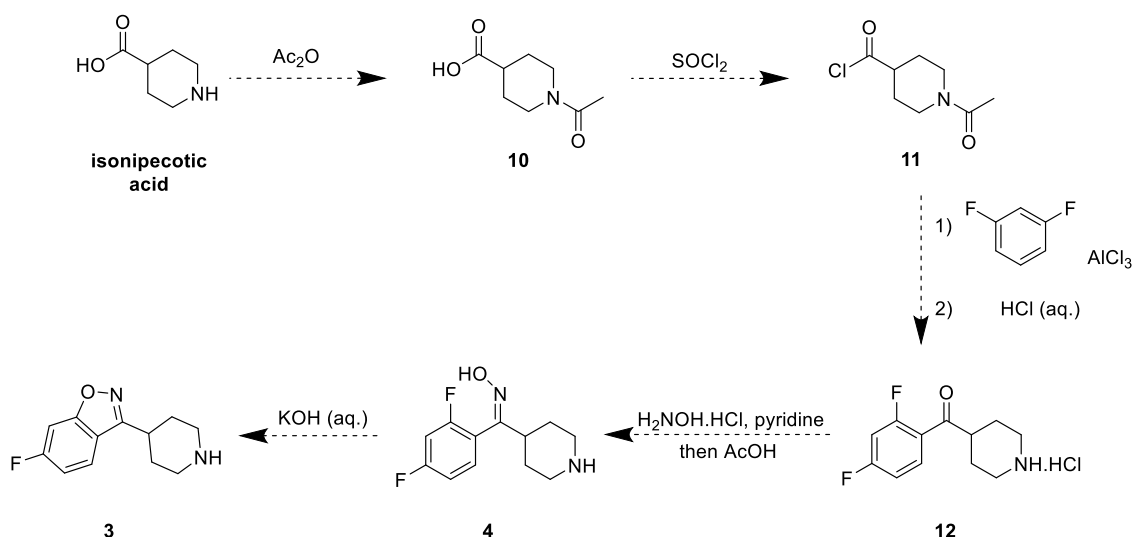
Figure 9. Three- and four-carbon linker analogues of risperidone.

1.6.1 Synthetic Chemistry

Synthesis of two extended-linker analogues of risperidone (**8** and **9**) will require the use of commercially available starting materials. This builds on earlier work by Durrant who generated three- and four-carbon linker benzyl-protected pyridopyrimidones as precursors for

these analogues.⁹⁸ Durrant's research explored catalytic hydrogenation for benzyl deprotection but was found to be unsuccessful after multiple attempts. This project aims to utilise the methodology developed by Durrant to synthesise the protected pyridopyrimidones, establish a suitable method for *O*-debenzylation and complete the synthesis of risperidone analogues **8** and **9**.

In the synthesis of truncated and unsaturated analogues of risperidone, Zareie *et al.*⁹⁷ employed known methodology for the synthesis of the benzisoxazole fragment (**Scheme 1**). Acetylation of the amine starting material was followed by a Friedel-Crafts acylation. This was followed by generation of an oxime (**4**) that was used in a nucleophilic aromatic substitution reaction to afford benzisoxazole **3**. This chemistry is well established and was used in the synthesis of risperidone itself so was expected to be straight-forward.

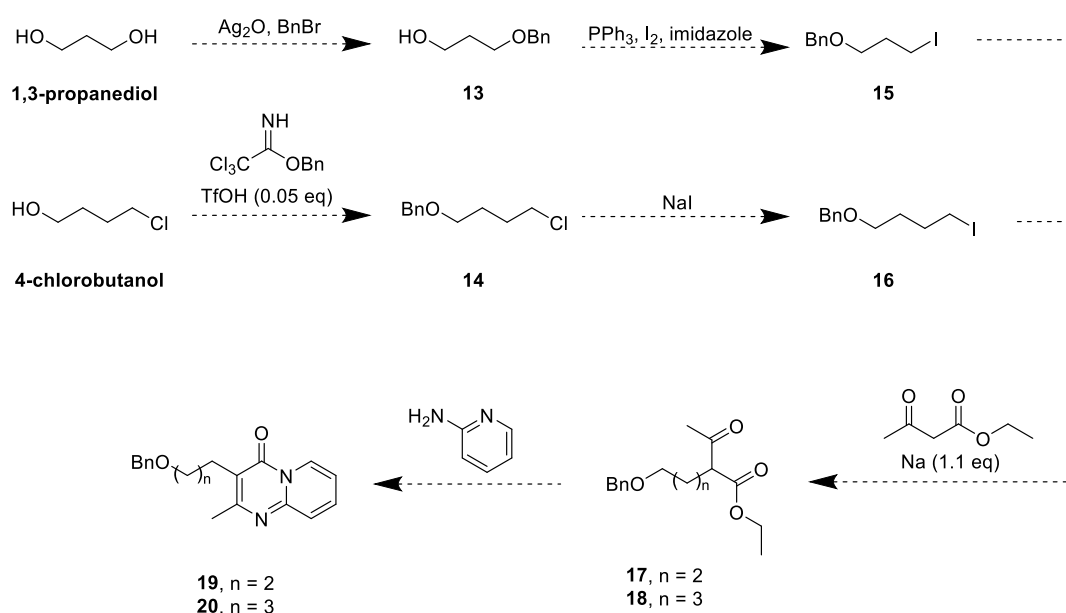


Scheme 1. Proposed synthesis of benzisoxazole **3**.

Durrant's synthesis of extended linker coupled benzyl protected pyridopyrimidones differs from methodology used in the commercial production of risperidone which employs a cyclic starting material that does not require protecting groups for pyridopyrimidone synthesis.⁹⁸ The synthetic route developed by Durrant for the extended-linker analogues involved benzyl monoprotection of alcohol functionality in the first step. Two different starting materials were required: 1,3-propanediol for the three-carbon analogue and 4-chlorobutanol for the four-

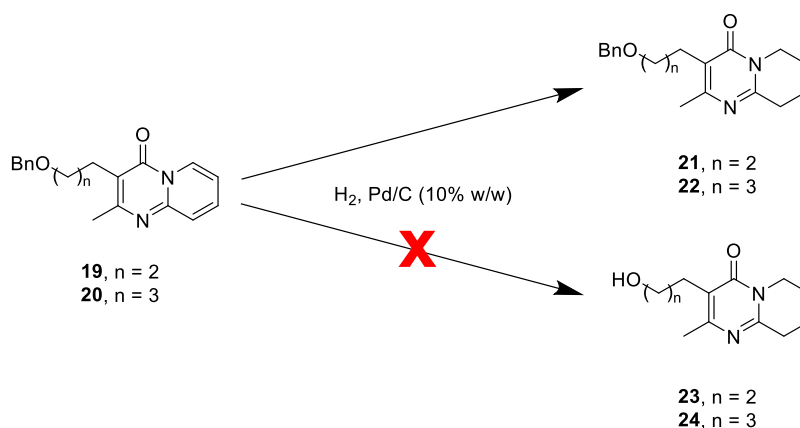
carbon analogue. The choice of the latter is due to the unavailability of 1,4-butanediol, which is a controlled substance in New Zealand as it is a prodrug for the class B narcotic GHB.⁹⁹

Benzyl protection of these starting materials required two different methods. A silver oxide mediated method was used for selective monoprotection of 1,3-propanediol and while an acid-catalysed method was used for benzyl protection of 4-chlorobutanol (**Scheme 2**). Appel and Finkelstein reactions were then required to yield iodoalkanes **15** and **16**, respectively, in preparation for subsequent alkylation reactions with ethyl acetoacetate. The alkylated products **17** and **18** afforded from these reactions were then subject to condensation with 2-aminopyridine. These reactions yield extended linker coupled pyridopyrimidones **19** and **20**.



Scheme 2. Proposed synthesis of extended linker coupled pyridopyrimidones **19** and **20**.

Palladium-catalysed hydrogenation was then required to afford saturated pyridopyrimidones **21** and **22**. Durrant⁹⁸ suggested the use of catalytic hydrogenation for saturation of the pyridine ring could simultaneously remove the benzyl protecting group and afford alcohols **23** and **24**. Unfortunately, this method only hydrogenated the pyridine ring, delivering **21** and **22** (**Scheme 3**). Therefore, debenzylation is required in a separate step.



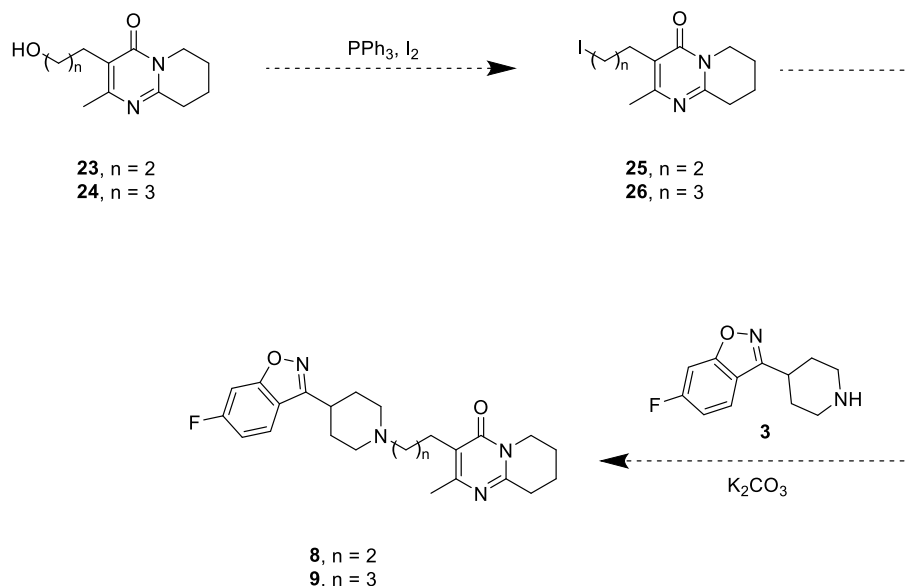
Scheme 3. Outcome of Durrant's Pd-catalysed hydrogenation reactions.⁹⁸

Multiple methods have been employed for the cleavage of benzyl ethers in the literature. TiCl_4 facilitates Lewis acid-mediated deprotection under mild conditions and can provide good selectivity, particularly in the total synthesis of natural products.¹⁰⁰⁻¹⁰² Hydrogenolysis by transfer hydrogenation may also be suitable as reactions can be carried out in MeOH, a solvent that **21** and **22** are soluble in.¹⁰³⁻¹⁰⁴ Oxidative cleavage of benzyl ethers can be achieved with DDQ, as this reagent has been applied to debenzylation in the synthesis of a range of substrates, including steroids, heterocycles and highly functionalised natural product.¹⁰⁵⁻¹⁰⁷ The use of photoirradiation at 365 nm has also been demonstrated to aid in *O*-debenzylation of simple substrates.¹⁰⁸ In the current work, DDQ, TiCl_4 and Pd/C catalysed hydrogenolysis under more forcing conditions were explored for deprotection of **21** and **22** as these methods were expected to be compatible with the functional groups present in the molecules and will afford **23** and **24** (Scheme 4).



Scheme 4. Proposed DDQ-mediated deprotection of **21** and **22**.

Following deprotection, alcohols **23** and **24** will be subject to Appel reactions similar to those previously described (**Scheme 5**).⁹⁷ This will provide iodides **25** and **26** which will then be coupled with benzisoxazole **3** using procedures established for the synthesis of risperidone, yielding the required three- and four-carbon extended linker analogues of risperidone (**8**, **9**).



Scheme 5. Proposed synthesis of analogues **8** and **9**.

1.6.2 *In Vitro* Assays

The cytotoxicity of analogues **8** and **9** will be explored using MTT assays according to methodology described by VUW researchers.⁹⁷ Flow cytometry can also be utilised to assess cell viability. IL-6 and IL-12p40 from cell culture supernatants will be measured using sandwich ELISA (Enzyme-Linked Immunosorbent Assay) according to previously established methodology.⁹⁷ IFN- γ , TNF- α , MCP-1 and IL-10 will be measured using a cytokine bead array mouse inflammatory kit according to previously established methodology.⁹⁷

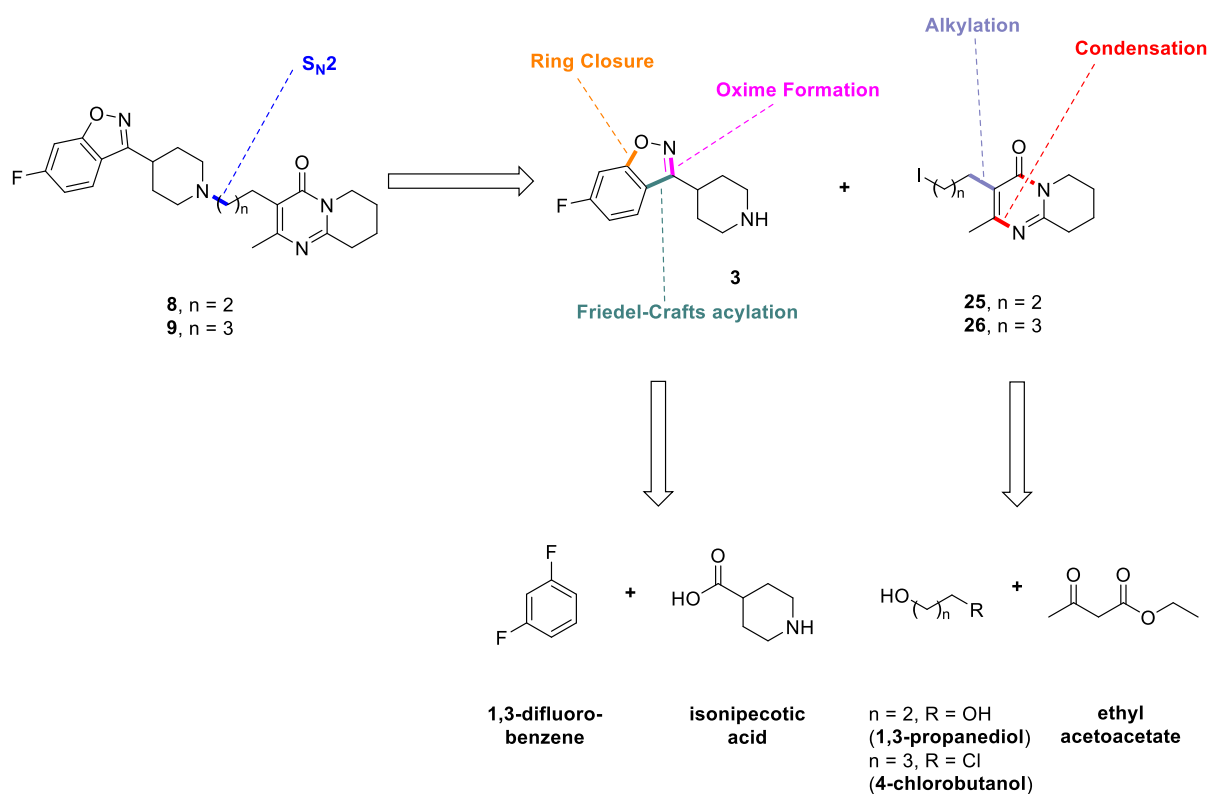
RAW 264.7 cells were chosen for assessment of cell viability, as well as pro- and anti-inflammatory cytokine production. Prior research has shown this cell type to give comparable results to BMM Φ when used in studies on risperidone and truncated analogues.⁹⁷ Macrophages are known to drive inflammatory processes that cause damage in this disease and BMM Φ have been used in MS studies.¹⁰⁹ Furthermore, some MS treatments are effective due to the way in

which they modulate macrophage responses in the CNS, thus making BMM Φ a good *in vitro* model.¹¹⁰⁻¹¹¹ Therefore, the related RAW 264.7 cells, readily available in our lab, are expected to provide a reasonable model for obtaining preliminary results.

2 Synthesis of Risperidone Analogues

2.1 Retrosynthesis

Synthesis of the extended linker analogues **8** and **9** relies on S_N2 coupling of the benzisoxazole fragment (**3**) and the extended linker coupled pyridopyrimidones **25** and **26** (**Scheme 6**). Synthesis of **3** will require a Friedel-Crafts acylation, formation of an oxime and ring closure through a nucleophilic aromatic substitution. Integration of the extended linkers will be required at the beginning of the synthesis with an alkylation to ethyl acetoacetate, the product of which will be subject to a condensation reaction with 2-aminopyridine. Generation of the desired analogues **8** and **9** will couple the benzisoxazole with a pyridopyrimidone in a base-mediated S_N2 reaction.



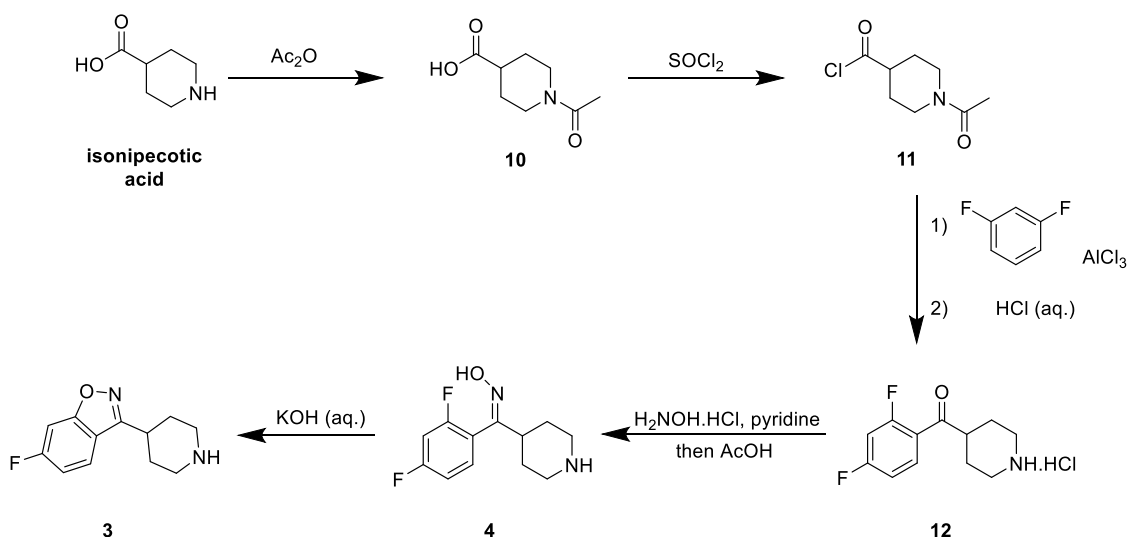
Scheme 6. Retrosynthesis of extended linker analogues of risperidone.

The first disconnection at the amine, as well as the three disconnections of benzisoxazole **3**, should be applicable in the synthesis of analogues **8** and **9** as they have been applied to the

commercial synthesis of risperidone. Furthermore, the addition of one and two methylenes in analogues **8** and **9**, respectively, does not introduce new functionality so should not hinder these reactions. The disconnections described for the extended linker coupled pyridopyrimidones **25** and **26** have been established as viable routes and have the possibility of being applied to synthesis of analogues with longer alkyl spacers.

2.2 Synthesis of the Benzisoxazole Fragment

To begin, attention was centred on the synthesis of benzisoxazole **3** following established methodology.⁹⁷ This route begins with acetylation of the amine starting material, followed by conversion of the carboxylic acid to an acyl chloride, a Friedel-Crafts acylation, formation of an oxime, and concludes with a ring closure through nucleophilic aromatic substitution (**Scheme 7**). This route will be described in detail below.

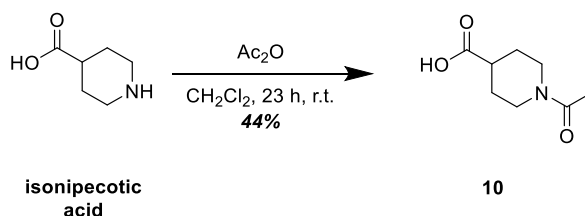


Scheme 7. Synthetic route to yield benzisoxazole **3**.

2.2.1 Isonipecotic Acid Acetylation

Commercially available isonipecotic acid was used as a starting material and was acetylated using acetic anhydride (**Scheme 8**). Formation of the *N*-acetylated product (**10**) was confirmed by the ^1H and ^{13}C NMR spectra which were consistent with those previously reported.⁹⁷

Interestingly, in the ^1H NMR spectrum, eight different shifts (one integrating for two protons) are observed for the nine protons in the piperidine ring although only five might be expected due to the apparent symmetry of the molecule. This is likely due to the product being present as a mixture of nitrogen rotamers (**Figure 10**). The piperidine ring is likely to adopt an energy minimised chair conformation with the $-\text{CO}_2\text{H}$ group found equatorial to reduce 1,3-diaxial interactions. In this conformation, two rotamer structures are possible at the amide where the oxygen will be oriented perpendicular relative to the ring system. These two conformers, or rotamers,¹¹² appear to be present in equal amounts in solution which would account for the ^1H spectrum observed.



Scheme 8. Acetylation of isonipecotic acid.

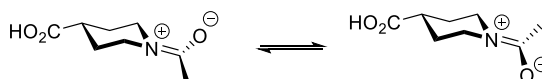
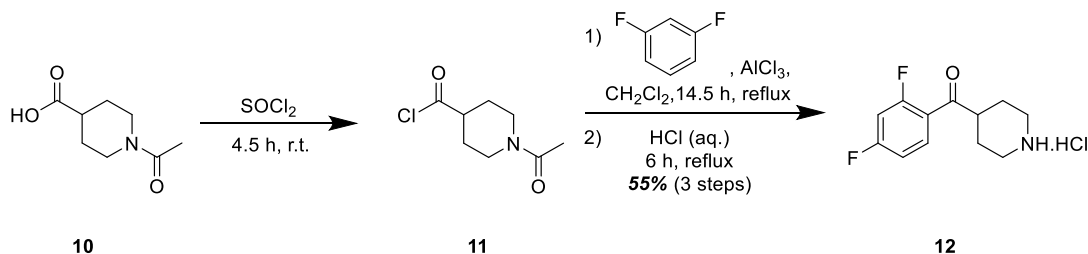


Figure 10. Possible nitrogen rotamers of **10**.

2.2.2 Friedel-Crafts Acylation of **10**

The *N*-acetylated product was then reacted with neat thionyl chloride to provide the corresponding acid chloride (**11**) (**Scheme 9**). This activated the acid for the subsequent Friedel-Crafts acylation. To avoid hydrolysis, the acid chloride intermediate was immediately subjected to the Friedel-Crafts acylation with 1,3-difluorobenzene using AlCl_3 as the Lewis acid. The fluorine atoms of 1,3-difluorobenzene stabilise the ring by resonance and act as ortho/para directors for the reaction while the steric hindrance caused by the fluorine atoms prevents formation of the ortho/ortho regioisomer, resulting in the observed formation of only the desired product. The Friedel-Crafts acylation product was immediately treated with 6 M

HCl to cleave the acetate group which provided the desired amine HCl salt (**12**), with ^1H and ^{13}C NMR data consistent with those previously reported.⁹⁷



Scheme 9. Friedel-Crafts acylation of **10**.

Analysis of the ^1H NMR spectrum clearly showed the introduction of aromatic protons with a triplet of doublets at 7.88 ppm (1H) and a multiplet at 7.10 ppm (2H). Cleavage of the acetate group was also confirmed by the loss of the methyl shift at 2.10 ppm. The loss of the molecules rotameric properties was also observed in the ^1H NMR spectrum, where the axial and equatorial protons at the 9- and 10-positions of the piperidine ring now have four shifts instead of seven distinct signals (**Figure 11**). A significant downfield shift of the proton at C-8 from 2.69 ppm to 3.62 ppm was noted, caused by the deshielding of the aromatic ring.

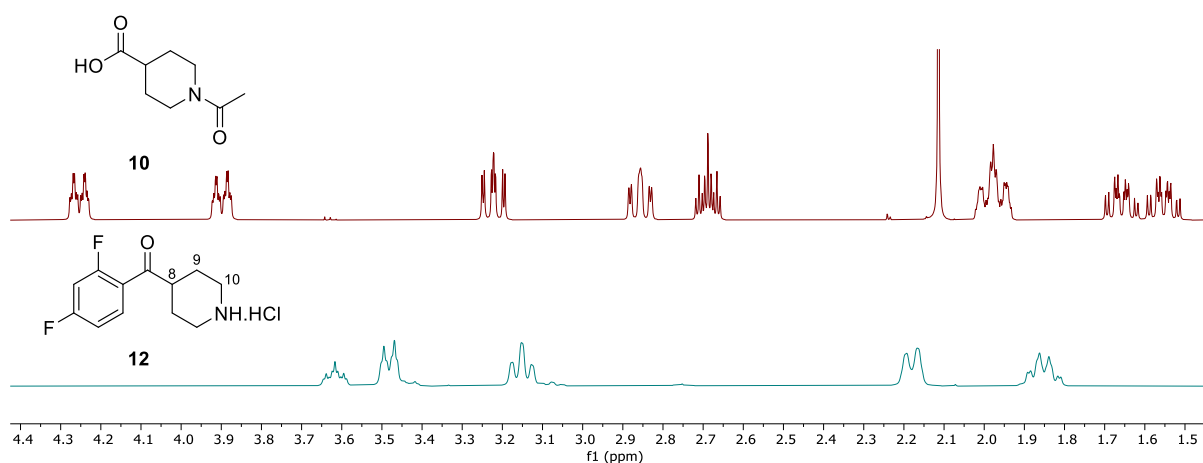


Figure 11. Comparison of ^1H NMR spectra of *N*-acetylated acid **10** and Friedel-Crafts product **12**.

The ^{13}C NMR spectrum showed the loss of the carboxylic acid functionality at 179.4 ppm and the presence of a ketone further downfield at 201.7 ppm. The aromatic carbons are seen to couple to the two fluorines, causing splitting of the ^{13}C NMR signals similar to what is observed in ^1H NMR with neighbouring protons. Standard ^{13}C NMR pulse sequences utilise C-H decoupling to prevent this peak splitting. C-F decoupling is not usually employed, thus splitting due to carbon-fluorine coupling is observed in the ^{13}C spectrum. In the case of **12**, each carbon covalently bonded to a fluorine exhibits splitting into a doublet of doublets at 166.1 ppm and 162.1 ppm, both of which have one large J -coupling of approximately 255 Hz and a smaller J -coupling of approximately 14 Hz (**Figure 12**). The larger coupling being between the carbon and the attached fluorine while the finer splitting is likely a three-bond coupling to the fluorine on the meta-position.

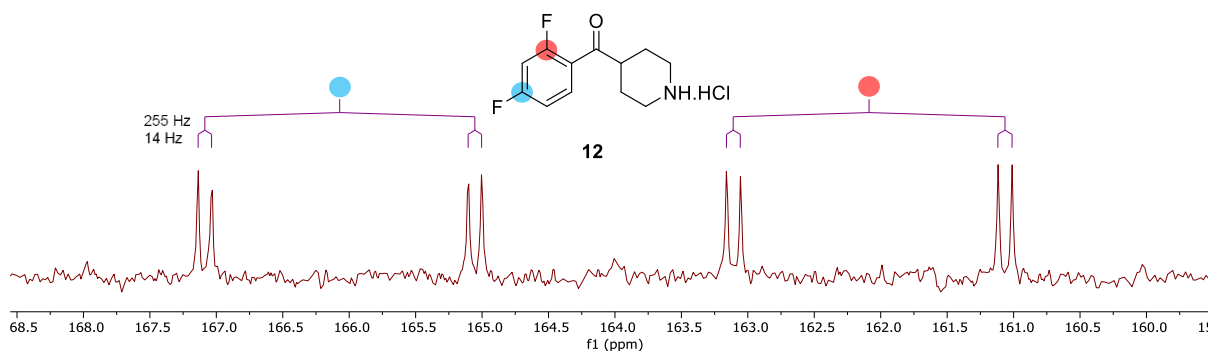
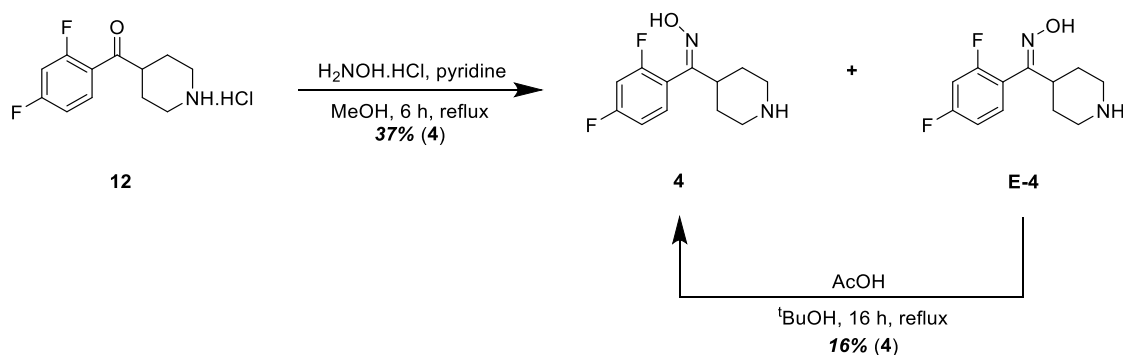


Figure 12. Splitting of ^{13}C peaks caused by fluorine coupling to neighbouring carbons in product **12**.

2.2.3 Oxime Formation

Synthesis of oxime **4** from ketone **12** utilised hydroxylamine hydrochloride with excess pyridine and methanol as solvents (**Scheme 10**). The *Z*-oxime (**4**) was obtained as a mixture with its *E*-isomer (**27**) (0.35:1 *Z*:*E* ratio) based on comparison of the integrals of the aromatic peaks in the ^1H NMR spectrum. This ratio varied but was always in favour of the formation of the *E*-oxime. Recrystallisation from MeOH enabled isolation of the desired *Z*-oxime **4** as white needle-like crystals. The supernatant was treated with acetic acid in *t*-butanol to convert the remaining *E*-isomer to further *Z*-isomer. A 4:1 mixture of *Z*:*E* isomers was found in the crude reaction mixture. The *E*-isomer is essentially unreactive in the subsequent aromatic substitution

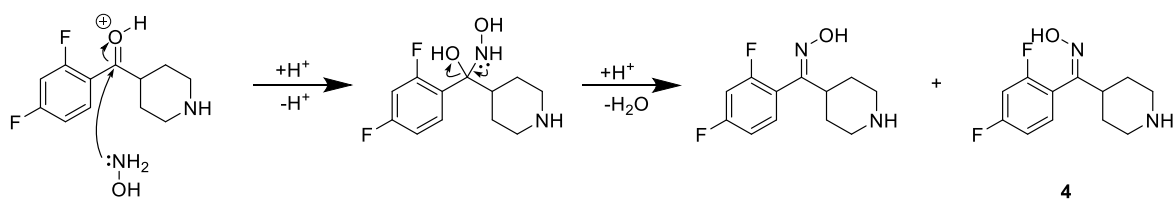
step due to the hydroxyl group being positioned away from the fluorinated carbon. Recycling of the *E*-isomer is desirable synthetically as it maximises the amount of *Z*-isomer obtained, improving the overall yield. This *E* to *Z* conversion reaction was only repeated once as the yield acquired was sufficient for the following steps.



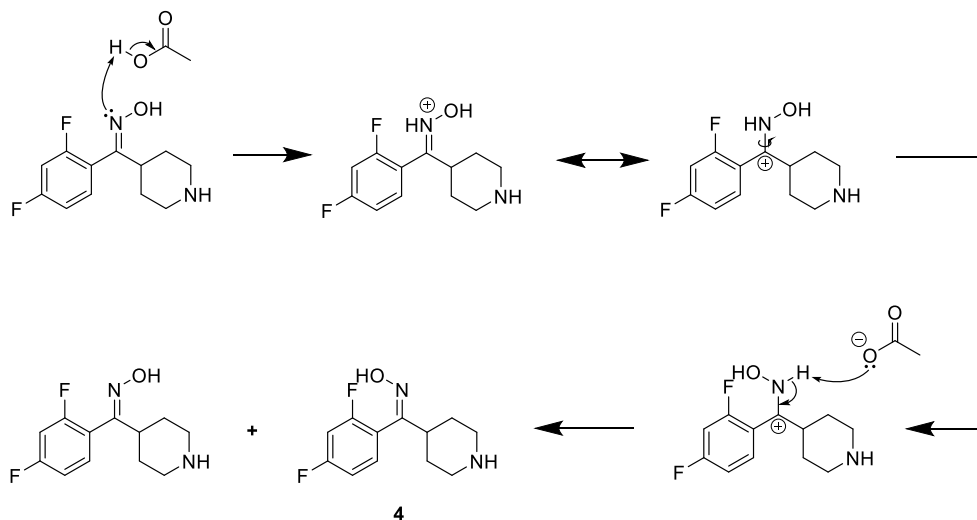
Scheme 10. Synthesis of *Z*-oxime **4**.

The most notable change in the ^1H NMR spectrum upon oxime formation was an upfield shift of the proton of C-8 from 3.62 ppm to 2.91 ppm, likely due to reduction in deshielding with conversion from a ketone to an oxime. The NMR data were consistent with those previously reported.⁹⁷ HRMS also supported this assignment.

Mechanistically, formation of the oxime begins with attack of NH_2OH at the carbonyl (**Scheme 11**). Proton transfer, followed by the loss of water results in the formation of both *E*- and *Z*-isomers, with a preference for the *E*-isomer based on sterics. After separation, treatment of the *E*-isomer with a weak acid causes isomerisation (**Scheme 12**). This proceeds via protonation of the oxime, leading to a resonance structure with a single C-N bond that is rotatable. In this way, rotation about the C-N bond, followed by deprotonation of the amine triggering reformation of the C=N bond, will yield a mixture of *E*- and *Z*-isomers. Preferential formation of the *Z*-oxime under acidic conditions may be as a result of hydrogen bonding to the fluorine, stabilising this conformation before reformation of the C=N bond.



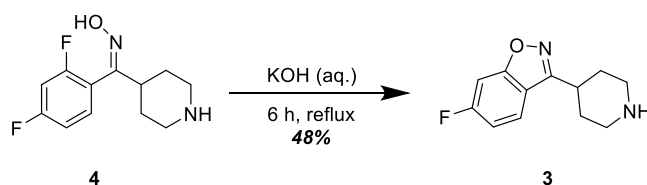
Scheme 11. Proposed mechanism of oxime formation.



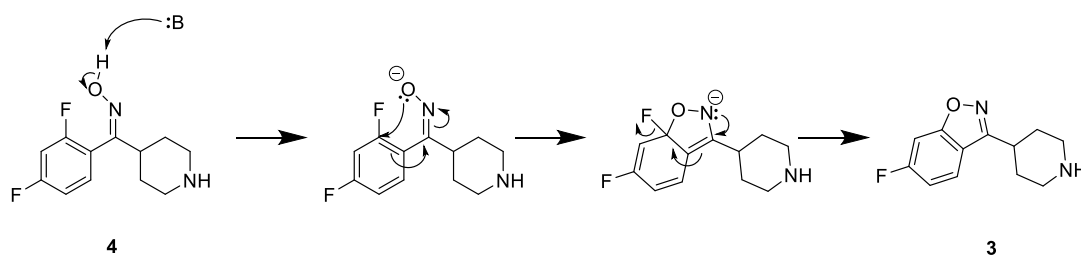
Scheme 12. Proposed mechanism of oxime isomeric conversion.

2.2.4 Benzisoxazole Ring Closing

Completion of the benzisoxazole fragment utilised aqueous KOH to deprotonate the oxime, inducing a nucleophilic aromatic substitution (**Schemes 13 and 14**) Any residual *E*-oxime will likely be unreactive due to the unfavourable orientation of the hydroxyl group.

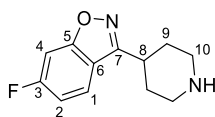


Scheme 13. Synthesis of benzisoxazole **3**.



Scheme 14. Proposed mechanism of benzisoxazole formation.

Benzisoxazole **3** was fully characterised using ^1H , ^{13}C , COSY, HSQC and HMBC NMR spectroscopy as full NMR assignment is not available in the literature (**Table 2**). Structural determination will also aid in characterisation of the final risperidone analogues and help define key HMBC correlations that are required to confirm the final condensation reactions have been successful.



3

Table 2. Tabulated NMR spectroscopic data (500 MHz, CDCl₃) for benzisoxazole **3**.

Position	¹³ C			¹ H			COSY	HMBC
	δ (ppm)	mult.	J _{CF} (Hz)	δ (ppm)	mult.	³ J _{HH} (Hz)		
C-1	122.7	CH	d, 11.1	7.68	dd	8.6, 5.1	2	3, 4, 5, 6, 7
C-2	112.4	CH	d, 25.2	7.04	td	8.9, 2.3	1	3, 4, 5, 6
C-3	164.1	C	d, 250.4	-	-	-	-	-
C-4	97.6	CH	d, 26.8	7.23	dd	8.6, 2.3	-	2, 3, 5, 6
C-5	164.0	C	d, 13.5	-	-	-	-	-
C-6	117.4	C	-	-	-	-	-	-
C-7	161.4	C	-	-	-	-	-	-
C-8	35.1	CH	-	3.19	tt	11.7, 3.7	9a, 9b	7, 9
C-9	31.7	CH ₂	-	a) 2.04	dd	12.9, 3.3	8, 9b	8, 9, 10
				b) 1.93	qd	11.8, 4.0	8, 9a, 10a	8, 9, 10
C-10	46.6	CH ₂	-	a) 3.23	dt	12.4, 3.6	9b, 10b	8, 9, 10
				b) 2.81	td	12.1, 2.8	10b	8, 9, 10

The first peak assigned was the ¹³C shift at 164.1 ppm. This has a large J_{CF}-coupling (250.4 Hz), typical of a fluorinated aromatic carbon,¹¹³⁻¹¹⁴ therefore it was designated as C-3. The aromatic peaks observed in the ¹H NMR spectrum at 7.23 ppm and 7.04 ppm were identified as the protons at positions neighbouring C-3 based on the two-bond J_{CF}-couplings (26.8 Hz and 25.2 Hz, respectively) observed in the ¹³C spectrum. The ¹H shift at 7.23 ppm has no COSY correlations so can be assigned as the proton at C-4. COSY correlations are observed between the ¹H shifts at 7.68 ppm and 7.04 ppm which can be assigned as C-1 and C-2, respectively. The ¹³C shift that represents C-1 has a small J_{CF}-coupling (11.1 Hz), likely due to a three-bond coupling to the fluorine. A similar small J_{CF}-coupling (13.5 Hz) is observed for the ¹³C shift at 164.0 ppm so can be assigned to C-5. The HSQC shows this position is unprotonated, providing further evidence for its assignment.

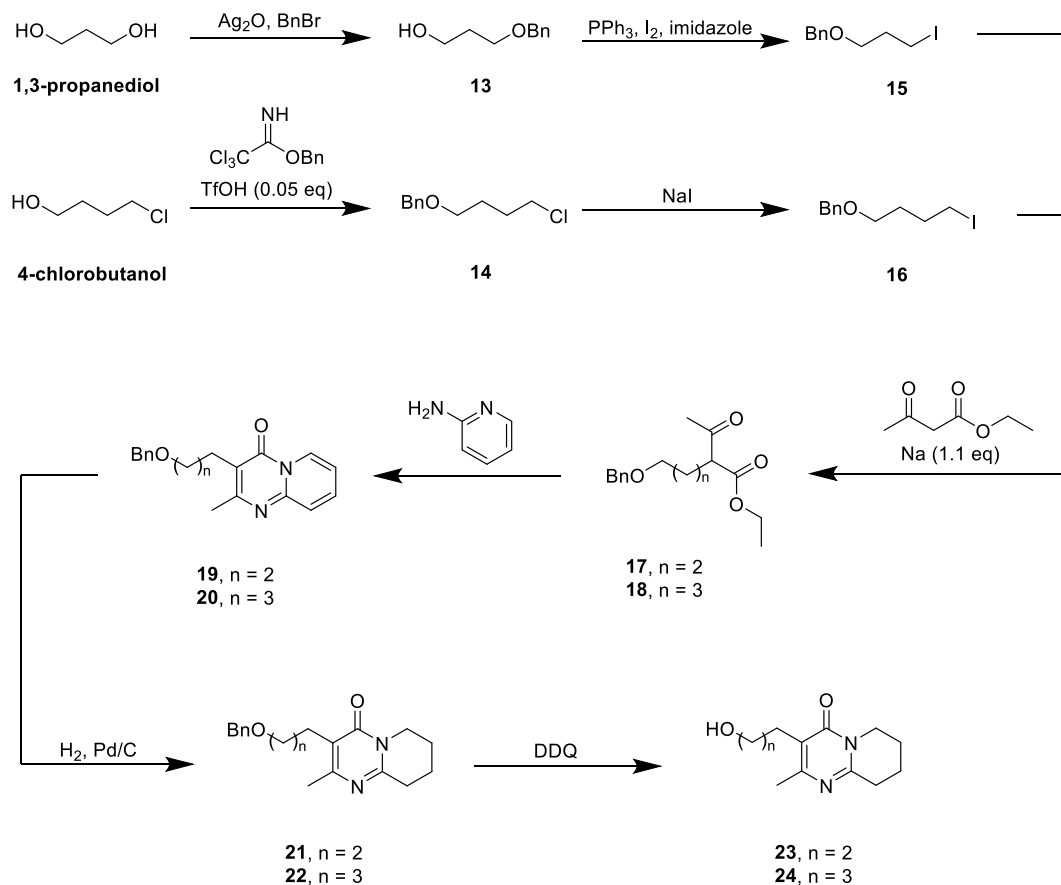
The triplet of triplets at 3.19 ppm in the ^1H NMR spectrum can be assigned to the proton on C-8, as the splitting observed would be caused by separate coupling to the neighbouring axial and equatorial protons. The ^1H shift at 3.19 ppm exhibits HMBC correlations to the ^{13}C shift found at 161.4 ppm. The proton at position C-1 also has an HMBC correlation to this ^{13}C shift. Due to these correlations, this carbon can likely be assigned as C-7. Strong deshielding from the neighbouring nitrogen would also account for the downfield shift observed. The protons of C-1, C-2 and C-4 all exhibit HMBC correlations to the ^{13}C shift at 117.4 ppm. This aromatic shift is found further upfield when compared to carbons C-5 and C-7. As all other aromatic shifts have been assigned, this shift can be assigned to C-6.

The piperidine ring is likely to adopt a low energy chair conformation, resulting in different environments for the axial and equatorial protons at positions C-9 and C-10. This is seen in the HSQC spectrum where the ^{13}C shifts at 46.6 ppm and 31.7 ppm both have two hydrogens bonded, each with distinct environments. The COSY spectrum shows the proton of C-8 to have a correlation to the ^1H shifts at 2.04 ppm and 1.93 ppm, both bound to the ^{13}C methylene at 31.7 ppm. Therefore it can be assigned as C-9. The ^1H shift at 1.93 ppm exhibits a COSY correlation to the protons at 3.23 ppm. The HSQC spectrum shows these protons to be attached to the carbon at 31.7 ppm in the ^{13}C NMR spectrum which can therefore be assigned as C-10. The ^1H shift at 2.81 ppm is assigned as the other proton of the C-10 methylene based on the HSQC spectrum.

2.3 Synthesis of Extended Linker Pyridopyrimidones

Synthesis of the extended linker pyridopyrimidones required the use of two different starting materials, 1,3-propanediol and 4-chlorobutanol, for synthesis of the three- and four-carbon analogues, respectively (**Scheme 15**). Benzyl protection of the alcohol functionality was to be followed by Appel and Finkelstein reactions, respectively, in preparation for alkylation with ethyl acetoacetate. The alkylated ethyl acetoacetates **17** and **18** would then be subjected to condensation reactions with 2-aminopyridine to give unsaturated extended linker coupled pyridopyrimidones **19** and **20**. Pd/C catalysed hydrogenation can then be used to saturate the pyridine ring. As previous work also unsuccessfully attempted to use Pd/C for *O*-debenzylation, an alternative method was required.⁹⁸ DDQ, TiCl_4 and Pd/C catalysed

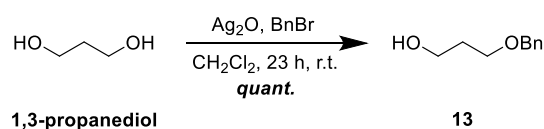
hydrogenolysis under more forcing conditions was planned to be used to facilitate this deprotection as it should be compatible with the functionality of the pyridopyrimidones.



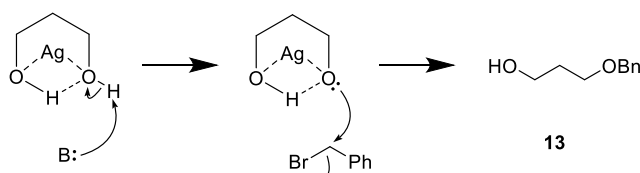
Scheme 15. Proposed synthetic route tetrahydropyridopyrimidones **23** and **24**.

2.3.1 Preparation of the Three-Carbon Alkylated Ethyl Acetoacetate

Synthesis of the three-carbon analogue (**8**) began with monoprotection of 1,3-propanediol using benzyl bromide and Ag_2O as per the methodology employed by Durrant (**Scheme 16**).^{98, 115} Synthesis of **13** was successful with a quantitative yield and high ratio of mono:diprotected product (1:0.07), calculated by comparison of the integrals of the benzylic peaks in the ^1H NMR spectrum. It is proposed that high selectivity for monoprotection is achieved by coordination of the two oxygen atoms with the silver atom (**Scheme 17**).¹¹⁵ Internal hydrogen bonding increases the acidity of only one of the hydroxyl protons, allowing for its deprotonation, thus creating a good nucleophile for attack on benzyl bromide.



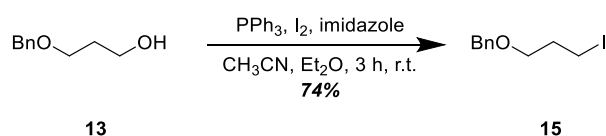
Scheme 16. Benzyl protection of 1,3-propanediol.



Scheme 17. Proposed mechanism of Ag_2O mediated 1,3-propanediol.

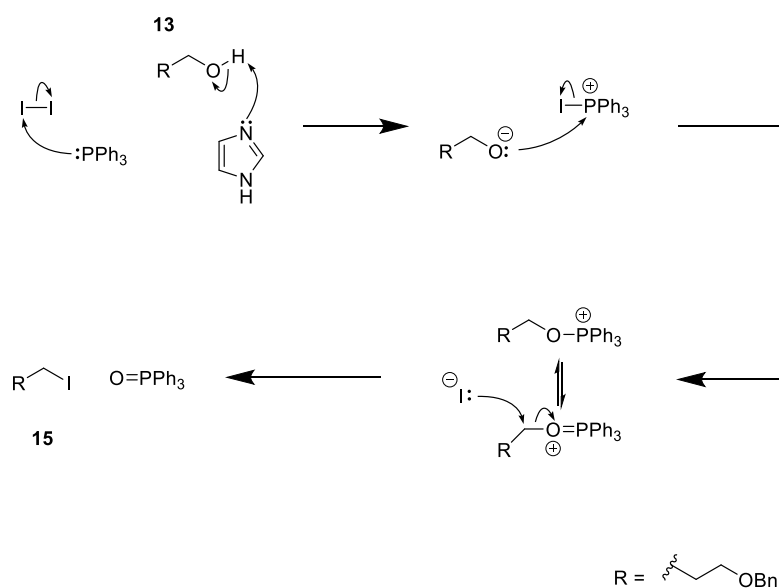
The presence of a benzylic CH_2 singlet at 4.53 ppm in the ^1H NMR spectrum alongside the appearance of a complex multiplet at 7.40-7.27 ppm confirmed the benzyl protection was successful. Shifts in the alkyl chain protons were also consistent with literature data.¹¹⁶ This product was able to be used without further purification as the dual-protected alcohol should be unreactive in the subsequent step.

An Appel reaction was then utilised to convert the protected diol **13** to the iodoalkane **15** in preparation for the following alkylation reaction (**Scheme 18**). Applying the methodology reported separately by Muñoz and Durrant, alcohol **13** was treated with PPh_3 and imidazole in Et_2O .^{98, 117} Subsequent addition of CH_3CN aided in solubilisation of the PPh_3 . Iodine was added at 0°C , then the reaction allowed to warm to room temperature and stir for 6 hours. Following workup, the desired iodide **15** was obtained in a 74% yield and was used without further purification in the subsequent step.



Scheme 18. Appel reaction of **13**.

The Appel reaction begins mechanistically by the attack of PPh_3 on iodine, forming a phosphonium salt while the imidazole is able to deprotonate the alcohol (**Scheme 19**). The resulting alkoxide can then displace the iodine of the phosphonium salt. The free iodide can break the carbon-oxygen bond via an $\text{S}_{\text{N}}2$ reaction, yielding the desired haloalkane product **15**, driven by the favourable formation of a phosphine-oxygen double bond. As this method stated that iodine be added last, the phosphonium salt will only form upon I_2 addition.



Scheme 19. Proposed Appel reaction mechanism.

Analysis of the ^1H NMR spectrum of **15** showed the peak at 3.79 ppm of alcohol **13**, representing the protons neighbouring the unprotected hydroxyl, exhibited an upfield shift to 3.31 ppm in the product due to a reduction in deshielding afforded by the less electronegative iodine. In the ^{13}C NMR spectrum, the shift representing the substituted carbon moves from 62.2 ppm in alcohol **13** to 3.6 ppm in the iodide product **15** (**Figure 13**). These data are consistent with those previously reported.¹¹⁷

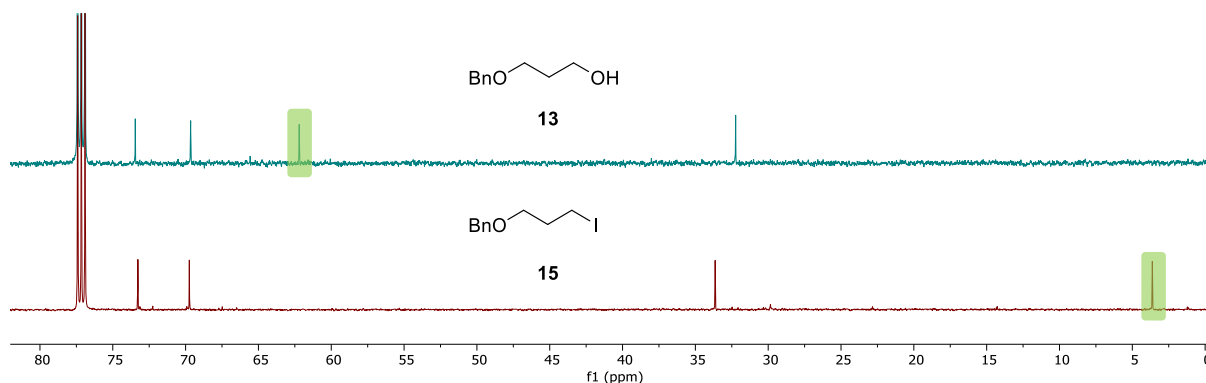
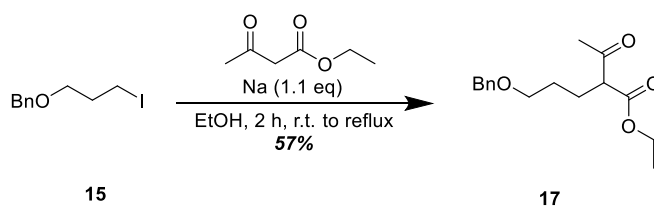


Figure 13. Comparison of ^{13}C NMR spectra of alcohol **13** and iodide **15**. Highlighted in green are the terminal carbon shifts.

Following the methodology reported separately by Hasseroth and Durrant, the substituted ethyl acetoacetate **17** was synthesised from iodoalkane **15** (**Scheme 20**).^{98, 118} This method required addition of freshly cut sodium to anhydrous ethanol. Subsequent refluxing was followed by the addition of ethyl acetoacetate, then iodoalkane **15**. After 2.5 hours the reaction was cooled, filtered through a silica plug twice then purified by column chromatography. A 40:1 CH_2Cl_2 :EtOAc solvent system was employed following the methodology of Durrant.⁹⁸ Compound **17** was isolated with a respectable 57% yield although some co-eluting impurities were found in the ^1H NMR spectrum, attributed to streaking caused by the combination of CH_2Cl_2 as the mobile phase, the stationary phase and compound **17**.



Scheme 20. Alkylation reaction of **15** with ethyl acetoacetate to give **17**.

Mechanistically, the addition of sodium to anhydrous ethanol was required first to form sodium ethoxide. Subsequent addition of ethyl acetoacetate leads to the formation of the enolate via deprotonation at the α -position. Addition of the iodoalkanes allows for nucleophilic attack in an $\text{S}_{\text{N}}2$ type reaction to afford the desired alkylated products.

Formation of the three-carbon alkylated product **17** was confirmed by NMR spectroscopy and HRMS analysis, the data of which were consistent with those previously reported.¹¹⁸ Notably, the appearance of ¹³C shifts at 203.4 ppm and 169.9 ppm was indicative of a ketone and ester, respectively (**Figure 14**). The triplet at 3.31 ppm in the ¹H NMR spectrum in iodoalkane **15** was replaced with a quartet at 1.95 ppm in **17**, indicative of a loss of iodine and the formation of a new covalent C-C bond to a methine. The presence of two methyl peaks in the ¹H NMR spectrum, a singlet at 2.21 ppm and a triplet at 1.26 ppm, provide further evidence that the alkylation was successful. These data are consistent with those previously reported.^{98, 118}

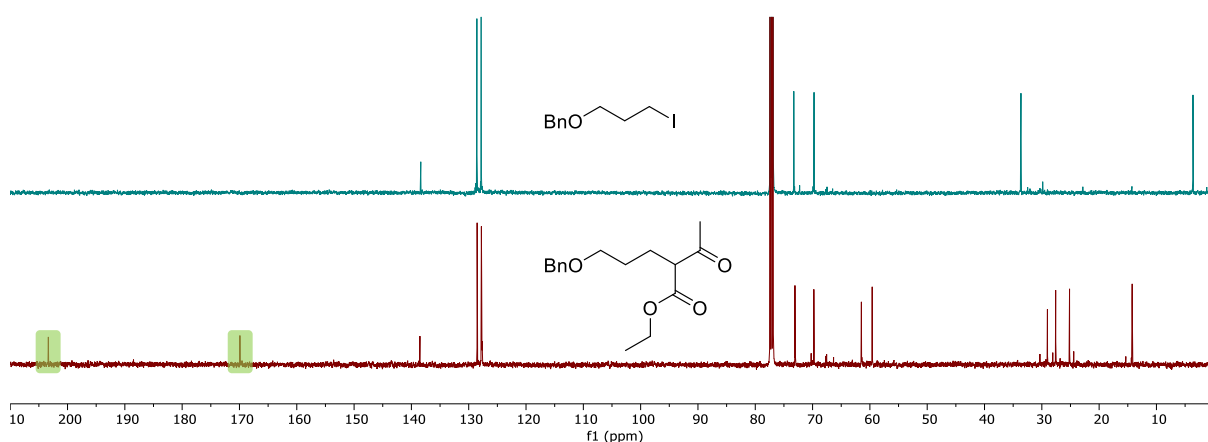
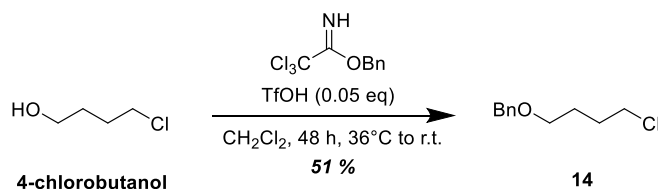


Figure 14. Comparison of ¹³C NMR spectra of iodide **15** and alkylated product **17**. Highlighted in green are shifts indicative of ketone (left) and ester (right) functionalities.

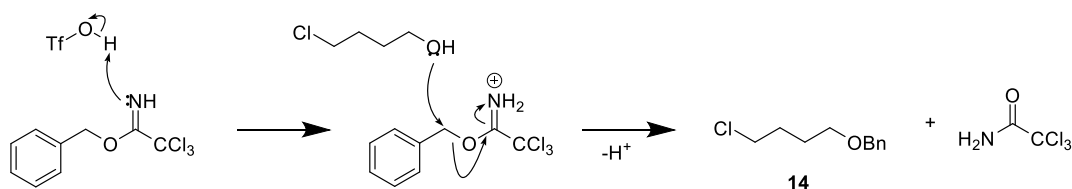
2.3.2 Preparation of the Four-Carbon Alkylated Ethyl Acetoacetate

Due to the unavailability of 1,4-butanediol, 4-chlorobutanol was used and an alternative Bn-protection method was employed for protection of the four-carbon linker analogue. Following Durrant's methodology, the alcohol functionality of 4-chlorobutanol was protected using benzyl trichloroacetimidate and catalytic triflic acid (**Scheme 21**).⁹⁸ A 4:1 ratio of **14**:alcohol was obtained following silica plug filtration of the base-quenched reaction mixture. The product was contaminated with a small amount of residual trichloroacetimidate based on the integration (8H) of the aromatic region of the ¹H NMR spectrum. The presence of the benzyl protecting group was confirmed by the appearance of a benzylic CH₂ singlet at 4.51 ppm in the ¹H NMR spectrum. Shifts in the alkyl chain protons matched those previously reported.¹¹⁹ This

process likely begins mechanistically with protonation of the imine, giving an electrophilic cation (**Scheme 22**). This charged species will readily react with the alcohol, yielding a benzyl ether (**14**) and trichloroacetamide as a byproduct.

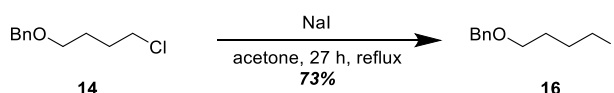


Scheme 21. Benzyl protection of 4-chlorobutanol.



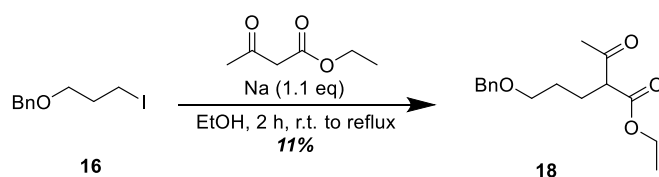
Scheme 22. Proposed mechanism of benzyl protection of 4-chlorobutanol.

A Finkelstein reaction was then employed for halide substitution of **14** in anticipation of the subsequent alkylation step as the iodine is a superior leaving group to chlorine (**Scheme 23**). Compound **14** was taken up in dry acetone with NaI and refluxed for 27 hours to provide the desired iodoalkane **16** as an orange oil. Similar to the synthesis of **15**, an upfield shift in the protons attached to the halogen bonded carbon was observed in the ^1H NMR spectrum, from 3.57 ppm in chloroalkane **14** to 3.21 ppm in the iodide product **16**. This change was again expected due to the reduced deshielding afforded by the less electronegative iodine. These data are consistent with those previously reported.¹¹⁹



Scheme 23. Finkelstein reaction of **14**.

The methodology utilised for the synthesis of **17** was applied to the synthesis of the four-carbon linked ethyl acetoacetate **18** (**Scheme 24**). Chromatographic isolation of the four-carbon product **18** employed 9:1 hexanes:EtOAc which proved to be more successful in separation of a pure product. Despite a crude yield of 80%, a disappointing 11% yield was achieved following purification. Surprisingly, after several hours under high vacuum, a large portion of **18** was lost with no change in the intensity of the yellow colour of the oil. This loss of volume could be attributed to possible volatility of the product.



Scheme 24. Alkylation reaction of ethyl acetoacetate to give **18**.

The four-carbon alkylated product **18** was first synthesised by Durrant but full structural assignment remained ambiguous.⁹⁸ Therefore the structure of **18** was fully assigned based on the NMR data as follows. These data are also available in **Table 3** alongside the numbering system used for position assignments.

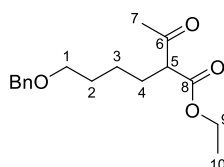


Table 3. Tabulated NMR spectroscopic data (500 MHz, CDCl₃) for alkylation product **18**.

Position	¹³ C		¹ H			COSY	HMBC
	δ (ppm)	mult.	δ (ppm)	mult.	³ J _{HH} (Hz)		
C-1	70.0	CH ₂	3.46	t	6.4	2	2, 3, PhCH ₂
C-2	29.6	CH ₂	1.63	m	-	1, 3	1, 3, 4
C-3	24.3	CH ₂	1.38	m	-	2, 4	4, 10
C-4	28.1	CH ₂	1.86	m	-	3, 5 (weak)	2, 3, 5, 6, 8
C-5	60.0	CH	3.40	t	7.4	4	3, 4, 6, 8
C-6	203.4	C	-	-	-	-	-
C-7	28.9	CH ₃	2.21	s	-	-	5, 6
C-8	169.9	C	-	-	-	-	-
C-9	61.4	CH ₂	4.19	qd	7.1, 0.9	10	8, 10
C-10	14.2	CH ₃	1.26	t	7.1	9	9
Ar	138.6	C	-	-	-	-	-
Ar	128.5	CH	7.36-7.26	m	-	Ar	Ar
Ar	127.8	CH	7.36-7.26	m	-	Ar	Ar
Ar	127.7	CH	7.36-7.26	m	-	Ar	Ar
PhCH ₂	73.0	CH ₂	4.48	s	-	-	1, Ar

The COSY spectrum confirms a four-carbon chain with methylene peaks found at 3.46 ppm, 1.86 ppm, 1.63 ppm and 1.38 ppm in the ¹H NMR spectrum (**Figure 15**). The triplet at 3.46 ppm in the ¹H NMR spectrum is likely at position C-1 due the increased deshielding of the neighbouring oxygen atom and splitting caused by coupling to the two protons at C-2. The ¹H shift at 1.63 ppm exhibits COSY correlations to the protons at C-1 and the shift at 1.38 ppm. This would place these shifts at positions C-2 and C-3, respectively. The protons at C-3 also have a COSY correlation to methylene protons at 1.86 ppm in the ¹H NMR spectrum, therefore assigning it at C-4. The C-4 protons have a COSY correlation to a single proton at 3.40 ppm in the ¹H NMR spectrum, placing it at C-5 and the internal end of the chain. The ¹H NMR

spectrum shows two methyl groups present at 2.21 ppm, as a singlet, and 1.26 ppm, as a triplet. Based on these multiplicities, they can be assigned to C-7 and C-10, respectively. The protons of C-10 also exhibit a COSY correlation to two protons at 4.19 ppm in the ^1H NMR spectrum which can be assigned to C-9. The two most downfield shifts in the ^{13}C NMR spectrum at 203.4 ppm and 169.9 ppm are typical of a ketone and an ester, respectively. An HMBC correlation from the protons of C-9 to the ^{13}C peak at 169.9 ppm allows it to be assigned as C-8. Therefore, the ^{13}C peak at 203.4 ppm must be the carbonyl at C-6. The methyl of C-7 also has a strong HMBC correlation to C-6, providing further evidence for this assignment. The CH_2 singlet at 4.48 ppm in the ^1H NMR spectrum is typical of benzylic protons and also exhibits a three-bond HMBC correlation to C-1, confirming the benzyl protecting group remained intact. A complex multiplet integrating for five protons in the aromatic region provide further evidence for this assignment.

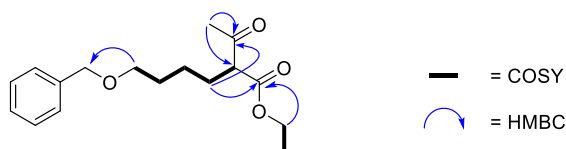


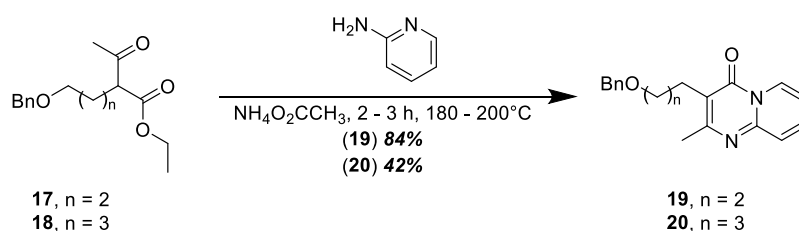
Figure 15. Key COSY and HMBC correlations of **18**.

2.3.3 Condensation of **17** and **18** with 2-aminopyridine

Prior work by Durrant found that methodology for condensation of a linker with 2-aminopyridine in the synthesis of risperidone was not transferable to condensation reactions with the alkylated ethyl acetoacetates **17** and **18**.⁹⁸ Durrant trialed a range of reaction conditions and reagents, ultimately finding ammonium acetate to be an effective reagent for the reaction that was performed neat (**Table 4**). This method proved to be very simple and reproducible (**Scheme 25**).

Table 4. Reaction conditions investigated by Durrant toward the condensation of **17** and 2-aminopyridine to form **19**.⁹⁸

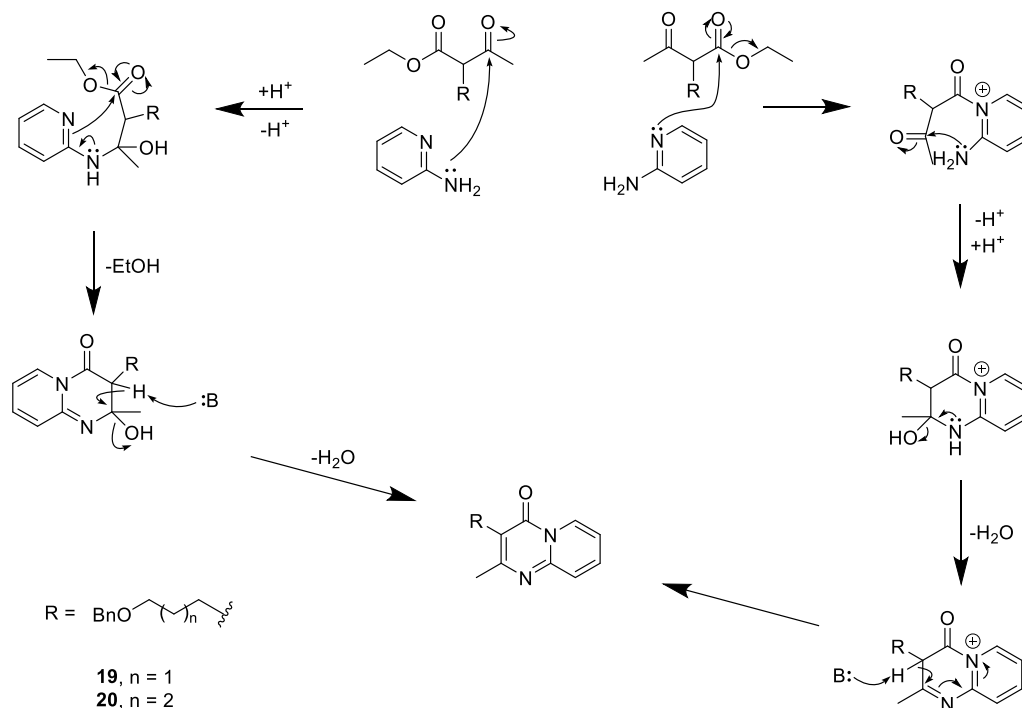
Entry	Method	Time	Temp. °C	Outcome (Yield)
1	P ₂ O ₅	Overnight	160	17
2	<i>p</i> -TsOH / Toluene	48 Hrs	Reflux	17 and 19
3	P ₂ O ₅	Overnight	170	By-product and 17
4	<i>p</i> -TsOH / Xylene	Overnight	Reflux	17 and 19
5	NH ₄ O ₂ CCH ₃	2 Hrs	120	17
6	H ₃ PO ₄ 85%	4 Hrs	120	17
7	H ₃ PO ₄ 100%	4 Hrs	120	17
8	<i>p</i> -TsOH / Xylene	Overnight	Reflux	19 (57%)
9	P ₂ O ₅	Overnight	180	By-product and 17
10	NH ₄ O ₂ CCH ₃	Overnight	180	19 (85%)
11	NH ₄ O ₂ CCH ₃	3.5 Hrs	180	19 (74%)
12	<i>p</i> -TsOH / Xylene	Overnight	Reflux	19 (42%)
13	NH ₄ O ₂ CCH ₃	2.5 Hrs	250	19 (63%)



Scheme 25. Condensation of 2-aminopyridine with **17** and **18**.

Synthesis of the three-carbon pyridopyrimidone **19** using this method was simple, time-efficient and high yielding, affording a product without additional purification steps required. A plausible mechanism for formation of pyridopyrimidones **19** and **20** begins with attack of the primary amine at the carbonyl (**Scheme 26**). Subsequent formation of an imine leads to cyclisation by nucleophilic attack, resulting in the loss of ethanol. Deprotonation at the α -position causes aromatisation via the loss of water, yielding **19** and **20**. Alternatively, this process may begin with attack of the pyridine at the carbonyl of the ester, leading to a

favourable loss of ethanol. Cyclisation by nucleophilic attack of the amine at the carbonyl, followed by proton transfer results in the loss of water and the formation of an imine. Aromatisation can then proceed to afford the desired product. It is also possible that imine formation could proceed first, followed by formation of the α,β -unsaturated ketone and again, the desired product attained after cyclisation.



Scheme 26. Possible mechanisms of the condensation of **17** and **18** with 2-aminopyridine.

Small and impure samples of these condensation products were found to have unusual NMR behaviour, possibly due to the pH of the sample or salt impurities present. Following workup of the condensation reaction, the ^1H NMR spectrum of the crude product showed only one of the four pyridine ring protons to be fully resolved while the three remaining pyridine ring protons were not observed as distinct peaks (**Figure 16**). The shifts representing the alkyl chain and methyl group were present in their expected positions. Nonetheless, HRMS analysis showed the desired product **19** to be present, prompting chromatographic purification.

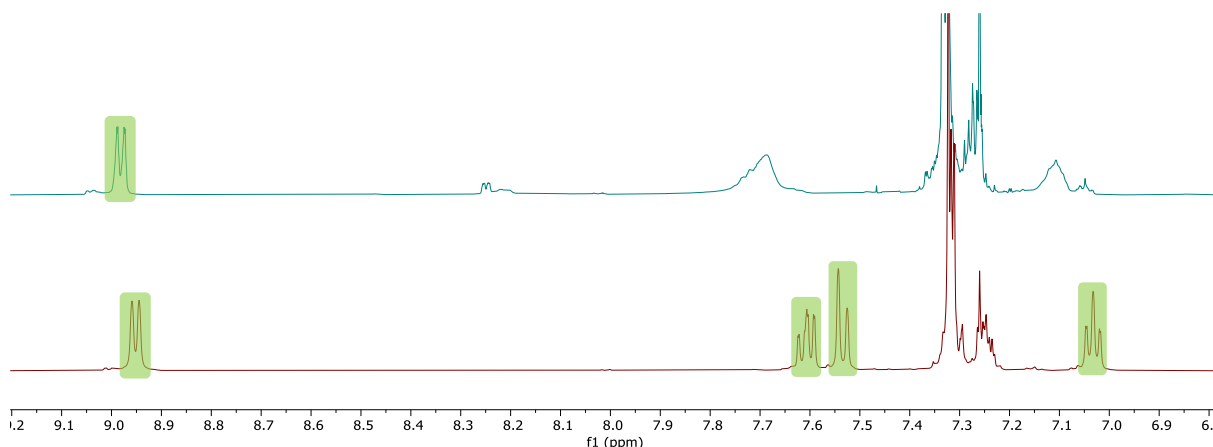


Figure 16. Comparison of ^1H NMR spectra of 2-aminopyridine condensation crude reaction mixture (top) and purified (bottom) **19**. Pyridine ring shifts are highlighted in green

TLC analysis of the crude product showed a distinctly bright purple spot under 254 nm UV light, a likely property of the product **19** due to its extensive conjugation. This spot was quite broad in 9:1 EtOAc:acetone, therefore 0.5% triethylamine was added to the solvent system, giving a more compact band. Purification by flash chromatography employing the aforementioned solvent system yielded **19** with NMR spectroscopic data that agreed with those previously reported.⁹⁸ This time a larger sample (>10 mg) was submitted for ^1H NMR analysis and all of the expected peaks were clearly resolved. This suggests that accurate NMR analysis of these pyridopyrimidones is sensitive to concentration or purity. Full structural assignment of **19** and **20** was ambiguous in the literature.⁹⁸ Therefore, the structure of **19** was fully assigned based on the NMR spectroscopic data in **Table 5**.

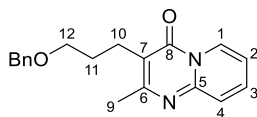


Table 5. Tabulated NMR spectroscopic data (500 MHz, CDCl₃) for pyridopyrimidone **19**.

Position	¹³ C		¹ H		³ J _{HH} (Hz)	COSY	HMBC
	δ (ppm)	mult.	δ (ppm)	mult.			
C-1	127.1	CH	8.95	d	7.0	2	2, 3, 5, 8
C-2	114.8	CH	7.03	t	6.8	1, 3	1, 4
C-3	134.9	CH	7.61	ddd	9.0, 6.5, 1.4	2, 4	1, 5
C-4	125.7	CH	7.53	d	8.8	3	2, 5
C-5	148.5	C	-	-	-	-	-
C-6	161.5	C	-	-	-	-	-
C-7	115.7	C	-	-	-	-	-
C-8	158.0	C	-	-	-	-	-
C-9	22.4	CH ₃	2.51	s	-	-	6, 7
C-10	23.7	CH ₂	2.81	t	7.5	10	6, 7, 8, 11, 12
C-11	28.4	CH ₂	1.91	m		11, 12	7, 10, 12
C-12	70.0	CH ₂	3.55	t	6.3	11	10, 11, PhCH ₂
Ar	138.7	C	-	-	-	-	-
Ar	128.4	CH	7.35-7.22	m	-	Ar	Ar
Ar	127.7	CH	7.35-7.22	m	-	Ar	Ar
Ar	127.6	CH	7.35-7.22	m	-	Ar	Ar
PhCH ₂	72.9	CH ₂	4.50	s	-	-	12, Ar

Two pathways of COSY correlations are found, one for three shifts representing the alkyl chain, which is consistent with the starting material **17**, and the other connecting four protons that would be present in the pyrimidine ring.

The aromatic protons found at 8.95 ppm, 7.03 ppm, 7.61 ppm and 7.53 ppm in the ¹H NMR are likely the protons of the pyrimidine based their downfield shifts and COSY correlations. The doublet at 8.95 ppm in the ¹H NMR is likely at position C-1 as it experiences strong deshielding from the neighbouring aromatic nitrogen and has only one COSY correlation. The

^1H shift at 7.03 ppm has a COSY correlation to the proton at C-1 as well as the proton found at 7.61 ppm, placing these shifts at C-2 and C-3, respectively. The proton of C-3 also has a COSY correlation to the doublet found at 7.53 ppm in the ^1H NMR which would place this shift at C-4.

HMBC correlations from the protons of C-1, C-3 and C-4 are observed to the ^{13}C shift at 148.5 ppm, providing evidence for its assignment as C-5. No HMBC evidence is observed for the proton of C-2 to C-5, which is not unexpected as a four-bond correlation is less likely.

The methyl singlet at 2.51 ppm in the ^1H NMR has no COSY correlations, therefore must be C-9. HMBC correlations from the protons of C-9 to ^{13}C shifts at 161.5 ppm and 115.7 ppm are likely three and two-bond correlations, respectively. The more downfield shift is likely C-6 which means the ^{13}C shift at 115.7 ppm is likely C-7. The protons of C-10 and C-11 also make three and two-bond HMBC correlations, respectively, to C-7, providing further evidence for its assignment. HMBC correlations are observed from the protons of C-10 to the ^{13}C shift at 158.0 ppm, assigning it as the carbonyl at C-8. A weak HMBC correlation is found from the protons of C-1 to this proposed carbonyl position, providing further evidence for its assignment.

Similar signals were observed for the four-carbon linked pyridopyrimidone **20** and thus the assignments were made accordingly (**Figure 17**). The main point of difference was two upfield multiplets in the ^1H NMR spectrum at 1.75 ppm and 1.67 ppm assigned to C-12 and C-11, respectively, based on COSY correlations through the alkyl chain.

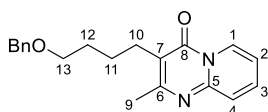


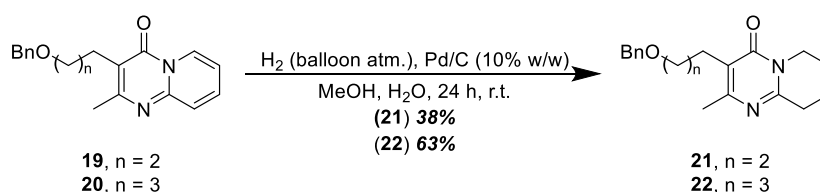
Figure 17. Numbered carbon environments for pyridopyrimidone **20**.

2.3.4 Pd/C Catalysed Hydrogenation of Pyridopyrimidones **19** and **20**

Pd/C catalysed hydrogenation of heterocyclic substrates is a well studied area of medicinal chemistry due to the importance of these structures as pharmacophores.¹²⁰⁻¹²¹ Hydrogenation of pyridine-based rings is possible under mild conditions.¹²² Selective hydrogenation of

quinolones is achievable with the use of more specialised Pd/C-based catalyst supports.¹²³ The use of catalytic Pd/C under a hydrogen atmosphere can also be utilized for hydrogenative *O*-debenzylation in the synthesis of hydrogenated pyridopyrimidines.¹²⁴ Extensive literature searches found the only application of Pd/C catalysed hydrogenation on a pyridopyrimidone system was in the commercial synthesis of risperidone.¹²⁵ This patent describes it to be a resource efficient and high yielding process forgoing the use of organic solvents.

Hydrogenation of the pyridine ring of **19** and **20** was required before deprotection. Prior work by Durrant planned to use Pd/C catalysed hydrogenation to obtain hydrogenated and deprotected pyridopyrimidones **23** and **24** in one step.⁹⁸ Unfortunately, this method only yielded hydrogenated products. These reactions required a Fischer-Porter vessel, allowing for high pressures (5 atm.) and relatively fast reaction times (24 hours). Regrettably, this apparatus was unavailable so a Schlenk tube with a hydrogen balloon attached was used in its place when first trialled on **19** (**Scheme 27**). This set up did not facilitate high pressures so a longer reaction time was expected, with periodic refilling of the H₂ balloon required. After four days, TLC analysis showed a small amount of **19** remained and the formation of a slightly more polar, less UV active species. A reduction in UV activity was expected due to the reduction in conjugation of the anticipated product. Careful chromatography allowed for isolation of the required hydrogenated pyridopyrimidone **21**. This procedure was repeated for hydrogenation of the four-carbon pyridopyrimidone **22**, with similar observations of reduced polarity and UV activity upon TLC analysis.



Scheme 27. Hydrogenation of **19** and **20**.

Structural elucidation of **21** utilised 2D NMR spectroscopic data for assignment of all ¹³C and ¹H shifts. The ¹H NMR spectrum showed a large upfield shift for the protons at positions C-1 to C-4, from > 7 ppm in **19** to 3.90 ppm, 1.94 ppm, 1.84 ppm and 2.86 ppm, respectively. These

assignments are supported by the COSY and HSQC spectra. This change is expected to be an effect of the reduced conjugation of the system.

Interestingly, the relative ^{13}C shifts of C-6 and C-8 appear to switch (**Figure 18**). In the HMBC spectrum of **19**, the proton of C-1 has a three-bond correlation to C-8 and the protons of C-9 exhibit a two-bond correlation to C-6. Evidence in the HMBC spectrum of **21** suggests that C-6 experiences a slight upfield shift to 158.1 ppm while C-8 shifts downfield to 162.7 ppm in the ^{13}C NMR spectrum. In the HMBC spectrum of **21**, C-1 no longer has an HMBC correlation to C-8 while C-9 maintains its two-bond correlation to C-6 (**Figure 19**). C-10 maintains its HMBC correlation to C-8, confirming these assignments.

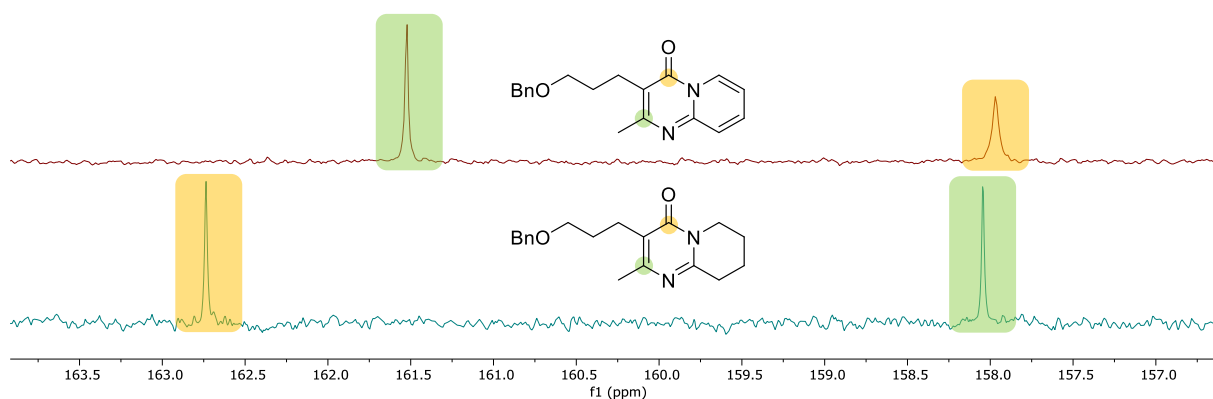


Figure 18. Comparison of ^{13}C shifts of C-6 and C-8 in **19** (top) and **21** (bottom).

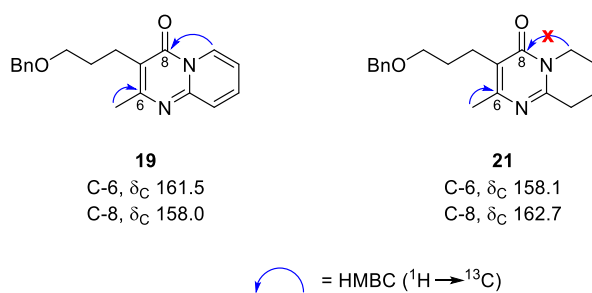


Figure 19. Comparison of ^{13}C shifts of C-6 and C-8 in **19** and **21**.

A study of non-alkylated pyridopyrimidones found that in unsaturated pyridopyrimidones like **19**, the imine carbon (C-6) will have the furthest downfield ^{13}C shift, followed by the amide

carbon.¹²⁶ The structural assignment of non-alkylated pyridopyrimidones remains ambiguous in the literature.¹²⁷⁻¹²⁸ It is postulated the changes in chemical shifts observed in the ¹³C NMR spectrum of **21** are caused by a resonance effect as the unsaturated pyridopyrimidone can exist in three resonance structures due to the extensive conjugation of the system (**Figure 20**). In a saturated substrate, such as **21**, the electrons will be more localised as the system is less conjugated. The carbonyl carbon will be more deshielded than the imine as a result, causing the observed “switch” of chemical shifts.

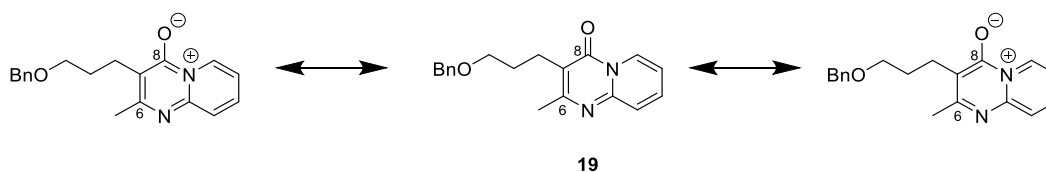


Figure 20. Possible resonance structures of **19**.

Repetition of the hydrogenation of **19** employed different equipment due to the unavailability of the Schlenk tube at the time. A wider 50 mL round bottom flask with a hydrogen balloon attached was used instead (**Figure 21**). Compared to the Schlenk tube, the volume of the reaction mixture relative to the size of the flask was much smaller. It was expected that vigorous stirring would increase the surface area of the reaction mixture, allowing for more efficient incorporation of H₂ gas into solution. After five days, TLC analysis showed the presence of the expected hydrogenated species, as well as a much more polar species ($R_f = 0.1$, 5:1 EtOAc:acetone) only visible under 254 nm UV light. Purification of this mixture yielded the hydrogenated product **21** (12%), as well as the hydrogenated and debenzylated pyridopyrimidone **23** (56%). (**Figure 22**). NMR analysis showed **21** to be lacking the characteristic CH₂ peak at ~ 4.5 ppm in the ¹H NMR spectrum as well as the complex multiplet at ~ 7.3 ppm found in previous Bn-protected pyridopyrimidones. Slight shifts were observed for peaks in the alkyl chain which was confirmed to remain intact by COSY correlations. Connectivity to the pyridopyrimidone was verified by HMBC correlations similar to those previously discussed. HRMS confirmed the presence of the deprotected tetrahydropyridopyrimidone **23**.

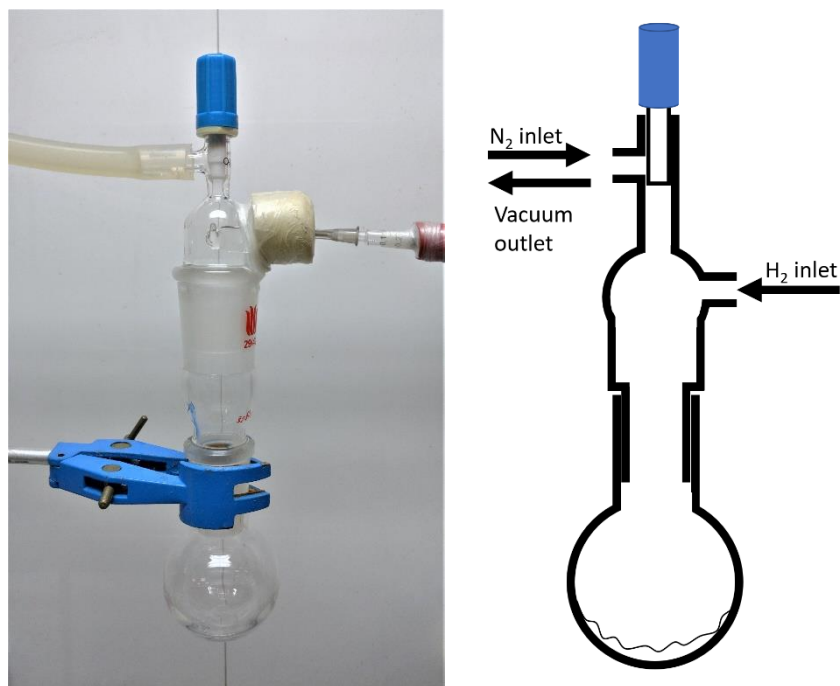


Figure 21. Photo (left) and schematic (right) of apparatus used for second hydrogenation attempt.

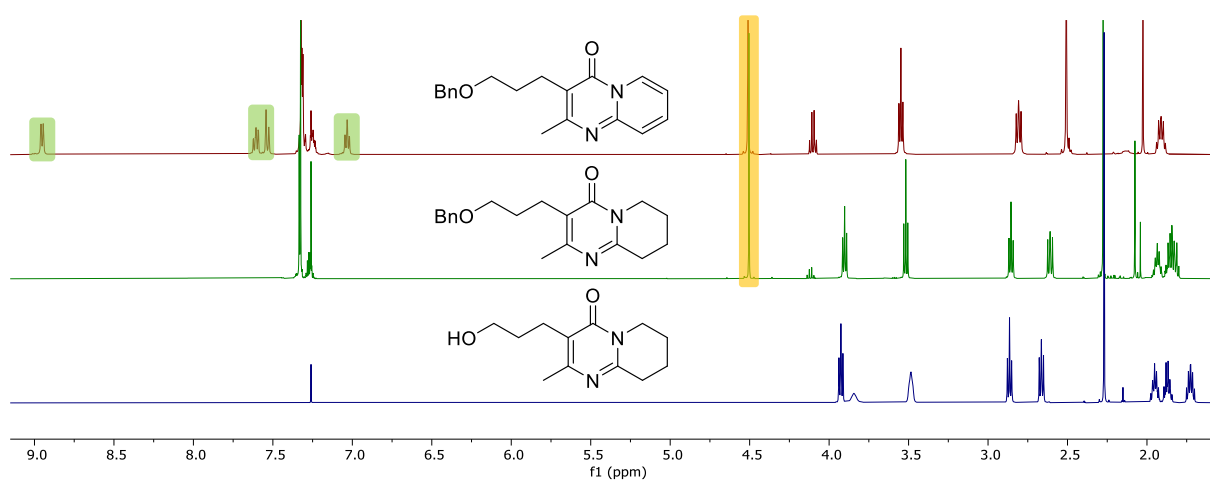
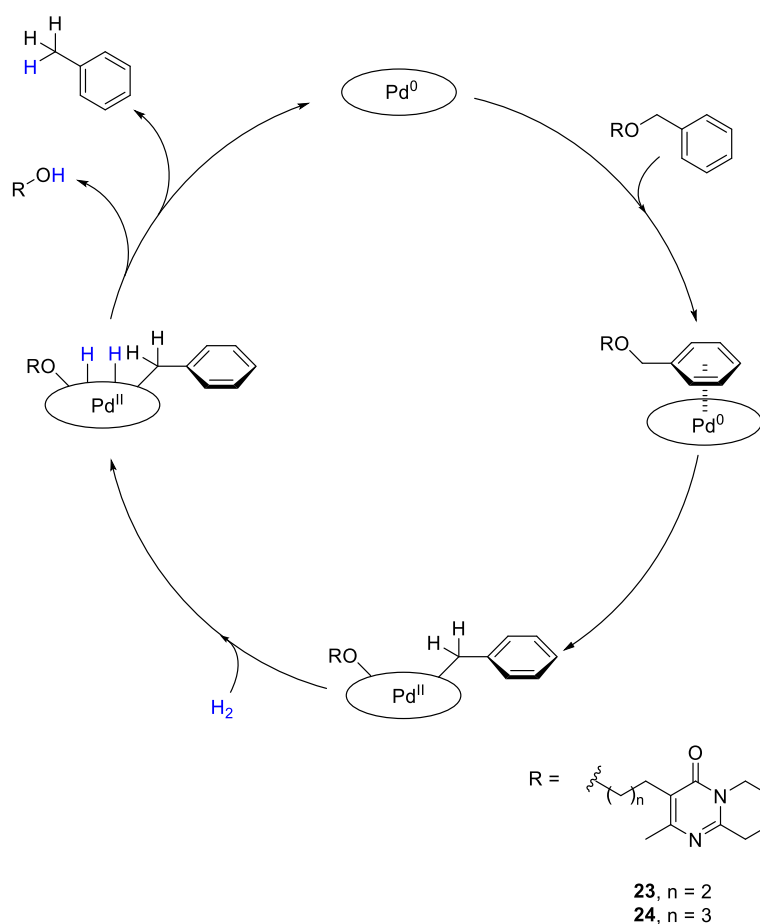


Figure 22. Comparison of ¹H NMR spectra of **19** (top), tetrahydropyridopyrimidone **21** (middle) and deprotected tetrahydropyrimidone **23** (bottom). Highlighted are unsaturated pyridine shifts (green) and benzylic shifts (yellow).

This result was surprising as Durrant's experiments with higher H₂ pressures did not yield any deprotected product.⁹⁸ Interestingly, benzyl ether hydrogenolysis using Pd/C can be inhibited

in the presence of added ammonia, ammonium acetate or pyridine.¹²⁹ However, It is unlikely that ammonium acetate is the reason for the lack of deprotection observed by Durrant as any residual ammonium acetate would have been removed during the aqueous workup of the previous step.

Mechanistically it is expected that the palladium catalysed hydrogenative debenzylolation occurred via a catalytic cycle beginning with the aromatic ring π -stacking with the palladium catalyst (**Scheme 28**). Pd^0 then inserts into the C-O bond. Addition of H_2 gas to the system allows for hydrogen transfer, releasing the debenzylated alcohol and toluene as a byproduct, thus reducing Pd^{II} and resetting the cycle.



Scheme 28. Mechanism of palladium catalysed hydrogenative *O*-debenzylolation.

2.4 Debenzylation Attempts

An efficient route for *O*-debenzylation was required for synthesis of the two analogues. Early work by Durrant found that deprotection by means of catalytic hydrogenation was a dead end despite multiple attempts.⁹⁸ However, hydrogenation of **19** in the current research found that the use of a larger reaction flask caused partial deprotection and afforded a mixture of **21** and **23**. Unfortunately, the deprotection was slow and did not go to completion after five days, therefore a more efficient route was sought. Deprotections of **19** and **22** with DDQ and TiCl₄ were attempted. These substrates were chosen because large stocks were available thanks to prior work by Durrant.⁹⁸ This allowed for multiple small scale deprotection attempts without the pressure of limited material. Tests on substrates with varying conjugation and different alkyl chain lengths could also establish if the order of hydrogenation, then deprotection was strictly required.

2.4.1 DDQ-mediated Deprotection Attempts

DDQ was trialled first for debenzylation of **19**. While DDQ is known to be an effective agent for oxidative cleavage of the more labile *p*-methoxybenzyl (PMB) and *p*-methylbenzyl (MBn) protecting groups,¹³⁰⁻¹³² DDQ-mediated *O*-debenzylation is often slower.^{107, 133} The first deprotection attempt on **19** using 3 equivalents of DDQ was difficult to monitor by TLC due to the apparent formation of multiple byproducts. ¹H NMR analysis of the crude reaction mixture after 24 hours indicated only approximately 1:12 conversion based on the integration of the new benzaldehyde peak at 10.03 ppm, relative to the existing benzylic shift at 4.51 ppm. The appearance of shifted peaks with a similar splitting pattern to **19** suggested that DDQ was effective for *O*-debenzylation, albeit rather slowly.

This prompted another attempt, increasing the amount of DDQ to 20 equivalents. The solubility of DDQ was poor so it is unlikely the total quantity was dissolved in the reaction. ¹H NMR analysis after 24 hours showed an increase in benzaldehyde formation. The appearance of a triplet at 2.87 ppm suggested transformation of **19** into a new species. Gradient flash chromatography (5:1 EtOAc:acetone then 1:1 EtOAc:acetone) was employed, yielding **19** (4 mg, 15%) as well as another far more polar product (1 mg). The ¹H NMR spectrum of this polar species showed an apparently debenzylated product that was lacking the characteristic benzylic peak at 4.51 ppm and the complex multiplet in the aromatic region. Surprisingly, only

one of the protons (C-1) of the pyridine ring was observable (**Figure 23**). 2D NMR confirmed this observation as no COSY correlations were found in this region. These shifts should be retained in the product, suggesting that while deprotecting **19**, DDQ was also interacting with the substrate in an undesired way and causing degradation.

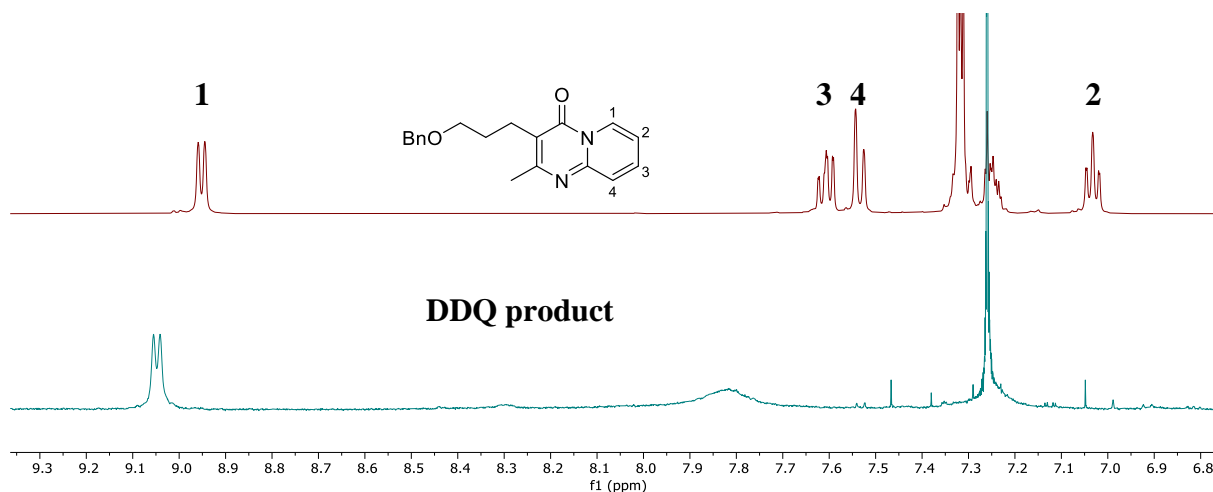


Figure 23. Stacked ¹H NMR of protected alcohol **19** (top) and unknown DDQ-mediated deprotection product (bottom).

These results demonstrate that DDQ was unlikely to be suitable for debenzylolation of the pyridopyrimidone substrates. Long reaction times resulted in only partial deprotection, as well as formation of unidentifiable byproducts. Therefore, other methods of debenzylolation were investigated.

2.4.2 TiCl₄-mediated Deprotection Attempts

Attention was then turned toward the use of TiCl₄ as an alternative method of deprotection. TiCl₄ is known to rapidly debenzylate benzyl ethers, making it an appealing alternative to DDQ.¹³⁴ TiCl₄-mediated debenzylolation has been used in the total synthesis of monocillin VII, a macrolactone containing a ketone and a pyran ring.¹³⁵ Treatment with 10 equivalents of TiCl₄ provided the expected product in an impressive 89% yield. Within the research group, TiCl₄ was used for debenzylolation in the final steps of syntheses of TAN-2483B analogues.¹³⁶ These highly functionalised compounds were isolated in yields of 56 – 72% following ten minute

reaction times. Interestingly, in the synthesis of leucascandrolide A, TiCl_4 was successfully used to facilitate allylation of an intermediate compound without deprotection of a benzyl ether.¹³⁷ Unfortunately, no literature was available on the reactivity of pyridopyrimidones in the presence of TiCl_4 .

The first use of TiCl_4 to debenzylate **19** using 5 equivalents of TiCl_4 was difficult to monitor by TLC as the acid continued to react on the silica. Following aqueous workup, TLC analysis of the crude reaction mixture showed a broad, 254 nm UV active species at $R_f = 0.22$ (1:1 EtOAc:acetone), which was subsequently separated by column chromatography. Initial ^1H NMR analysis of one isolated fraction showed only one of the pyridine protons to be present, similar to what was found with the DDQ debenzylation attempt. Upon combination of all fractions containing the same pure compound, all of the expected proton shifts were present, signifying successful deprotection (**Figure 24**). This suggested that accurate NMR analysis of **27** is sensitive to concentration. Consequently, it also suggests the previous deprotection using DDQ may have been successful, but due to the small quantity isolated (1 mg), accurate NMR analysis was not possible.

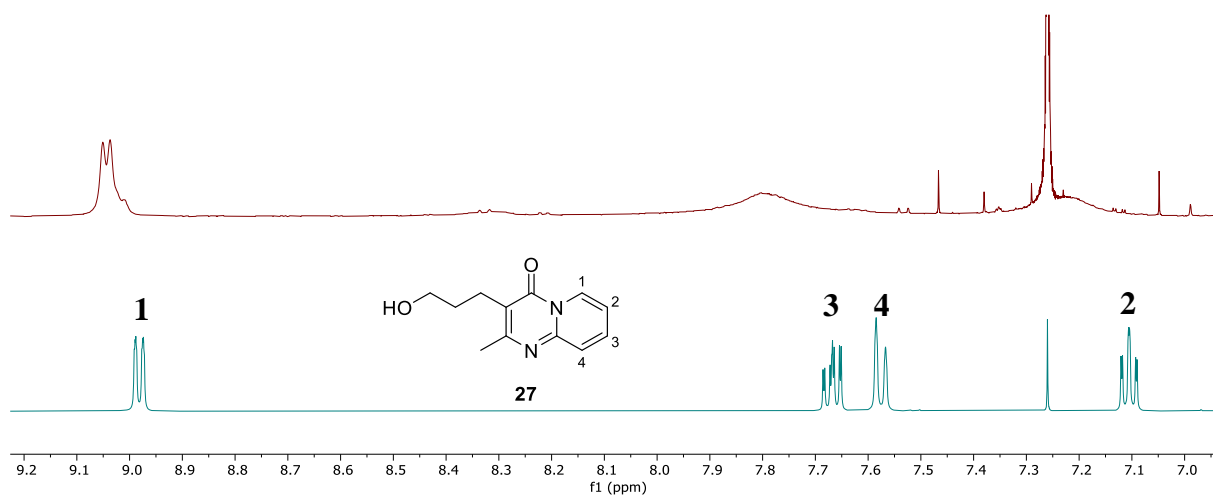
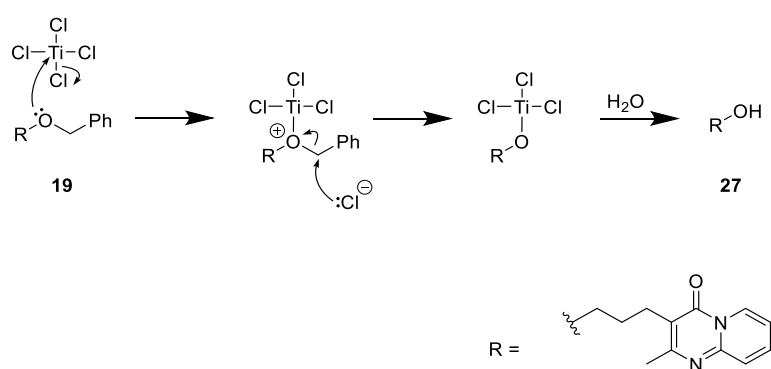


Figure 24. Stacked ^1H NMR spectra of one fraction of chromatographed TiCl_4 reaction product (top) and combined fractions of TiCl_4 reaction product (bottom).

The ^1H NMR spectrum of **27** showed the alkyl chain peaks to have shifted by up to 0.08 ppm when compared to **19**. The 2D NMR data confirmed the connectivity of the alkyl chain to the pyridopyrimidone remained unchanged. The ^{13}C NMR spectrum showed the loss of phenyl

ring shifts and the shift characteristic of benzylic position at 72.9 ppm, indicative of successful deprotection. A broad -OH stretch at 3231 cm^{-1} was noted in the IR spectrum of **27** that was not present in the starting material. HRMS supported these observations, confirming the desired product had been isolated in a 49% yield.

Mechanistically it is proposed this reaction begins with attack of the oxygen on the titanium, leading to loss of a chlorine (**Scheme 29**). The free chlorine can then attack the benzylic position, breaking the C-O bond and forming benzyl chloride as a result. Subsequent hydrolysis will provide the deprotected alcohol.



Scheme 29. Proposed mechanism of TiCl_4 -mediated deprotection.

The success of the deprotection of **19** prompted an attempt towards deprotection of **22**. Employing the aforementioned procedure, chromatographic separation with a more polar solvent system (acetone + 0.5% triethylamine) yielded the anticipated alcohol **24** (41%). The success of the TiCl_4 deprotection method on both saturated and unsaturated substrates changed the aim of the project from synthesis of two analogues to four analogues. These four variants having three- and four-carbon alkyl linkers and the pyridopyrimidine being either saturated or unsaturated (**Figure 25**). The use of additional analogues in biological assays will hopefully provide more insight into the immunomodulatory mode of action of risperidone.

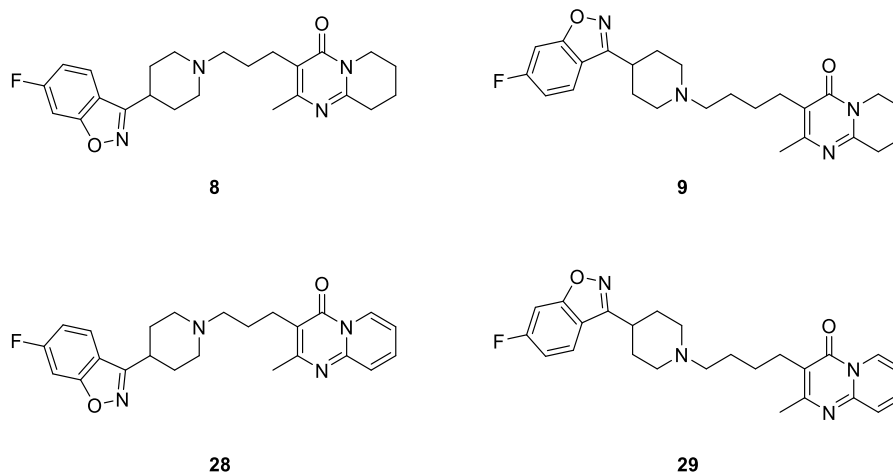
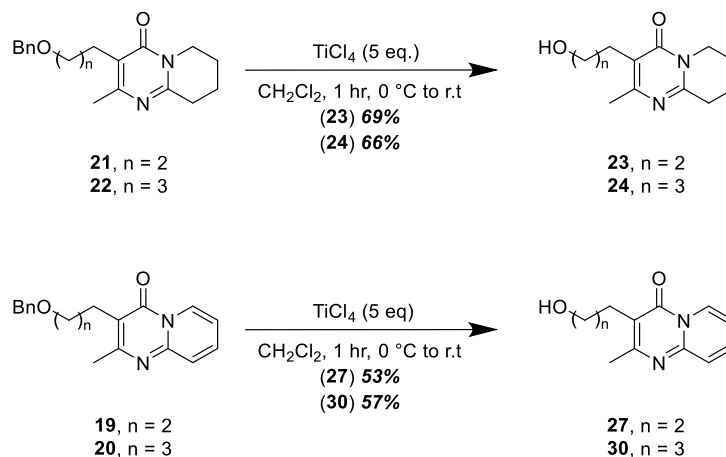


Figure 25. The four proposed risperidone analogues.

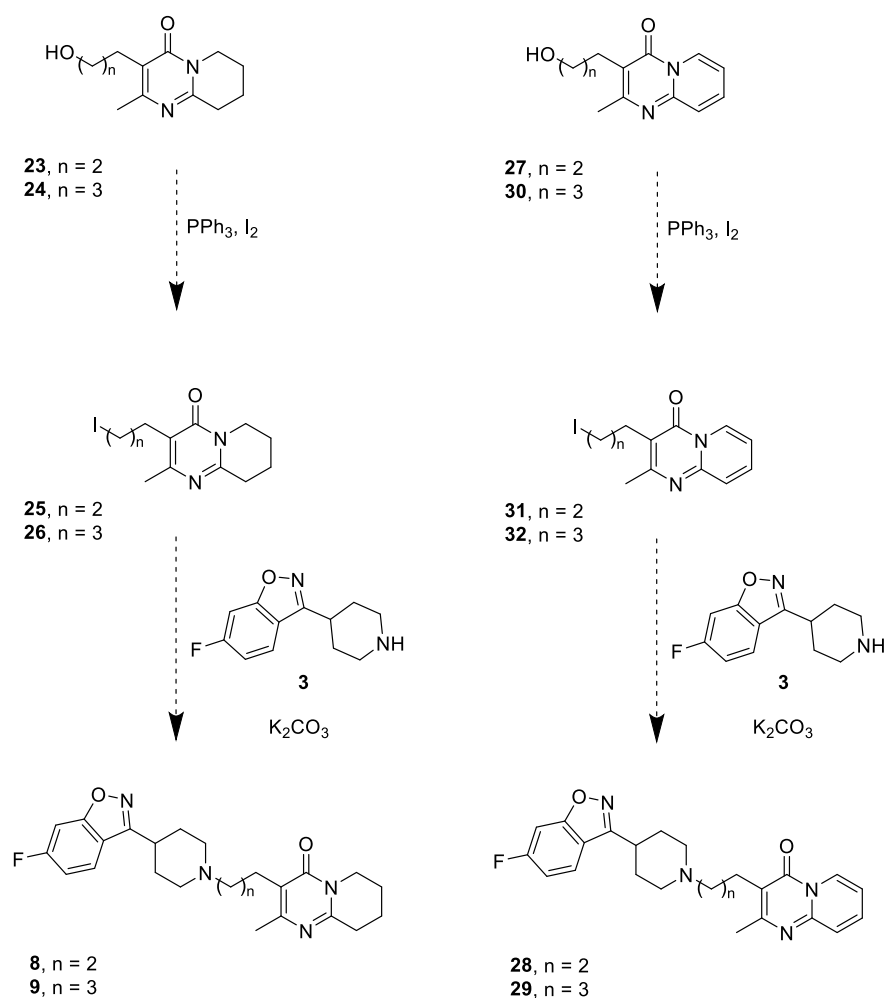
Deprotection of **19** was scaled up, with a more exhaustive extraction method providing a cleanly debenzylated product in a slightly improved yield (53%). Scale up of the deprotection of **22** also had an improved yield (66%). The aforementioned method was applied to the deprotection of **21** and **20** (**Scheme 30**). Observations in the NMR data similar to previous deprotected products confirmed the success of these debenzylation reactions.



Scheme 30. TiCl_4 -mediated benzyl-deprotection of pyridopyrimidones **19**, **20**, **21** and **22**.

2.5 Completion of the Synthesis of **8**, **9**, **28** and **29**

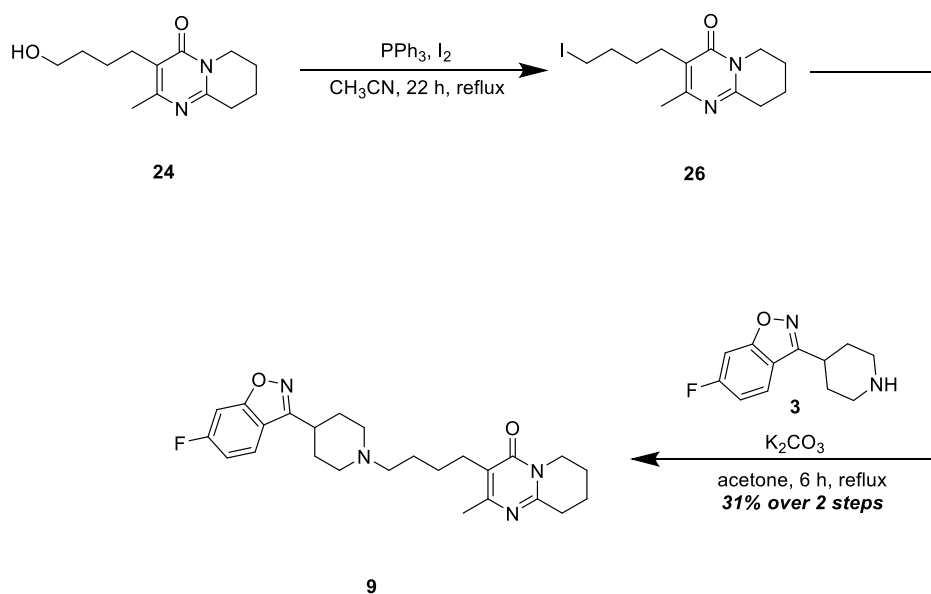
With the four deprotected pyridopyrimidones in hand, an Appel reaction was required to replace the hydroxyl with an iodide group in preparation for the final base-mediated coupling reactions (**Scheme 31**). Following the methodology of Zareie *et al.*, approximately 2 equivalents of PPh_3 and 1.5 equivalents of iodine were to be added to acetonitrile at $0\text{ }^\circ\text{C}$.⁹⁷ The pyridopyrimidone can then be added and the reaction heated at reflux overnight. Following workup, the iodide product was to be used immediately in the subsequent coupling with amine **3**. Chromatographic purification of the Appel product would be avoided to prevent possible degradation on silica gel.



Scheme 31. Proposed synthesis of analogues **8**, **9**, **28** and **29** via Appel reactions yielding iodides **25**, **26**, **31** and **32**.

2.5.1 Synthesis of Four-Carbon Saturated Analogue **9**

During the Appel reaction of **24** toward synthesis of **9**, it was demonstrated that the addition of iodine to the dissolved PPh_3 resulted in the formation of a precipitate (**Scheme 32**). This is likely a phosphonium salt formed via a similar mechanism to the earlier Appel reaction (see **Section 2.3.1**). The reaction was halted after 19 hours as reaction monitoring by TLC analysis was impossible due to streaking of the triphenylphosphine oxide byproduct (**Figure 26**). Addition of triethylamine to the mobile phase did not allow for resolution of individual species as it had in previous steps. Fortunately, the prescribed aqueous workup removed the PPh_3O byproduct and afforded iodide **26** in a reasonable yield.



Scheme 32. Synthesis of analogue **9**.

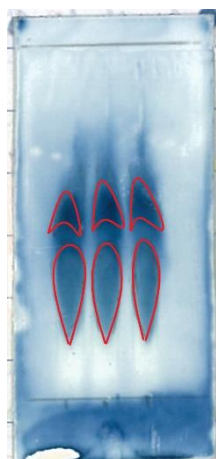


Figure 26. Triplicate TLC analysis (acetone + 0.5% triethylamine) of crude reaction mixture pre-workup for Appel reaction on **24**. Stained with ceric ammonium molybdate. 254 nm UV active spots are outlined in red.

The ^1H NMR spectrum of **26** showed the presence of a small amount of PPh_3O (1:40) which was expected to be unreactive in the subsequent step. The biggest change when comparing the ^1H NMR spectra of alcohol **24** and iodide **26** was the moderate upfield shift of the halogen neighbouring protons. A shift from 3.71 ppm in alcohol **24** to 3.21 ppm in iodide **26** was observed with a small change in the J -couplings of these triplets (6.2 Hz and 6.9 Hz, respectively). These observations are similar to those noted in the synthesis of two-carbon linker pyridopyrimidones by Zareie *et al.*⁹⁷

Iodide **26** was immediately subjected to a coupling reaction with the benzisoxazole-linked piperidine **3**. Using approximately equimolar amounts of iodide **26**, amine **3** and K_2CO_3 , the mixture was heated at reflux. After six hours, TLC analysis was unconvincing due to the presence of multiple products. Four UV active species were present as well as two that stained with ceric ammonium molybdate dip (**Figure 27**). TLC analysis the following day showed that the addition of further K_2CO_3 (0.5 equivalents) had not pushed the reaction to completion. As a result, the reaction was halted, the aqueous workup followed and the crude reaction product analysed by NMR spectroscopy. Future syntheses withheld the addition of extra base due to its ineffectiveness.

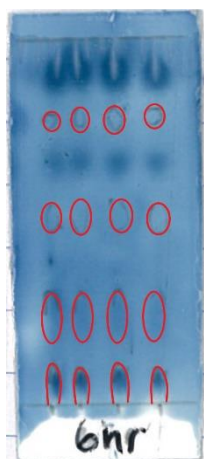


Figure 27. Quadruplicate TLC analysis (acetone + 0.5% triethylamine) of the crude reaction mixture of the coupling reaction towards **9**. Stained with ceric ammonium molybdate. 254 nm UV active spots are outlined in red.

The ^1H NMR spectrum of the crude reaction mixture showed the presence of similar shifts to those of the two fragments **3** and **26**, albeit slightly shifted. The largest change in chemical shifts were noted for protons located nearest to the point of coupling, the amine. In particular, the piperidine ring protons of **3** and the terminal protons of the alkyl chain of **26**, exhibited the greatest change in shifts.

The peaks representative of the piperidine ring protons were found to be much less resolved than all other shifts found in the crude mixture. Comparing the ^1H NMR spectra of benzisoxazole **3** and analogue **9** showed the triplet of triplets and doublet of triplets, representing H-8' and H-10'a respectively, to be significantly less resolved in crude reaction mixture (**Figure 28**). This effect had been noted in the earlier 2-aminopyridine condensation step where some peaks did not resolve with impure samples. A slight upfield shift was also noted for protons H-8' and H-10'a in the crude product. HRMS analysis confirmed the presence of the desired product **9** with a found mass of 439.2512 that matched the calculated value for $\text{C}_{25}\text{H}_{32}\text{FN}_4\text{O}_2^+ [\text{M}+\text{H}]^+$ 439.2504 with $\Delta = 1.9$ ppm.

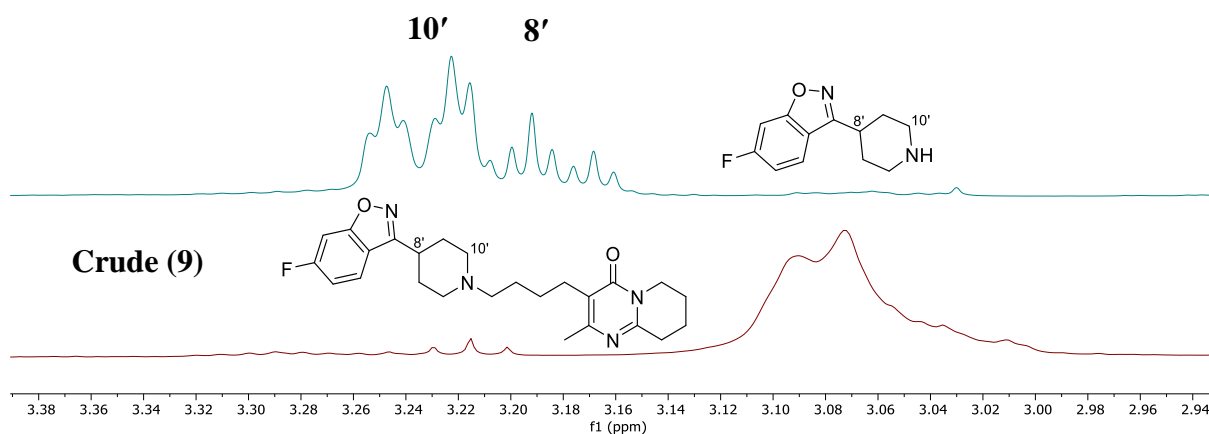


Figure 28. Stacked ¹H NMR spectra of benzisoxazole **3** (top) and crude condensation product **9** (bottom), focussed on shifts representative of positions C-8' and C-10'.

TLC analysis of the crude reaction mixture revealed a distinctly flat spot visible under 254 nm UV irradiation. Isolation of this species utilised diol-functionalised silica gel in a pipette column to avoid acid-mediated degradation associated with traditional silica gel. Fortunately, clean separation was achieved to afford the first analogue (**9**).

COSY NMR analysis demonstrated that connectivity was maintained throughout the alkyl chain, as well as in the pyridine ring of the pyridopyrimidone. HMBC correlations within the fused heterocycle were similar to those previously discussed (see **Section 2.3.3**). Connectivity of the piperidine ring to the benzisoxazole was confirmed by HMBC and COSY correlations as previously discussed (see **Section 2.2.4**). NMR analysis of the whole product confirmed that the coupling was successful, with an HMBC correlation from the protons of C-13 to C-10' (**Figure 29**).

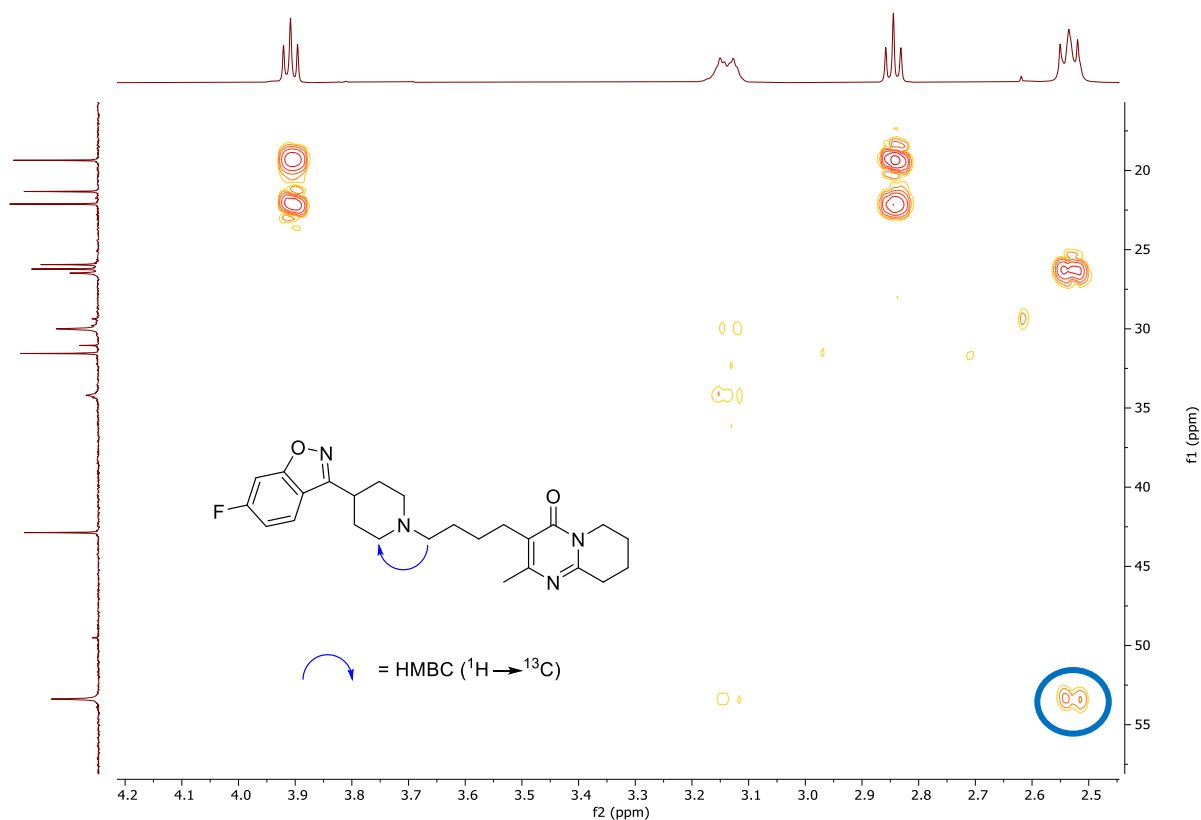


Figure 29. Expansion of HMBC spectrum of **9** with the key correlation circled.

Again, it was found that weakly concentrated NMR samples did not allow for adequate resolution of all peaks, similar to previous analyses of small quantities of **19** and **27**. In an attempt to circumvent this issue the use of D₂O was trialled in place of the usual CDCl₃. Surprisingly, ¹H NMR analysis in D₂O provided a more resolved spectrum (**Figure 30**), however poor solubility did not allow for collection of ¹³C and 2D NMR spectra from this sample. Instead, larger quantities (> 10 mg) of analogue **9** were found to provide well-resolved spectra in CDCl₃.

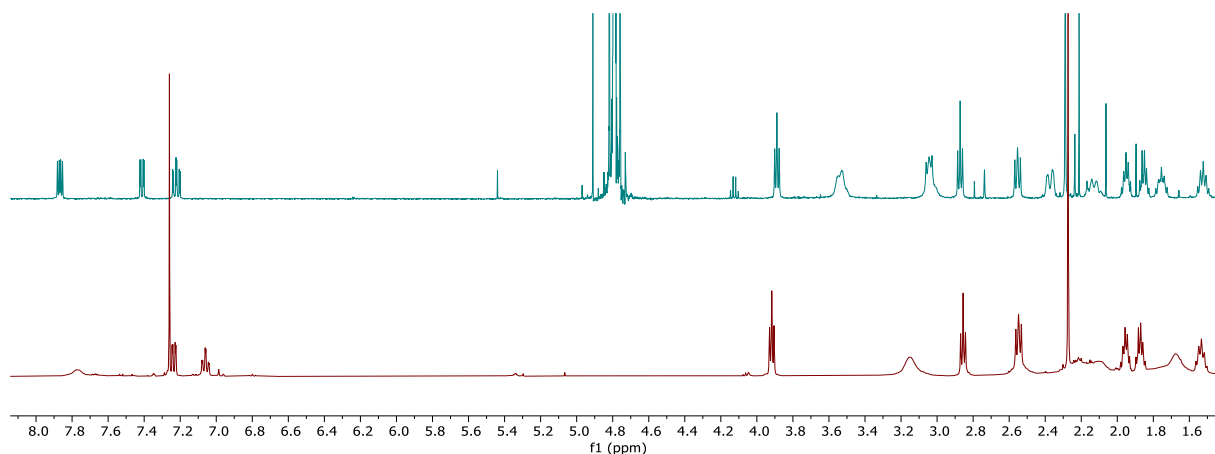
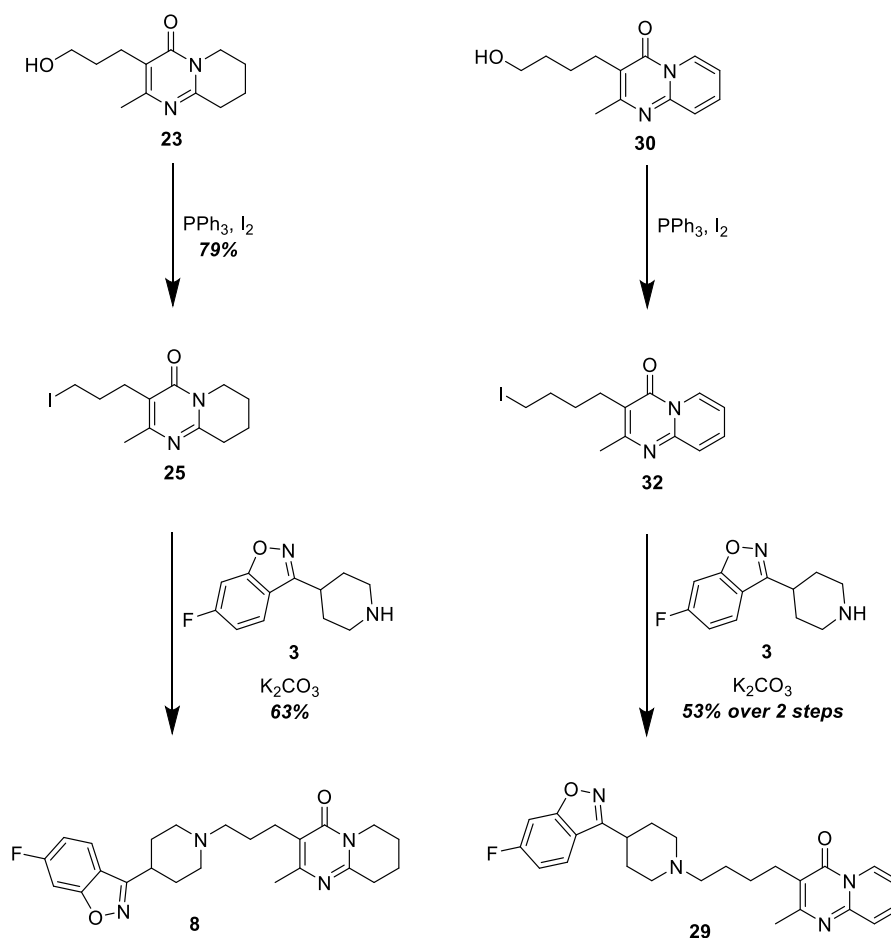


Figure 30. Comparison of ^1H NMR spectra of analogue **9** in D_2O (top) and CDCl_3 (bottom).

2.5.2 Synthesis of Analogues **8**, **28** and **29**

Synthesis of analogues **8** and **29** employed the same procedure as for synthesis of analogue **9** (**Scheme 33**). Appel reaction of **23** and **30** yielded iodides **25** and **32**, the formation of which was confirmed by HRMS. These iodide products were used immediately in coupling reactions with **3**. Chromatographic separation as previously described yielded the desired analogues **8** and **29**. Fortunately, adequate quantities were synthesised for full structural elucidation by NMR spectroscopy. The ^1H NMR spectra of both **8** and **29** showed similar shifts in peaks to **9**, when compared to the starting material (**Figure 31**).



Scheme 33. Synthesis of analogues **8** and **29**.

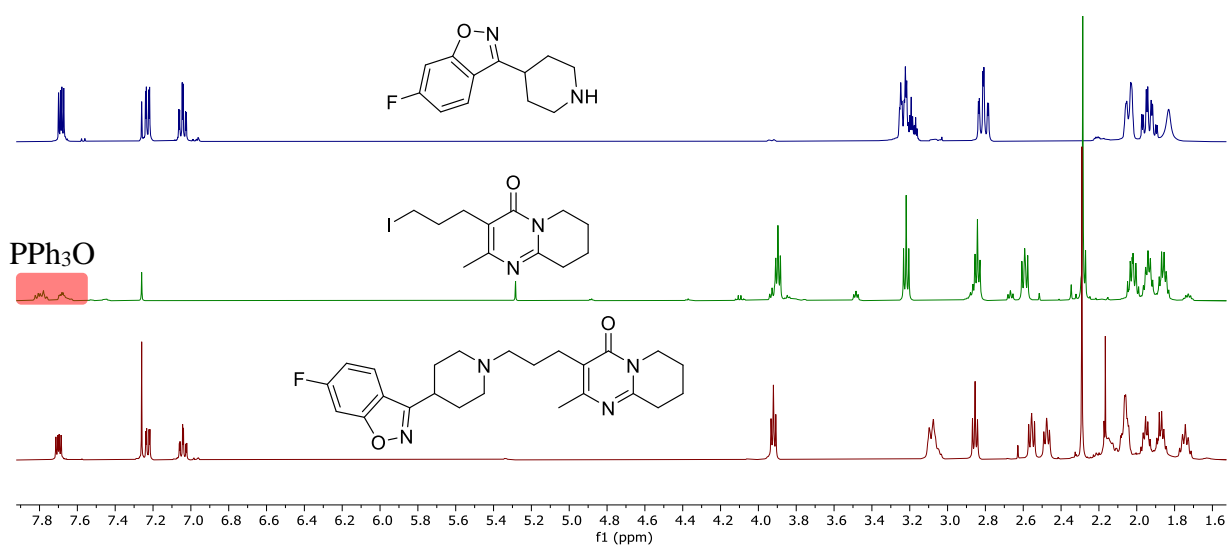
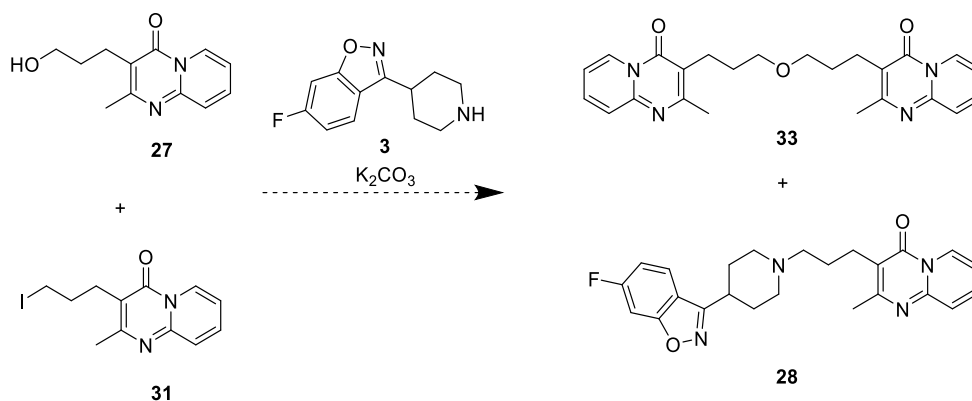
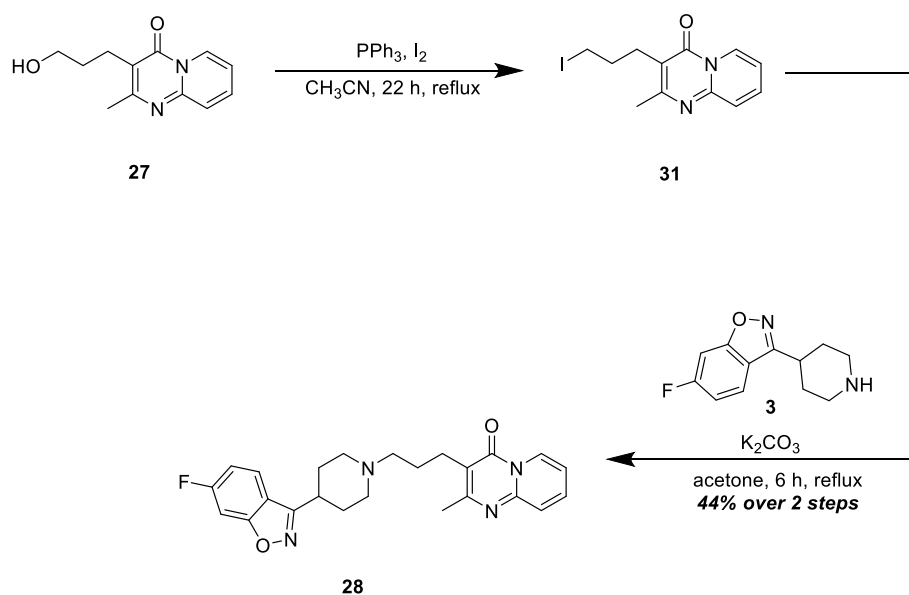


Figure 31. Stacked ^1H NMR spectra of benzisoxazole **3** (top), iodide **25** (middle) and analogue **8** (bottom). Residual PPh_3O is highlighted in red.

Synthesis of **28** was less efficient. Two attempts of the Appel reaction on this substrate resulted in only partial conversion of the alcohol to the iodide **31** (2:1 and 0.32:1 **27**:**31** by comparison of integrals in the ^1H NMR spectrum). These mixtures were used in the subsequent coupling reaction without further purification as it was expected the alcohol would be unreactive. The hydroxyl proton would likely be less labile than the amine proton of benzisoxazole **3**. However, if the alcohol were to react with the iodide, a dimeric product (**33**) could form (**Scheme 34**). Fortunately, the coupling with **3** proceeded smoothly and no dimeric product was identified (**Scheme 35**). The final analogue **28** was isolated in sufficient quantity (10.3 mg, 67%) for definitive NMR analysis.



Scheme 34. Possible products of an alcohol (**27**) and iodide (**31**) mixture in the final condensation reaction.



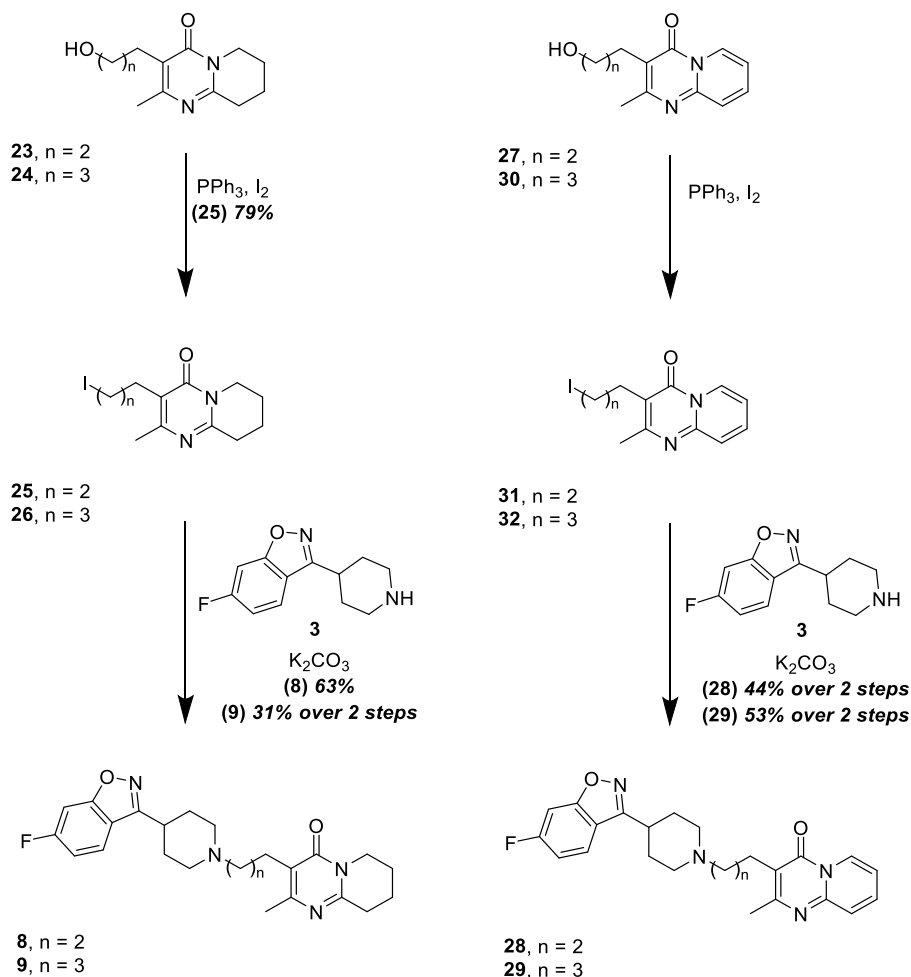
Scheme 35. Synthesis of analogue **28**.

The transformation of all four substrates from an alcohol to an iodide showed some consistency in the observed ^1H NMR shifts (**Table 6**). The halogen-neighbouring protons of three-carbon iodides **25** and **31** experienced an upfield shift of 0.27 ppm and 0.28 ppm, respectively. Similar protons in four-carbon iodides **26** and **32** experienced upfield shifts of 0.50 ppm and 0.49 ppm, respectively. These protons in all four iodides were found to have J -couplings of 6.9 Hz, larger than in the alcohol in all cases.

Table 6. Comparison of terminal triplet shifts and J -couplings of Appel starting materials and products.

Analogue	Alcohol δ (ppm)	Iodide δ (ppm)	Difference δ (ppm)
	($^3J_{\text{HH}}$ Hz)	($^3J_{\text{HH}}$ Hz)	($^3J_{\text{HH}}$ Hz)
3-Carbon Saturated	3.49 (5.9)	3.22 (6.9)	- 0.27 (+ 1.0)
3-Carbon Unsaturated	3.54 (5.8)	3.26 (6.9)	- 0.28 (+ 1.1)
4-Carbon Saturated	3.71 (6.2)	3.21 (6.9)	- 0.50 (+ 0.7)
4-Carbon Unsaturated	3.72 (6.3)	3.23 (6.9)	- 0.49 (+ 0.6)

With the synthesis of analogue **28** complete, four risperidone analogues had successfully been generated (**Scheme 36**). According to the methodology of West, samples of analogues **8**, **9**, **28** and **29** were quantified by NMR using nitromethane as an internal standard.¹³⁸ 10mM solutions of each analogue were made in DMSO in anticipation of the biological testing to follow.



Scheme 36. Synthesis of analogues **8**, **9**, **28** and **29**.

3 *In Vitro* Assays

To investigate the *in vitro* activity of the four synthesised risperidone analogues, **8**, **9**, **28** and **29** were added to the culture medium of LPS-stimulated RAW264.7 macrophages at increasing concentrations. Zareie *et al.* previously found risperidone to cause a modest decrease in MTT metabolism in RAW264.7 cells treated at concentrations of 80 μ M or greater.⁹⁷ Cytokine levels of the supernatant were also measured by ELISA according to the methodology of Zareie *et al.*⁹⁷ Anti-inflammatory cytokine production was demonstrated to be significantly increased at risperidone concentrations of 60 μ M and above. Pro-inflammatory cytokine production was found to be significantly decreased at risperidone concentrations as low as 20 μ M. The current research uses risperidone as a positive control for comparison of the results from assays of **8**, **9**, **28** and **29**. In the MTT assay, risperidone results were comparable to the findings of Zareie *et al.* except for at concentrations of 80 and 100 μ M where the decrease in MTT metabolism was to a lesser degree than previously observed. This observed difference could be due to dilution of the stock risperidone solution with DMSO, instead of 0.1 M acetic acid as previously used. ELISA results with risperidone treatment were comparable to previous work.⁹⁷

3.1 MTT and ELISA Assay Results

3.1.1 MTT Assay Results

Treatment with three-carbon unsaturated analogue **28** resulted in similarly non-toxic activity to risperidone regarding its effect on MTT metabolism at concentrations up to 80 μ M (**Figure 32**). At 100 μ M, treatment with **28** appeared to cause a small reduction in MTT metabolism compared to risperidone.

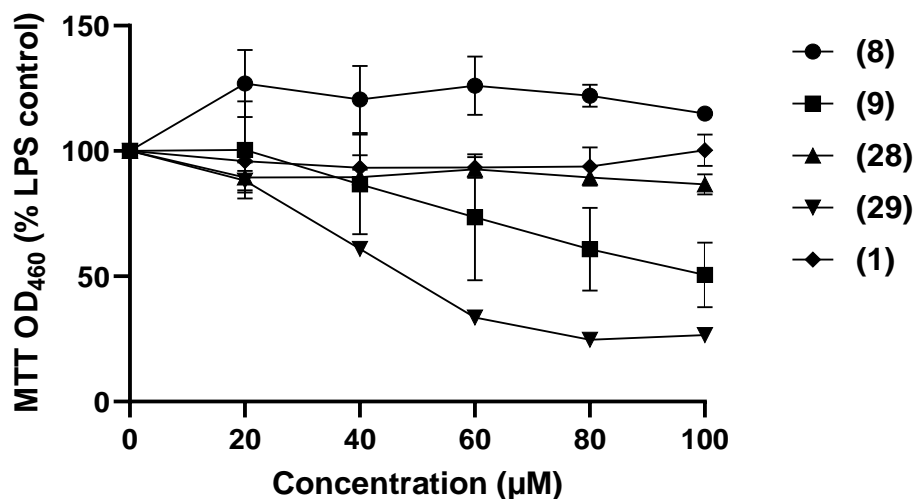


Figure 32. RAW264.7 cell viability measured by MTT assay. Presented as a percentage of vehicle control. RAW 264.7 cells were plated at 50,000 cells/well, primed with IFN- γ (20 U/mL), and stimulated with LPS for 24 hours in increasing concentrations of analogues **8**, **9**, **28**, **29** and risperidone at 1% DMSO. Shown are means and SEM of triplicate wells from one experiment.

Surprisingly, treatment with saturated three-carbon analogue **8** resulted in a significant increase in MTT metabolism at concentrations of 60 μ M and above when compared to the vehicle control. This apparent increase may be as a result of the readings lying outside the optimal range of the optical density reader. This may mean that MTT metabolism was not increased as a result of treatment with **8**. However, it is unlikely that MTT metabolism is negatively affected by **8**.

Treatment with four-carbon saturated analogue **9** caused a large and significant decrease in MTT metabolism at concentrations of 80 μ M and above. Compound **29** was found to significantly inhibit MTT metabolism at concentrations of 40 μ M and greater.

In summary, varied effects on cell viability were seen with the four analogues **8**, **9**, **28** and **29**. The four-carbon linker analogues **9** and **29** led to decreased MTT metabolism, with the unsaturated analogue **29** shown to be the greatest inhibitor of MTT metabolism compared to all other treatments at concentrations of 40 μ M and above. The three-carbon linker analogues **8** and **28** behaved in a similar manner to risperidone itself, with little decrease in cell viability as seen by MTT metabolism.

3.1.2 IL-12 ELISA Results

At concentrations of 40 μM and greater, all analogues significantly inhibited production of pro-inflammatory cytokine IL-12 when compared to control (**Figure 33**). In comparison to risperidone treated cells at concentrations of 60 μM and greater, analogue treatment resulted in significantly greater inhibition of IL-12 production. The attenuation of IL-12 production observed in the supernatant of **9** and **29** treated cells may be a result of the reduction in cell viability inferred from the MTT assay. Thus, fewer living cells are present to produce this inflammatory cytokine.

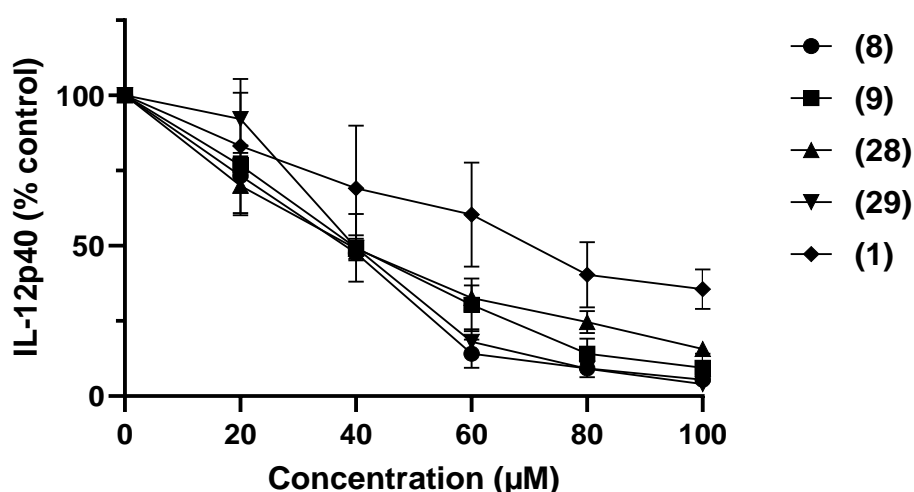


Figure 33. IL-12 in the supernatant measured by ELISA.

The results for risperidone treatment were comparable to those of Zareie *et al.* who demonstrated IL-12 production to be reduced linearly upon treatment with risperidone at concentrations of up to 60 μM .⁹⁷ At concentrations greater than 60 μM no further change in IL-12 production was observed. Risperidone is proven to be a suitable positive control for this experiment.

3.1.3 IL-10 ELISA Results

The ELISA results of treatment with the risperidone analogues on quantities of anti-inflammatory cytokine IL-10 were varied (**Figure 34**). Treatment with three-carbon linker analogues **8** and **28** resulted in no significant change in IL-10 production when compared to vehicle control across all concentrations tested. Treatment with four-carbon analogues **9** and **29** treatment at 20 μ M and 40 μ M concentrations resulted in a significant increase in IL-10 production, greater than 200% of control. This was significantly more than the increase observed for risperidone (**1**). At 60 μ M, the level of IL-10 production is comparable to risperidone treatment while concentrations of 80 μ M and greater resulted in levels of IL-10 comparable to vehicle control.

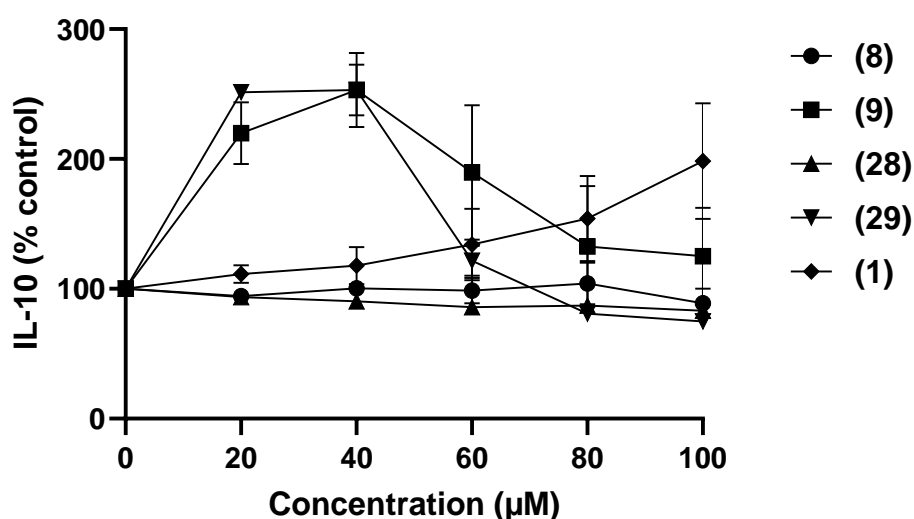


Figure 34. IL-10 in the supernatant measured by ELISA.

3.2 Discussion

3.2.1 Cell Viability

These results show that, like risperidone, neither of the three-carbon linker analogues inhibits MTT metabolism and therefore, have no negative effect on cell viability. Interestingly, four-carbon linker analogues **9** and **29** were found to significantly reduce cell viability at

concentrations of 80 μM and 40 μM , respectively. These results will need to be verified by flow cytometry.

The suppression of MTT metabolism associated with **9** and **29** treatment is apparently due to the longer alkyl spacer in these compounds. These four-carbon linker analogues have two additional methylenes, compared to risperidone, separating the piperidine and the pyridopyrimidone moieties. This longer alkyl chain has more rotatable bonds which increases the flexibility of these molecules and expands the number of structural conformations these molecules can adopt. A greater number of conformations may increase the number of protein binding sites accessible to these molecules.

A flexible molecule can adopt different conformations, allowing it to access more than one dissimilar binding site. An example of this is acarbose, an antidiabetic drug that adopts different conformations to inhibit the activity of both glucoamylase and 4- α -glucanotransferase (**Figure 35**).¹³⁹⁻¹⁴⁰ The binding affinity of acarbose for each protein is different due to the variations in the amino acids and their positions in the active site. Extending the linker of risperidone may have a similar effect and allow for off-target protein binding. This promiscuity could result in inhibition of multiple key metabolic pathways, thus explaining the reduction in cell viability associated with **9** and **29** treatment.

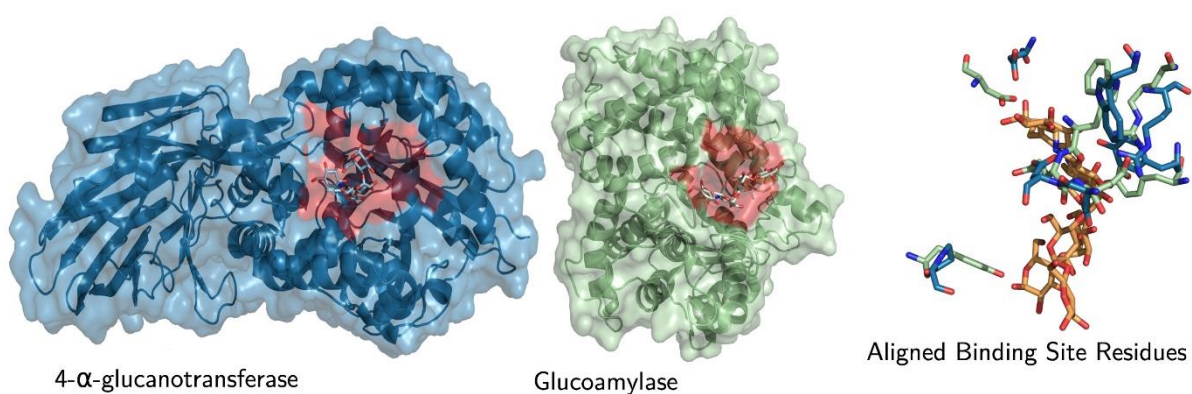


Figure 35. Acarbose binding site alignments in 4- α -glucanotransferase and glucoamylase. Binding sites are highlighted in red and ligands are presented in orange. Adapted from Haupt *et al. Drug Promiscuity in PDB: Protein Binding Site Similarity Is Key. PLOS ONE* **2013**, 8 (6), e65894.¹⁴¹

Alternatively, a longer alkyl chain could make the ligand compatible with proteins that have similar binding sites and open up new therapeutic areas. For example, the antiviral drug brivudine inhibits virus replication by binding to thymidine kinase.¹⁴² Brivudine can also bind to human heat shock protein (HSP), conferring potential anticancer activity.¹⁴³ The active sites of these proteins share five residues in similar positions, including two phenylalanines that are crucial for π -stacking interactions in the binding pocket.

It is plausible that the conformational flexibility of **9** and **29** may allow for binding to many proteins with structurally similar active sites, similar to brivudine. The increased toxicity of **29**, compared to **9**, at lower concentrations may be attributed to the increase in π -stacking interactions possible with the unsaturated pyridopyrimidone. Inhibition of multiple key metabolic pathways as a result of this promiscuity could explain the observed reduction in cell viability. Alternatively, reduced MTT metabolism may be due to direct inhibition of the enzymatic reduction of MTT to formazan.

3.2.2 Immunomodulatory Activity

Compounds **8** and **28** induced suppression of IL-12 production follows a similar concentration-dependent curve as risperidone treatment. This suggests a similar mode of action between **8**, **28** and risperidone. Compounds **8** and **28** did not affect IL-10 production significantly while even at low concentrations, both four-carbon analogues **9** and **29** demonstrated significant IL-10 amplification properties. Compared to control, a 200% increase in IL-10 production was observed at sub-toxic concentrations.

Compared to risperidone, an IL-12 suppression response was associated with **8** and **28** while an increase in IL-10 production was associated with **9** and **29**. These observations may be a result of enhanced binding of the analogues within the active site of a protein afforded by the extended linker. As the mode of action associated with the immunomodulatory activity of risperidone is unknown, the types of binding interactions possible can only be postulated.

A range of binding pocket interactions could be possible, including adjacent, shallow and deep pocket interactions. An adjacent pocket allows a bivalent ligand, such as risperidone, to bind in the main active site as well as an adjacent pocket simultaneously.¹⁰ A shallow pocket ligand-protein interaction is less likely as these are usually associated with protein-protein interactions.¹⁴⁴ Deep, hydrophobic pockets in a protein are very common sites for small

molecules to bind as the large amount of hydrophobic residues present favour interactions with organic molecules.¹⁴⁵⁻¹⁴⁷

The extended linker of an analogue may allow for a second pharmacophore to be favourably positioned to make an adjacent pocket interaction. For example, the benzisoxazole pharmacophore of risperidone binds in a deep hydrophobic pocket in the D₂ receptor, and the pyridopyrimidone extends into an adjacent binding pocket.¹⁰ The benzisoxazole moiety of **9** was not modified so this would allow it to access the same hydrophobic pocket of the D₂ receptor as risperidone. However, ligand-protein interactions in the extended binding pocket are likely to change due to the increased distance between the piperidine ring and the pyridopyrimidone moiety (**Figure 36**). Key stabilising interactions, such as those with Trp100, may be lost and result in a less stable binding interaction. Alternatively, the pyridopyrimidone moiety may extend into a different binding pocket that creates a more stable ligand-protein interaction. The potential π -stacking interactions of unsaturated analogues **28** and **29** would also alter the binding profile of these compounds in an adjacent pocket.

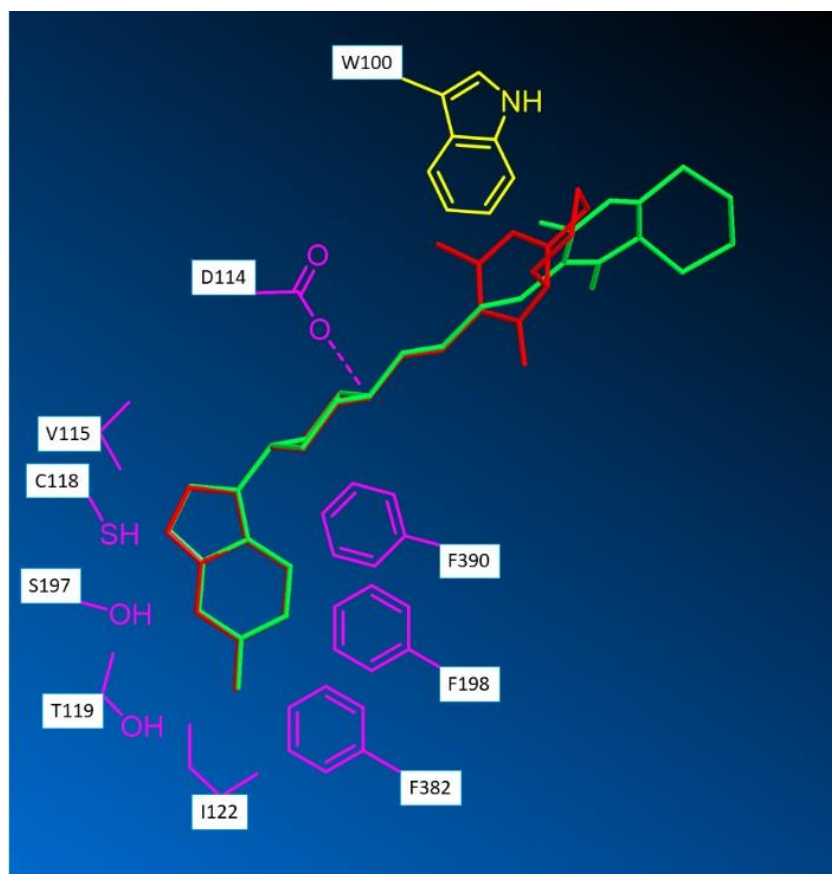


Figure 36. Overlay of **9** (green) and risperidone (red), demonstrating their proposed positions in relation to a tryptophan residue (yellow) in the D₂ receptor.

If the pharmacophore were to bind in a deep hydrophobic pocket of an unknown protein, a longer alkyl spacer may reduce unfavourable drug-protein interactions if the unbound moiety resided outside the binding pocket (**Figure 37**). In this proposed situation, risperidone may have weaker ligand-protein interactions due to the steric hindrance caused by the non-binding moiety at the entrance of the pocket. This could explain the enhanced IL-12 suppression attributed to **8** and **28**.

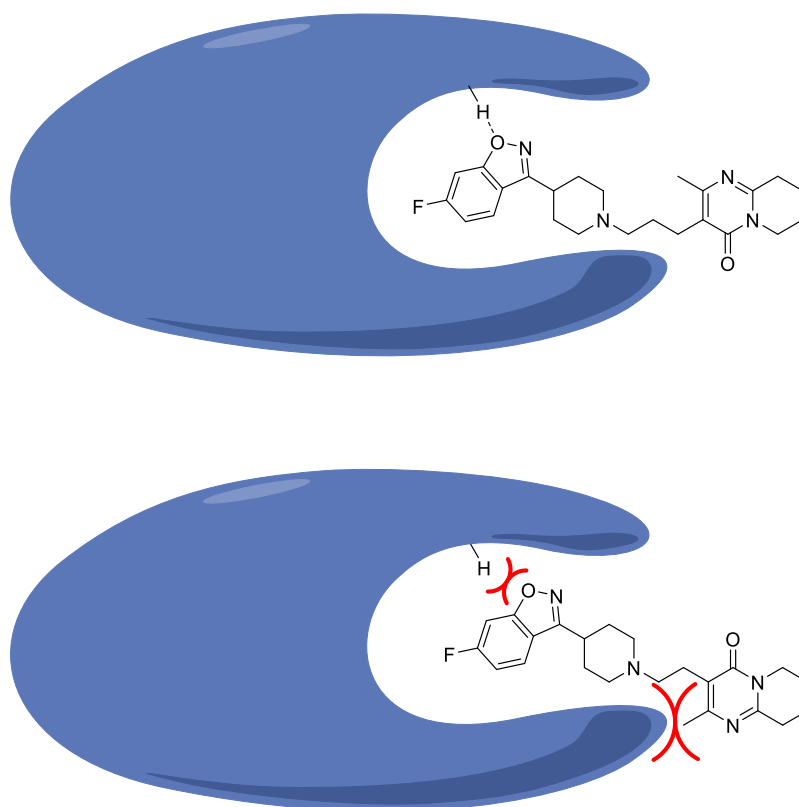


Figure 37. Proposed deep-pocket ligand-protein interactions of **8** (top) and risperidone (bottom).

A longer alkyl spacer may also prevent unfavourable intramolecular interactions within the ligand when binding to protein. A protein with a wide, shallow binding pocket could restrict the size of the molecule it is able to accommodate (**Figure 38**). Flexibility about the alkyl chain may be required for the pharmacophore to establish strong ligand-receptor interactions whilst minimising unfavourable intramolecular interactions. Analogues with longer alkyl spacers have an increased number of rotatable bonds. Therefore, a molecule like **9** would be more likely to have a strong binding interaction with a protein. If such a protein were part of the IL-10 pathway, this could explain the enhanced IL-10 production observed.

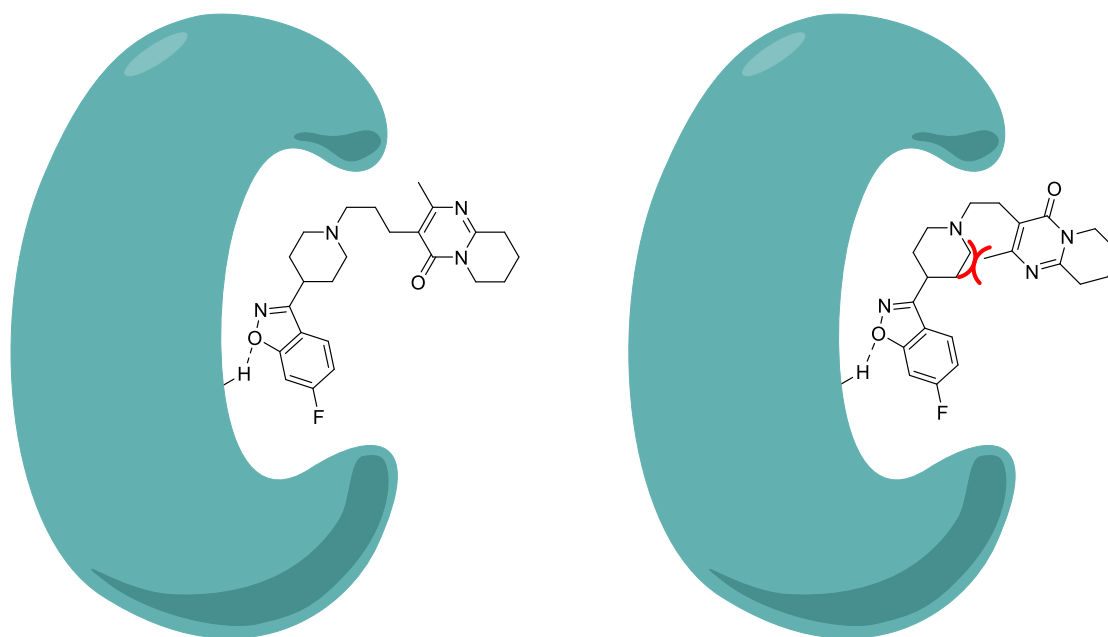
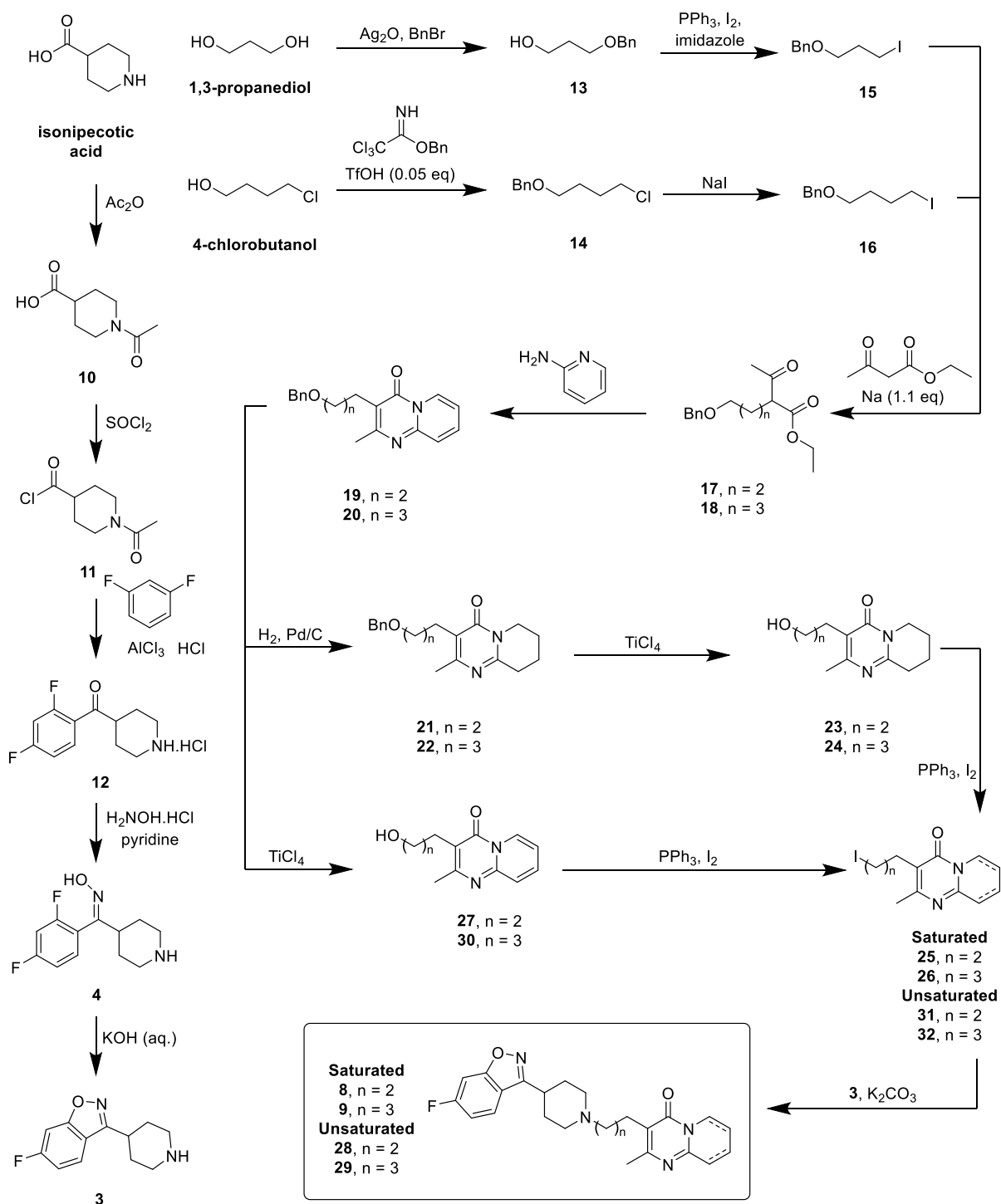


Figure 38. Proposed shallow-pocket ligand-protein interactions of **8** (left) and risperidone (right).

4 Summary and Future Work

4.1 Summary

Four risperidone analogues (**8**, **9**, **28**, **29**) were successfully synthesised (**Scheme 37**), exceeding the initial aim of generating two analogues (**8**, **9**). This project was a continuation of Durrant's preliminary work, from which a method was required for deprotection of the benzyl-protected hydrogenated pyridopyrimidones **21** and **22**.⁹⁸ Interestingly, here, catalytic hydrogenation was found to be applicable for debenzylation, contrary to previous reports. This method was rather slow so, fortunately, TiCl_4 was subsequently found to be a suitable reagent. TiCl_4 -mediated deprotection was also demonstrated to be applicable to formation of unsaturated pyridopyrimidones **27** and **30**. This allowed for synthesis of four analogues, now including unsaturated variants **28** and **29**. Fortunately, the Appel and coupling reactions to follow were straight-forward and all four analogues were generated.



Scheme 37. Overall synthetic route for risperidone analogues 8, 9, 28 and 29.

Preliminary immunomodulatory studies were also performed. *In vitro* assays of analogues 8, 9, 28 and 29 in RAW264.7 cells found both four-carbon analogues (9, 29) to be cytotoxic while 8 and 28 had no observable effect on cell viability, similar to risperidone. Suppression of IL-

IL-12 production was observed with all four compounds, however for **9** and **29** this may be as a result of cytotoxicity. Analogues **8** and **28** suppressed IL-12 production to a greater extent than risperidone. Analogues **9** and **29** greatly amplified IL-10 production at low concentrations while **8** and **28** had no effect on IL-10 production at all concentrations tested. Unfortunately, time did not permit for further repetitions of these assays nor measurement of IFN- γ , TNF- α , MCP-1 and IL-6 production in RAW264.7 cells and BMM Φ . These will be followed up in the near future.

4.2 Future Work

The successful synthesis of four risperidone analogues and their *in vitro* assay results encourages further investigation into the potential of risperidone and these analogues as immunomodulatory agents.

Additional *in vitro* testing is required to corroborate the results observed in the current research. Due to time constraints the proposed ELISAs to detect IL-6, TNF- α , IFN- γ and MCP-1 were not completed. Assays revealing the effects of the synthesised analogues on the profiles of these signalling molecules in RAW264.7 and BMM Φ cells will further reveal potential immunomodulatory activity. The strong increase in IL-10 production associated with low (sub-toxic) concentrations of four-carbon analogues **9** and **29** is of particular interest due to their more potent anti-inflammatory effect when compared to risperidone. Similar experiments using lower concentrations of these analogues will provide more detailed information of the anti-inflammatory effect associated with **9** and **29** treatment.

Optimisation of the TiCl₄ deprotection of the benzyl ether in the synthesis of the pyridopyrimidone fragment could improve the overall yield by modifying the reaction times and workup conditions. Alternatively, the DDQ debenzylation method could be trialled again, using larger quantities for NMR analysis to confirm whether this reagent is applicable to deprotection of a pyridopyrimidone system. The Pd/C catalysed hydrogenation-*O*-debenzylolation should be repeated to confirm the reproducibility of the deprotection and to optimise for higher yields. A dual hydrogenation and debenzylation step would prevent the need for a separate deprotection as well as the associated purification, reducing the number of steps and potentially increasing the overall yield.

Alternative routes towards synthesis of the current analogues could be also more efficient stepwise and thus, improve the overall yield. A Stille reaction could be used for integration of the extended alkyl chain onto a pyridopyrimidone substrate, removing the need for protecting groups altogether.¹²⁷ However, the use of tin reagents may be unfavourable due to the current trends towards green synthesis so a Suzuki reaction could be applied instead.

Synthesis and testing of higher homologues, such as those with five- and six-carbon linkers (**34**, **36** and **35**, **37**, respectively) would be informative (**Figure 39**). The methodology applied to the synthesis of three-carbon analogues **8** and **28** should be transferable due to the availability of diol starting materials for both proposed analogues and the lack of additional functionality.

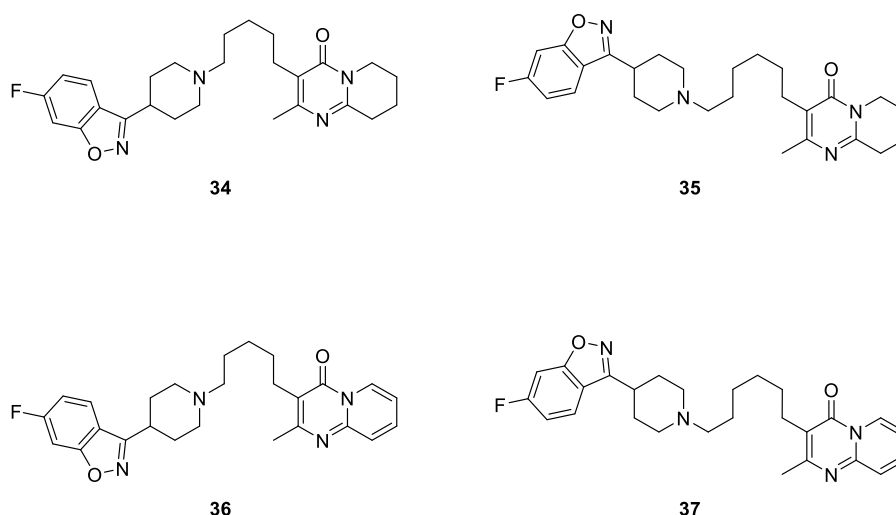


Figure 39. Proposed five- and six-carbon linker analogues of risperidone.

Structure rigidification is a common approach in the optimisation of drugs.¹⁴⁸ Further modification of the current three- and four-carbon analogues with a more restricted linker would also provide more structure activity relationship data with *in vitro* testing. Differentially positioned *E*- and *Z*-alkenes (**38** - **41**) could aid in the elucidation the mode of action of these compounds (**Figure 40**).

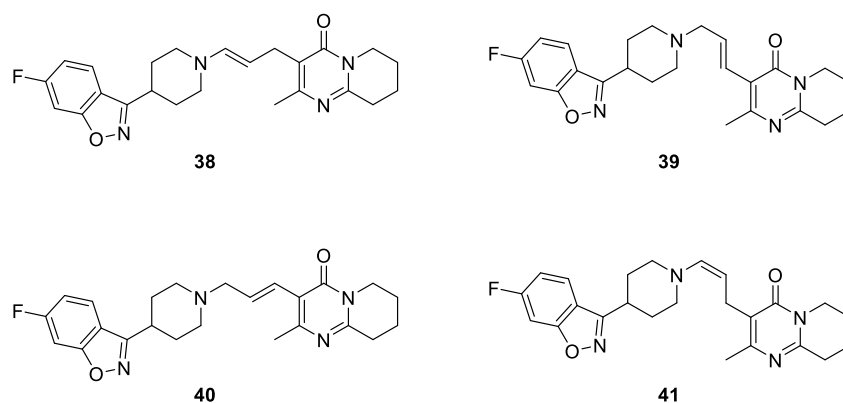


Figure 40. Proposed rigidified analogues of **8**.

Furthermore, the synthesis of biotin-linked risperidone and analogues for use with affinity chromatography could aid in discovery of new ligand-protein interactions. Attachment of a biotin tag to the benzisoxazole and pyridopyrimidinone moieties separately could help in identification of protein targets with varying affinities for these two potential pharmacophores. Molecular modelling could then be used to identify putative binding pockets for target proteins captured, furthering our understanding of the activity of risperidone and its analogues.

5 Experimental

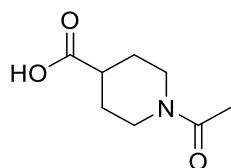
5.1 Synthetic Chemistry Experimental

5.1.1 General Methods

Unless otherwise noted, the following general conditions were applied. Reactions were performed under an atmosphere of dry argon using standard syringe techniques. Reaction solvents (CH_2Cl_2 , Et_2O) were dispensed from an Innovative Technologies Inc. PureSolv™ solvent purification system. Dry acetone was stored over activated 3Å molecular sieves for 24 hours before use. Molecular sieves were activated by drying under high-vacuum at 350 °C for 4 hrs. Workup solvents were used from the bottle as received from the supplier. All water was distilled and reaction glassware was oven dried at 130 °C overnight, assembled hot and cooled under vacuum. Reagents were purchased from Sigma-Aldrich unless otherwise specified. NMR spectra were collected on a JEOL JMTC-500/54/JJ NMR spectrometer at 22 ± 1 °C with a field strength of 11.74 T. ^{13}C NMR were proton-decoupled. Chemical shift (δ) is reported in parts per million (ppm) to the nearest 0.01 ppm for ^1H and 0.1 ppm for ^{13}C . ^1H and ^{13}C NMR spectra in CDCl_3 were referenced to residual solvent peaks with ^1H NMR (CHCl_3) $\delta = 7.26$ ppm and ^{13}C NMR (CDCl_3) $\delta = 77.16$ ppm. ^1H spectra in D_2O were referenced to the residual solvent peak (D_2O) $\delta = 4.79$ ppm. ^{13}C spectra in D_2O were unreferenced. Multiplicities are described as d (doublet), t (triplet), q (quartet), quin. (quintet), m (multiplet), br. (broad) and apparent (app.). Where identifiable, impurity peaks are not reported. Full spectral data are available in the supplementary information. Atom numbering in this section is for the purposes of description only and does not necessarily reflect the IUPAC name. Mass spectra were collected on an Agilent 6530 LCMS QToF using ESI and were processed using Mestrelab® Mestrenova (V. 14.0.0) and Agilent® MassHunter (V. B.06.01). Infrared spectra were collected using neat samples on a Bruker Alpha FTIR ATR spectrometer and are reported in cm^{-1} . All chromatography was with hexanes b.p. 40-60 °C, ethyl acetate, CH_2Cl_2 and acetone, with 0.5% triethylamine, on silica and TLC staining was with ceric ammonium molybdate unless otherwise noted.

5.1.2 Procedures and Experimental Data

1-Acetylpiperidine-4-carboxylic acid (**10**)



To a solution of isonipecotic acid (4.124 g, 31.9 mmol) and CH_2Cl_2 (65 mL), acetic anhydride (3.40 mL, 36.0 mmol) dissolved in CH_2Cl_2 (6.5 mL) was added dropwise. The reaction was stirred at room temperature for 23 hours, then concentrated *in vacuo*. The resulting white solid was recrystallised from ethanol to afford acid **10** as a white powder (2.439 g, 14.2 mmol, 45%).

m.p. 181.2 – 183.0 °C

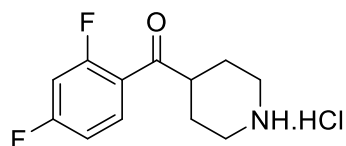
^1H NMR (500 MHz, D_2O) δ_{H} 4.25 (dtd, $J = 13.3, 3.9, 1.8$ Hz, 1H), 3.90 (dtd, $J = 13.9, 4.0, 1.8$ Hz, 1H), 3.22 (ddd, $J = 14.3, 11.6, 2.9$ Hz, 1H), 2.86 (ddd, $J = 13.9, 11.8, 3.1$ Hz, 1H), 2.69 (tt, $J = 11.4, 4.0$ Hz, 1H), 2.11 (s, 3H), 2.04 – 1.91 (m, 2H), 1.66 (dtd, $J = 13.4, 11.5, 4.2$ Hz, 1H), 1.55 (dtd, $J = 13.6, 11.6, 4.2$ Hz, 1H).

^{13}C NMR (126 MHz, D_2O) δ_{C} 179.4, 172.2, 46.0, 41.3, 40.4, 27.8, 27.4, 20.4.

HRMS: m/z $\text{C}_8\text{H}_{14}\text{NO}_3^+$ $[\text{M}+\text{H}]^+$ calcd. 172.0968, found 172.0963 (Δ 2.9 ppm).

The experimental data obtained matches those previously reported.⁹⁷

4-(2',4'-Difluorobenzoyl)piperidine hydrochloride (**12**)



A solution of acid **10** (499 mg, 2.92 mmol) in thionyl chloride (neat, 5.0 mL, 69 mmol) was stirred at room temperature for 4.5 hours. Et_2O (5 mL) was added and the solution concentrated *in vacuo*. The resulting red solid, acid chloride **11**, was used without further purification. To a solution of acid chloride **11** in CH_2Cl_2 (5 mL), AlCl_3 (1.022 g, 9 mmol) and 1,3 difluorobenzene (0.36 mL, 3.67 mmol) were added and heated at reflux for 14.5 hours. The resulting brown solution was cooled and poured into an ice/water mixture (32 g, 50% w/w). This mixture was

extracted with CH₂Cl₂ (3 x 30 mL), the organic fractions combined, dried (MgSO₄) and concentrated *in vacuo* to provide a viscous brown oil (592 mg) which was used without further purification. This oil was dissolved in 6M HCl (5 mL) and heated at reflux for 6 hours. The reaction mixture was then cooled, extracted with CH₂Cl₂ (3 x 30 mL) and the aqueous portion was concentrated *in vacuo* to provide hydrochloride salt **12** as a beige powder (420 mg, 1.61 mmol, 55% over 3 steps).

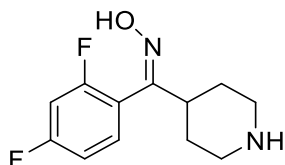
¹H NMR (500 MHz, D₂O) δ_H 7.88 (td, *J* = 8.8, 6.5 Hz, 1H), 7.15 – 7.05 (m, 2H), 3.62 (tt, *J* = 11.0, 3.6 Hz, 1H), 3.48 (dt, *J* = 13.1, 3.9 Hz, 2H), 3.15 (br t, *J* = 12.6 Hz, 2H), 2.18 (br d, *J* = 14.7 Hz 2H), 1.86 (m, 2H).

¹³C NMR (126 MHz, D₂O) δ_C 201.7, 166.1 (dd, *J* = 255.4, 14.1 Hz), 162.1 (dd, *J* = 256.0, 14.0 Hz) 132.7 (m), 120.7 (d, *J* = 11.0 Hz), 112.5 (d, *J* = 21.2 Hz), 105.1 (t, *J* = 26.5 Hz), 44.1, 43.2, 24.4.

HRMS: *m/z* C₁₂H₁₄F₂NO⁺ [M+H]⁺ calcd. 226.1038, found 226.1047 (Δ 4.0 ppm).

The experimental data obtained matches those previously reported.⁹⁷

(*Z*)-2,4-Difluorophenyl-(4-piperidiny)l)methanone oxime (**4**)



To a solution of pyridine (0.72 mL, 8.94 mmol) and hydroxylamine hydrochloride (129 mg, 1.86 mmol) in MeOH (9 mL), ketone **12** (201 mg, 0.77 mmol) was added and heated at reflux for 7 hours. The reaction mixture was cooled and concentrated *in vacuo* to provide a 1:0.35 mixture of *E*- and *Z*-isomers. This solid was recrystallised from methanol to provide *Z*-oxime **4** as white needle-like crystals (68 mg, 0.28 mmol, 37%). The remaining supernatant was concentrated *in vacuo*, dissolved in *t*-butanol (10 mL) and glacial acetic acid (2 mL) and heated at reflux for 19 hours. The reaction mixture was cooled and concentrated *in vacuo* to provide a beige solid that was recrystallised from methanol to provide further **4** as white needle-like crystals (29.5 mg, 0.12 mmol, 16%). Total combined yield of **4**: 97.3 mg, 0.40 mmol, 53%.

m.p. 233 – 239 °C

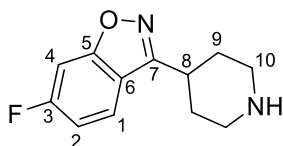
¹H NMR (500 MHz, D₂O) δ_{H} 7.29 (m, 1H), 7.14 – 7.05 (complex m, 2H), 3.45 (dt, J = 13.1, 3.8 Hz, 2H), 3.04 (td, J = 12.7, 3.0 Hz, 2H), 2.91 (tt, J = 11.3, 3.5 Hz, 1H), 2.09 (br d, 2H), 1.77 (dtd, J = 15.6, 11.8, 4.0 Hz, 2H).

¹³C NMR (126 MHz, D₂O) δ_{C} 163.4 (dd, J = 248.9, 12.1 Hz) 158.7 (dd, J = 248.0, 12.1 Hz) 157.1, 129.9 (dd, J = 10.0, 5.6 Hz) 116.3 (dd, J = 18.5, 4.0 Hz) 112.0 (dd, J = 22.0, 3.3 Hz, 104.3 (t, J = 26.0 Hz), 43.5, 38.8, 25.5.

HRMS: m/z C₁₂H₁₅F₂N₂O⁺ [M+H]⁺ calcd. 241.1147 found 241.1156 (Δ 3.7 ppm).

The experimental data obtained matches those previously reported.⁹⁷

6-Fluoro-3-(piperidin-4-yl)benzo[d]isoxazole (3)



A solution of KOH (614 mg, 11 mmol) dissolved in H₂O (2.00 mL) was added to oxime **4** (55.1 mg, 0.23 mmol) and heated at reflux for 6.5 hours. The solution was cooled and extracted with CH₂Cl₂ (3 x 10 mL). The organic fractions were combined, dried (MgSO₄) and concentrated *in vacuo* to provide benzisoxazole **3** as an off white powder (41.7 mg, 0.19 mmol, 83%).

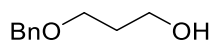
¹H NMR (500 MHz, CDCl₃) δ_{H} 7.68 (dd, J = 8.6, 5.1 Hz, 1H, H-1), 7.23 (dd, J = 8.6, 2.1 Hz, 1H, H-4), 7.04 (td, J = 8.9, 2.3 Hz, 1H, H-2), 3.23 (dt, J = 12.4, 3.6 Hz, 2H, H-10a), 3.19 (tt, J = 11.7, 3.7 Hz, 1H, H-8) 2.81 (td, J = 12.1, 2.8 Hz, 2H, H-10b), 2.04 (dd, J = 12.9, 3.3 Hz, 2H, H-9a), 1.93 (qd, J = 11.8, 4.0 Hz, 2H, H-9b).

¹³C NMR (126 MHz, CDCl₃) δ_{C} 164.1 (d, J = 250.4 Hz, C, C-3), 164.0 (d, J = 13.5 Hz, C, C-5), 161.4 (C, C-7), 122.7 (d, J = 11.1 Hz, CH, C-1), 117.4 (C, C-6), 112.4 (d, J = 25.2 Hz, CH, C-2), 97.6 (d, J = 26.8 Hz, CH, C-4), 46.6 (CH₂, C-10), 35.1 (CH, C-8), 31.7 (CH₂, C-9).

HRMS: m/z C₁₂H₁₄FN₂O⁺ [M+H]⁺ calcd. 221.1085, found 221.1085 (Δ 0.0 ppm).

The experimental data obtained matches those previously reported.⁹⁷

3-(Benzyloxy)propan-1-ol (**13**)



To a solution of Ag_2O (1.672 g, 7.28 mmol) suspended in CH_2Cl_2 (18 mL), 1,3-propanediol (0.48 mL, 6.65 mmol) was added. The solution was stirred for 15 minutes until small clumps of Ag_2O formed in the clear solution. The solution was then cooled in an ice-salt bath for 10 minutes. Benzyl bromide (0.82 mL, 6.94 mmol) was added dropwise over 15 minutes. The ice bath was removed and the solution stirred for 23 hours, after which a precipitate was free flowing in solution. The solution was filtered through a silica plug and concentrated *in vacuo* to afford **13** as a yellow oil (1.106 g, 6.65 mmol, 100%) containing 20:1 mono:dibenzylated product which was used without purification in the subsequent step.

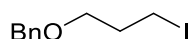
^1H NMR (500 MHz, CDCl_3) δ_{H} 7.40-7.27 (complex m, 5H), 4.53 (s, 2H), 3.79 (t, $J = 5.7$ Hz, 2H), 3.67 (t, $J = 5.7$ Hz, 2H), 1.88 (quin, $J = 5.7$ Hz, 2H).

^{13}C NMR (126 MHz, CDCl_3) δ_{C} 128.6, 127.9, 127.8, 73.5, 69.7, 62.2, 32.2.

HRMS: m/z $\text{C}_{10}\text{H}_{15}\text{O}_2^+$ $[\text{M}+\text{H}]^+$ calcd. 167.1067, found 167.1065 (Δ 1.2 ppm).

The experimental data obtained matches those previously reported.^{98, 116}

3-Benzyloxy-1-iodopropane (**15**)



To alcohol **13** (1.106 g, 6.65 mmol), PPh_3 (2.645 g, 10.1 mmol), imidazole (1.111 g, 16.3 mmol) and dry Et_2O (36 mL) were added. The resulting solution was cooled in an ice bath and CH_3CN (12 mL) added. Once the PPh_3 had dissolved, a solution of I_2 (2.494 g, 9.83 mmol) in Et_2O (13 mL) was added dropwise, causing the formation of a white precipitate. The solution was allowed to warm to room temperature and stir for 2.5 hours, after which further I_2 (1.416 g, 5.58 mmol) was added as a solid directly to the reaction mixture and stirring continued for a further 3.5 hours. The solution was then filtered through cotton wool and rinsed with Et_2O . Sat. aqueous NaHCO_3 (20 mL) was added to the filtered solution which was stirred vigorously and the phases separated. The organic layer was washed with sat. aqueous $\text{Na}_2\text{S}_2\text{O}_3$ (3x 20 mL), brine (1x 20 mL) and concentrated *in vacuo* to give a yellow oil. The oil was then taken up in 5:1 hexanes: EtOAc (20 mL) and shaken to produce a white precipitate in a clear solution.

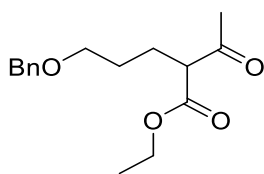
Filtration through a silica plug and concentration of the filtrate *in vacuo* afforded iodide **15** as a yellow oil (1.257 g, 4.92 mmol, 74%). (74% over 2 steps).

¹H NMR (500 MHz, CDCl₃) δ_{H} 7.40 – 7.27 (complex m, 5H), 4.52 (s, 2H), 3.55 (t, $J = 5.7$ Hz, 2H), 3.31, (t, $J = 6.8$ Hz, 2H), 2.10 (tt, $J = 6.8, 5.8$ Hz, 2H).

¹³C NMR (126 MHz, CDCl₃) δ_{C} 138.4, 128.6, 127.8 (2 overlapping peaks), 73.3, 69.7, 33.6, 3.6.

The experimental data obtained matches those previously reported.^{98, 117}

Ethyl 2-acetyl-5-(benzyloxy)pentanoate (**17**)



To a solution of freshly cut sodium (0.55 g, 2.4 mmol) dissolved in EtOH (10 mL, dried over 3 Å sieves) was added ethyl acetoacetate (0.25 mL, 1.97 mmol) and the reaction heated at reflux. Once refluxing, a solution of iodide **15** (480 mg, 1.74 mmol) in EtOH (2 mL) was added dropwise. Reflux was continued for 2.5 hours after which the solution was cooled, filtered through a silica plug with ethanol (3 x 5 mL) and concentrated *in vacuo* to give a yellow oil and white precipitate. This slurry was taken up in 5:1 PE:EtOAc, filtered through a silica plug and concentrated *in vacuo* to afford a yellow oil. Silica gel chromatography (40:1 CH₂Cl₂:EtOAc) provided **17** as a slightly yellow oil that was used immediately (275 mg, 0.99 mmol, 57%).

R_f 0.33 (40:1 CH₂Cl₂:EtOAc)

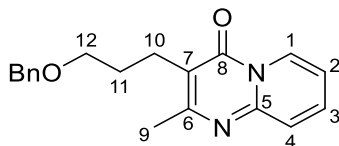
¹H NMR (500 MHz, CDCl₃) δ_{H} 7.36 – 7.27 (complex m, 5H), 4.49 (s, 2H), 4.19 (qd, $J = 6.9, 2.3$ Hz, 2H), 3.48 (td, $J = 6.3, 1.5$ Hz, 2H), 3.46 (t, $J = 7.6$ Hz, 2H), 2.21 (s, 3H), 1.95 (q, $J = 7.7$ Hz, 2H), 1.61 (m, 2H), 1.26 (t, $J = 7.1$ Hz, 3H).

¹³C NMR (126 MHz, CDCl₃) δ_{C} 203.4, 169.9, 138.5, 128.5, 127.8, 127.7, 73.1, 69.8, 61.5, 59.6, 29.0, 27.6, 25.2, 14.2.

HRMS: m/z C₁₆H₂₃O₄⁺ [M+H]⁺ calcd. 279.1591, found 279.1591 (Δ 0.0 ppm).

The experimental data obtained matches those previously reported.^{98, 118}

3-(3-(Benzyloxy)propyl)-2-methyl-4H-pyrido[1,2-*a*]pyrimidin-4-one (19)



A mixture of pentanoate **17** (1.277 g, 4.56 mmol), 2-aminopyridine (434 mg, 4.6 mmol) and ammonium acetate (12.484 g, 0.16 mol) was set to stir vigorously at 180 °C for 3.5 hours. Upon reaching 120 °C, the ammonium salt melted providing a viscous 2-phase solution which became a single brown phase at 180 °C. The reaction mixture was then cooled, diluted with H₂O (20 mL) and extracted with CH₂Cl₂ (3 x 20 mL). The organic fractions were combined, washed with sat. aqueous NaHCO₃ (20 mL) and brine (20 mL), then dried (MgSO₄) and concentrated *in vacuo* to afford **19** as a viscous brown oil (1.196 g, 3.88 mmol, 85% crude yield). Silica gel chromatography (EtOAc + 0.5% triethylamine) provided the title compound (**19**) as a slightly yellow oil (901 mg, 2.92 mmol, 64%).

R_f 0.25 (EtOAc + 0.5% triethylamine).

¹H NMR (500 MHz, CDCl₃) δ_H 8.95 (d, *J* = 7.0 Hz, 1H, H-1), 7.61 (ddd, *J* = 9.0, 6.5, 1.4 Hz, 1H, H-3), 7.53 (d, *J* = 8.8 Hz, 1H, H-4), 7.35 – 7.22 (complex m, 5H, Bn), 7.03 (t, *J* = 6.8 Hz, 1H, H-2), 4.51 (s, 2H, PhCH₂), 3.55 (t, *J* = 6.3 Hz, 2H, H-12), 2.81 (t, *J* = 7.5 Hz, 2H, H-10), 2.51 (s, 3H, H-9), 1.96 – 1.87 (m, 2H, H-11).

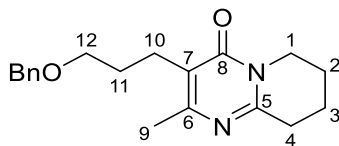
¹³C NMR (126 MHz, CDCl₃) δ_C 161.5 (C, C-6), 158.0 (C, C-8), 148.5 (C, C-5), 138.7 (C, Bn), 134.9 (CH, C-3), 128.4 (CH, Bn), 127.7 (CH, Bn), 127.6 (CH, Bn), 127.1 (CH, C-1), 125.7 (CH, C-4), 115.7 (C, C-7), 114.8 (CH, C-2), 72.9 (CH₂, PhCH₂), 70.0 (CH₂, C-12), 28.4 (CH₂, C-11), 23.7 (CH₂, C-10), 22.4 (CH₃, C-9).

HRMS: *m/z* C₁₉H₂₁N₂O₂⁺ [M+H]⁺ calcd. 309.1598, found 309.1601 (Δ 1.0 ppm).

IR: (neat) ν_{max} 2928, 2856, 1735, 1665, 1635, 1531, 1474, 1427, 1327, 1095, 1044, 768, 731, 697 cm⁻¹.

The experimental data obtained matches those previously reported.⁹⁸

3-(3-(Benzyloxy)propyl)-2-methyl-6,7,8,9-tetrahydro-4H-pyrido[1,2- α]pyrimidin-4-one
(21)



A Schlenk tube fitted with a Youngs tap was charged with **19** (112 mg, 0.36 mmol), palladium on activated carbon (10% w/w, 11.2 mg, 0.11 mmol), MeOH (0.8 mL) and H₂O (0.7 mL). The tube was flushed with N₂ and evacuated 5 times, then charged with H₂ under balloon pressure. Stirring for 4 days provided a suspension that was filtered through Celite[®] to afford a clear solution that was concentrated *in vacuo* to provide a yellow oil. Silica gel chromatography (5:1 EtOAc:Acetone + 0.5% triethylamine) provided the title compound (**21**) as a yellow oil (42.4 mg, 0.14 mmol, 38%).

R_f 0.35 (5:1 EtOAc: acetone).

¹H NMR (500 MHz, CDCl₃) δ _H 7.35 – 7.26 (m, 5H, Bn), 4.50 (s, 2H, PhCH₂), 3.90 (t, *J* = 6.2 Hz, 2H, H-1), 3.52 (t, *J* = 6.3 Hz, 2H, H-12), 2.86 (t, *J* = 6.7 Hz, 2H, H-4), 2.61 (t, *J* = 7.8 Hz, 2H, H-10), 2.28 (s, 3H, H-9), 1.97 – 1.90 (m, 2H, H-2), 1.89 – 1.79 (m, 4H, H-3,11).

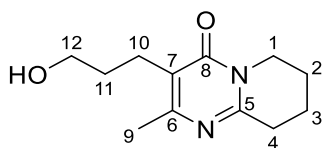
¹³C NMR (126 MHz, CDCl₃) δ _C 162.7 (C, C-8), 158.1 (C, C-6), 155.9 (C, C-5), 138.8 (C, Bn) 128.5(CH, Bn), 127.7 (CH, Bn), 127.6 (CH, Bn), 121.2 (C, C-7), 72.9 (CH₂, PhCH₂), 70.1 (CH₂, C-12), 42.8 (CH₂, C-1), 31.4 (CH₂, C-4), 28.2 (CH₂, C-11), 23.1 (CH₂, C-10), 22.1 (CH₂, C-2), 21.2 (CH₃, C-9), 19.4 (CH₂, C-3).

HRMS: *m/z* C₁₉H₂₅N₂O₂⁺ [M+H]⁺ calcd. 313.1911, found 313.1898 (Δ 4.2 ppm).

IR: (neat) ν_{\max} 2947, 2861, 1652, 1534, 1192, 1099, 738, 698 cm⁻¹.

The experimental data obtained matches those previously reported.⁹⁸

3-(3-Hydroxypropyl)-2-methyl-6,7,8,9-tetrahydro-4H-pyrido[1,2-*a*]pyrimidin-4-one (23)



A solution of benzyl ether **21** (34.7 mg, 0.11 mmol) in CH₂Cl₂ (0.44 mL) was cooled to 0 °C and 1M TiCl₄ in CH₂Cl₂ (0.56 mL, 0.56 mmol, 5 equiv.) was added dropwise resulting in the formation of a yellow precipitate. The solution was then allowed to warm to room temperature and stir for 1 hour. The reaction mixture was then poured into ice cold sat. aqueous NaHCO₃ (20 mL). This solution was extracted with CH₂Cl₂ (3 x 10 mL) and EtOAc (10 mL). The organic fractions were combined, dried (MgSO₄) and concentrated *in vacuo* to provide a yellow oil. Purification by silica gel chromatography (Acetone + 0.5% triethylamine) provided alcohol **23** as an off-white amorphous solid (17.1 mg, 0.77 mmol, 69%).

R_f 0.28 (acetone + 0.5% triethylamine).

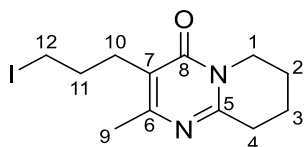
¹H NMR (500 MHz, CDCl₃) δ_H 3.93 (t, *J* = 6.2 Hz, 2H, H-1), 3.49 (br. t, *J* = 5.9 Hz, 2H, H-12), 2.86 (t, *J* = 6.6 Hz, 2H, H-4), 2.66 (t, *J* = 6.7 Hz, 2H, H-10), 2.27 (s, 3H, H-9), 1.98 – 1.92 (m, 2H, H-2), 1.90 – 1.83 (m, 2H, H-3), 1.73 (ddt, *J* = 7.9, 6.6, 5.7 Hz, 2H, H-11).

¹³C NMR (126 MHz, CDCl₃) δ_C 164.1 (C, C-8), 159.3 (C, C-6), 156.0 (C, C-5), 120.5 (C, C-7), 60.4 (CH₂, C-12), 43.2 (CH₂, C-1), 31.5 (CH₂, C-4), 31.1 (CH₂, C-11), 22.1 (CH₂, C-2), 21.4 (CH₂, C-10), 21.2 (CH₃, C-9), 19.3 (CH₂, C-3).

HRMS: *m/z* C₁₂H₁₉N₂O₂⁺ [M+H]⁺ calcd. 223.1441, found 223.1442 (Δ 0.4 ppm).

IR: (neat) ν_{max} 3407, 2931, 2868, 1633, 1528, 1190, 1057, 1041, 729, 606 cm⁻¹.

3-(3-Iodopropyl)-2-methyl-6,7,8,9-tetrahydro-4H-pyrido[1,2-*a*]pyrimidin-4-one (25)



I₂ (32.3 mg, 0.13 mmol) was added to a solution of PPh₃ (44.9 mg, 0.17 mmol) in CH₃CN (1.20 mL) at 0 °C and stirred for 30 minutes to give an orange solution. A solution of alcohol **23** (18.3 mg, 0.08 mmol) in CH₃CN (0.60 mL) was added and the reaction mixture heated at reflux

for 20 hours to give a dark orange solution. The reaction mixture was cooled and concentrated *in vacuo*, then taken up in EtOAc (10 mL) and H₂O (10 mL). The organic layer was washed with H₂O (5x 10 mL), then 1M HCl (10 mL). The aqueous layers were combined and extracted with EtOAc (20 mL). CH₂Cl₂ (20 mL) was added to the aqueous phase and the pH adjusted to 7 by addition of sat. aqueous NaHCO₃. The phases were separated and the aqueous layer extracted with CH₂Cl₂ (2x 20 mL). The CH₂Cl₂ layers were combined, dried (Na₂SO₄) and concentrated *in vacuo* to provide iodide **25** as a yellow solid (21.7 mg, 0.06 mmol, 79%).

m.p. 96 - 100 °C

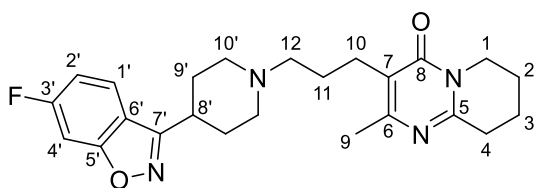
¹H NMR (500 MHz, CDCl₃) δ_H 3.90 (t, *J* = 6.2 Hz, 2H, H-1), 3.22 (t, *J* = 6.9 Hz, 2H, H-12), 2.84 (t, *J* = 6.6 Hz, 2H, H-4), 2.59 (t, *J* = 7.7 Hz, 2H, H-10), 2.29 (s, 3H, H-9), 2.06 – 1.98 (m, 2H, H-11), 1.94 (quin, *J* = 6.1 Hz, 2H, H-2), 1.89 – 1.83 (m, 2H, H-3).

¹³C NMR (126 MHz, CDCl₃) δ_C 162.7 (C, C-8), 158.4 (C, C-6), 156.1 (C, C-5), 119.9 (C, C-7), 42.8 (CH₂, C-1), 32.2 (CH₂, C-11), 31.5 (CH₂, C-4), 27.4 (CH₂, C-10), 22.1 (CH₂, C-2), 21.4 (CH₃, C-9), 19.3 (CH₂, C-3), 6.8 (CH₂, C-12).

HRMS: *m/z* C₁₂H₁₈IN₂O⁺ [M+H]⁺ calcd. 333.0458, found 333.0456 (Δ 0.6 ppm)

IR: (neat) ν_{max} 3389, 2952, 2869, 1651, 1525, 1436, 1397, 1231, 1193, 755, 707, 494 cm⁻¹.

3-(3-(4-(6-Fluorobenzo[d]isoxazol-3-yl)piperidin-1-yl)propyl)-2-methyl-6,7,8,9-tetrahydro-4H-pyrido[1,2-α]pyrimidin-4-one (8)



Iodide **25** (20.0 mg, 0.06 mmol) was dissolved in acetone (1.30 mL). Amine **3** (13.7 mg, 0.06 mmol) was added followed by K₂CO₃ (9.6 mg, 0.07 mmol). The reaction mixture was heated at reflux for 6.5 hours resulting in a dark yellow solution that was cooled and concentrated *in vacuo* to afford a dark orange solid that was then suspended in H₂O (5 mL) and stirred for 1 hour. The water was filtered off, the remaining solid taken up in CH₂Cl₂ and concentrated *in vacuo* to afford a dark orange solid (22.0 mg, 0.05 mmol, 86% crude yield). Purification by

pipette column using diol (acetone) provided analogue **8** as a slightly yellow film (16.1 mg, 0.038 mmol, 63%).

R_f 0.16 (acetone + 0.5% triethylamine)

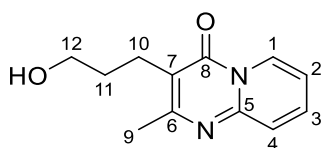
¹H NMR (500 MHz, CDCl₃) δ_H 7.70 (dd, *J* = 8.7, 5.1 Hz, 1H, H-1'), 7.23 (dd, *J* = 8.5, 2.1 Hz, 1H, H-4'), 7.04 (td, *J* = 8.9, 2.2 Hz, 1H, H-2'), 3.92 (t, *J* = 6.2 Hz, 2H, H-1), 3.09 (complex m, 3H, H-8',10'a), 2.85 (t, *J* = 6.7 Hz, 2H, H-4), 2.55 (t, *J* = 7.6 Hz, 2H, H-10), 2.48 (t, *J* = 7.5 Hz, 2H, H-12), 2.29 (s, 3H, H-9), 2.21 – 2.13 (complex m, 2H, H-10'b), 2.10 – 2.04 (complex m, 4H, H-9'), 1.95 (m, 2H, H-2), 1.87 (m, 2H, H-3), 1.79 – 1.70 (m, 2H, H-11).

¹³C NMR (126 MHz, CDCl₃) δ_C 164.1 (d, *J* = 251.2 Hz, C, C-3'), 164.0 (d, *J* = 14.0 Hz, C, C-5'), 162.8 (C, C-8), 161.3 (C, C-7'), 158.0 (C, C-6), 155.8 (C, C-5), 122.8 (d, *J* = 14.0 Hz, CH, C-1'), 121.2 (C, C-7), 117.4 (C, C-6'), 112.5 (d, *J* = 25.4 Hz, CH, C-2'), 97.5 (d, *J* = 26.7 Hz, CH, C-4'), 58.5 (CH₂, C-12), 53.6 (CH₂, C-10'), 42.8 (CH₂, C-1), 34.7 (CH, C-8'), 31.6 (CH₂, C-4), 30.6 (CH₂, C-9'), 25.5 (CH₂, C-11), 24.3 (CH₂, C-10), 22.1 (CH₂, C-2), 21.4 (CH₃, C-9), 19.4 (CH₂, C-3).

HRMS: *m/z* C₂₄H₃₀FN₄O₂⁺ [M+H]⁺ calcd. 425.2347, found 425.2351 (Δ 0.9 ppm)

IR: (neat) ν_{max} 2926, 2805, 2765, 1643, 1613, 1531, 1447, 1270, 1120, 955, 835, 730 cm⁻¹.

3-(3-hydroxypropyl)-2-methyl-4H-pyrido[1,2-*a*]pyrimidin-4-one (**27**)



A solution of benzyl ether **19** (99.2 mg, 0.32 mmol) dissolved in CH₂Cl₂ (1.30 mL) was cooled to 0 °C and 1M TiCl₄ in CH₂Cl₂ (1.60 mL, 1.6 mmol, 5 equiv.) was added dropwise resulting in the formation of a yellow precipitate. The flask was then allowed to warm to room temperature and stir for 1 hour. The reaction mixture was then poured into ice cold sat. aqueous NaHCO₃ (40 mL). This solution was extracted with CH₂Cl₂ (3 x 30 mL) and EtOAc (30 mL). The organic fractions were combined, dried (MgSO₄) and concentrated *in vacuo* to provide a yellow oil. Purification by silica gel chromatography (1:1 EtOAc:Acetone + 0.5% triethylamine) provided the alcohol **27** as a yellow solid (37.2 mg, 0.17 mmol, 53%).

R_f 0.26 (1:1 EtOAc: acetone)

m.p. 85.6 – 89.0 °C

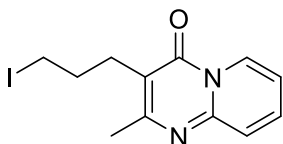
¹H NMR (500 MHz, CDCl₃) δ_H 8.98 (d, *J* = 7.2 Hz, 1H, H-1), 7.67 (ddd, *J* = 9.0, 6.6, 1.6 Hz, 1H, H-3), 7.58 (br. dt, *J* = 9.0, 1.2 Hz, 1H, H-4), 7.11 (ddd, *J* = 7.2, 6.6, 1.4 Hz, 1H, H-2), 3.54 (t, *J* = 5.8 Hz, 2H, H-12), 2.87 (t, *J* = 6.8 Hz, 2H, H-10), 2.52 (s, 3H, H-9), 1.83 (quin, *J* = 6.2 Hz, 2H, H-11).

¹³C NMR (126 MHz, CDCl₃) δ_C 162.6 (C, C-6), 159.2 (C, C-8), 148.4 (C, C-5), 135.2 (CH, C-3), 127.2 (CH, C-1), 125.8 (CH, C-4), 115.4 (CH, C-2), 115.1 (CH, C-7), 60.6 (CH₂, C-12), 31.2 (CH₂, C-11), 22.4 (CH₃, C-9), 22.1 (CH₂, C-10).

HRMS: *m/z* C₁₂H₁₅N₂O₂⁺ [M+H]⁺ calcd. 219.1128, found 219.1122 (Δ 2.7 ppm).

IR: (neat) ν_{max} 3231, 2923, 2863, 1655, 1629, 1527, 1473, 1419, 1253, 1228, 1062, 936, 769, 719, 698, 689, 429 cm⁻¹.

3-(3-Iodopropyl)-2-methyl-4*H*-pyrido[1,2-*α*]pyrimidin-4-one (31)

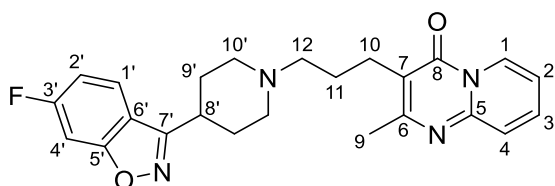


I₂ (27.2 mg, 0.107 mmol) was added to a solution of PPh₃ (36.4 mg, 0.139 mmol) in CH₃CN (1.20 mL) at 0 °C and stirred for 30 minutes. A solution of alcohol **27** (11.8 mg, 0.054 mmol) in CH₃CN (1.20 mL) was added and the reaction mixture heated at reflux for 21 hours to give an orange solution. The reaction mixture was then cooled and concentrated *in vacuo*, then taken up in EtOAc (10 mL) and H₂O (10 mL). The organic layer was washed with H₂O (5x 10 mL), then 1M HCl (10 mL). The aqueous layers were combined and extracted with EtOAc (20 mL). CH₂Cl₂ (20 mL) was added to the aqueous phase and the pH adjusted to 7 by addition of sat. aqueous NaHCO₃. The phases were separated and the aqueous layer extracted with CH₂Cl₂ (3x 20 mL). The CH₂Cl₂ layers were combined, dried (Na₂SO₄) and concentrated *in vacuo* to provide a yellow oil that was determined to be a 1:0.32 mixture of **32:27** by ¹H NMR analysis (12.2 mg, 0.037 mmol, 65% iodide yield). This was used in the next step without further purification.

¹H NMR (500 MHz, CDCl₃) δ_H 8.95 (ddd, *J* = 7.3, 1.6, 0.8 Hz, 1H), 7.64 – 7.61 (m, 1H), 7.53 (br. dt, *J* = 8.9, 1.1 Hz, 1H), 7.06 (ddd, *J* = 7.2, 6.5, 1.4 Hz, 1H), 3.26 (t, *J* = 6.9 Hz, 2H), 2.83 – 2.76 (m, 2H), 2.53 (s, 3H), 2.15 – 2.06 (m, 2H).

HRMS: *m/z* C₁₂H₁₄IN₂O⁺ [M+H]⁺ calcd. 329.0145, found 329.0151 (Δ 1.8 ppm).

3-(3-(4-(6-Fluorobenzo[d]isoxazol-3-yl)piperidin-1-yl)propyl)-2-methyl-4*H*-pyrido[1,2-*α*]pyrimidin-4-one (28)



A 1:0.32 mixture of **32:27** (11.9 mg, 0.036 mmol) was suspended in acetone (1.0 mL). Amine **3** (9.1 mg, 0.041 mmol) was added followed by K₂CO₃ (6.3 mg, 0.046 mmol). The reaction mixture was heated at reflux for 6 hours resulting in a cloudy yellow solution that was cooled and concentrated *in vacuo* to afford a viscous yellow oil that was then suspended in H₂O (5 mL) and stirred for 1 hour. The water was filtered off, the remaining solid concentrated *in vacuo* to afford a light brown solid (14.7 mg, 0.035 mmol, 97% crude yield). Purification by pipette column using diol (acetone) provided analogue **28** as a yellow film (10.3 mg, 0.024 mmol, 67%). (44% over 2 steps).

R_f 0.12 (acetone + 0.5% triethylamine)

¹H NMR (500 MHz, CDCl₃) δ_H 8.97 (ddd, *J* = 7.2, 1.6, 0.8 Hz, 1H, H-1), 7.70 (dd, *J* = 8.7, 5.1 Hz, 1H, H-1'), 7.63 (ddd, *J* = 9.0, 6.6, 1.6 Hz, 1H, H-3), 7.53 (dt, *J* = 8.9, 1.2 Hz, 1H, H-4), 7.23 (dd, *J* = 8.5, 2.1 Hz, 1H, H-4'), 7.08 – 7.02 (m, 2H, H-2,2'), 3.15 – 3.04 (complex m, 3H, H-8',10'a), 2.77 (t, *J* = 7.7 Hz, 2H, H-10), 2.54 (complex m, 5H, H-9,12), 2.24 – 2.15 (complex m, 2H, H-10'b), 2.14 – 2.04 (complex m, 4H, H-9'), 1.90 – 1.81 (m, 2H, H-11).

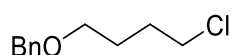
¹³C NMR (126 MHz, CDCl₃) δ_C 164.1 (d, *J* = 251.1 Hz, C, C-3'), 164.0 (d, *J* = 13.6 Hz, C, C-5'), 161.6 (C, C-6), 161.2 (C, C-7'), 158.1 (C, C-8), 148.5 (C, C-5), 134.9 (CH, C-3), 127.1 (CH, C-1), 125.9 (CH, C-4), 122.8 (d, *J* = 11.1 Hz, CH, C-1'), 117.4 (C, C-6'), 115.9 (C, C-7), 114.9 (CH, C-2), 112.5 (d, *J* = 25.3 Hz, CH, C-2'), 97.6 (d, *J* = 26.7 Hz, CH, C-4'), 58.5 (CH₂,

C-12), 53.6 (CH₂, C-10'), 34.7 (CH, C-8'), 30.6 (CH₂, C-9'), 25.6 (CH₂, C-11), 25.0 (CH₂, C-10), 22.7 (CH₃, C-9).

HRMS: m/z C₂₄H₂₆FN₄O₂⁺ [M+H]⁺ calcd. 421.2034, found 421.2035 (Δ 0.2 ppm).

IR: (neat) ν_{\max} 2927, 2805, 2766, 1663, 1635, 1614, 1530, 1474, 1416, 1121, 955, 768, 729 cm⁻¹.

4-Benzyloxy-1-chlorobutane (**14**)

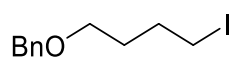


To a solution of 4-chlorobutanol (0.23 mL, 2.3 mmol) in CH₂Cl₂ (11 mL) at 36 °C, benzyl trichloroacetimidate (0.64 mL, 3.5 mmol) was added to give a cloudy yellow solution. Triflic acid (0.02 mL, 0.12 mmol) was added dropwise and the solution stirred for 3 hours before heat was removed and stirring continued for 45 hours. The cloudy yellow mixture was quenched by dropwise addition of pyridine (0.02 mL, 0.25 mmol). The solution was then concentrated *in vacuo* to provide a pink slurry. This was taken up in 14:1 PE:EtOAc and filtered through a silica plug. The filtrate was concentrated *in vacuo* to provide the title compound (**14**) as a colourless oil (234 mg, 1.18 mmol, 51%) containing a 4:1 ratio of **14**:4-chlorobutanol by ¹H NMR analysis. This was used in the next step without further purification.

¹H NMR (500 MHz, CDCl₃) δ_{H} 7.43 – 7.27 (m, 5H), 4.51 (s, 2H), 3.57 (t, J = 6.5 Hz, 2H), 3.51 (t, J = 6.2 Hz, 2H), 1.93 – 1.83 (m, 2H), 1.80 – 1.72 (m, 2H).

The experimental data obtained matches those previously reported.^{98, 119}

4-Benzyloxy-1-iodobutane (**16**)



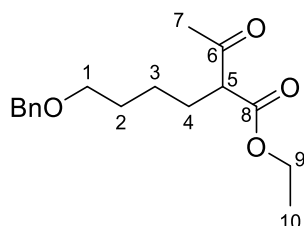
A solution of NaI (1.031 g, 3.5 mmol) dissolved in distilled acetone (5 mL) was added to **14** (234 mg, 1.79 mmol) giving a yellow solution that was heated at reflux for 27 hours. The resulting dark orange solution was concentrated *in vacuo* to provide a wet dark orange crystalline product that was taken up in Et₂O (5 mL), washed with water (2 x 5 mL), brine (5

mL) and dried (MgSO₄). Concentration *in vacuo* afforded iodide **16** as an orange oil (251 mg, 0.87 mmol, 73%). This was used in the next step without further purification.

¹H NMR (500 MHz, CDCl₃) δ_H 7.40 – 7.27 (m, 5H), 4.50 (s, 2H), 3.50 (t, *J* = 6.3 Hz, 2H), 3.21 (t, *J* = 7.1 Hz, 2H), 1.98 – 1.91 (app. quin, 2H), 1.73 (app quin, 2H).

The experimental data obtained matches those previously reported.^{98, 119}

Ethyl 2-acetyl-6-(benzyloxy)hexanoate (**18**)



To a solution of sodium (22 mg, 0.96 mmol) dissolved in ethanol (3 mL), ethyl acetoacetate (0.11 mL, 0.85 mmol) was added and the reaction heated at reflux. A solution of iodide **16** (227 mg, 0.78 mmol) dissolved in ethanol (2 mL) was then added dropwise, giving a brown solution. Reflux was continued for 2.5 hours, after which the reaction was cooled and concentrated *in vacuo* to give a brown slurry. The slurry was then taken up in 5:1 PE:EtOAc, filtered through a silica plug and concentrated *in vacuo* to provide a yellow oil (183.5 mg, 0.63 mmol, 80% crude). Purification by silica gel chromatography (9:1 PE:EtOAc) provided hexanoate **18** as a yellow oil (25.7 mg, 0.09 mmol, 11%). (4% over 3 steps).

R_f 0.18 (9:1 hexanes: EtOAc)

¹H NMR (500 MHz, CDCl₃) δ_H 7.36 – 7.26 (m, 5H, Bn), 4.48 (s, 2H, PhCH₂), 4.19 (qd, *J* = 7.1, 0.9 Hz, 2H, H-9), 3.46 (t, *J* = 6.4 Hz, 2H, H-1), 3.40 (t, *J* = 7.4 Hz, 1H, H-5), 2.21 (s, 3H, H-7), 1.90 – 1.82 (m, 2H, H-4), 1.67 – 1.60 (m, 2H, H-2), 1.42 – 1.33 (m, 2H, H-3), 1.26 (t, *J* = 7.1 Hz, 3H, H-10).

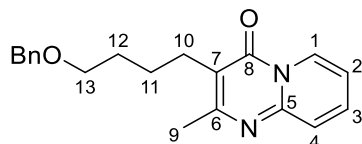
¹³C NMR (126 MHz, CDCl₃) δ_C 203.4 (C, C-6), 169.9 (C, C-8), 138.6 (C, Bn), 128.5 (CH, Bn), 127.8 (CH, Bn), 127.7 (CH, Bn), 73.0 (CH₂, PhCH₂), 70.0 (CH₂, C-1), 61.4 (CH₂, C-9), 60.0 (CH, C-5), 29.6 (CH₂, C-2), 28.9 (CH₃, C-7), 28.1 (CH₂, C-4), 24.3 (CH₂, C-3), 14.2 (CH₃, C-10).

HRMS: *m/z* C₁₇H₂₅O₄⁺ [M+H]⁺ calcd. 293.1747, found 293.1755 (Δ 2.7 ppm).

IR: (neat) ν_{\max} 2935, 2862, 1737, 1713, 1454, 1360, 1097, 737, 698 cm^{-1} .

The experimental data obtained matches those previously reported.⁹⁸

3-(4-(Benzyloxy)butyl)-2-methyl-4*H*-pyrido[1,2-*a*]pyrimidin-4-one (20)



A mixture of hexanoate **18** (20.7 mg, 0.07 mmol), 2-aminopyridine (7.5 mg, 0.08 mmol) and ammonium acetate (0.687 g, 8.9 mmol) was set to stir at 180 °C. At 120 °C the ammonium salt melted giving a viscous brown solution which became a clear brown mixture at 180 °C. After 1 hour, more ammonium acetate (1.106 g, 14.3 mmol) was added. After 3 hours, the reaction mixture was cooled and diluted with H₂O (10 mL). The aqueous solution was extracted with CH₂Cl₂ (4x 10 mL), the organic fractions combined and washed with sat. aqueous NaHCO₃ (10 mL) and brine (10 mL), then dried (MgSO₄) and concentrated *in vacuo* to provide a brown oil. Purification by silica gel chromatography (EtOAc + 0.5% triethylamine) provided the title compound (**20**) as a yellow oil (9.6 mg, 0.03 mmol, 42%).

R_f 0.37 (EtOAc + 0.5% triethylamine)

¹H NMR (500 MHz, CDCl₃) δ_{H} 8.97 (ddd, $J = 7.2, 1.6, 0.8$ Hz, 1H, H-1), 7.62 (ddd, $J = 9.0, 6.5, 1.6$ Hz, 1H, H-3), 7.54 (d, $J = 8.7$ Hz, 1H, H-4), 7.36 – 7.27 (m, 5H, Bn), 7.05 (ddd, $J = 7.2, 6.5, 1.4$ Hz, 1H, H-2), 4.50 (s, 2H, PhCH₂), 3.52 (t, $J = 6.4$ Hz, 2H, H-13), 2.74 (t, $J = 7.8$ Hz, 2H, H-10), 2.50 (s, 3H, H-9), 1.74 (m, 2H, H-12), 1.67 (m, 2H, H-11).

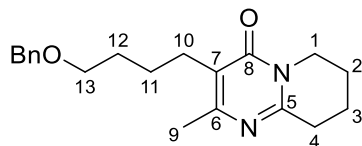
¹³C NMR (126 MHz, CDCl₃) δ_{C} 161.3 (C, C-6), 158.1 (C, C-8), 148.5 (C, C-5), 138.8 (C, Bn), 134.9 (CH, C-3), 128.5 (CH, Bn), 127.8 (CH, Bn), 127.6 (CH, Bn), 127.2 (CH, C-1), 125.8 (CH, C-4), 116.2 (C, C-7), 114.9 (CH, C-2), 73.1 (CH₂, PhCH₂), 70.4 (CH₂, C-13), 29.9 (CH₂, C-12), 26.8 (CH₂, C-10), 25.2 (CH₂, C-11), 22.6 (CH₃, C-9).

HRMS: m/z C₂₀H₂₃N₂O₂⁺ [M+H]⁺ calcd. 323.1754, found 323.1760 (Δ 1.9 ppm).

IR: (neat) ν_{\max} 2926, 2855, 1663, 1635, 1530, 1474, 1426, 1098, 768, 735, 696, 607 cm^{-1} .

The experimental data obtained matches those previously reported.⁹⁸

3-(4-(Benzyloxy)butyl)-2-methyl-6,7,8,9-tetrahydro-4H-pyrido[1,2- α]pyrimidin-4-one
(22)



A Schlenk tube fitted with a Youngs tap was charged with **20** (35.6 mg, 0.11 mmol), palladium with 10% activated carbon (4 mg, 10% w/w), MeOH (0.40 mL) and H₂O (0.35 mL). The tube was flushed with N₂ and evacuated 5 times, then charged with H₂ under balloon pressure. Stirring for 5 days provided a suspension that was filtered through Celite® to afford a clear solution that was concentrated *in vacuo* to provide a brown oil. Silica gel chromatography (EtOAc + 0.5% triethylamine) provided the title compound (**22**) as a clear oil (22.7 mg, 0.07 mmol, 63%).

R_f 0.16 (EtOAc + 0.5% triethylamine)

¹H NMR (500 MHz, CDCl₃) δ_{H} 7.35 – 7.26 (m, 5H, Bn), 4.49 (s, 2H, PhCH₂), 3.91 (t, J = 6.2 Hz, 2H, H-1), 3.50 (t, J = 6.6 Hz, 2H, H-13), 2.84 (t, J = 6.7 Hz, 2H, H-4), 2.53 (t, J = 7.7 Hz, 2H, H-10), 2.25 (s, 3H, H-9), 1.98 – 1.91 (m, 2H, H-2), 1.89 – 1.83 (m, 2H, H-3), 1.73 – 1.65 (m, 2H, H-12), 1.61 – 1.53 (m, 2H, H-11).

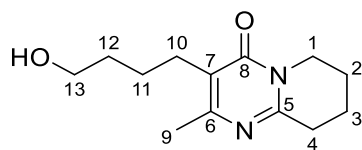
¹³C NMR (126 MHz, CDCl₃) δ_{C} 162.8 (C, C-8), 157.9 (C, C-6), 155.7 (C, C-5), 138.8 (C, Bn), 128.5 (CH, Bn), 127.8 (CH, Bn), 127.6 (CH, Bn), 121.5 (C, C-7), 73.1 (CH₂, PhCH₂), 70.5 (CH₂, C-13), 42.8 (CH₂, C-1), 31.6 (CH₂, C-4), 29.9 (CH₂, C-12), 26.1 (CH₂, C-10), 25.0 (CH₂, C-11), 22.2 (CH₂, C-2), 21.3 (CH₃, C-9), 19.4 (CH₂, C-3).

HRMS: m/z C₂₀H₂₇N₂O₂⁺ [M+H]⁺ calcd. 327.2067, found 327.2068 (Δ 0.3 ppm).

IR: (neat) ν_{max} 2934, 2860, 1649, 1531, 1190, 1096, 734, 698, 607 cm⁻¹.

The experimental data obtained matches those previously reported.⁹⁸

3-(4-Hydroxybutyl)-2-methyl-6,7,8,9-tetrahydro-4H-pyrido[1,2- α]pyrimidin-4-one (24)



A solution of **22** (209 mg, 0.64 mmol) dissolved in CH₂Cl₂ (2.5 mL) was cooled to 0 °C and 1M TiCl₄ in CH₂Cl₂ (3.2 mL, 3.2 mmol, 5 equiv.) was added dropwise resulting in the formation of a yellow precipitate. The flask was then allowed to warm to room temperature and stir for 1 hour. The reaction mixture was then poured into ice cold sat. aqueous NaHCO₃ (80 mL). This solution was extracted with CH₂Cl₂ (3 x 60 mL) and EtOAc (60 mL). The organic fractions were combined, dried (MgSO₄) and concentrated *in vacuo* to provide a yellow oil. Silica gel chromatography (Acetone + 0.5% triethylamine) provided alcohol **24** as a yellow oil (99.3 mg, 0.42 mmol, 66%).

R_f 0.39 (acetone + 0.5% triethylamine)

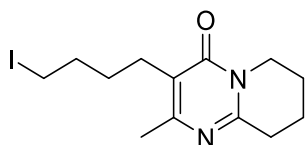
¹H NMR (500 MHz, CDCl₃) δ_{H} 3.92 (t, J = 6.2 Hz, 2H, H-1), 3.71 (t, J = 6.2 Hz, 2H, H-13), 2.89 (t, J = 6.6 Hz, 2H, H-4), 2.54 (t, J = 7.7 Hz, 2H, H-10), 2.29 (s, 3H, H-9) 1.99 – 1.92 (m, 2H, H-2), 1.91 – 1.84 (m, 2H, H-3), 1.67 – 1.53 (complex m, 4H, H-11,12).

¹³C NMR (126 MHz, CDCl₃) δ_{C} 162.8 (C, C-8), 157.8 (C, C-6), 155.8 (C, C-5), 121.6 (C, C-5), 62.5 (CH₂, C-13), 42.9 (CH₂, C-1), 32.3 (CH₂, C-12), 31.4 (CH₂, C-4), 25.6 (CH₂, C-10), 24.5 (CH₂, C-11), 22.1 (CH₂, C-2), 21.2 (CH₃, C-9), 19.3 (CH₂, C-3).

HRMS: m/z C₁₃H₂₁N₂O₂⁺ [M+H]⁺ calcd. 237.1598, found 237.1596 (Δ 0.8 ppm).

IR: (neat) ν_{max} 3284, 2925, 2859, 1637, 1529, 1414, 1191, 1096, 709 cm⁻¹.

3-(4-Iodobutyl)-2-methyl-6,7,8,9-tetrahydro-4H-pyrido[1,2- α]pyrimidin-4-one (26)



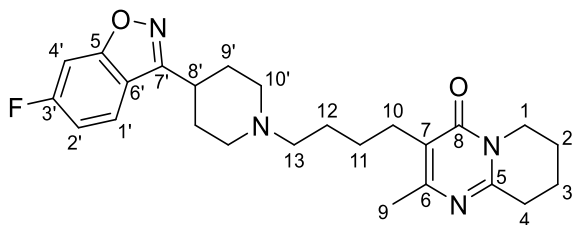
I₂ (51 mg, 0.20 mmol) was added to a solution of PPh₃ (67.1 mg, 0.26 mmol) in CH₃CN (1.80 mL) at 0 °C and stirred for 30 minutes to give an orange solution. A solution of alcohol **24** (29.3 mg, 0.12 mmol) in CH₃CN (0.5 mL) was added and the reaction mixture heated at reflux

for 22 hours to give a yellow solution. The reaction mixture was cooled and concentrated *in vacuo*, then taken up in EtOAc (15 mL) and H₂O (15 mL). The organic layer was washed with H₂O (5x 10 mL), then 1M HCl (10 mL). The aqueous layers were combined and extracted with EtOAc (20 mL). CH₂Cl₂ (20 mL) was added to the aqueous phase and the pH adjusted to 7 by addition of sat. aqueous NaHCO₃. The phases were separated and the aqueous layer extracted with CH₂Cl₂ (2x 20 mL). The CH₂Cl₂ layers were combined, dried (Na₂SO₄) and concentrated *in vacuo* to provide iodide **26** as a yellow oil (38.5 mg, 0.11 mmol, 90%). This was used in the next step without further purification.

¹H NMR (500 MHz, CDCl₃) δ_H 3.93 (t, *J* = 6.1 Hz, 2H), 3.21 (t, *J* = 6.9 Hz, 2H), 3.06 (t, *J* = 6.6 Hz, 2H), 2.52 (t, *J* = 7.8 Hz, 2H), 2.37 (s, 3H), 2.02 – 1.95 (m, 2H), 1.93 – 1.85 (m, 4H), 1.62 – 1.55 (m, 2H).

HRMS: *m/z*, C₁₃H₂₀IN₂O⁺ [M+H]⁺ calcd. 347.0615, found 347.0605 (Δ 2.9 ppm).

3-(4-(4-(6-Fluorobenzo[d]isoxazol-3-yl)piperidin-1-yl)butyl)-2-methyl-6,7,8,9-tetrahydro-4H-pyrido[1,2-*a*]pyrimidin-4-one (9)



Iodide **26** (35.1 mg, 0.101 mmol) was suspended in acetone (2.00 mL). Amine **3** (23.1 mg, 0.105 mmol) was added followed by K₂CO₃ (16.5 mg, 0.119 mmol). The reaction mixture was heated at reflux for 6 hours resulting in a cloudy grey solution that was cooled and concentrated *in vacuo* to afford a sticky grey solid that was then suspended in H₂O (5 mL) and stirred for 1 hour. The water was filtered off and the remaining solid purified by pipette column using diol (Acetone) provided analogue **9** as a clear film (16.1 mg, 0.037 mmol, 36%). (31% over 2 steps).

R_f 0.10 (acetone + 0.5% triethylamine)

¹H NMR (500 MHz, D₂O) δ_H 7.87 (dd, *J* = 8.9, 4.9 Hz, 1H), 7.42 (d, *J* = 8.9, 2.2 Hz, 1H), 7.22 (td, *J* = 9.2, 2.3 Hz, 1H), 3.89 (t, *J* = 6.3 Hz, 2H), 3.61 – 3.45 (complex m, 3H), 3.10 – 2.98 (complex m, 4H), 2.87 (t, *J* = 6.6 Hz, 2H), 2.55 (t, *J* = 7.8 Hz, 2H), 2.37 (br. d, *J* = 14.7 Hz

2H), 2.29 (s, 3H), 2.17 – 2.09 (complex m, 2H), 1.99 – 1.92 (m, 2H), 1.88 – 1.82 (m, 2H), 1.79 – 1.72 (m, 2H), 1.53 (quin, $J = 7.6$ Hz, 2H).

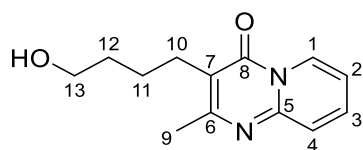
^1H NMR (500 MHz, CDCl_3) δ_{H} 7.75 (dd, $J = 8.7, 5.1$ Hz, 1H, H-1'), 7.22 (dd, $J = 8.5, 2.2$ Hz, 1H, H-4'), 7.04 (td, $J = 8.8, 2.1$ Hz, 1H, H-2'), 3.91 (t, $J = 6.2$ Hz, 2H, H-1), 3.14 (m, 3H, H-8',10'a), 2.84 (t, $J = 6.7$ Hz, 2H, H-4), 2.58 – 2.51 (m, 4H, H-11,12), 2.34 – 2.25 (complex m, 5H, H-9,10'b), 2.22 – 2.16 (complex, 2H, H-9'a), 2.14 – 2.07 (complex m, 2H, H-9'b), 1.98 – 1.91 (m, 2H, H-2), 1.89 – 1.83 (m, 2H, H-3), 1.70 – 1.62 (m, 2H, H-12), 1.56 – 1.49 (m, 2H, H-11).

^{13}C NMR (126 MHz, CDCl_3) δ_{C} 164.1, (d, $J = 250.8$ Hz, C, C-3') 164.0 (d, $J = 13.7$ Hz, C, C-5), 162.8 (C, C-8), 161.0 (C, C-7'), 158.0 (C, C-6), 155.8 (C, C-5), 122.9 (d, $J = 11.0$ Hz, CH, C-1'), 121.3 (C, C-7), 117.3 (C, C-6'), 112.6 (d, $J = 25.3$ Hz, CH, C-2'), 97.5 (d, $J = 26.8$ Hz, CH, C-4'), 58.7 (CH_2 , C-13), 53.4 (CH_2 , C-10'), 42.9 (CH_2 , C-1), 34.2 (CH, C-8'), 31.6 (CH_2 , C-4), 30.0 (CH_2 , C-9'), 26.5 (CH_2 , C-12), 26.2 (CH_2 , C-11), 25.9 (CH_2 , C-10), 22.1 (CH_2 , C-2) 21.3 (CH_3 , C-9), 19.4 (CH_2 , C-3).

HRMS: m/z $\text{C}_{25}\text{H}_{32}\text{FN}_4\text{O}_2^+$ $[\text{M}+\text{H}]^+$ calcd. 439.2504, found 439.2514 (Δ 2.3 ppm).

IR: (neat) ν_{max} 2931, 2807, 2768, 1641, 1613, 1530, 1447, 1271, 1189, 955, 836, 815, 728 cm^{-1} .

3-(4-Hydroxybutyl)-2-methyl-4H-pyrido[1,2- α]pyrimidin-4-one (30)



A solution of **20** (66.7 mg, 0.21 mmol) dissolved in CH_2Cl_2 (0.96 mL) was cooled to 0 °C and 1M TiCl_4 in CH_2Cl_2 (1.04 mL, 1.04 mmol, 5 equiv.) was added dropwise resulting in the formation of a dark red precipitate. The flask was then allowed to warm to room temperature and stir for 1 hour. The reaction mixture was then poured into ice cold sat. aqueous NaHCO_3 (30 mL). This solution was extracted with CH_2Cl_2 (3 x 20 mL) and EtOAc (20 mL). The organic fractions were combined, dried (MgSO_4) and concentrated *in vacuo* to provide a yellow oil. Silica gel chromatography (Acetone + 0.5% triethylamine) provided alcohol **30** as a yellow oil (27.3 mg, 0.12 mmol, 57%).

R_f 0.42 (acetone + 0.5% triethylamine)

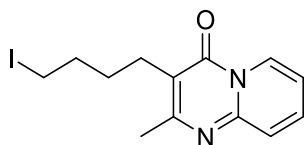
¹H NMR (500 MHz, CDCl₃) δ_H 8.96 (ddd, *J* = 7.2, 1.6, 0.8 Hz, 1H, H-1), 7.62 (ddd, *J* = 9.0, 6.6, 1.6 Hz, 1H, H-3), 7.53 (ddd, *J* = 9.0, 1.4, 0.9 Hz, 1H, H-4), 7.06 (ddd, *J* = 7.2, 6.5, 1.4 Hz, 1H, H-2), 3.72 (br. t, *J* = 6.3 Hz, 2H, H-13), 2.75 (t, *J* = 7.5 Hz, 2H, H-10), 2.51 (s, 3H, H-9), 1.73 – 1.61 (m, 4H, H-11,12).

¹³C NMR (126 MHz, CDCl₃) δ_C 161.5 (C, C-6), 158.2 (C, C-8), 148.5 (C, C-5), 134.9 (CH, C-3), 127.1 (CH, C-1), 125.9 (CH, C-4), 116.2 (C, C-7), 114.9 (CH, C-2), 62.7 (CH₂, C-13), 32.4 (CH₂, C-12), 26.3 (CH₂, C-10), 24.7 (CH₂, C-11), 22.6 (CH₃, C-9).

HRMS: *m/z* C₁₃H₁₇N₂O₂⁺ [M+H]⁺ calcd. 233.1285, found 233.1286 (Δ 0.4 ppm).

IR: (neat) ν_{max} 3448, 2945, 2928, 2856, 1657, 1631, 1527, 1471, 1368, 1219, 1134, 770, 572, 432 cm⁻¹.

3-(4-Iodobutyl)-2-methyl-4*H*-pyrido[1,2-*α*]pyrimidin-4-one (**32**)

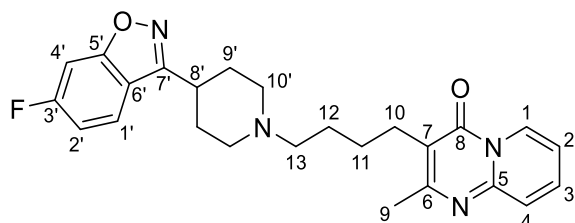


I₂ (30.5 mg, 0.12 mmol) was added to a solution of PPh₃ (39.4 mg, 0.15 mmol) in CH₃CN (1.20 mL) at 0 °C and stirred for 30 minutes to give a yellow solution. A solution of alcohol **30** (17.0 mg, 0.07 mmol) in CH₃CN (0.7 mL) was added and the reaction mixture heated at reflux for 21 hours to give a transparent orange solution. The reaction mixture was cooled and concentrated *in vacuo*, then taken up in EtOAc (10 mL) and H₂O (10 mL). The organic layer was washed with H₂O (5x 10 mL), then 1M HCl (10 mL). The aqueous layers were combined and extracted with EtOAc (20 mL). CH₂Cl₂ (20 mL) was added to the aqueous phase and the pH adjusted to 7 by addition of sat. aqueous NaHCO₃. The phases were separated and the aqueous layer extracted with CH₂Cl₂ (2x 20 mL). The CH₂Cl₂ layers were combined, dried (Na₂SO₄) and concentrated *in vacuo* to provide iodide **32** as a yellow oil (15.0 mg, 0.04 mmol, 60%). This was used in the next step without further purification.

¹H NMR (500 MHz, CDCl₃) δ_H 8.95 (br. d, *J* = 6.8 Hz, 1H), 7.64 – 7.60 (m, 1H), 7.52 (br. d, *J* = 9.0 Hz, 1H), 7.05 (td, *J* = 7.0, 1.7 Hz, 1H), 3.23 (t, *J* = 6.9 Hz, 2H), 2.72 (t, *J* = 7.6 Hz, 2H), 2.50 (s, 3H), 1.93 (quin, *J* = 7.5 Hz, 2H), 1.73 – 1.63 (m, 2H).

HRMS: m/z C₁₃H₁₆IN₂O⁺ [M+H]⁺ calcd. 343.0302, found 343.0306 (Δ 1.2 ppm).

3-(4-(4-(6-Fluorobenzo[d]isoxazol-3-yl)piperidin-1-yl)butyl)-2-methyl-4H-pyrido[1,2- α]pyrimidin-4-one (29)



Iodide **32** (14.5 mg, 0.042 mmol) was suspended in acetone (1 mL). Amine **3** (9.7 mg, 0.044 mmol) was added followed by K₂CO₃ (7.7 mg, 0.052 mmol). The reaction mixture was heated at reflux for 6.5 hours resulting in a cloudy grey solution that was cooled and concentrated *in vacuo* to afford a slightly yellow solid that was then suspended in H₂O (5 mL) and stirred for 1 hour. The water was filtered off, the remaining solid taken up in CH₂Cl₂ and concentrated *in vacuo* to afford a yellow film (17.1 mg, 0.039 mmol, 94% crude yield). Purification by pipette column using diol (acetone) provided analogue **29** as a yellow film (16.0 mg, 0.037 mmol, 88%). (53% over 2 steps).

R_f 0.15 (acetone)

¹H NMR (500 MHz, CDCl₃) δ _H 8.97 (ddd, J = 7.3, 1.6, 0.9 Hz, 1H, H-1), 7.74 (dd, J = 8.7, 5.1 Hz, 1H, H-1'), 7.63 (ddd, J = 9.0, 6.6, 1.6 Hz, 1H, H-3), 7.53 (dt, J = 9.0, 1.2 Hz, 1H, H-4), 7.23 (dd, J = 8.5, 2.1 Hz, 1H, H-4'), 7.08 – 7.02 (m, 2H, H-2,2'), 3.10 – 3.02 (m, 3H, H-8',10'a), 2.76 (t, J = 7.5 Hz, 2H, H-10), 2.52 (s, 2H, H-9), 2.44 (t, J = 7.4 Hz 2H, H-13), 2.30 – 2.04 (complex m, 6H, H-9',10'b), 1.69 (m, 2H, H-12), 1.63 (m, 2H, H-11).

¹³C NMR (126 MHz, CDCl₃) δ _C 164.1 (d, J = 251.5 Hz, C, C-3'), 164.0 (d, J = 13.5 Hz, C, C-5'), 161.5 (C, C-7'), 161.2 (C, C-6), 158.1 (C, C-8), 148.5 (C, C-5), 134.9 (CH, C-3), 127.2 (CH, C-1), 125.9 (CH, C-4), 122.9 (d, J = 11.6 Hz, CH, C-1'), 117.4 (C, C-6'), 116.1 (C, C-7), 114.9 (CH, C-2), 112.5 (d, J = 25.3 Hz, CH, C-2'), 97.6 (d, J = 26.5 Hz, CH, C-4'), 58.8 (CH₂, C-13), 53.6 (CH₂, C-10'), 34.5 (CH, C-8'), 30.3 (CH₂, C-9'), 26.8 (CH₂, C-12), 26.8 (CH₂, C-10), 26.5 (CH₂, C-11), 22.6 (CH₃, C-9).

HRMS: m/z C₂₅H₂₈FN₄O₂⁺ [M+H]⁺ calcd. 435.2191, found 435.2199 (Δ 1.8 ppm).

IR: (neat) ν_{max} 3067, 2807, 2767, 1662, 1635, 1613, 1530, 1474, 1426, 1249, 1121, 955, 768. 729 cm^{-1} .

5.2 *In Vitro* Assay Experimental

5.2.1 Cell Culture and *In Vitro* Experiments

5.2.1.1 Quantification of Analogues

Compounds to be quantified were **8**, **9**, **28** and **29**. Following the methodology of West,¹³⁸ the compound to be quantified was dissolved in CDCl_3 (500 μL) and an approximately equimolar amount of CH_3NH_2 , also dissolved in CDCl_3 , was added. The solutions were sonicated, transferred to 5 mm NMR tubes and sealed with parafilm. ^1H NMR spectra for quantification were collected on a JEOL JNM-ECZ600R NMR spectrometer with the settings described in **Table 7** applied.

Table 7. NMR parameters and settings for quantification experiments.

Parameter	Setting
Temperature	25 °C
Relaxation Delay	15.0 s
Pulse Angle	90.0°
Repetitions	64

5.2.1.2 Compounds for *In Vitro* Use

Analogues synthesised were dissolved in DMSO at a concentration of 10 mM and stored at room temperature until required. Risperidone (Kindly provided by Douglas Pharmaceuticals, Auckland, New Zealand) was dissolved in 0.1 M AcOH (Sigma-Aldrich, MO) at a concentration of 25 mM and stored at -80 °C until required. All stock compounds were stored in single use aliquots to prevent repeated freeze/thaw cycles. Compounds were diluted to the desired concentration in 1% DMSO and complete T-cell media (CTCM) for *in vitro* assays.

5.2.1.3 Culture and Maintenance of RAW 264.7 Macrophage Cell Line

RAW 264.7 cells were a kind gift from Dr. Helen Woolner. According to the methodology of Zareie,¹⁴⁹ 2×10^6 RAW264.7 cells were stored long term by re-suspending cells in cryopreservation medium (see **Appendix 6.2**) and kept in a liquid phase liquid nitrogen storage tank until required. Low passage numbers (<20) RAW264.7 cells were cultured from storage by first thawing the cryovial in a 37 °C water bath, after which its contents were immediately transferred into 9 mL of 37 °C CTCM and centrifuged at 400 x g for 5 minutes to remove the cryopreservation medium. The cell pellet was then re-suspended in 10 mL of 37 °C CTCM and transferred to a T25 tissue culture flask and incubated in a humidified incubator at 37 °C and 5% CO₂ until confluent. At 80% confluency, RAW264.7 cells were passaged by first removing culture medium and adding 5 mL of warm dPBS to wash non-adherent cells/debris to be discarded. 5 mL of cold dPBS is then added to the flask and adherent cells were lifted from the flask by using a cell scraper. The cell suspension was then aspirated and transferred to a 15 mL conical tube and centrifuged at 400 x g for 5 mins and re-suspended in 1 mL of dPBS. Live cells are counted by trypan blue exclusion. 1×10^6 cells are added to 15 mL of CTCM in a T75 culture flask and cultured until 80% confluent.

5.2.1.4 MTT Reduction Assay

Following completion of an experiment, 170 µL/well of supernatant was transferred to a sterile flat bottom 96 well plate and stored at -20 °C or used immediately. 50 µL/well of fresh CTCM warmed to 37 °C was added before adding 20 µL/well of MTT solution (see **Appendix 6.2**) was added to each well. Plates were incubated for a further 2 hours at 37 °C and 5% CO₂. After incubation, the reaction was stopped by adding 100 µL/well of MTT stop solution (see **Appendix 6.2**) and left overnight at 37 °C to solubilize formazan products. Absorbance was measured at 570 nm in a multi-well Enspire 2300 Multilabel plate reader (PerkinElmer, Wellesley, MA). Cell metabolism was calculated as percentage absorbance of indicated control wells.

5.2.2 Cytokine Assays

5.2.2.1 General ELISA Protocol

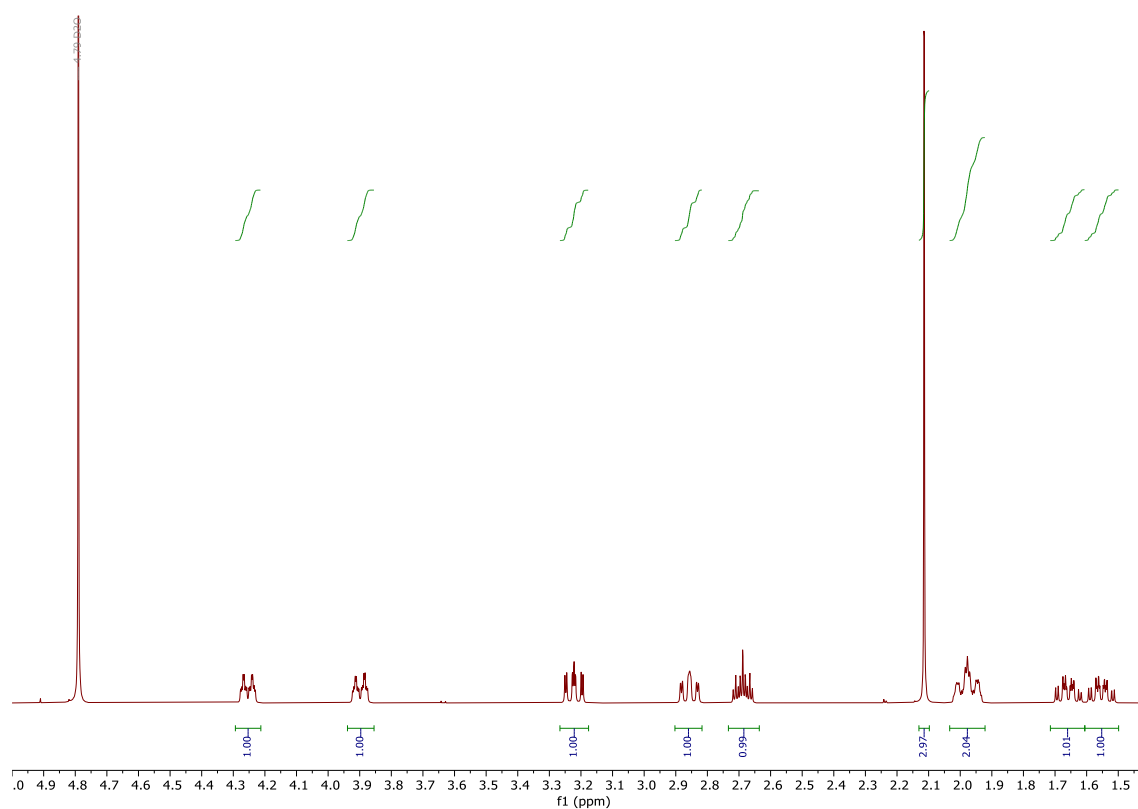
Enzyme linked immunosorbent assays (ELISA) were performed by coating 96-well Nunc

MaxiSorp plates (Thermo Fisher Scientific, MA) with a primary capture antibody in ELISA capture buffer and incubated overnight at 4 °C. Capture antibody solution was removed and plates were washed in wash buffer containing PBS with 0.01% Tween-20 (Sigma-Aldrich, MO) 4 times. Plates were blocked with 10% fetal calf serum (FCS) in dPBS for 2 hours at room temperature, then washed 3 times with wash buffer. 50 µL/well of cytokine standards and samples were then added to each well and incubated for 2 hours RT. The standard curve was prepared by serially diluting in the top two rows of the plate. Plates were then washed 4 times in wash buffer and 50 µL/well of the matched biotinylated secondary antibody was added and incubated RT. After 1 hour plates were washed 6 times in wash buffer and 50 µL/well of streptavidin-horseradish peroxidase (SA-HRP) was added and incubated for a further 1-hour room temperature protected from light. After incubation, plates are washed 8 times and tetramethyl benzidine (TMB) substrates A and B (BD Biosciences, NJ) were brought to room temperature and mixed to equal volumes. 100 µL/well of TMB reagent was added and the reaction was stopped with 100 µL/well 0.18M H₂SO₄. Details for specific ELISA's can be found in **Appendix 6.2**.

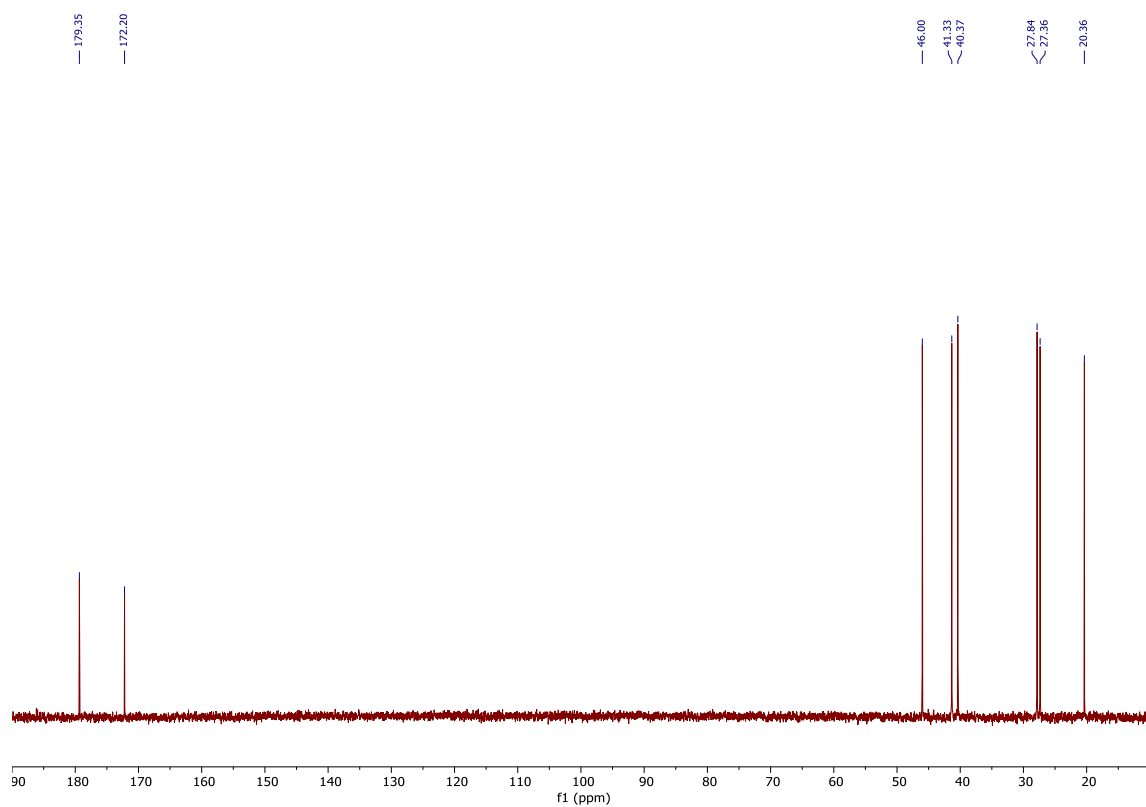
6 Appendix

6.1 NMR Spectra

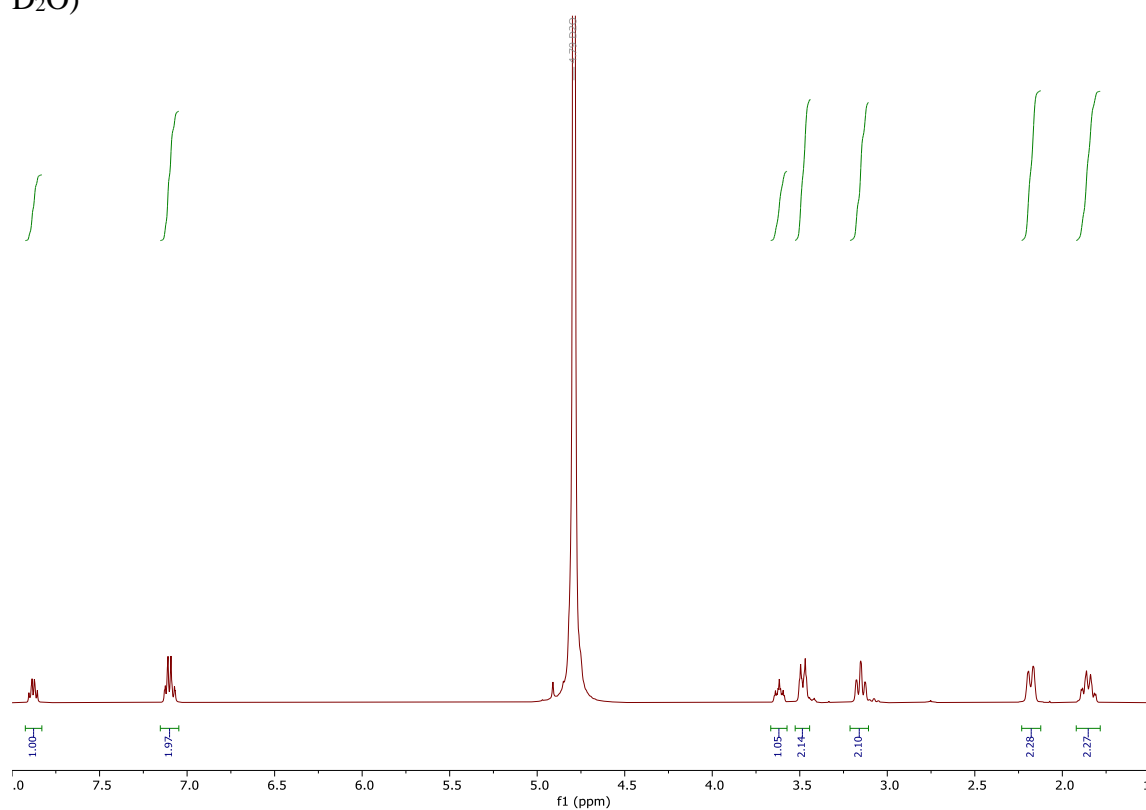
^1H NMR spectrum of 1-Acetylpiperidine-4-carboxylic acid (**10**) (500 MHz, D_2O)



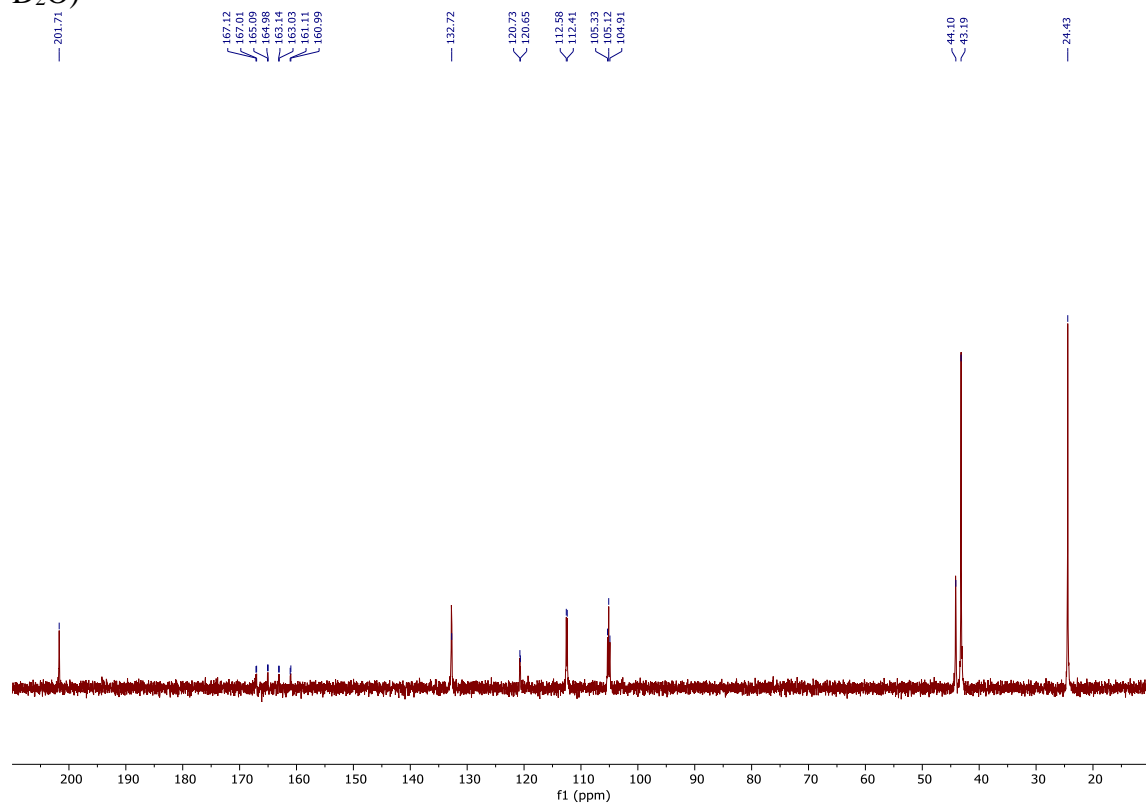
^{13}C NMR spectrum of 1-Acetylpiperidine-4-carboxylic acid (**10**) (126 MHz, D_2O)



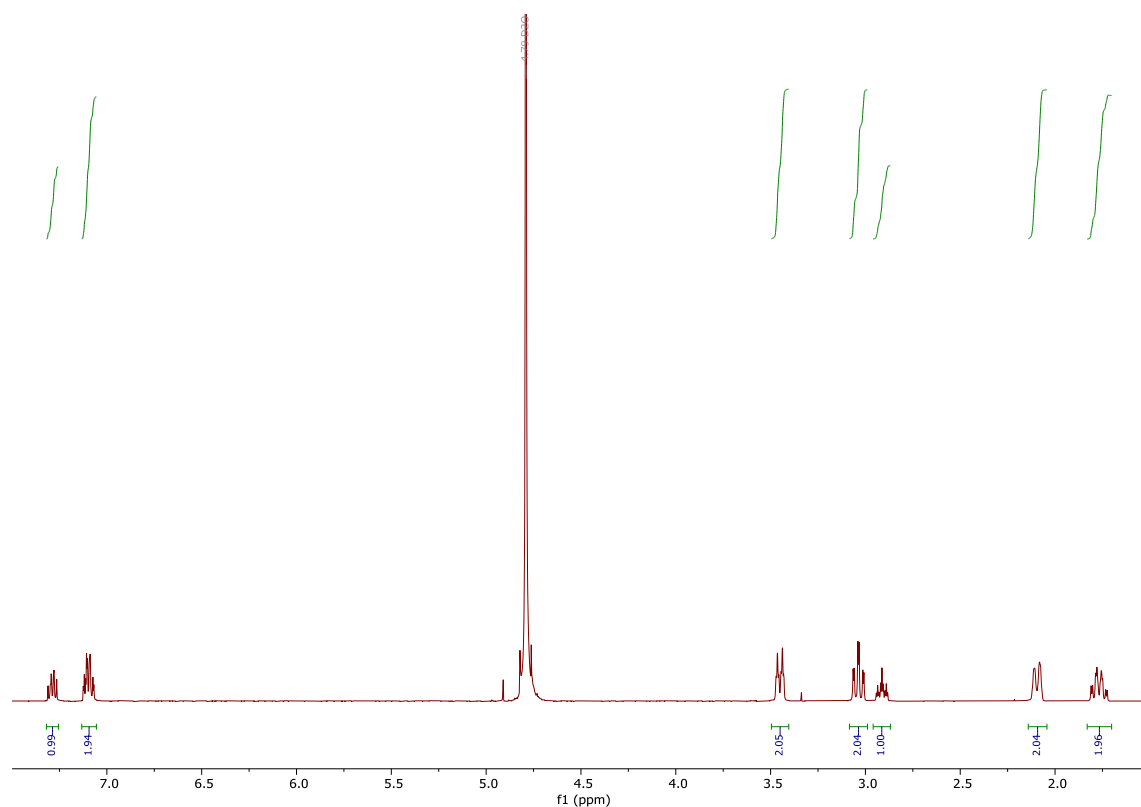
^1H NMR spectrum of 4-(2',4'-Difluorobenzoyl)piperidine hydrochloride (**12**) (500 MHz, D_2O)



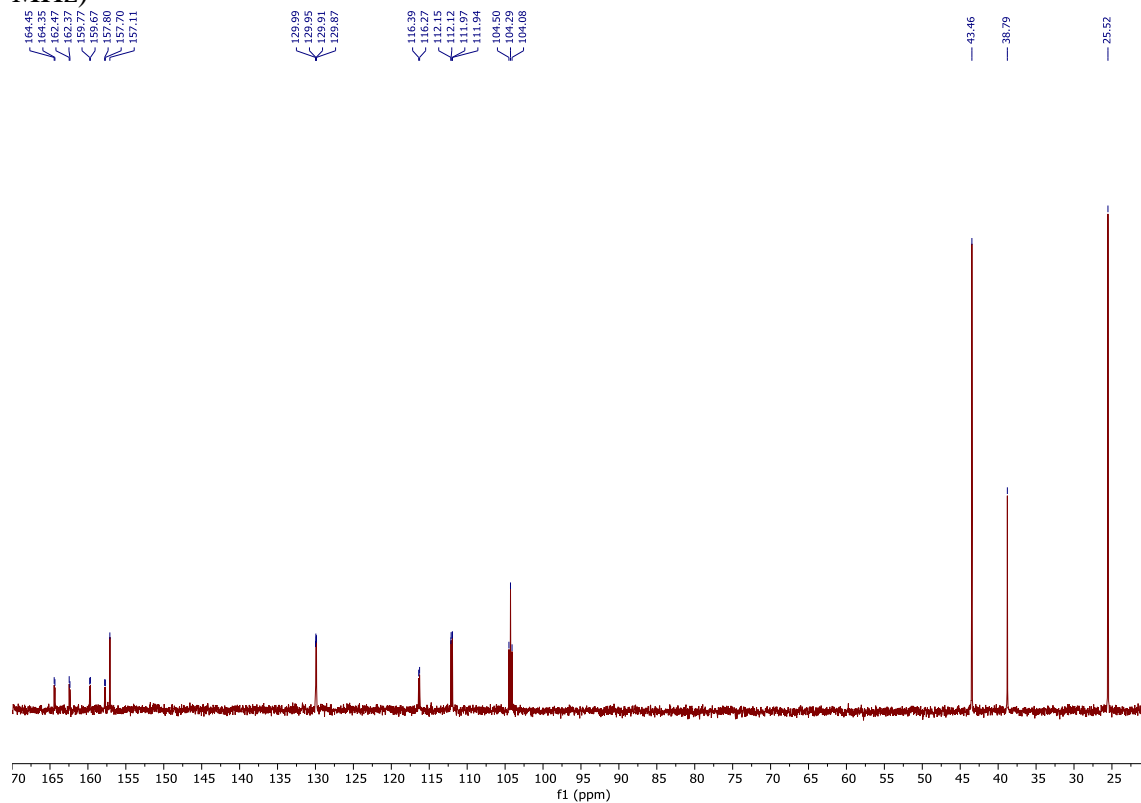
^{13}C NMR spectrum of 4-(2',4'-Difluorobenzoyl)piperidine hydrochloride (**12**) (126 MHz, D_2O)



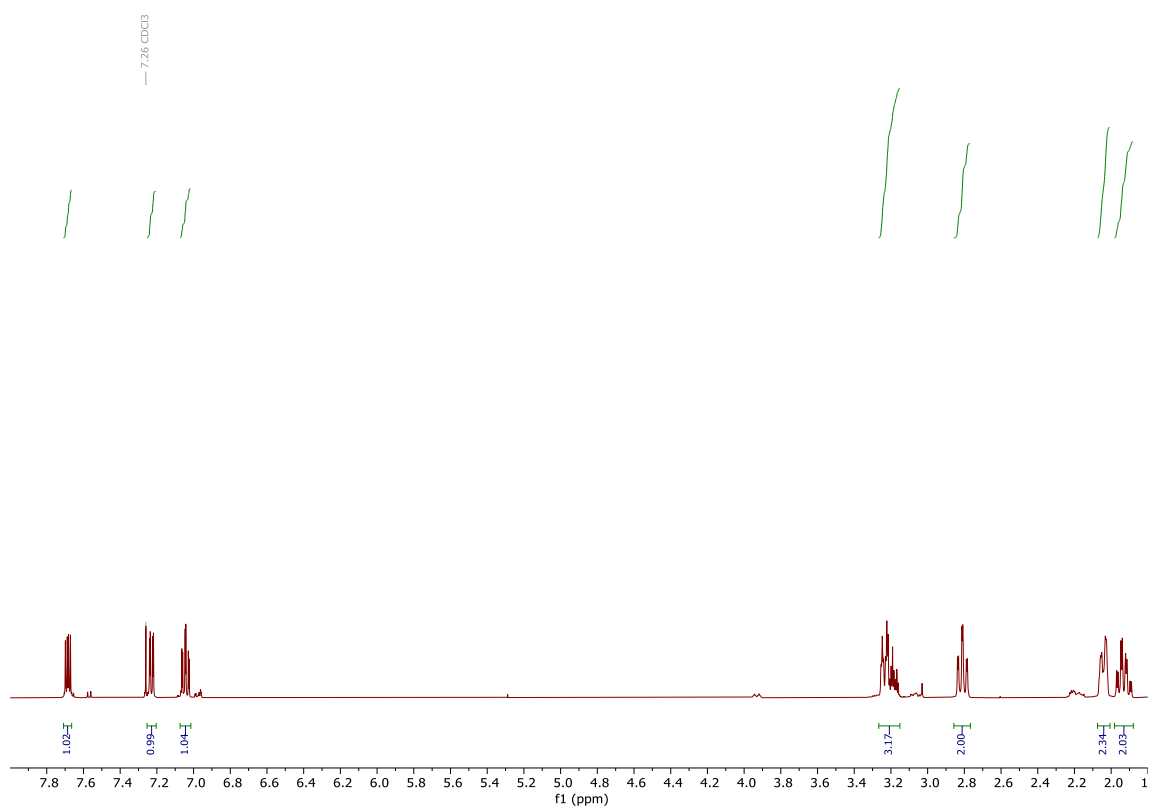
^1H NMR spectrum of (Z)-2,4-Difluorophenyl-(4-piperidiny)methanone oxime (**4**) (D_2O , 500 MHz)



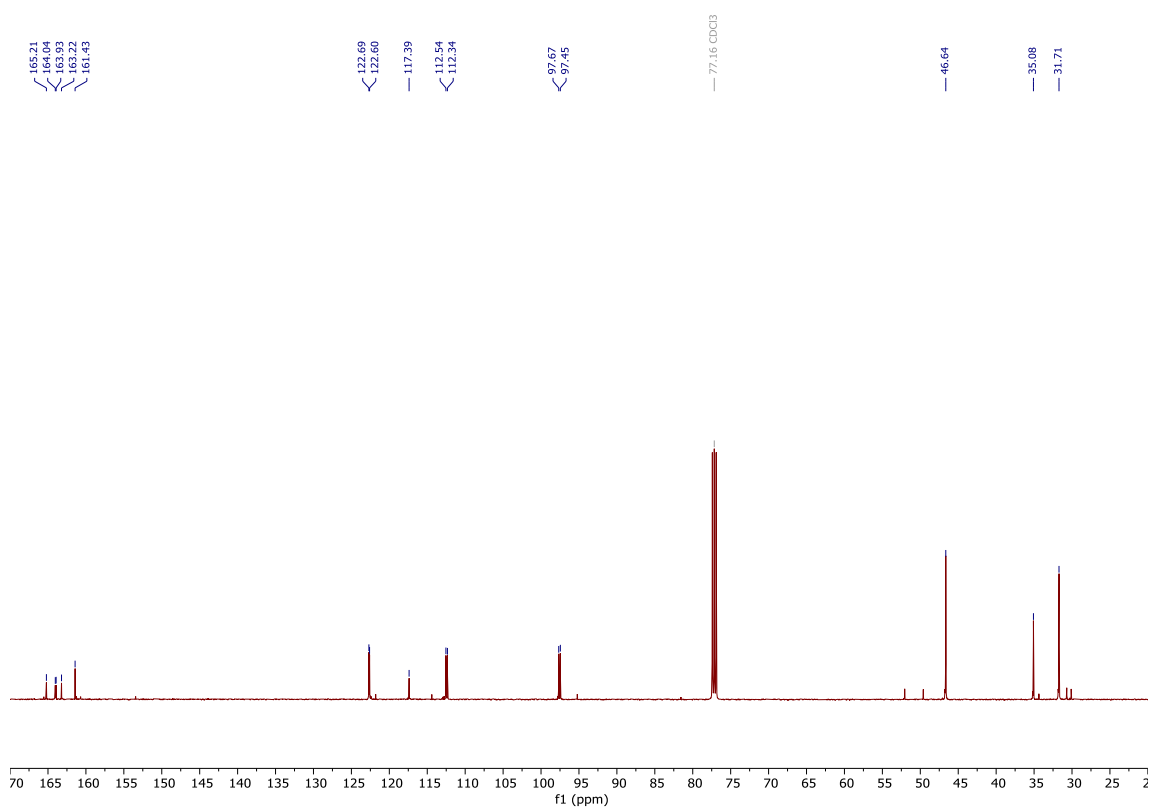
^{13}C NMR spectrum of (Z)-2,4-Difluorophenyl-(4-piperidiny)methanone oxime (**4**) (D_2O , 126 MHz)



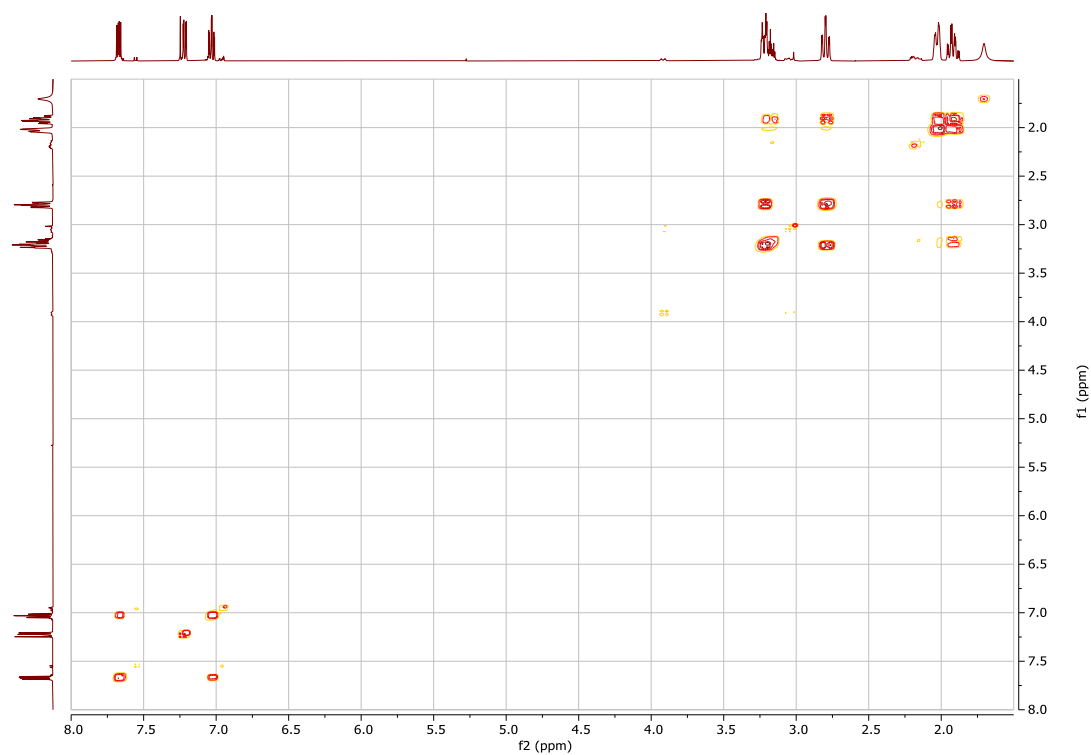
^1H NMR spectrum of 6-Fluoro-3-(piperidin-4-yl)benzo[*d*]isoxazole (**3**) (CDCl_3 , 500 MHz)



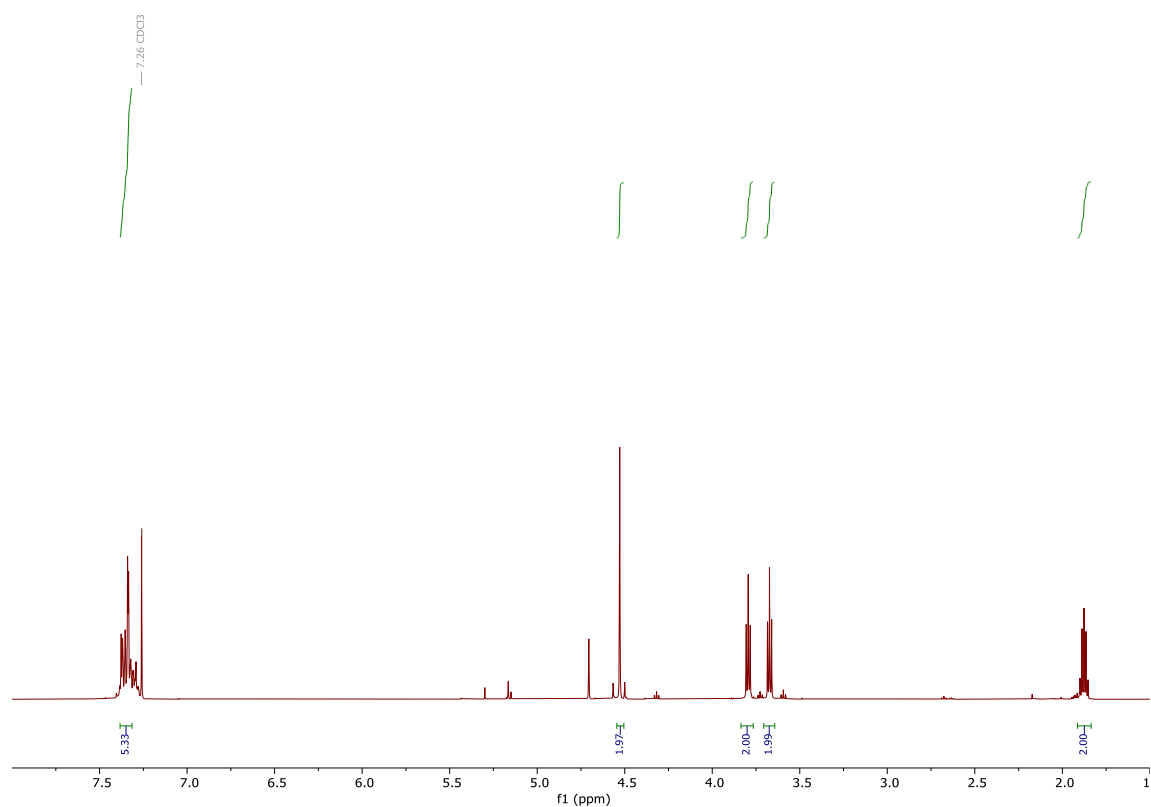
^{13}C NMR spectrum of 6-Fluoro-3-(piperidin-4-yl)benzo[*d*]isoxazole (**3**) (CDCl_3 , 126 MHz)



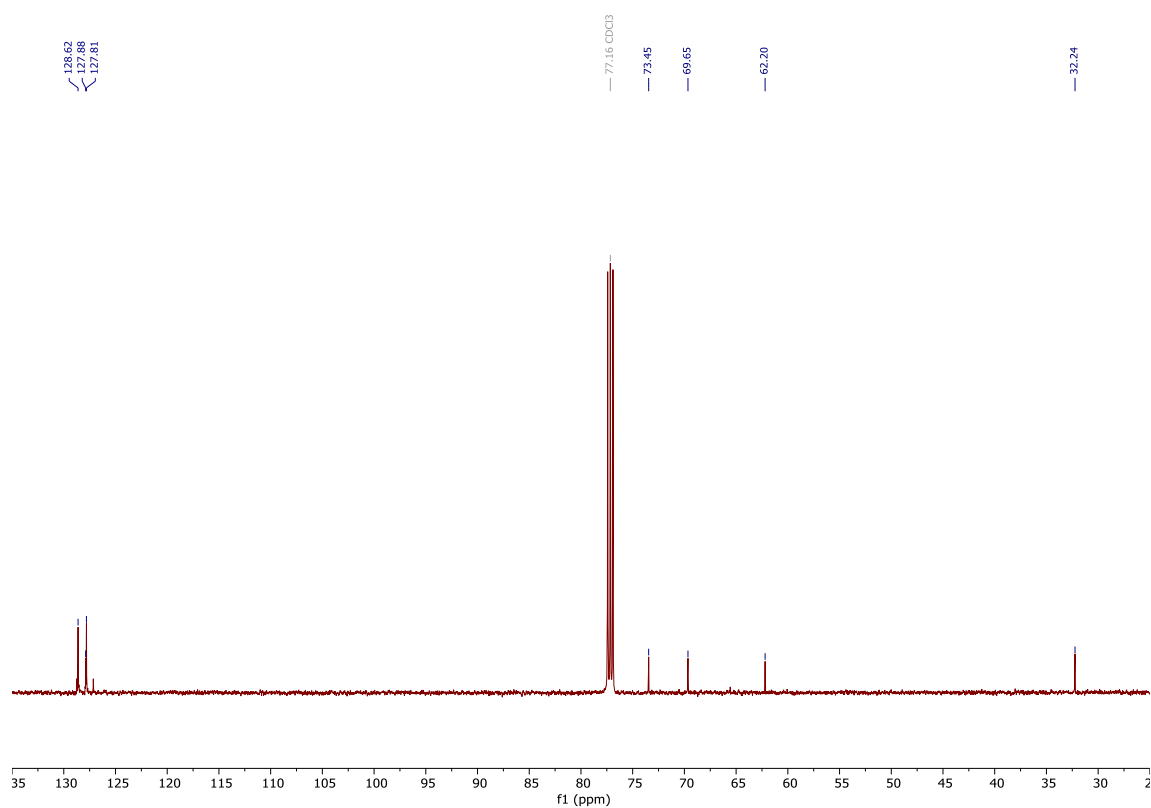
COSY NMR spectrum of 6-Fluoro-3-(piperidin-4-yl)benzo[d]isoxazole (**3**) (CDCl₃, 500 MHz)



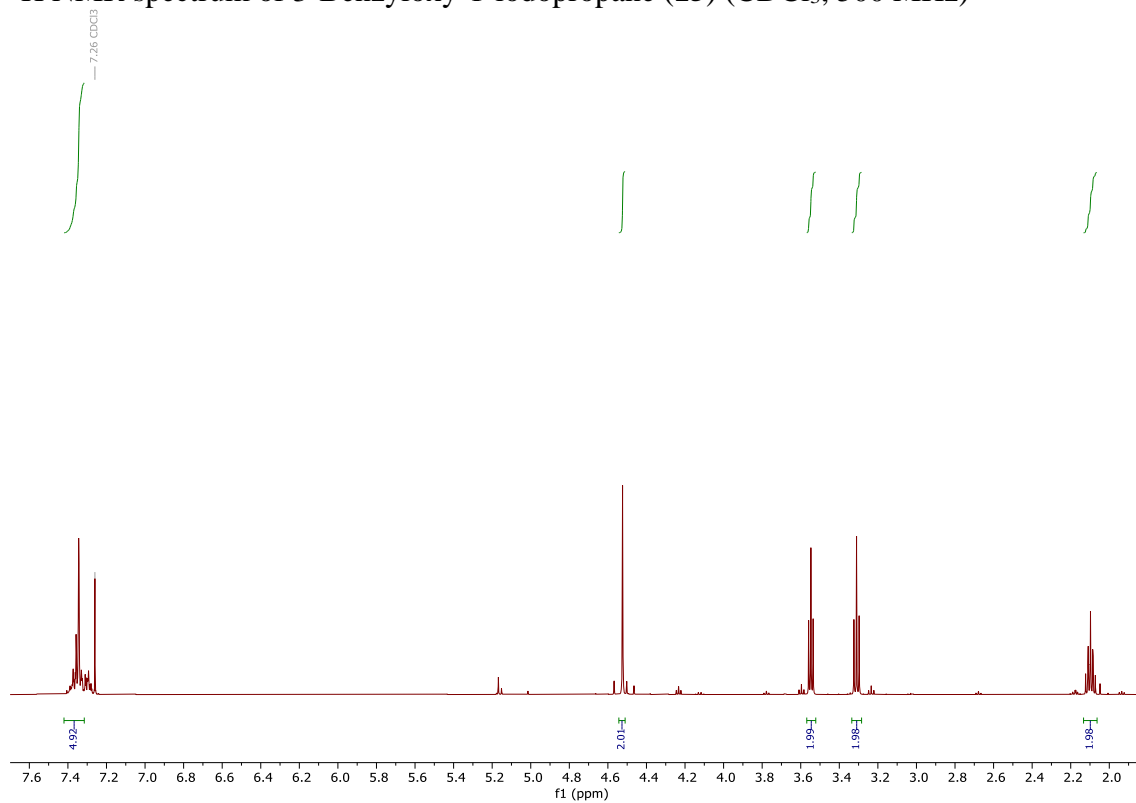
^1H NMR spectrum of 3-(Benzyloxy)propan-1-ol (**13**) (CDCl_3 , 500 MHz)



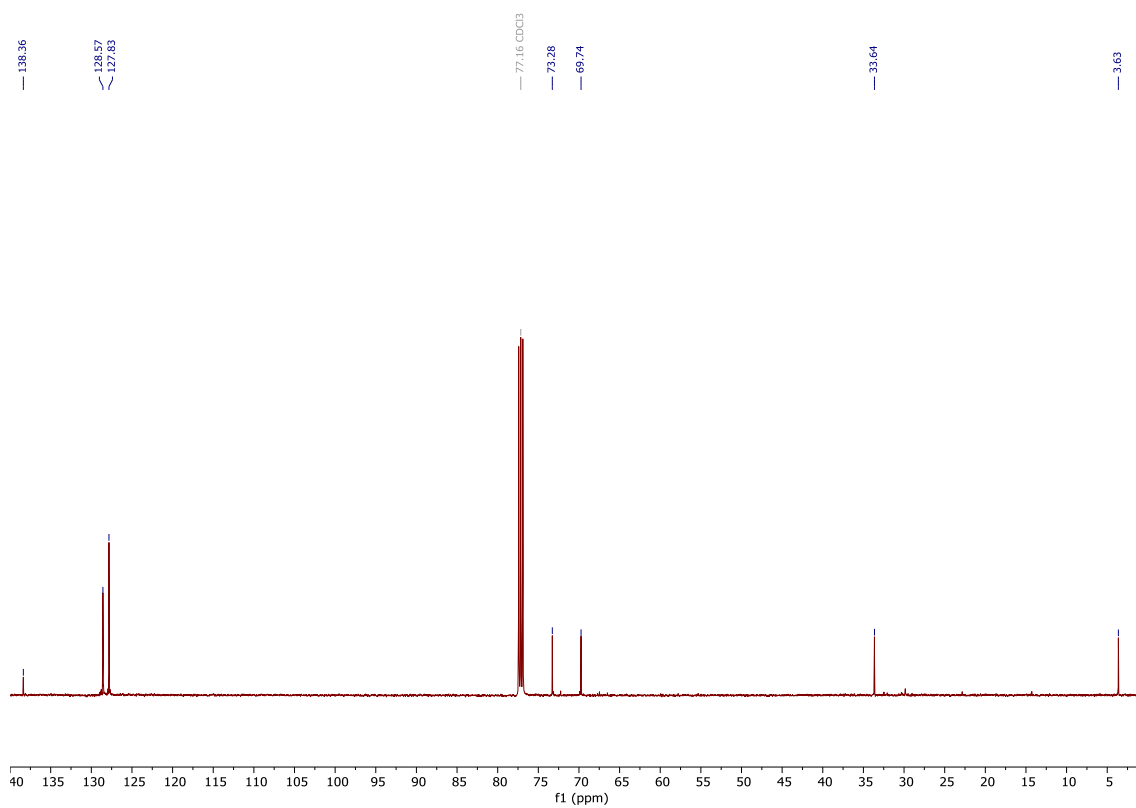
^{13}C NMR spectrum of 3-(Benzyloxy)propan-1-ol (**13**) (CDCl_3 , 126 MHz)



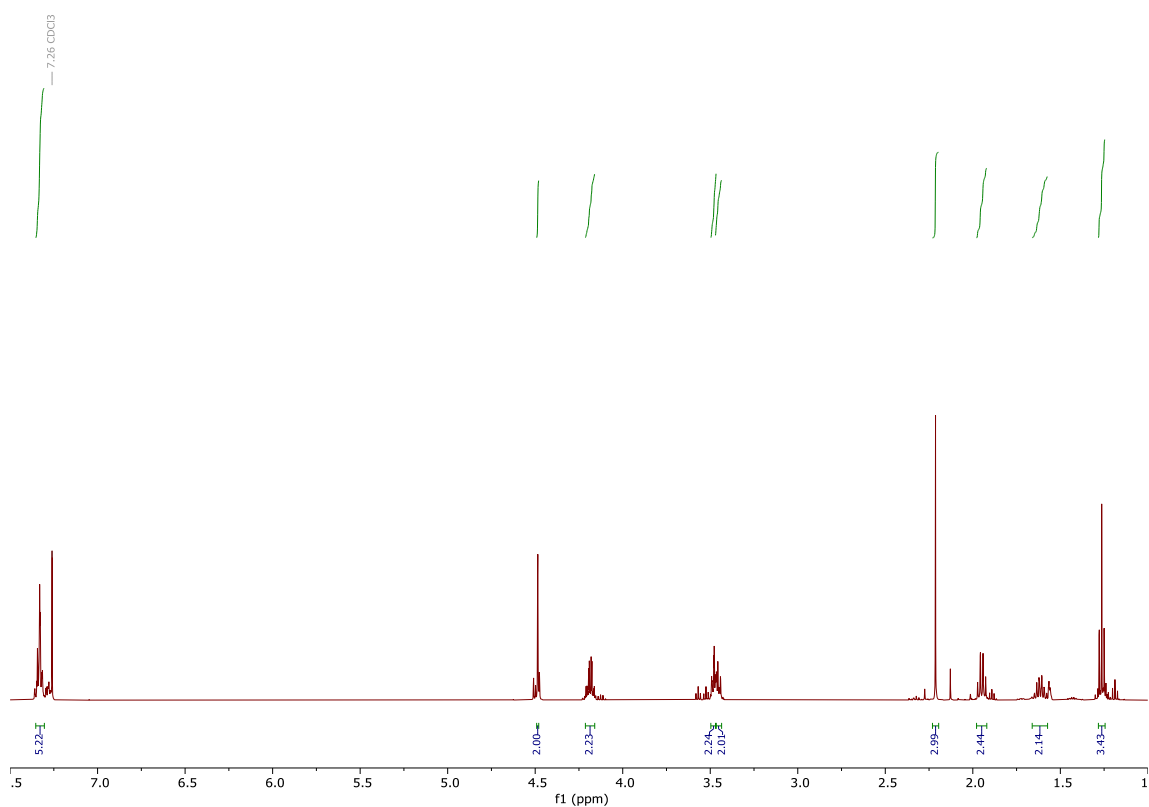
^1H NMR spectrum of 3-Benzyloxy-1-iodopropane (**15**) (CDCl_3 , 500 MHz)



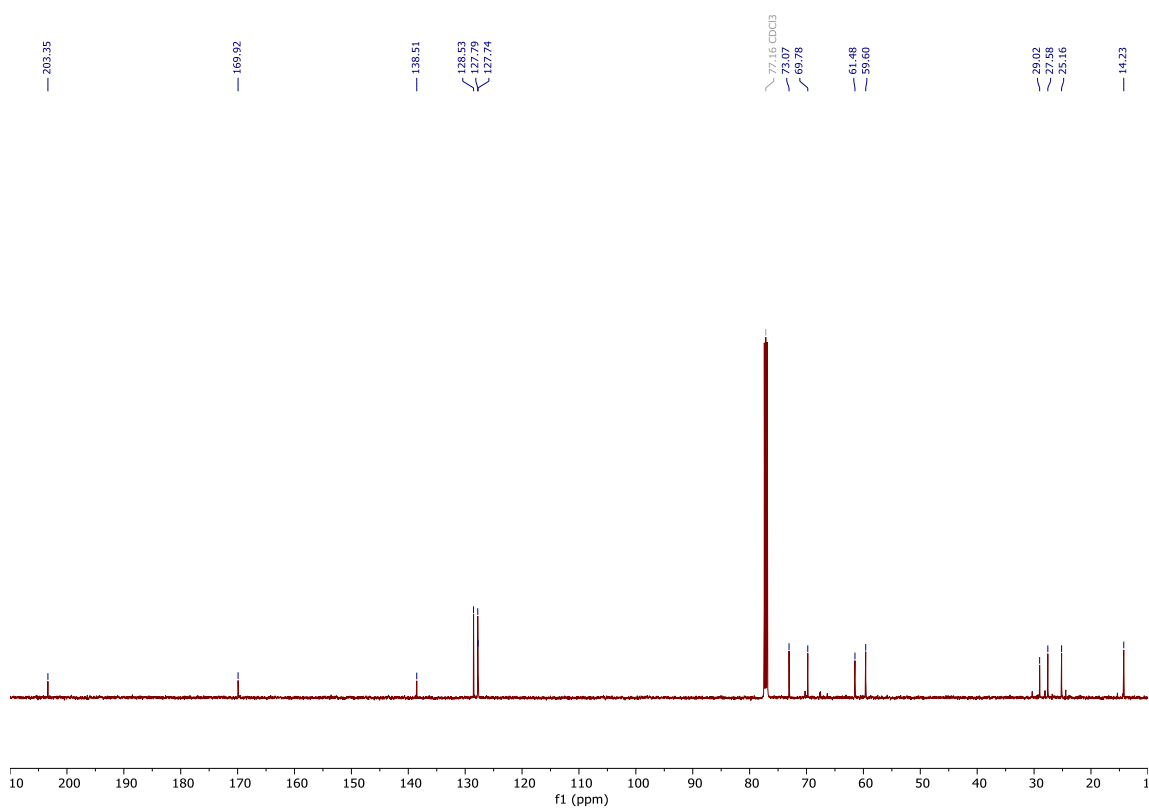
^{13}C NMR spectrum of 3-Benzyloxy-1-iodopropane (**15**) (CDCl_3 , 126 MHz)



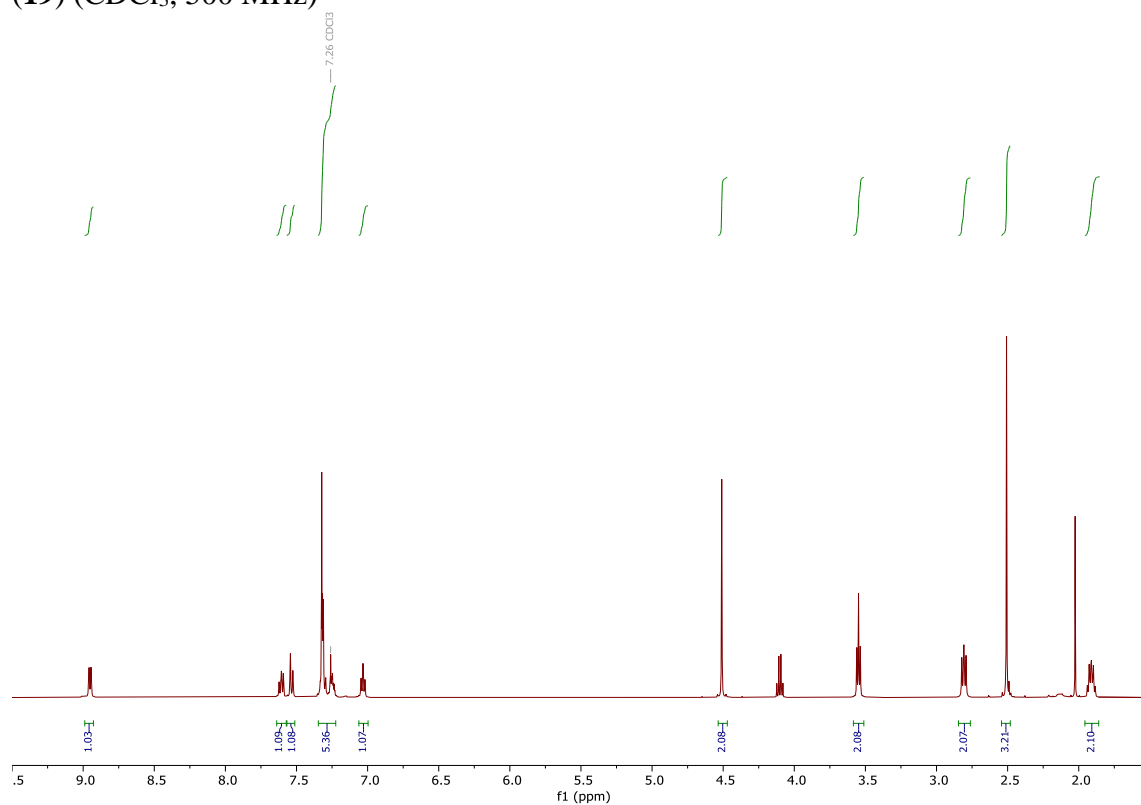
^1H NMR spectrum of Ethyl 2-acetyl-5-(benzyloxy)pentanoate (**17**) (CDCl_3 , 500 MHz)



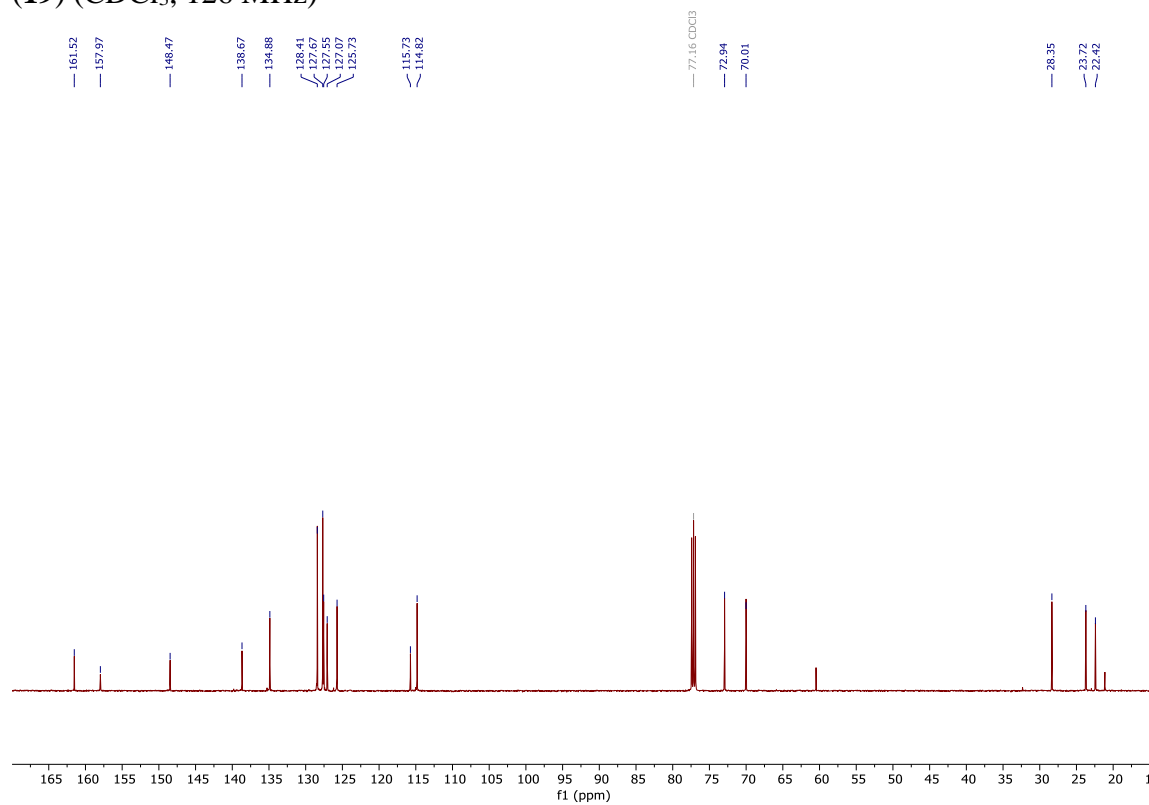
^{13}C NMR spectrum of Ethyl 2-acetyl-5-(benzyloxy)pentanoate (**17**) (CDCl_3 , 126 MHz)



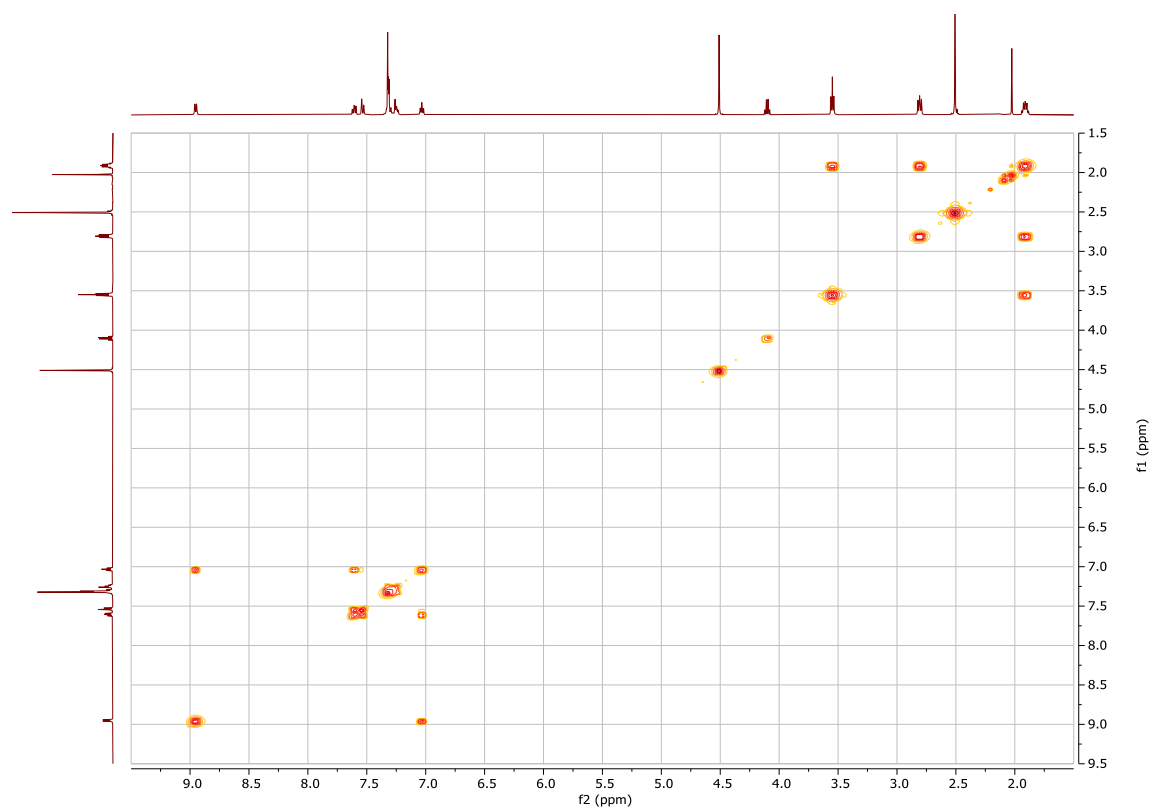
^1H NMR spectrum of 3-(3-(Benzyloxy)propyl)-2-methyl-4*H*-pyrido[1,2-*a*]pyrimidin-4-one (**19**) (CDCl_3 , 500 MHz)



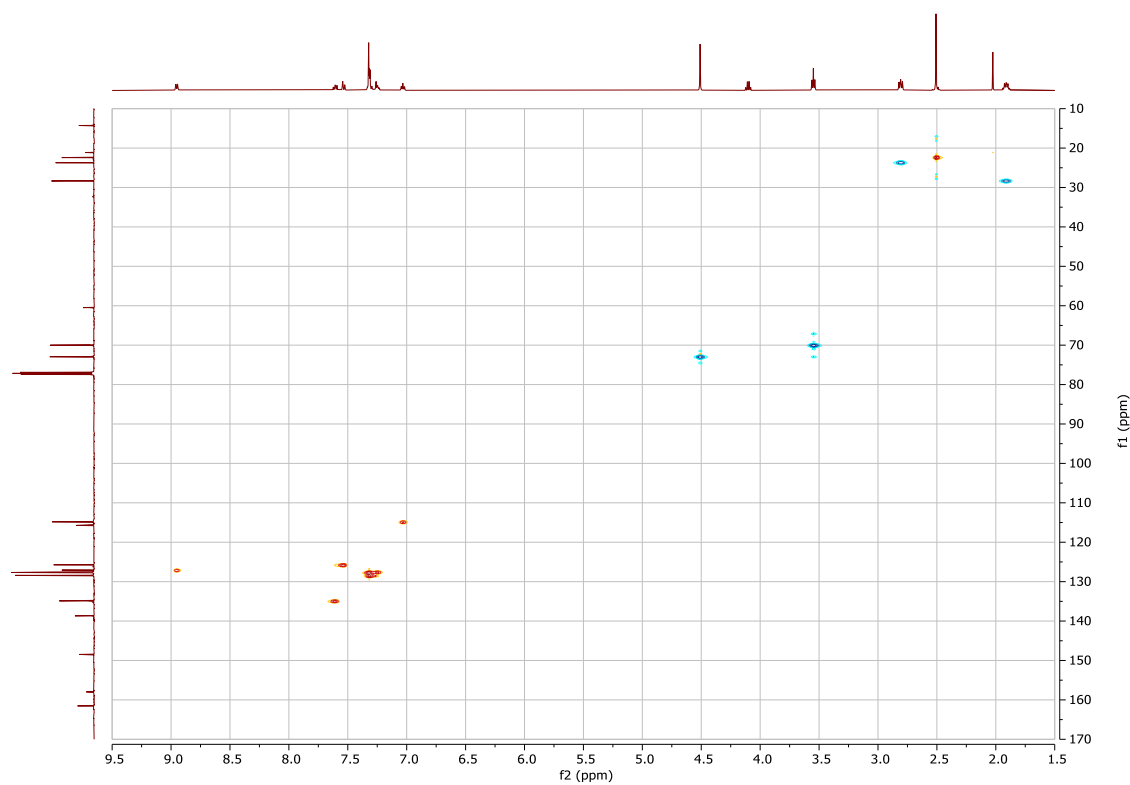
^{13}C NMR spectrum of 3-(3-(Benzyloxy)propyl)-2-methyl-4*H*-pyrido[1,2-*a*]pyrimidin-4-one (**19**) (CDCl_3 , 126 MHz)



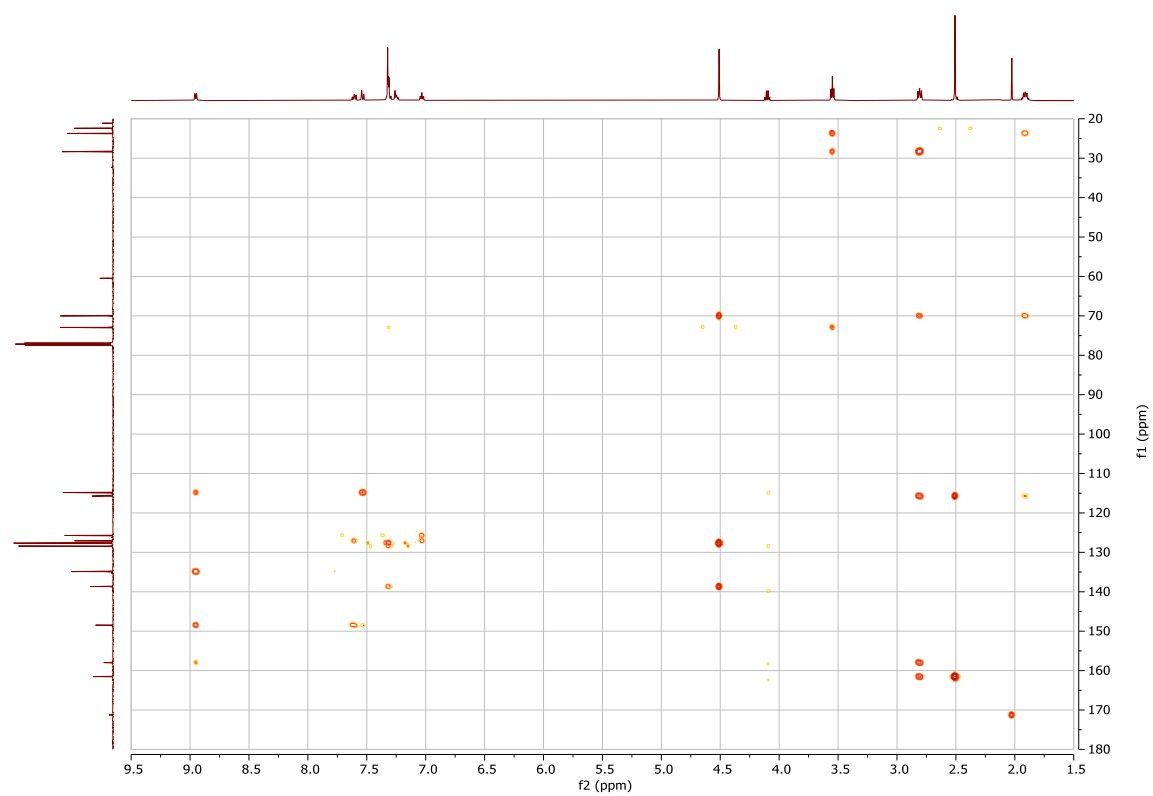
COSY NMR spectrum of 3-(3-(Benzyloxy)propyl)-2-methyl-4*H*-pyrido[1,2-*a*]pyrimidin-4-one (**19**) (CDCl₃, 500 MHz)



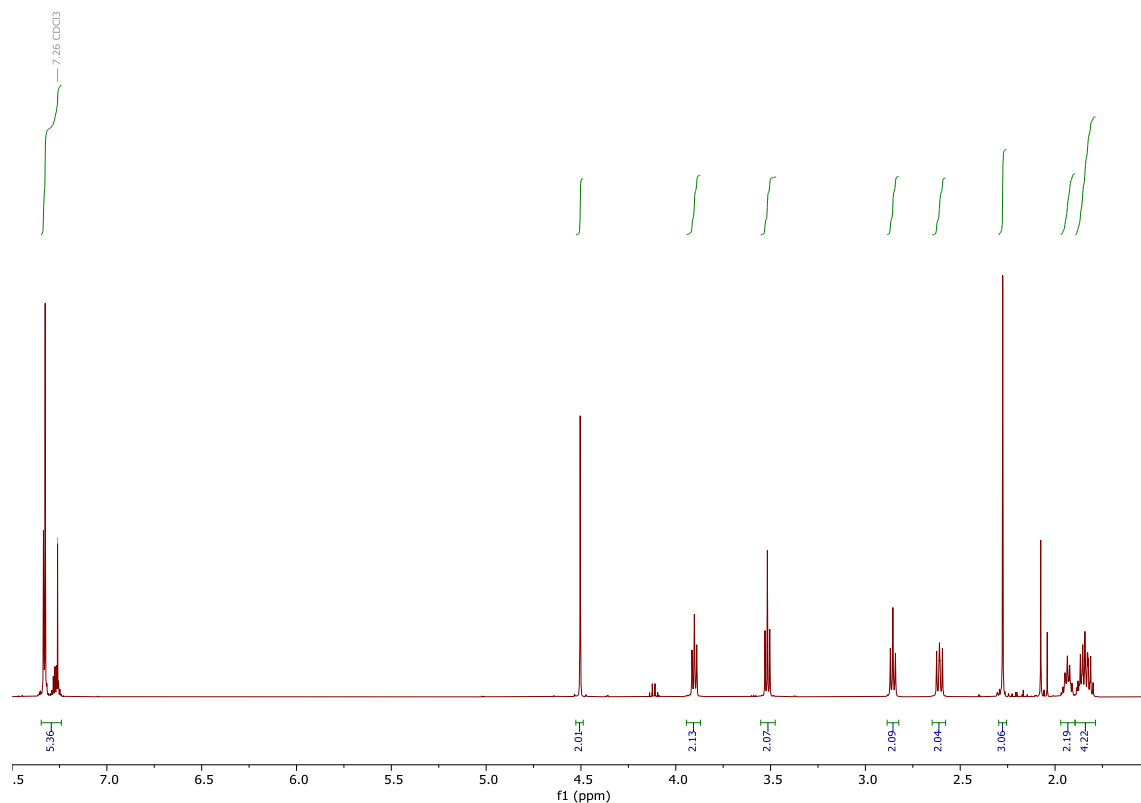
HSQC NMR spectrum of 3-(3-(Benzyloxy)propyl)-2-methyl-4*H*-pyrido[1,2-*a*]pyrimidin-4-one (**19**) (CDCl₃, 500 MHz)



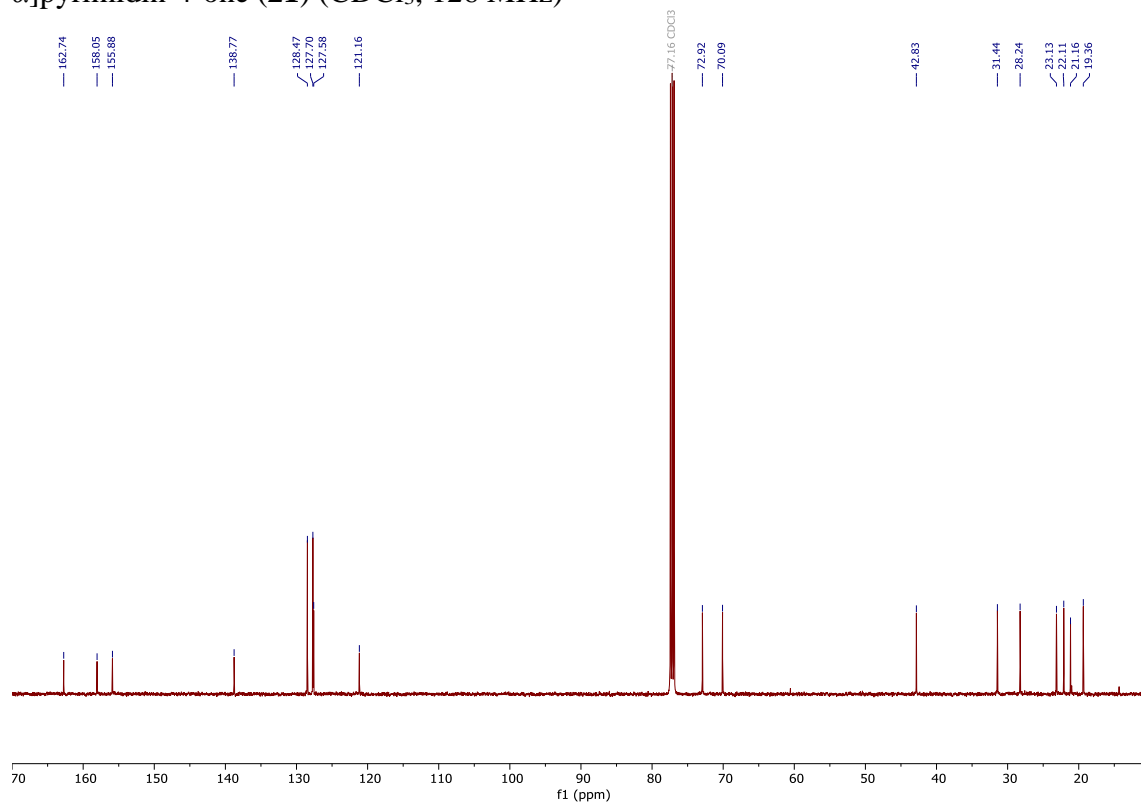
HMBC NMR spectrum of 3-(3-(Benzyloxy)propyl)-2-methyl-4*H*-pyrido[1,2-*a*]pyrimidin-4-one (**19**) (CDCl₃, 500 MHz)



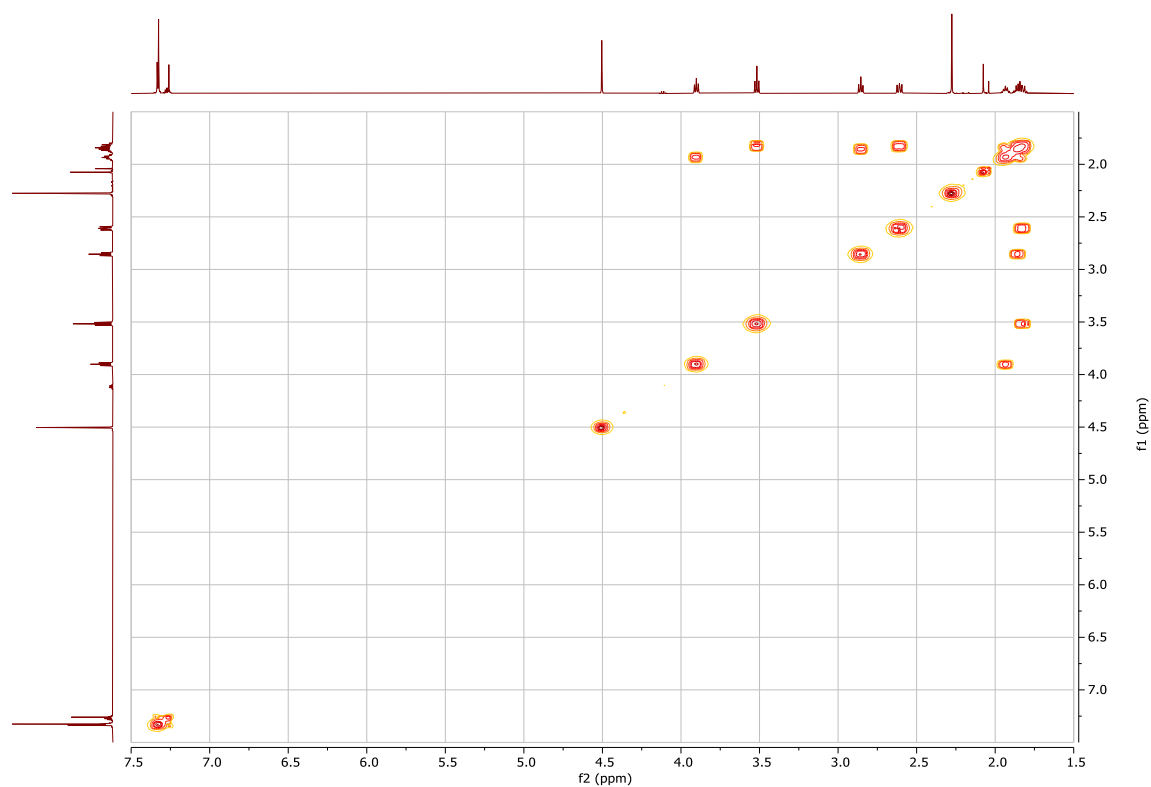
^1H NMR spectrum of 3-(3-(Benzyloxy)propyl)-2-methyl-6,7,8,9-tetrahydro-4*H*-pyrido[1,2- α]pyrimidin-4-one (**21**) (CDCl_3 , 500 MHz)



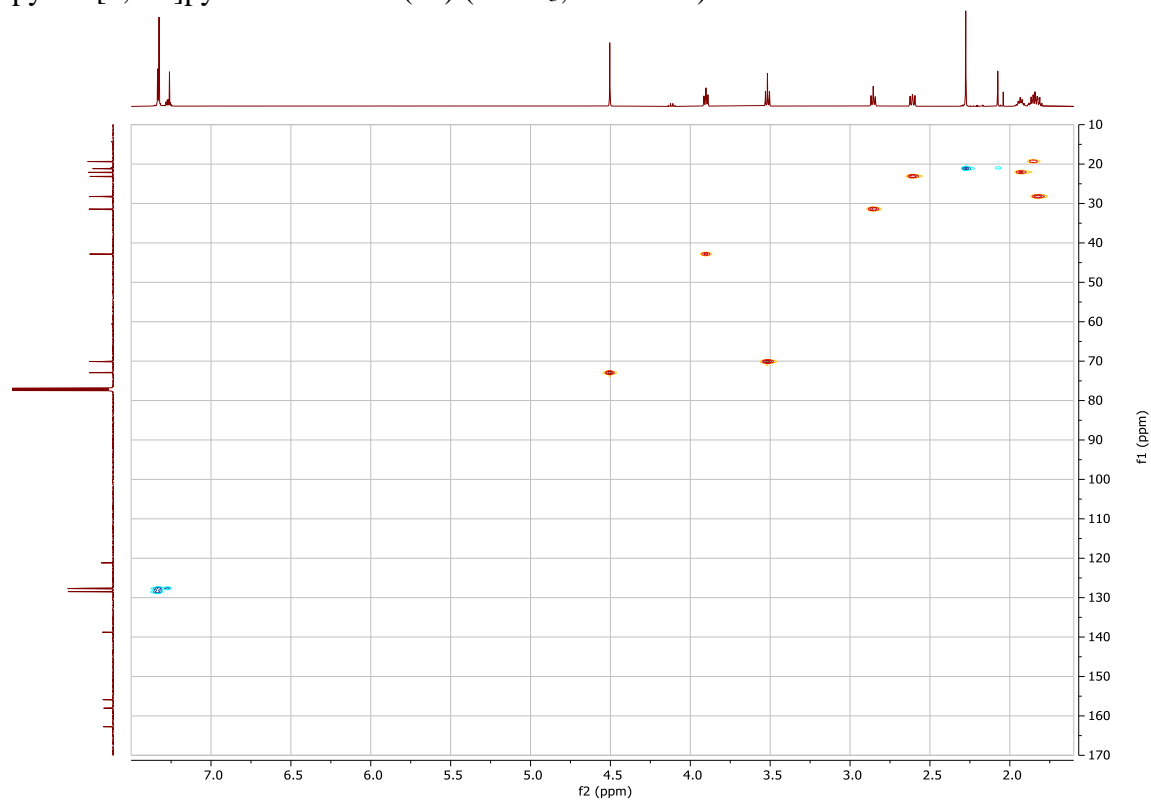
^{13}C NMR spectrum of 3-(3-(Benzyloxy)propyl)-2-methyl-6,7,8,9-tetrahydro-4*H*-pyrido[1,2- α]pyrimidin-4-one (**21**) (CDCl_3 , 126 MHz)



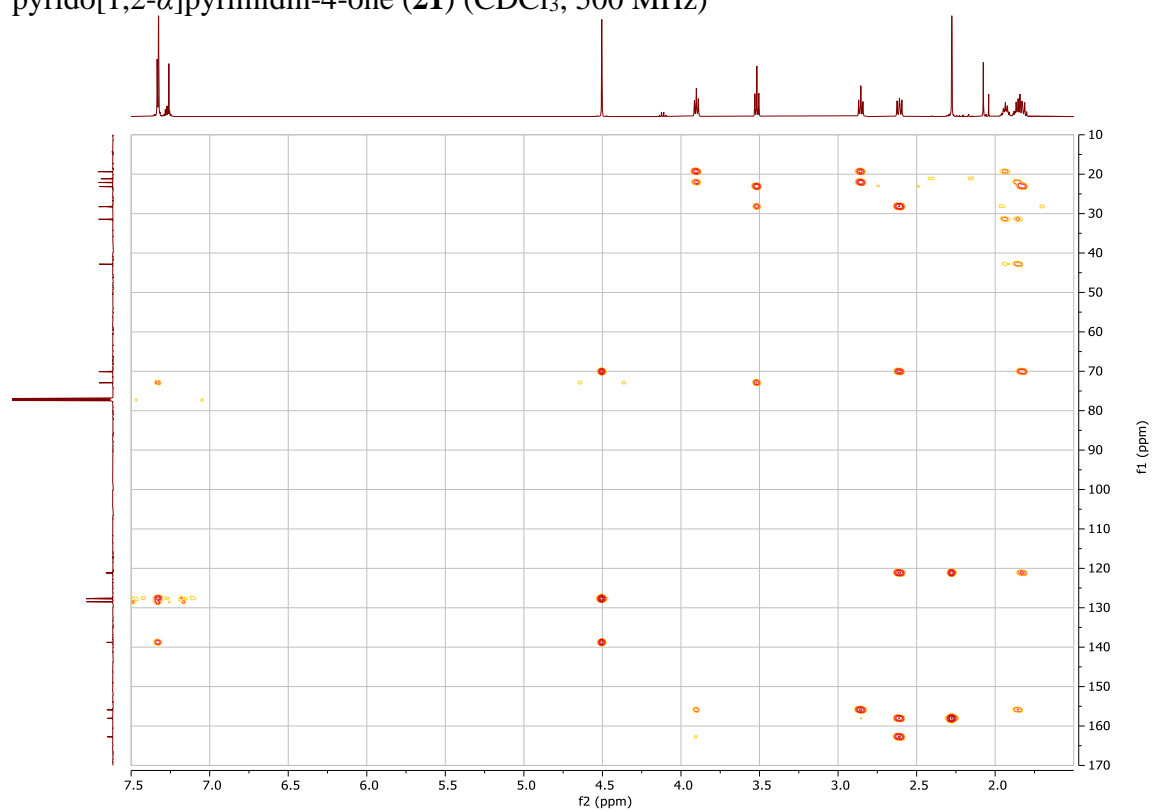
COSY NMR spectrum of 3-(3-(Benzyloxy)propyl)-2-methyl-6,7,8,9-tetrahydro-4H-pyrido[1,2-*a*]pyrimidin-4-one (**21**) (CDCl₃, 500 MHz)



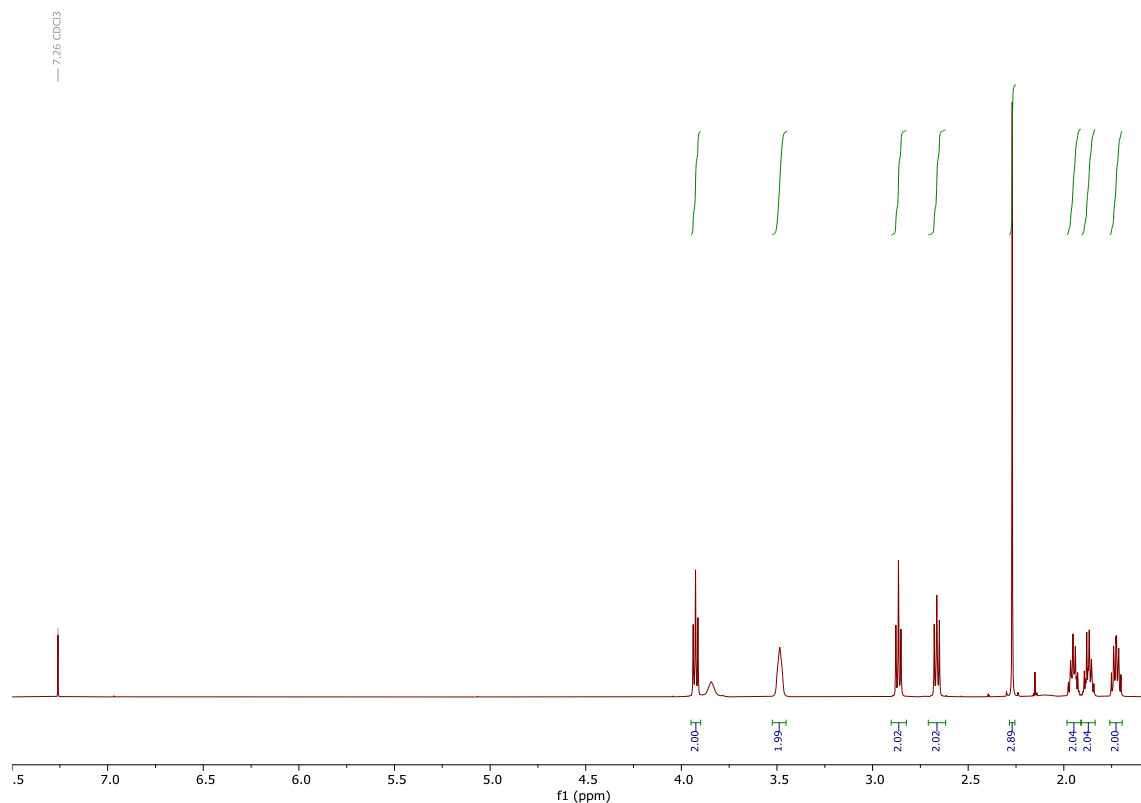
HSQC NMR spectrum of 3-(3-(Benzyloxy)propyl)-2-methyl-6,7,8,9-tetrahydro-4H-pyrido[1,2-*a*]pyrimidin-4-one (**21**) (CDCl₃, 500 MHz)



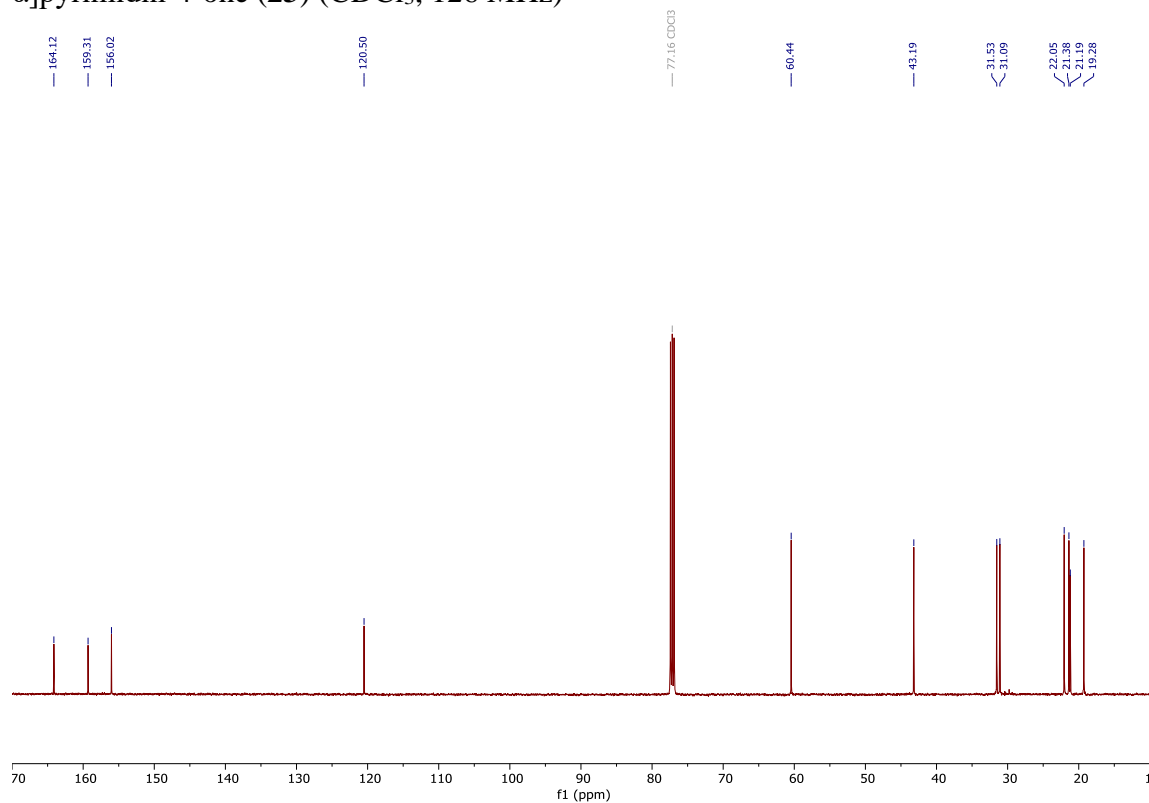
HMBC NMR spectrum of 3-(3-(Benzyloxy)propyl)-2-methyl-6,7,8,9-tetrahydro-4H-pyrido[1,2- α]pyrimidin-4-one (**21**) (CDCl₃, 500 MHz)



^1H NMR spectrum of 3-(3-Hydroxypropyl)-2-methyl-6,7,8,9-tetrahydro-4*H*-pyrido[1,2- α]pyrimidin-4-one (**23**) (CDCl_3 , 500 MHz)

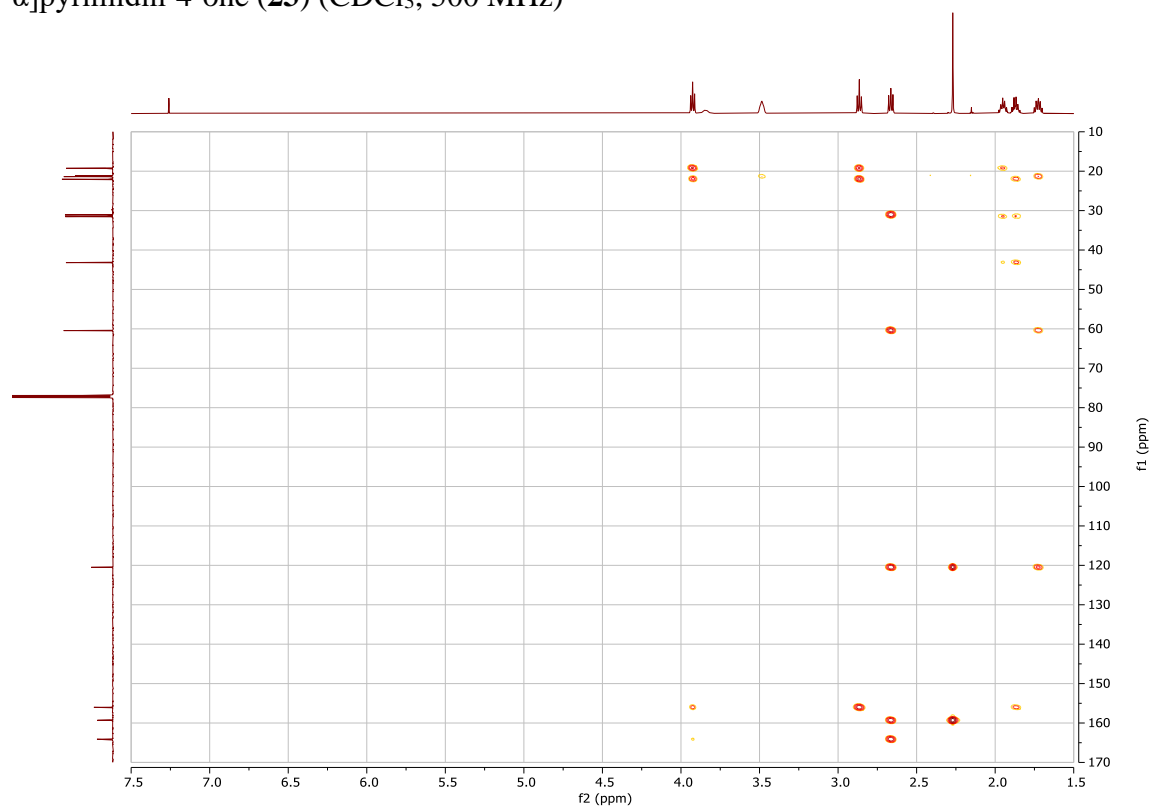


^{13}C NMR spectrum of 3-(3-Hydroxypropyl)-2-methyl-6,7,8,9-tetrahydro-4*H*-pyrido[1,2- α]pyrimidin-4-one (**23**) (CDCl_3 , 126 MHz)

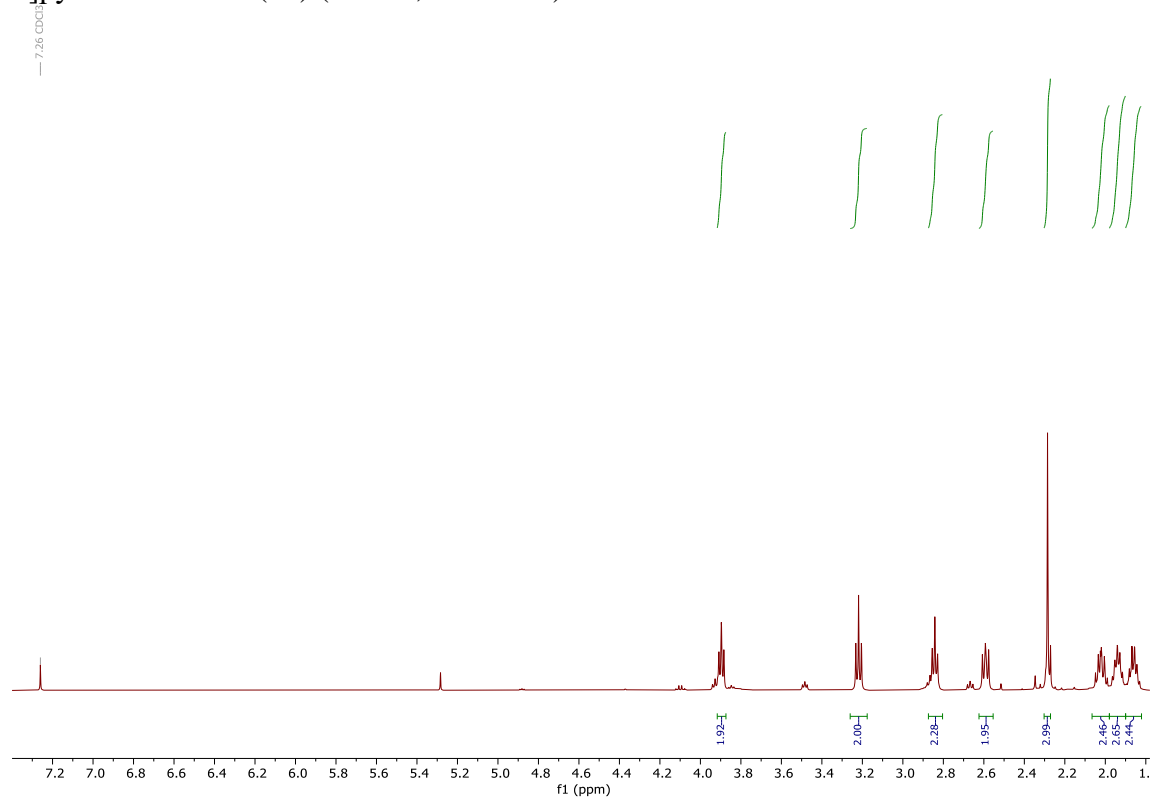


2D COSY NMR spectrum of compound **25**. The x-axis is labeled 'f2 (ppm)' and ranges from 1.5 to 7.5. The y-axis ranges from 1.5 to 7.5. The plot shows diagonal peaks and off-diagonal cross-peaks. A 1D ¹H NMR spectrum is projected along the top and left edges of the 2D plot. Cross-peaks are labeled with numbers 1 through 19, indicating correlations between protons.

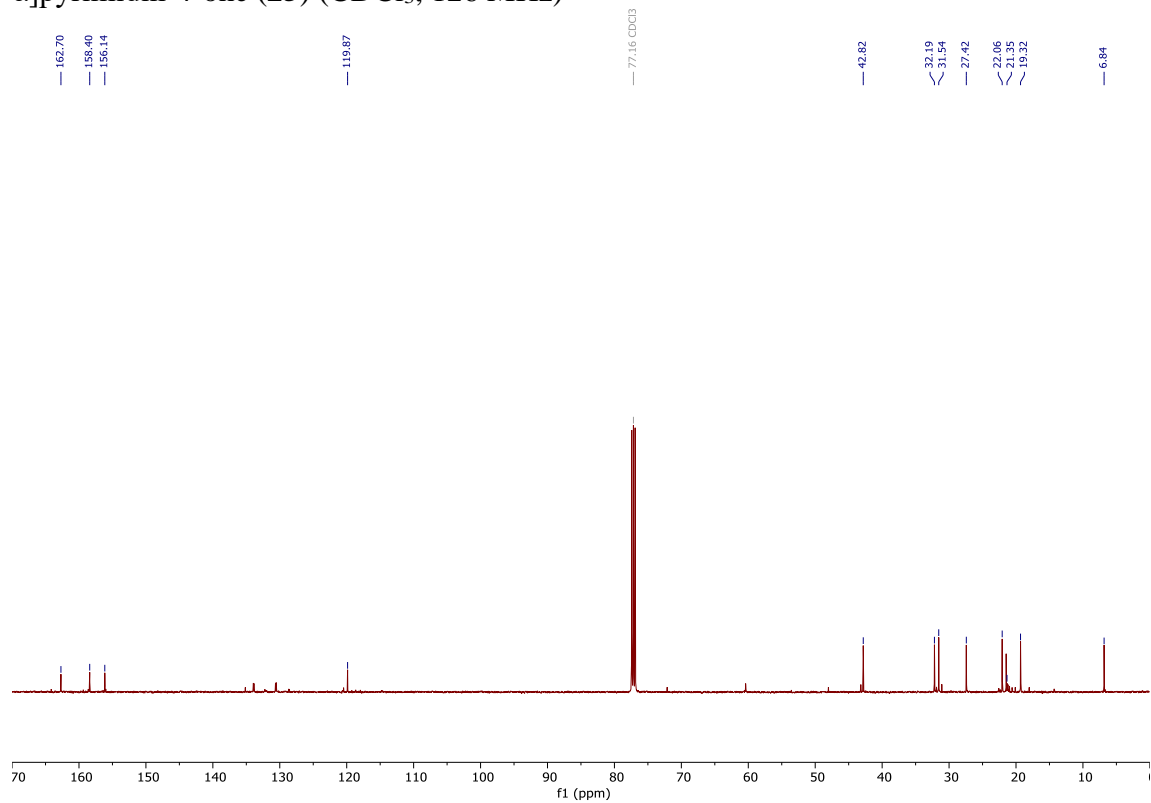
HMBC NMR spectrum of 3-(3-Hydroxypropyl)-2-methyl-6,7,8,9-tetrahydro-4*H*-pyrido[1,2- α]pyrimidin-4-one (**23**) (CDCl₃, 500 MHz)



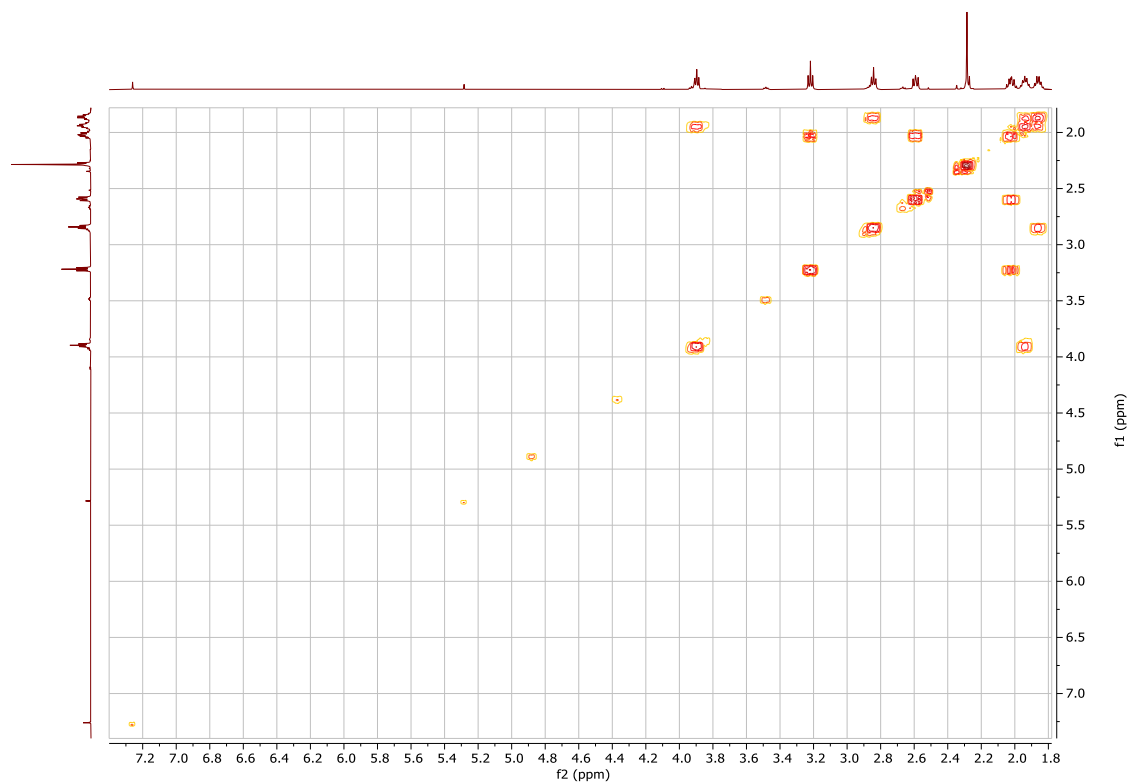
^1H NMR spectrum of 3-(3-Iodopropyl)-2-methyl-6,7,8,9-tetrahydro-4*H*-pyrido[1,2- α]pyrimidin-4-one (**25**) (CDCl_3 , 500 MHz)



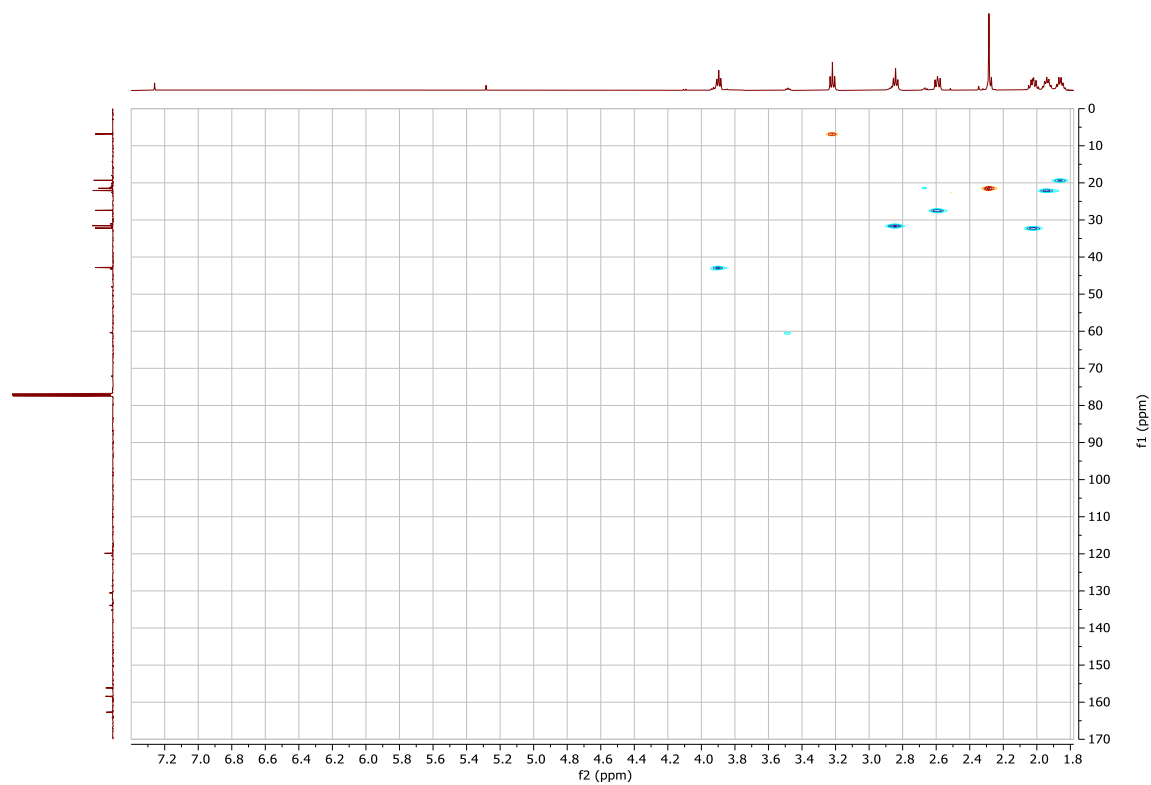
^{13}C NMR spectrum of 3-(3-Iodopropyl)-2-methyl-6,7,8,9-tetrahydro-4*H*-pyrido[1,2- α]pyrimidin-4-one (**25**) (CDCl_3 , 126 MHz)



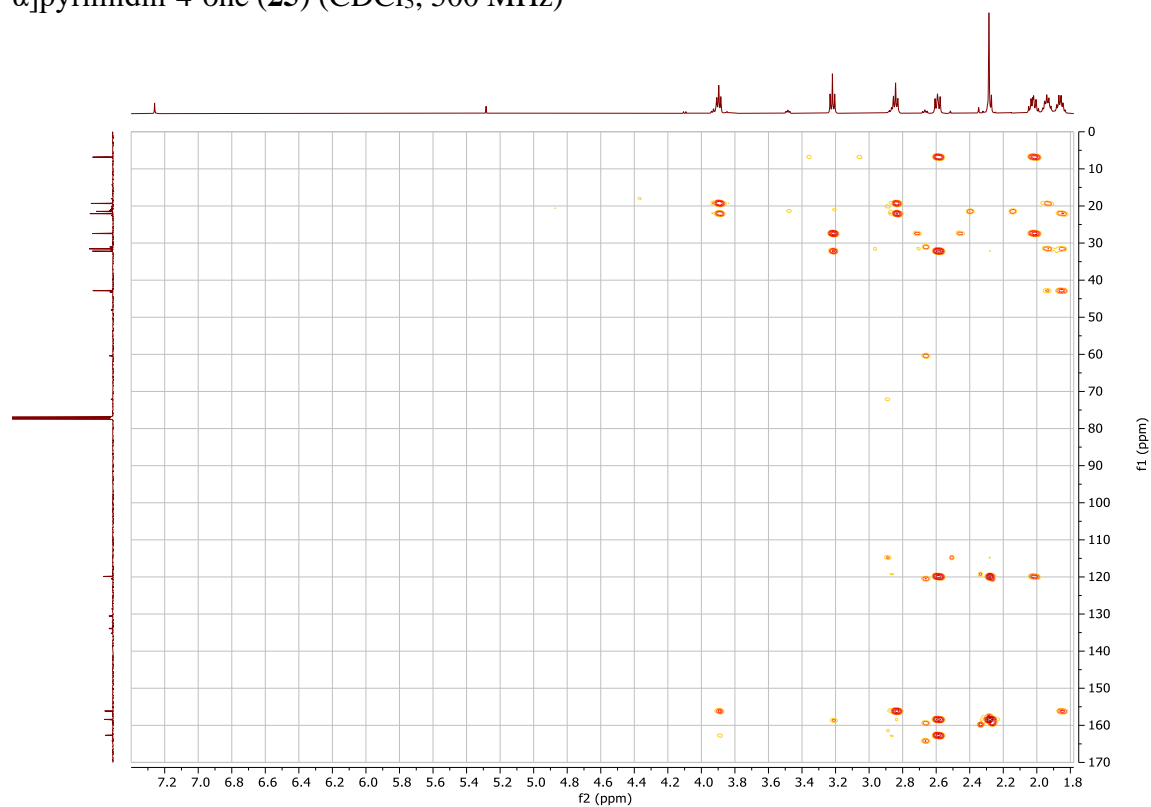
COSY NMR spectrum of 3-(3-Iodopropyl)-2-methyl-6,7,8,9-tetrahydro-4*H*-pyrido[1,2- α]pyrimidin-4-one (**25**) (CDCl₃, 500 MHz)



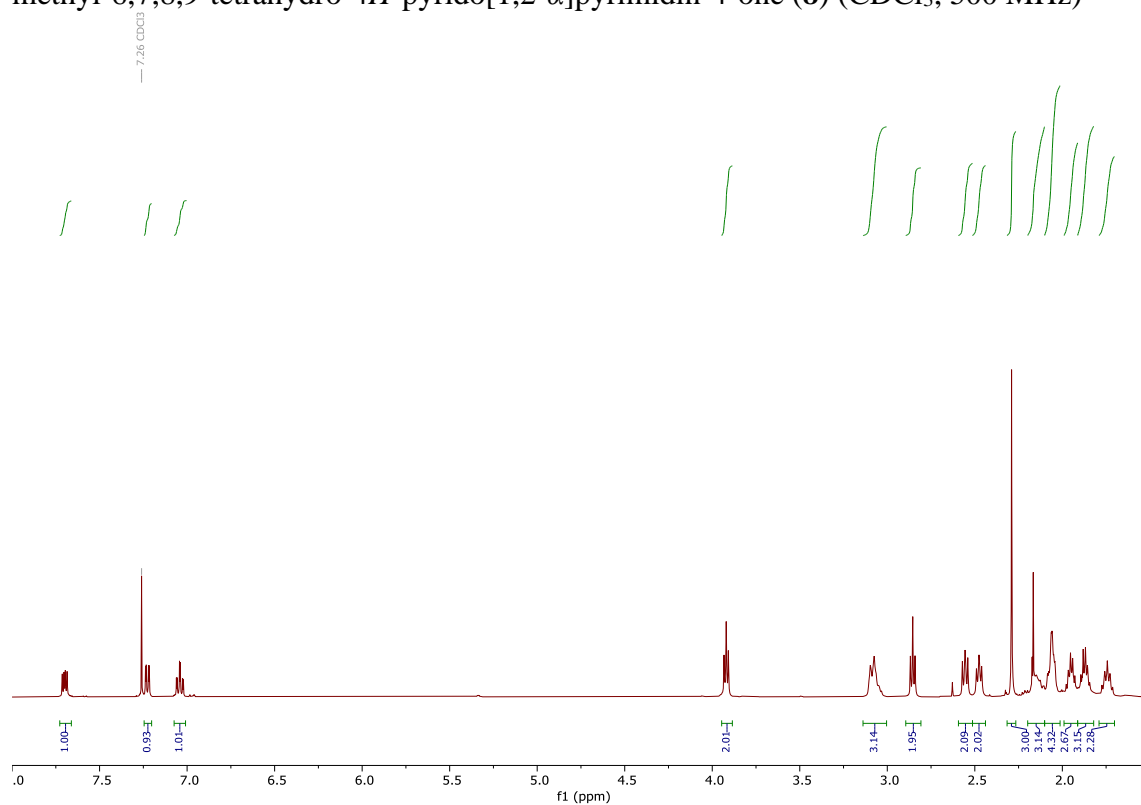
HSQC NMR spectrum of 3-(3-Iodopropyl)-2-methyl-6,7,8,9-tetrahydro-4*H*-pyrido[1,2- α]pyrimidin-4-one (**25**) (CDCl₃, 500 MHz)



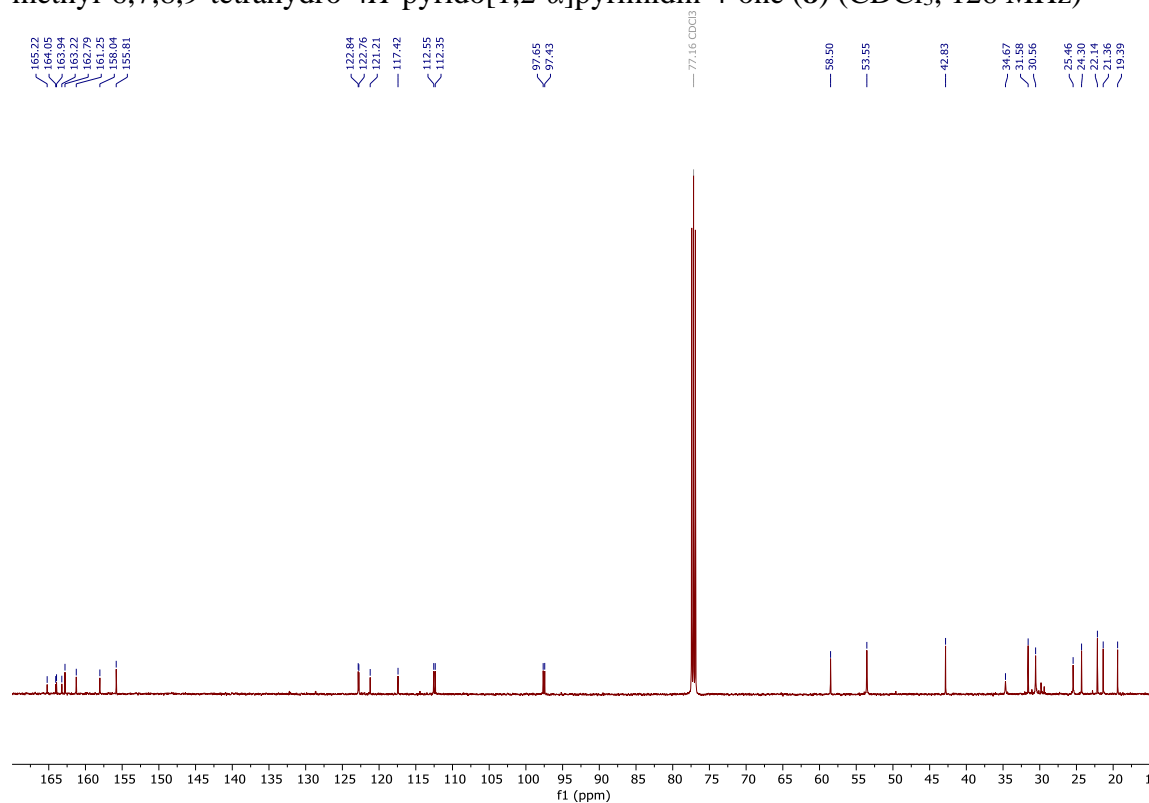
HMBC NMR spectrum of 3-(3-Iodopropyl)-2-methyl-6,7,8,9-tetrahydro-4*H*-pyrido[1,2- α]pyrimidin-4-one (**25**) (CDCl₃, 500 MHz)



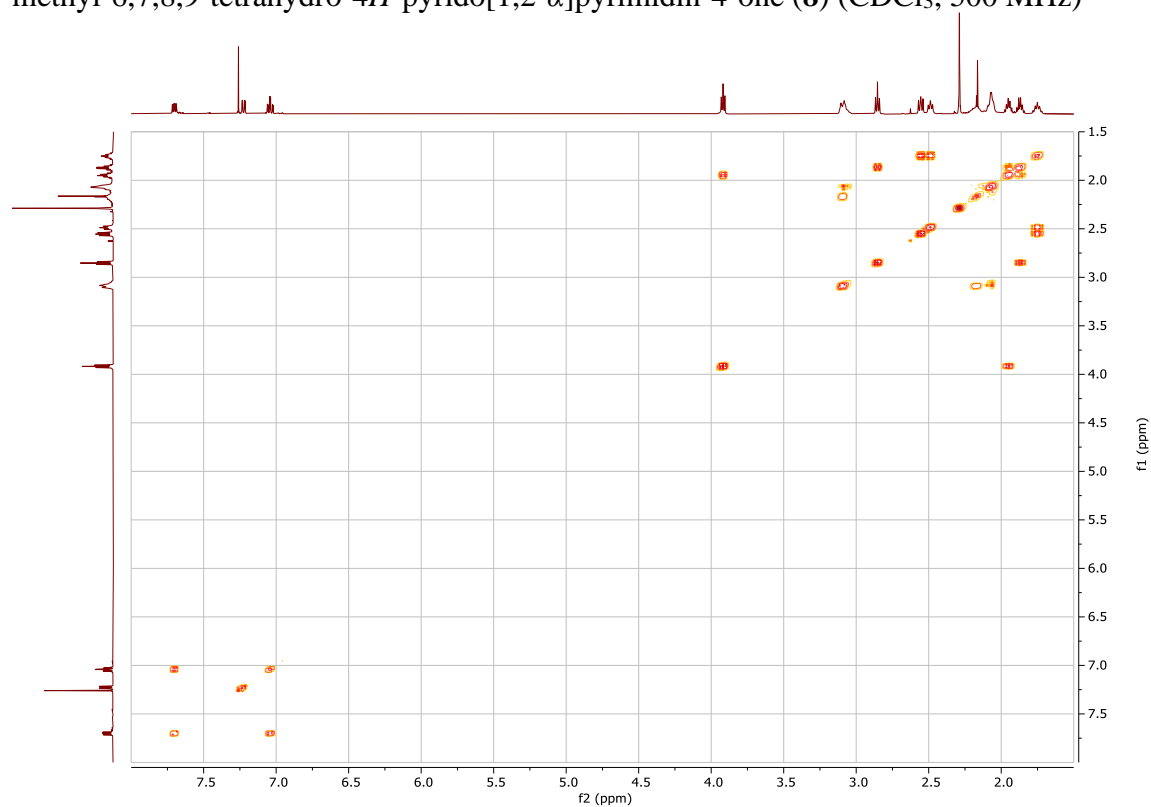
¹H NMR spectrum of 3-(3-(4-(6-Fluorobenzo[d]isoxazol-3-yl)piperidin-1-yl)propyl)-2-methyl-6,7,8,9-tetrahydro-4H-pyrido[1,2-α]pyrimidin-4-one (**8**) (CDCl₃, 500 MHz)



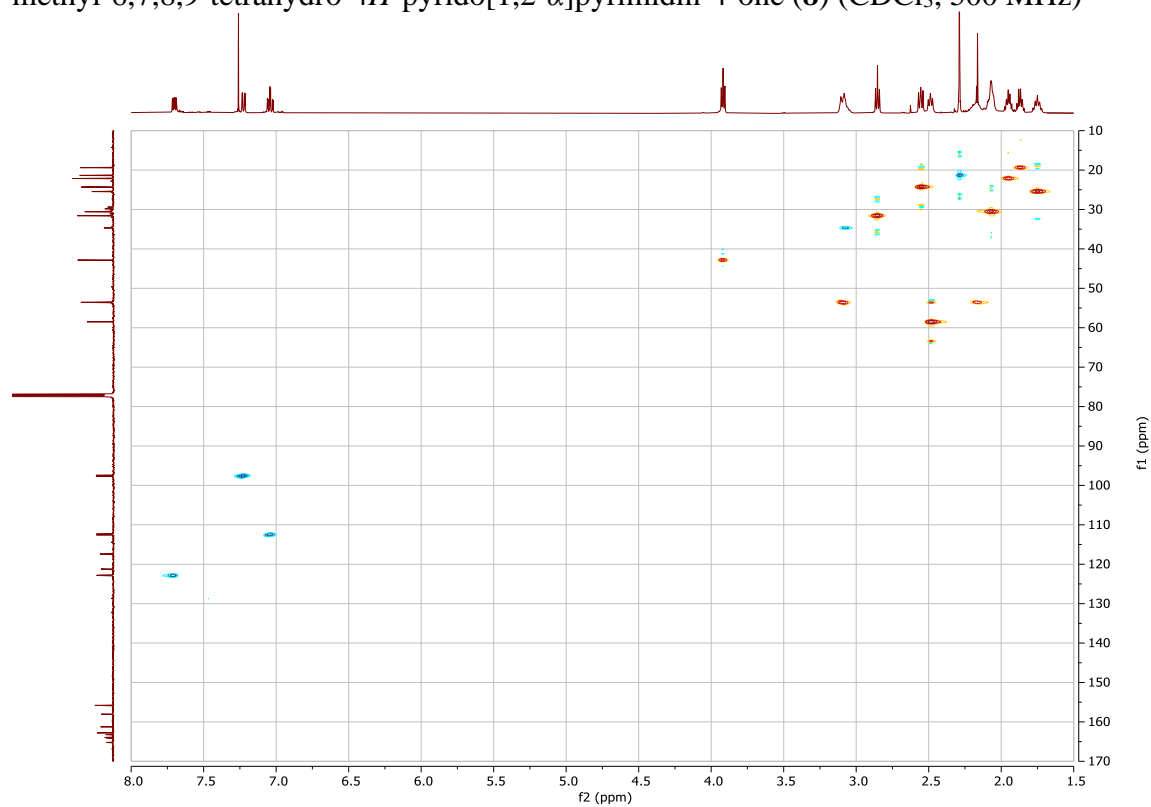
¹³C NMR spectrum of 3-(3-(4-(6-Fluorobenzo[d]isoxazol-3-yl)piperidin-1-yl)propyl)-2-methyl-6,7,8,9-tetrahydro-4H-pyrido[1,2-α]pyrimidin-4-one (**8**) (CDCl₃, 126 MHz)



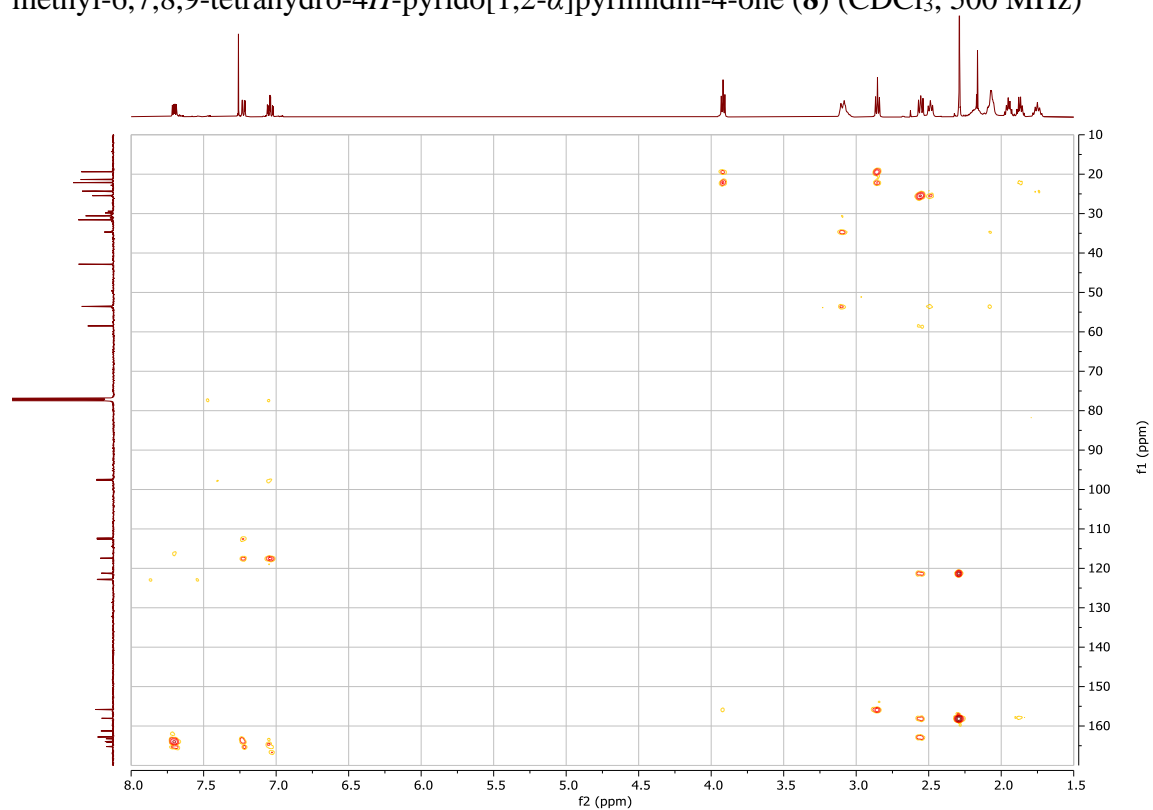
COSY NMR spectrum of 3-(3-(4-(6-Fluorobenzo[*d*]isoxazol-3-yl)piperidin-1-yl)propyl)-2-methyl-6,7,8,9-tetrahydro-4*H*-pyrido[1,2- α]pyrimidin-4-one (**8**) (CDCl₃, 500 MHz)



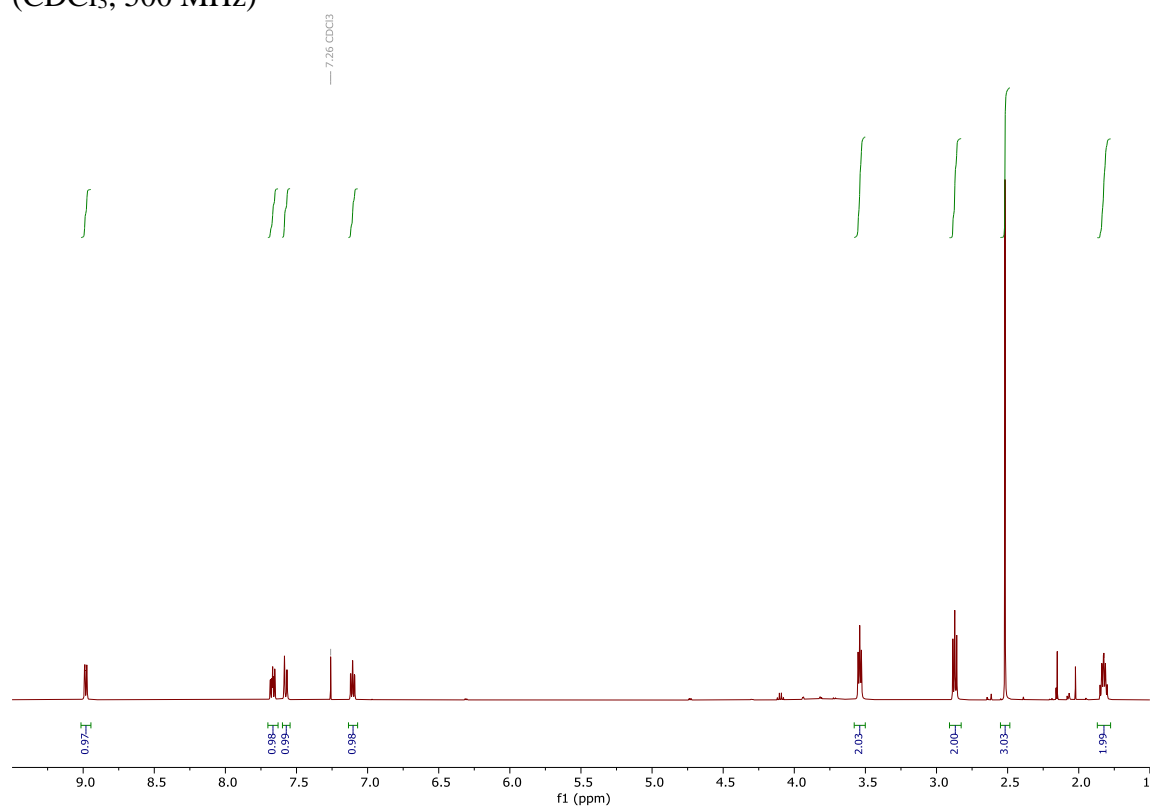
HSQC NMR spectrum of 3-(3-(4-(6-Fluorobenzo[*d*]isoxazol-3-yl)piperidin-1-yl)propyl)-2-methyl-6,7,8,9-tetrahydro-4*H*-pyrido[1,2- α]pyrimidin-4-one (**8**) (CDCl₃, 500 MHz)



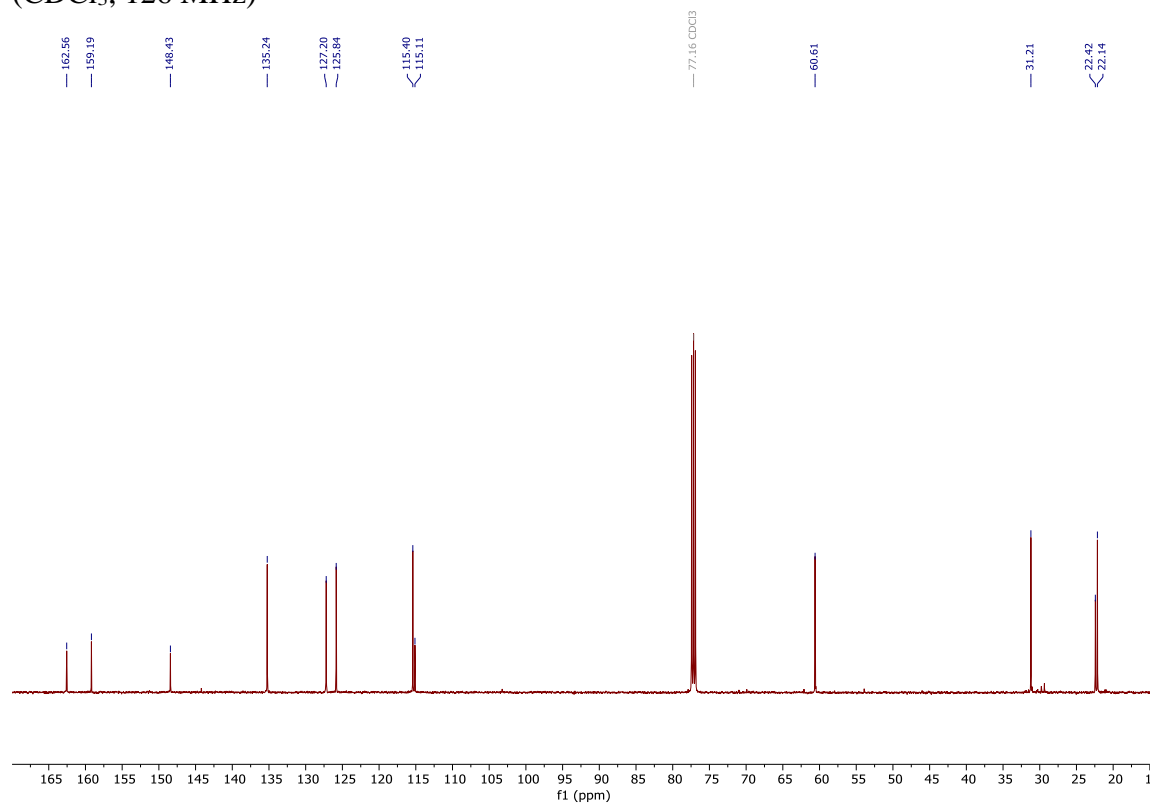
HMBC NMR spectrum of 3-(3-(4-(6-Fluorobenzo[d]isoxazol-3-yl)piperidin-1-yl)propyl)-2-methyl-6,7,8,9-tetrahydro-4*H*-pyrido[1,2- α]pyrimidin-4-one (**8**) (CDCl₃, 500 MHz)



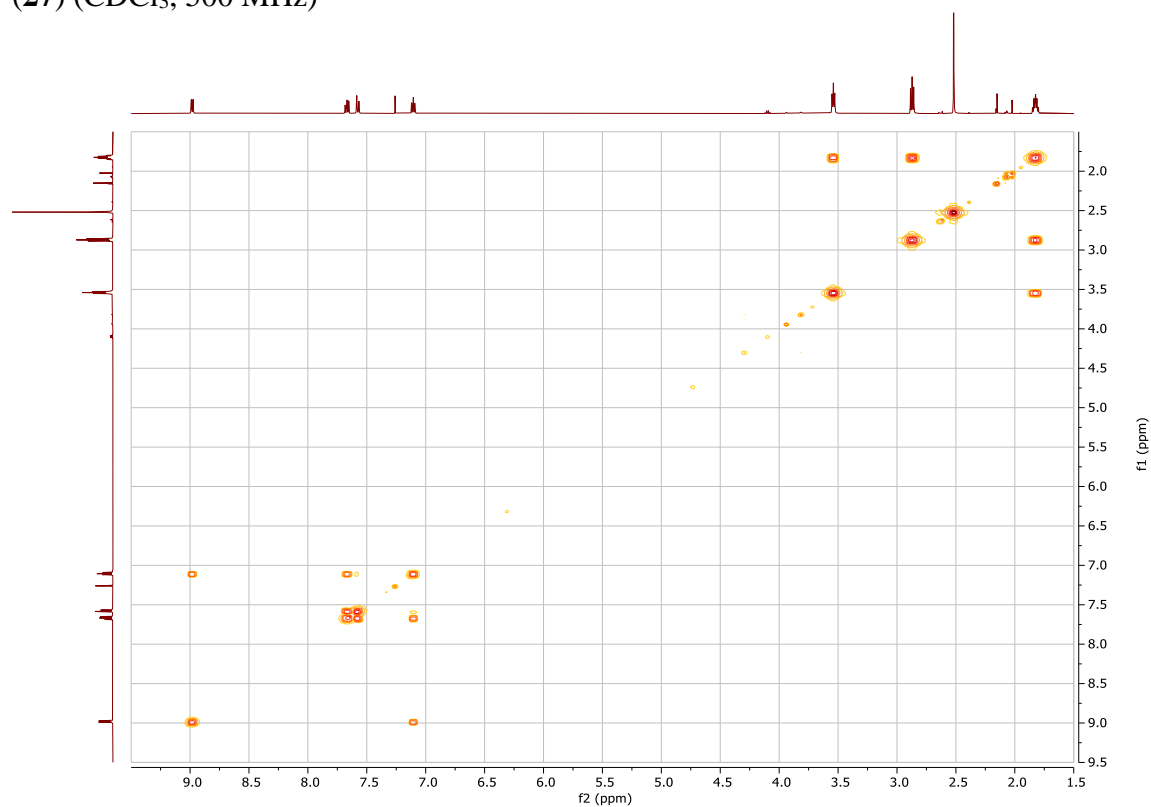
^1H NMR spectrum of 3-(3-hydroxypropyl)-2-methyl-4H-pyrido[1,2- α]pyrimidin-4-one (**27**) (CDCl_3 , 500 MHz)



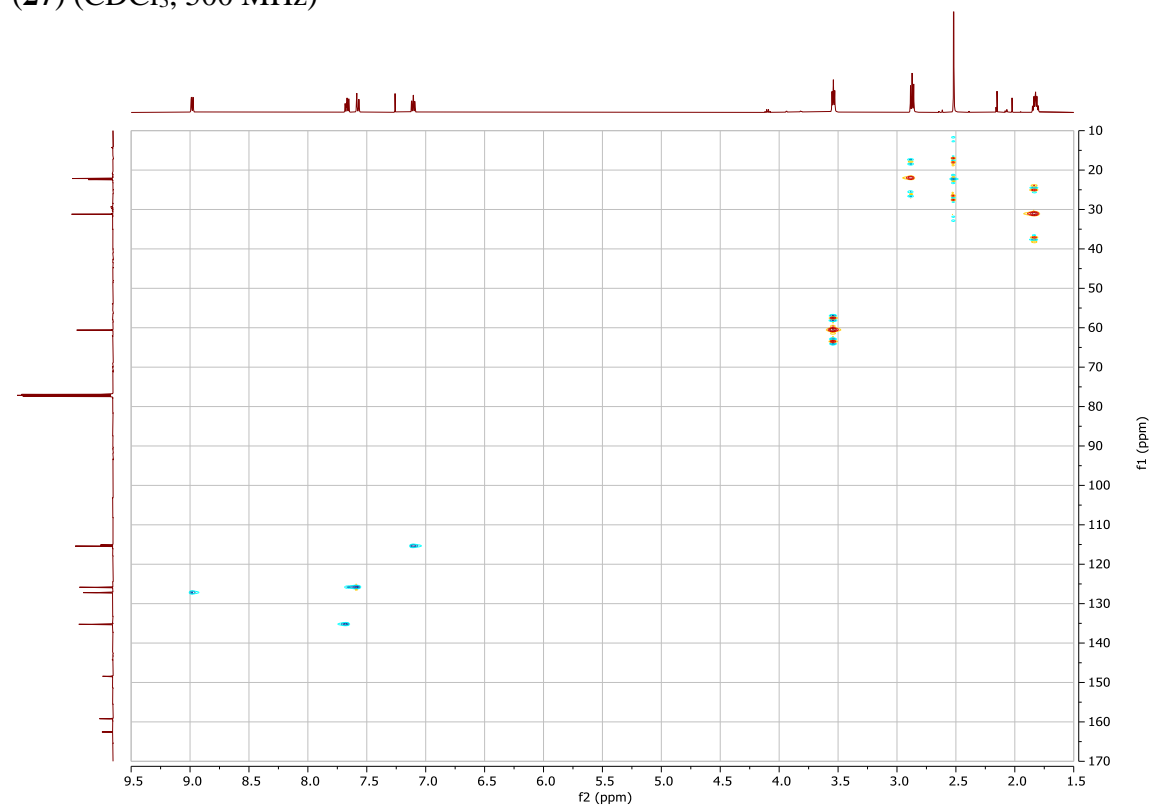
^{13}C NMR spectrum of 3-(3-hydroxypropyl)-2-methyl-4H-pyrido[1,2- α]pyrimidin-4-one (**27**) (CDCl_3 , 126 MHz)



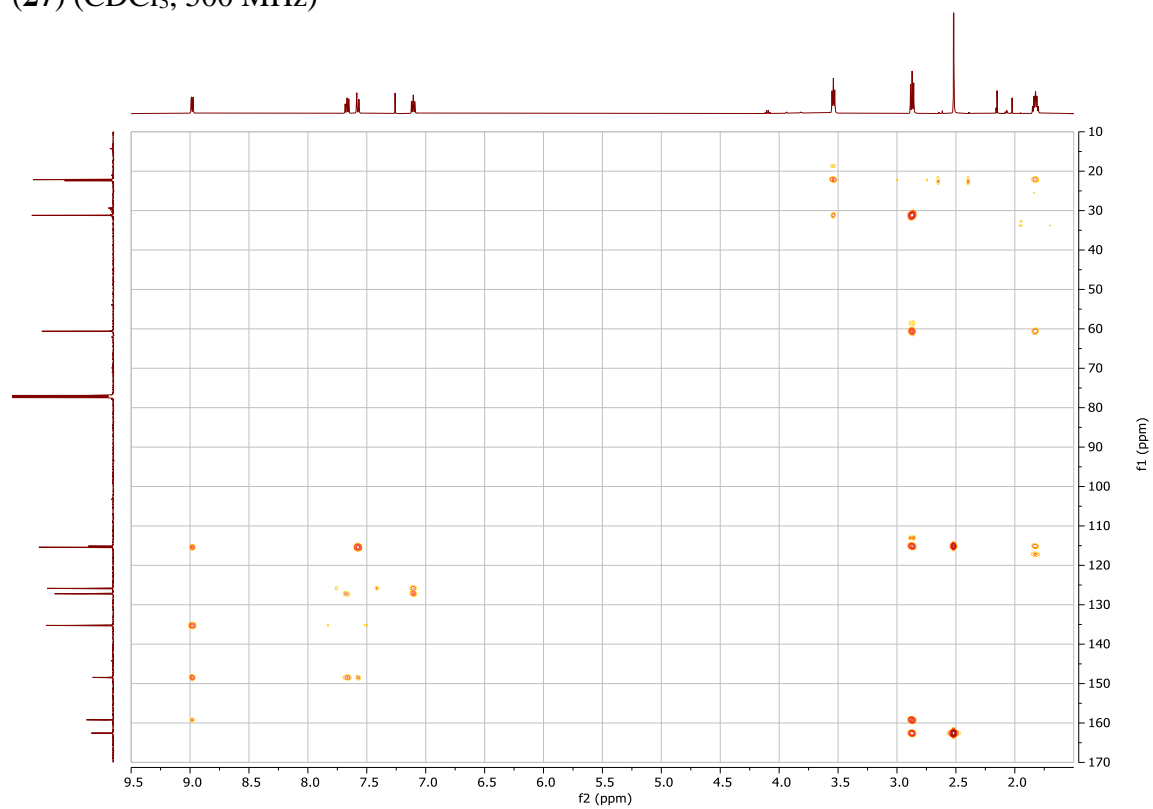
COSY NMR spectrum of 3-(3-hydroxypropyl)-2-methyl-4H-pyrido[1,2- α]pyrimidin-4-one (**27**) (CDCl₃, 500 MHz)



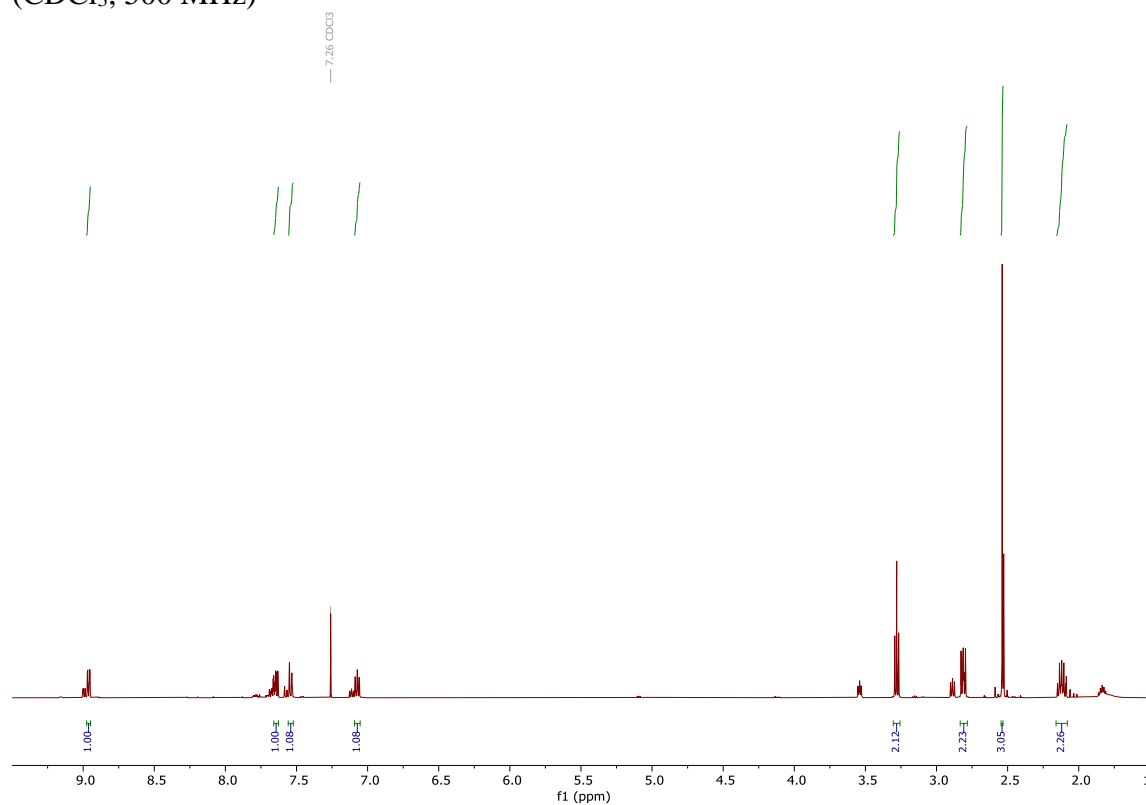
HSQC NMR spectrum of 3-(3-hydroxypropyl)-2-methyl-4H-pyrido[1,2- α]pyrimidin-4-one (**27**) (CDCl₃, 500 MHz)



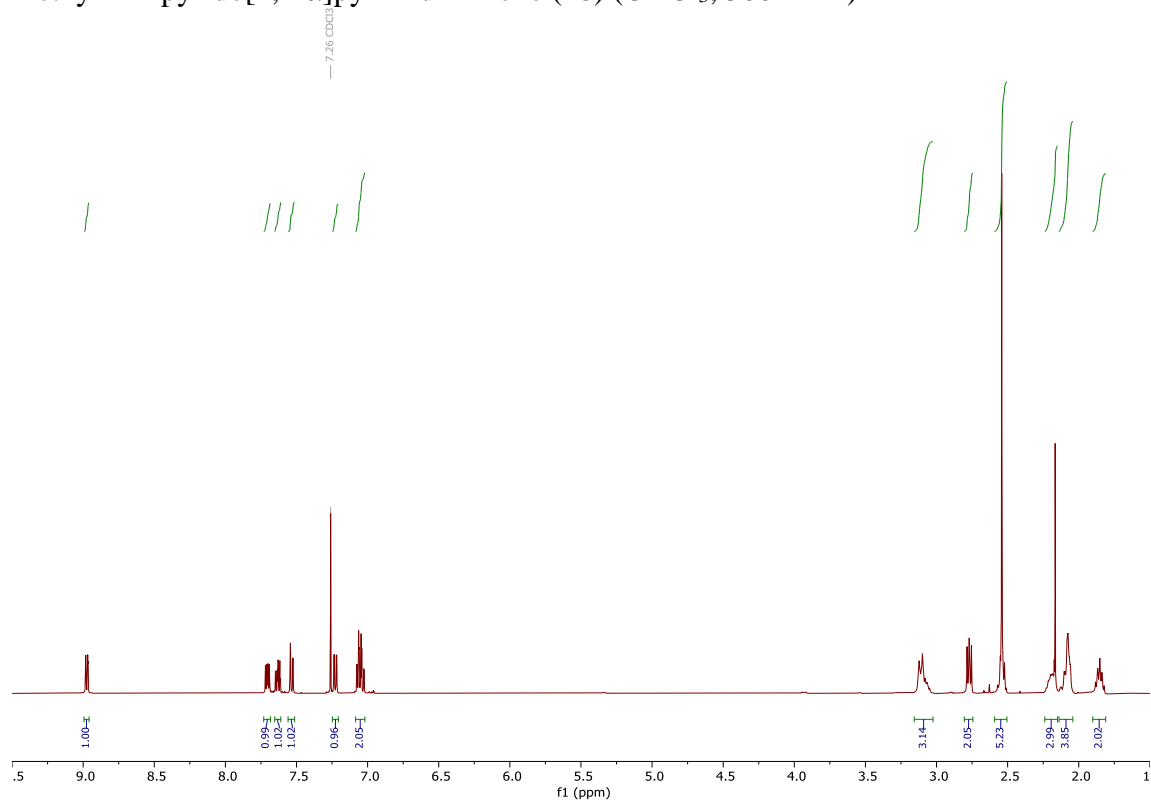
HMBC NMR spectrum of 3-(3-hydroxypropyl)-2-methyl-4H-pyrido[1,2- α]pyrimidin-4-one (**27**) (CDCl₃, 500 MHz)



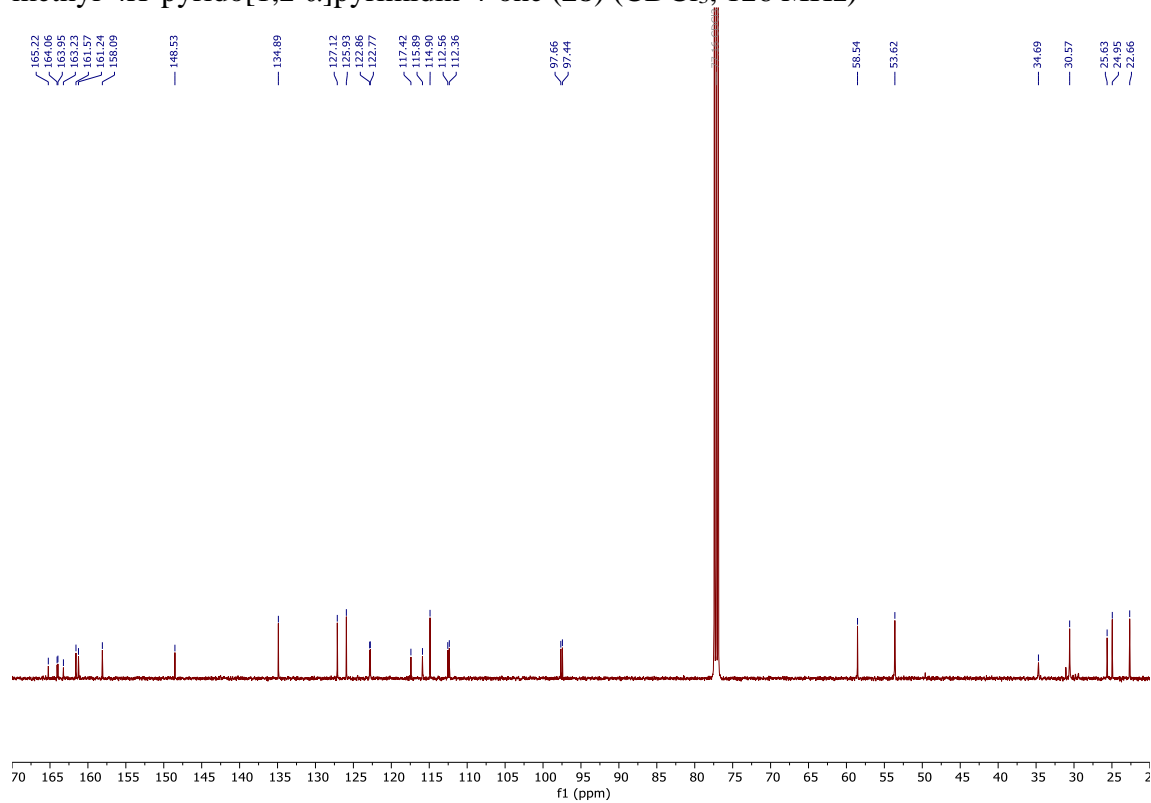
^1H NMR spectrum of 3-(3-Iodopropyl)-2-methyl-4*H*-pyrido[1,2- α]pyrimidin-4-one (**31**)
(CDCl_3 , 500 MHz)



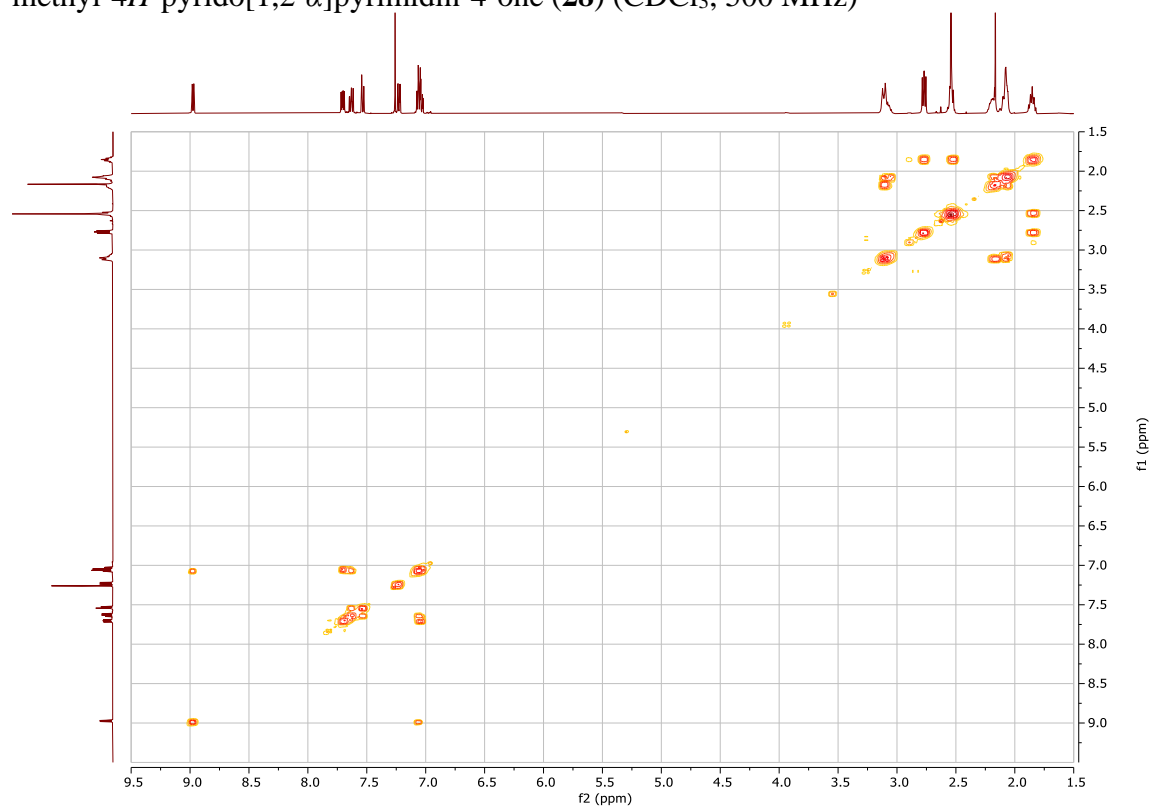
¹H NMR spectrum of 3-(3-(4-(6-Fluorobenzo[d]isoxazol-3-yl)piperidin-1-yl)propyl)-2-methyl-4*H*-pyrido[1,2-*a*]pyrimidin-4-one (**28**) (CDCl₃, 500 MHz)



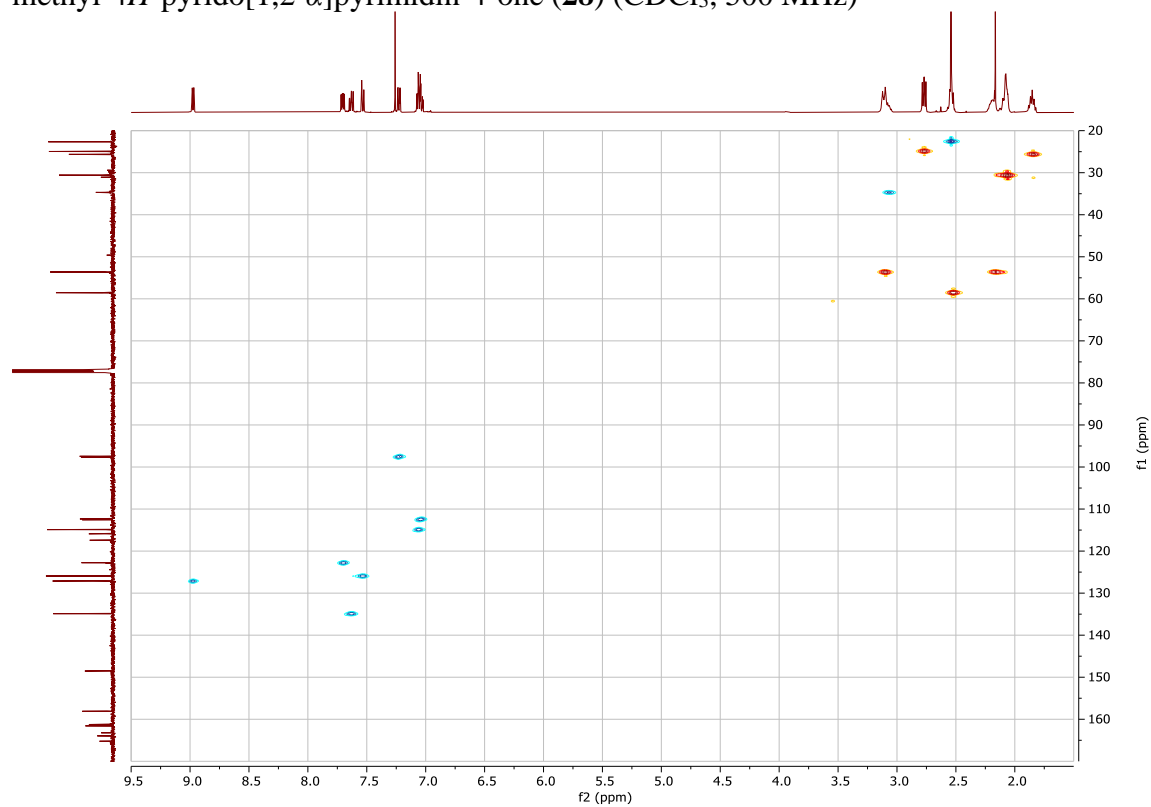
¹³C NMR spectrum of 3-(3-(4-(6-Fluorobenzo[d]isoxazol-3-yl)piperidin-1-yl)propyl)-2-methyl-4*H*-pyrido[1,2-*a*]pyrimidin-4-one (**28**) (CDCl₃, 126 MHz)



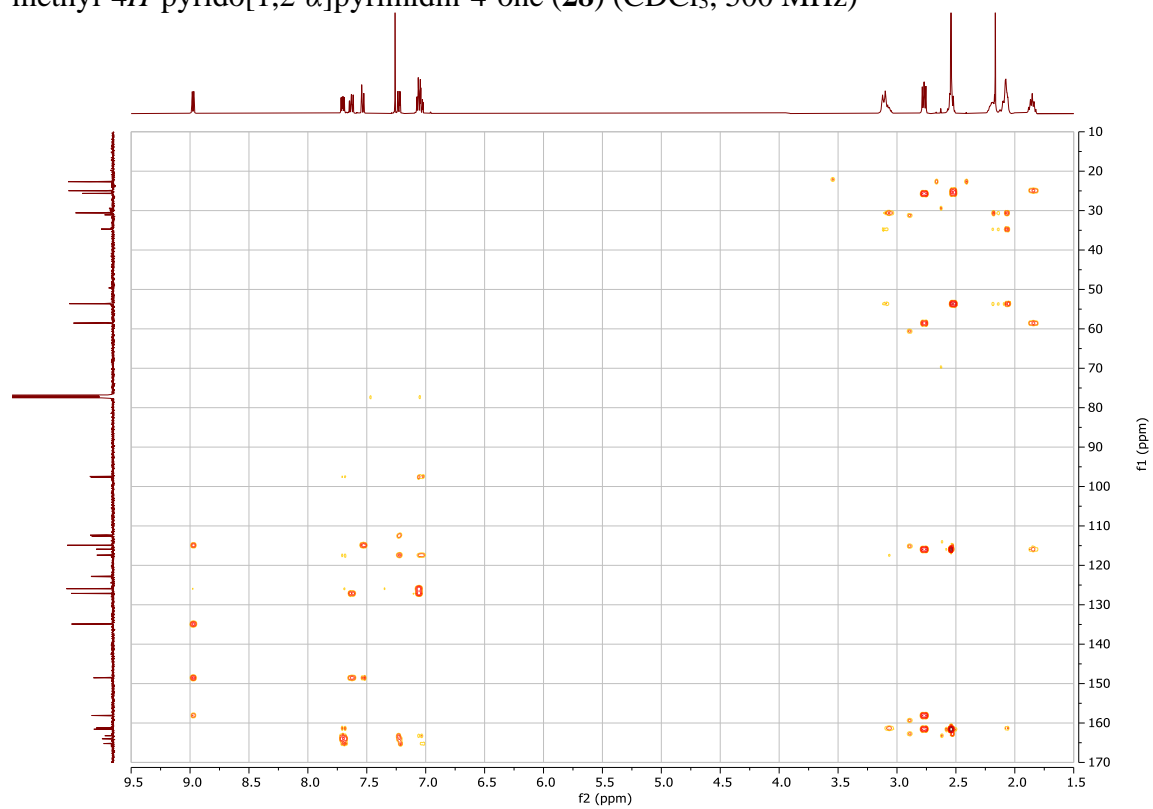
COSY NMR spectrum of 3-(3-(4-(6-Fluorobenzo[*d*]isoxazol-3-yl)piperidin-1-yl)propyl)-2-methyl-4*H*-pyrido[1,2-*a*]pyrimidin-4-one (**28**) (CDCl₃, 500 MHz)



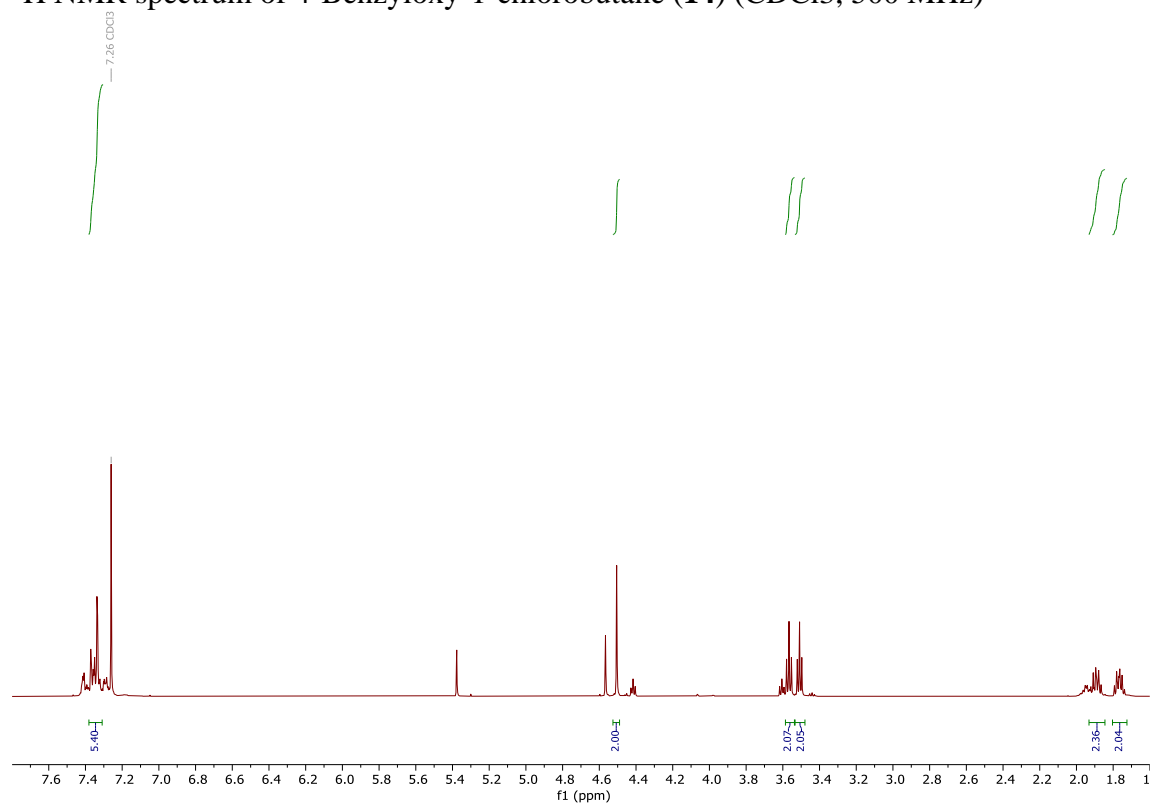
HSQC NMR spectrum of 3-(3-(4-(6-Fluorobenzo[*d*]isoxazol-3-yl)piperidin-1-yl)propyl)-2-methyl-4*H*-pyrido[1,2-*a*]pyrimidin-4-one (**28**) (CDCl₃, 500 MHz)



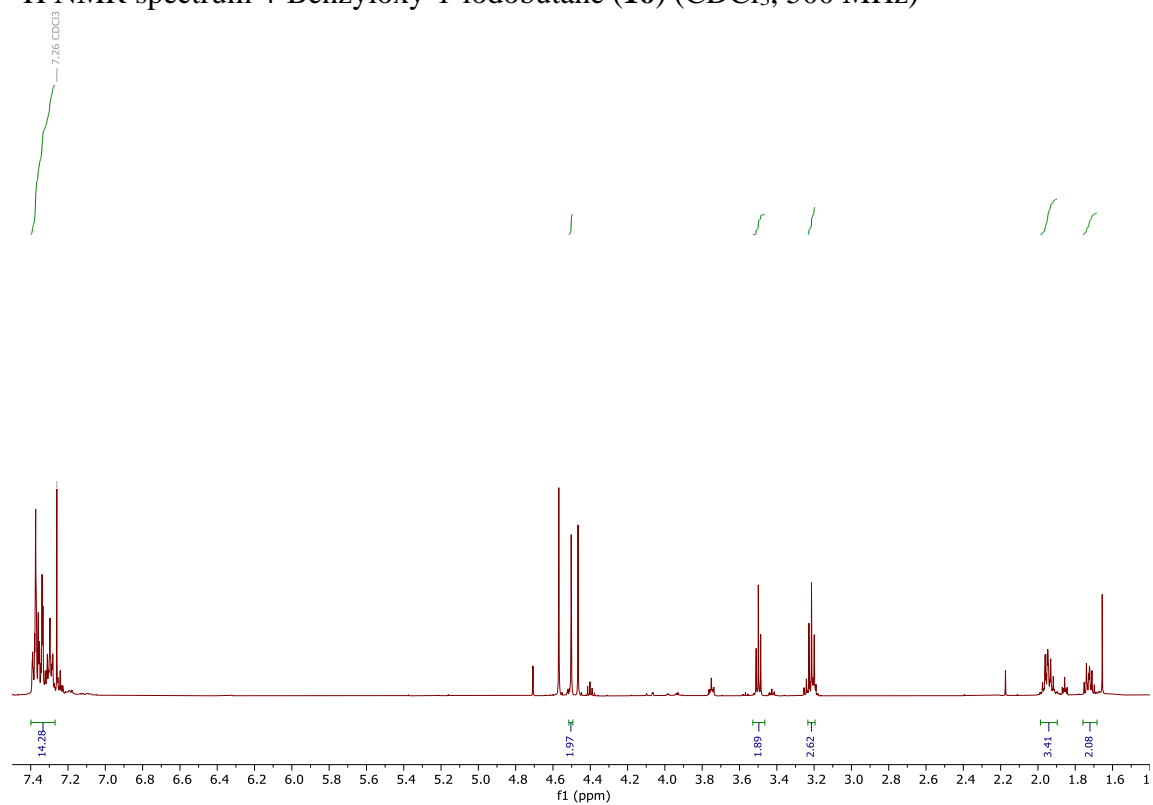
HMBC NMR spectrum of 3-(3-(4-(6-Fluorobenzo[d]isoxazol-3-yl)piperidin-1-yl)propyl)-2-methyl-4*H*-pyrido[1,2-*a*]pyrimidin-4-one (**28**) (CDCl₃, 500 MHz)



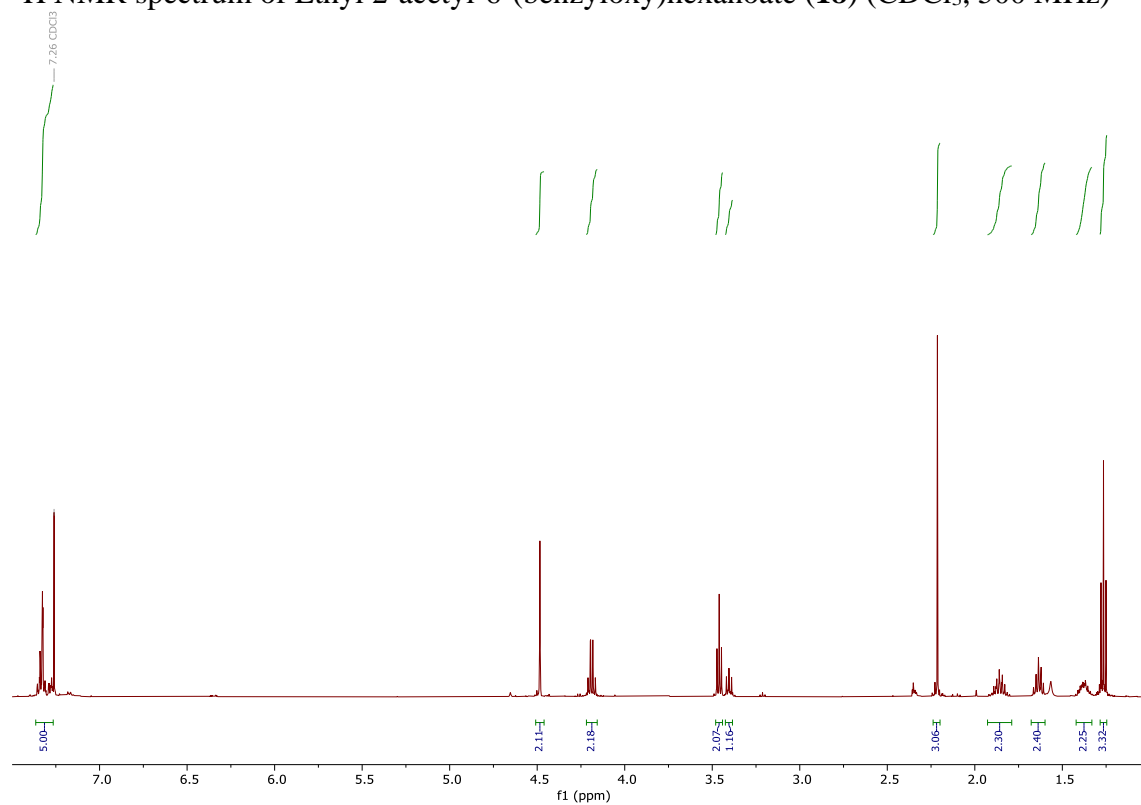
^1H NMR spectrum of 4-Benzyloxy-1-chlorobutane (**14**) (CDCl_3 , 500 MHz)



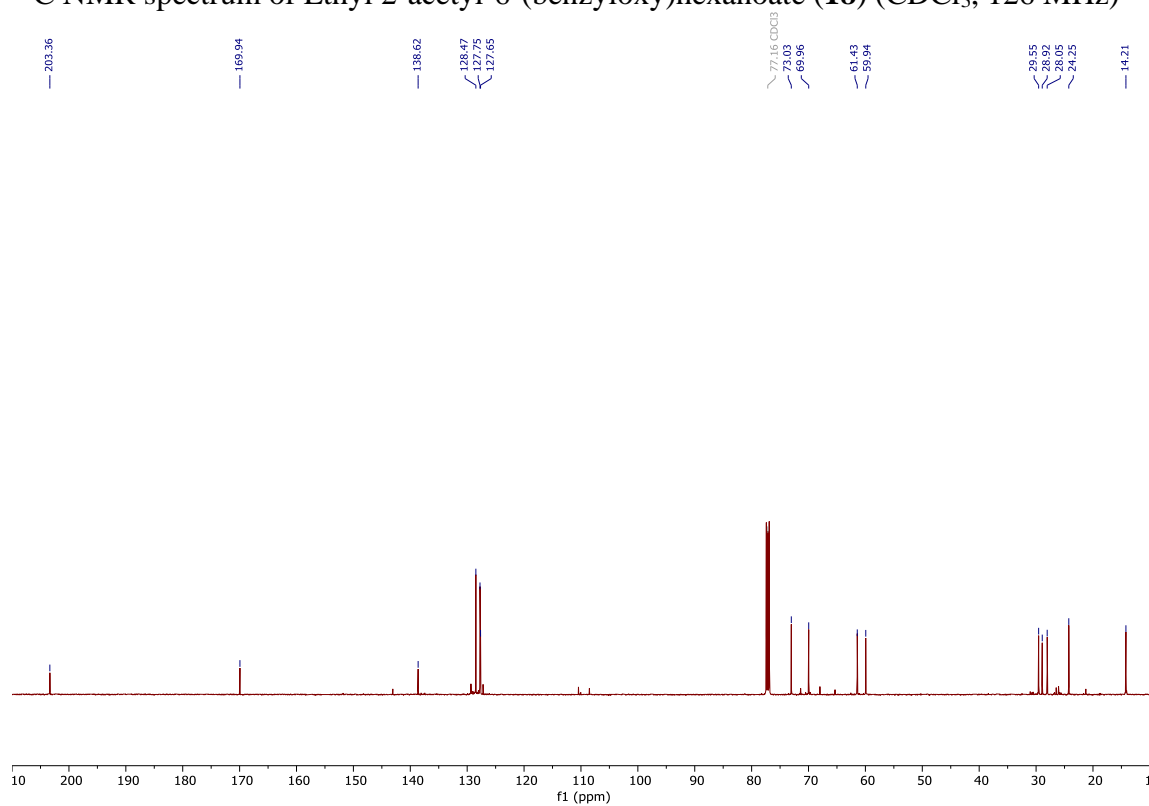
^1H NMR spectrum 4-Benzyloxy-1-iodobutane (**16**) (CDCl_3 , 500 MHz)



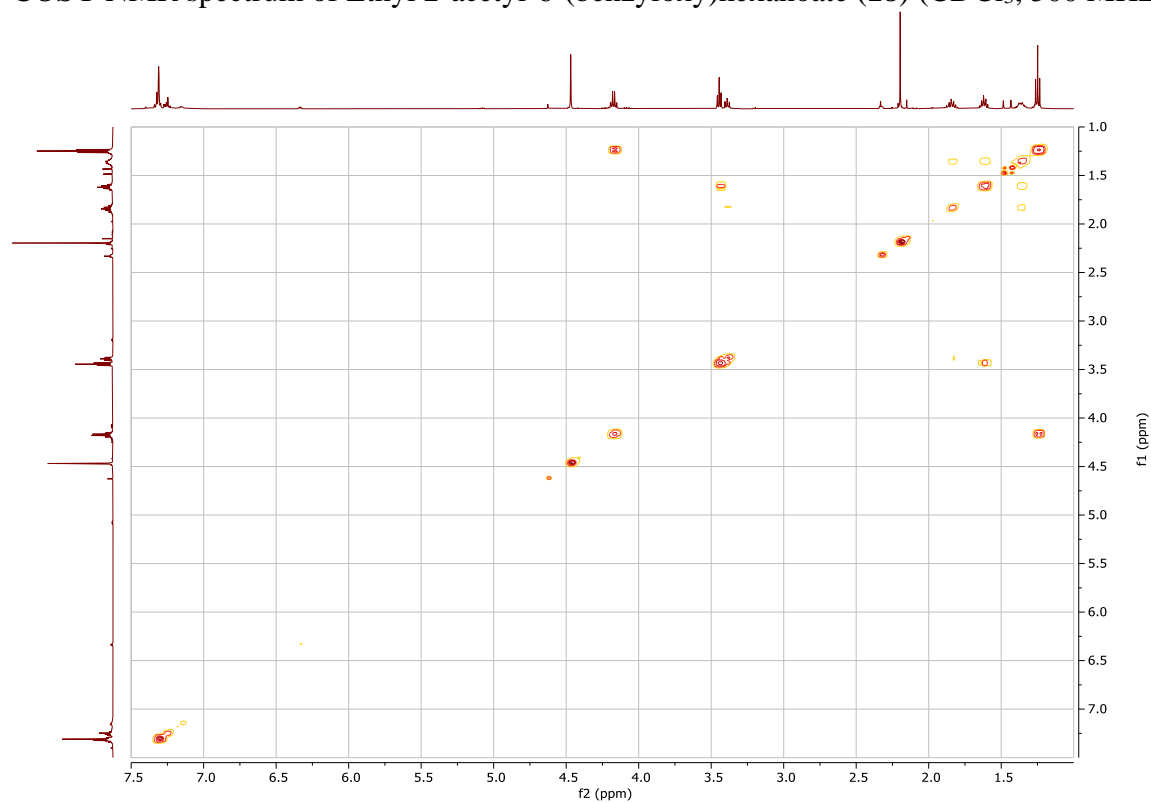
^1H NMR spectrum of Ethyl 2-acetyl-6-(benzyloxy)hexanoate (**18**) (CDCl_3 , 500 MHz)



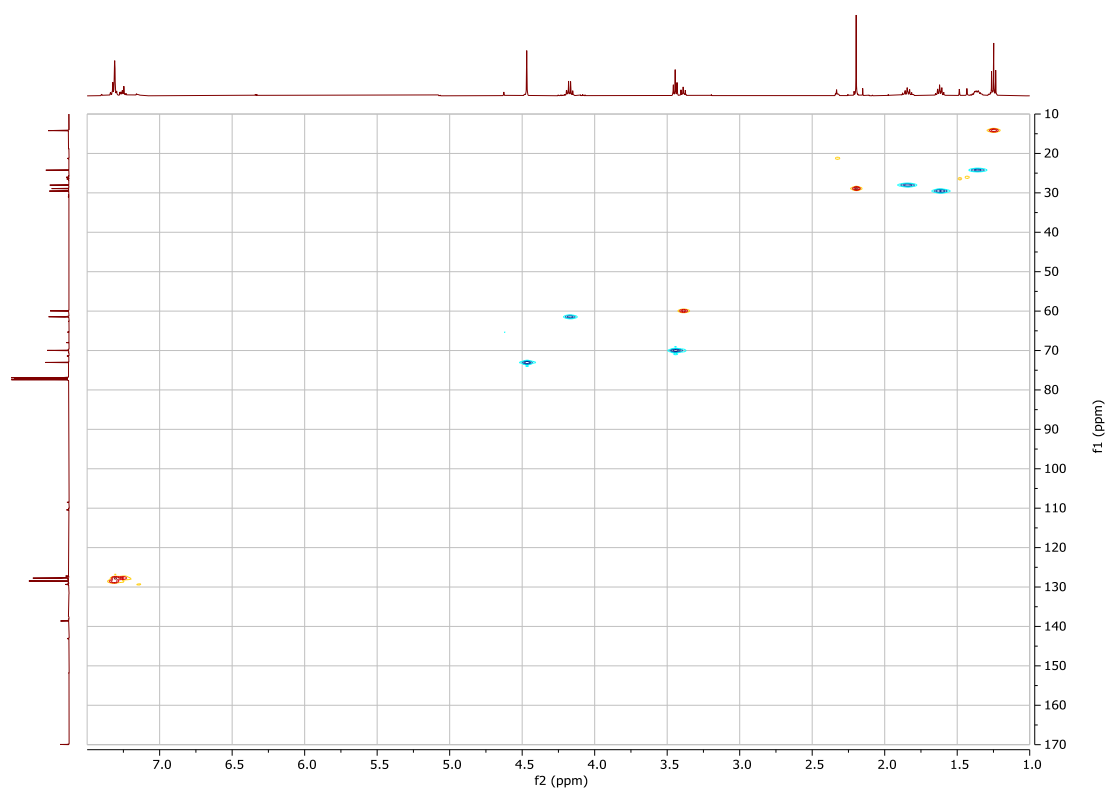
^{13}C NMR spectrum of Ethyl 2-acetyl-6-(benzyloxy)hexanoate (**18**) (CDCl_3 , 126 MHz)



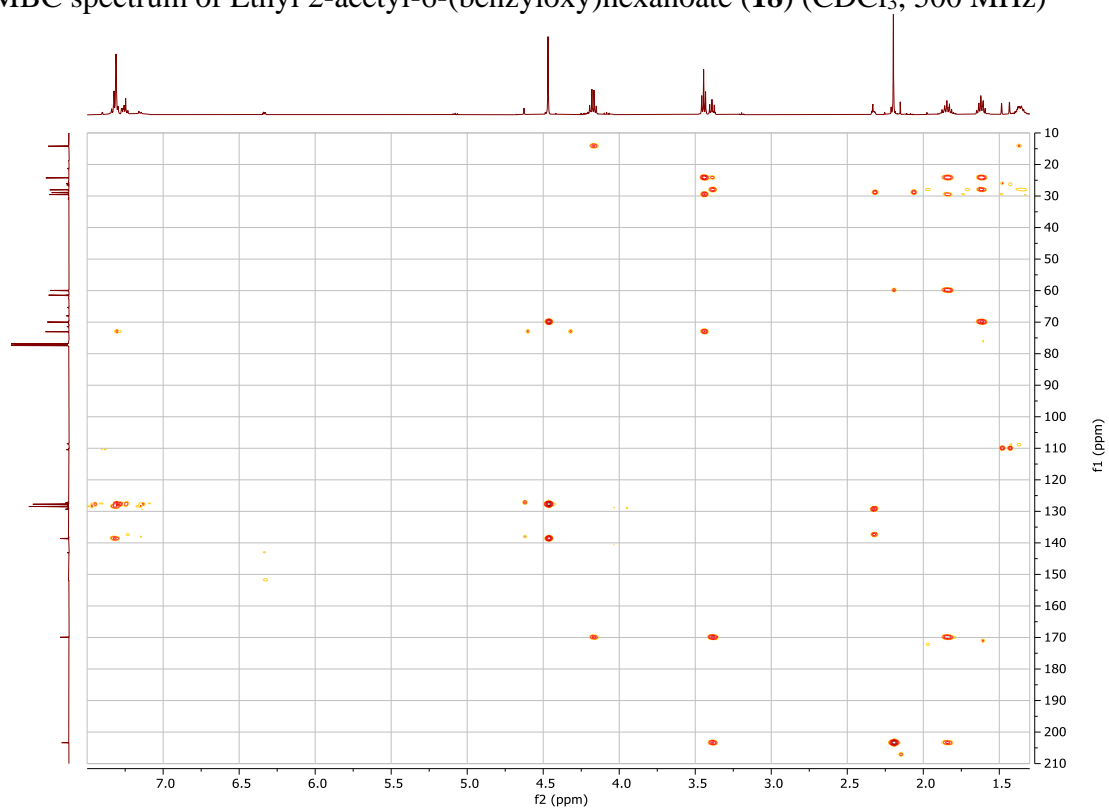
COSY NMR spectrum of Ethyl 2-acetyl-6-(benzyloxy)hexanoate (**18**) (CDCl₃, 500 MHz)



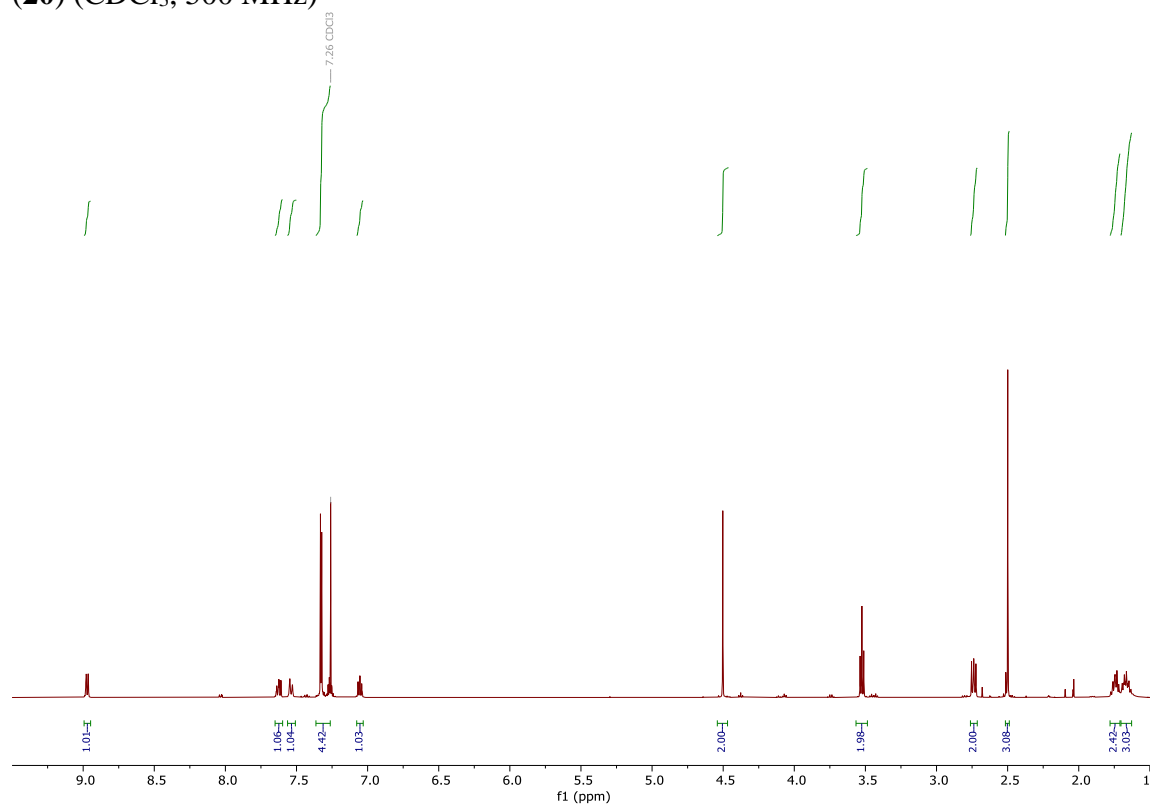
HSQC NMR spectrum of Ethyl 2-acetyl-6-(benzyloxy)hexanoate (**18**) (CDCl₃, 500 MHz)



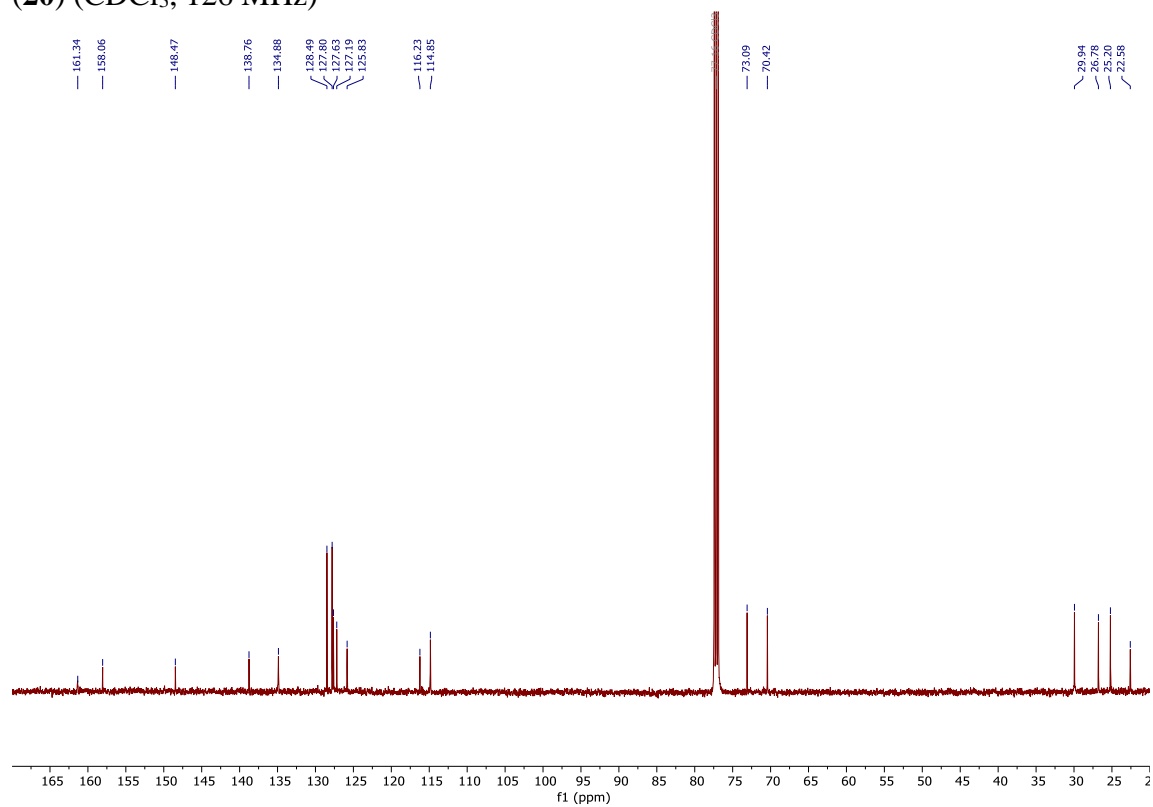
HMBC spectrum of Ethyl 2-acetyl-6-(benzyloxy)hexanoate (**18**) (CDCl₃, 500 MHz)



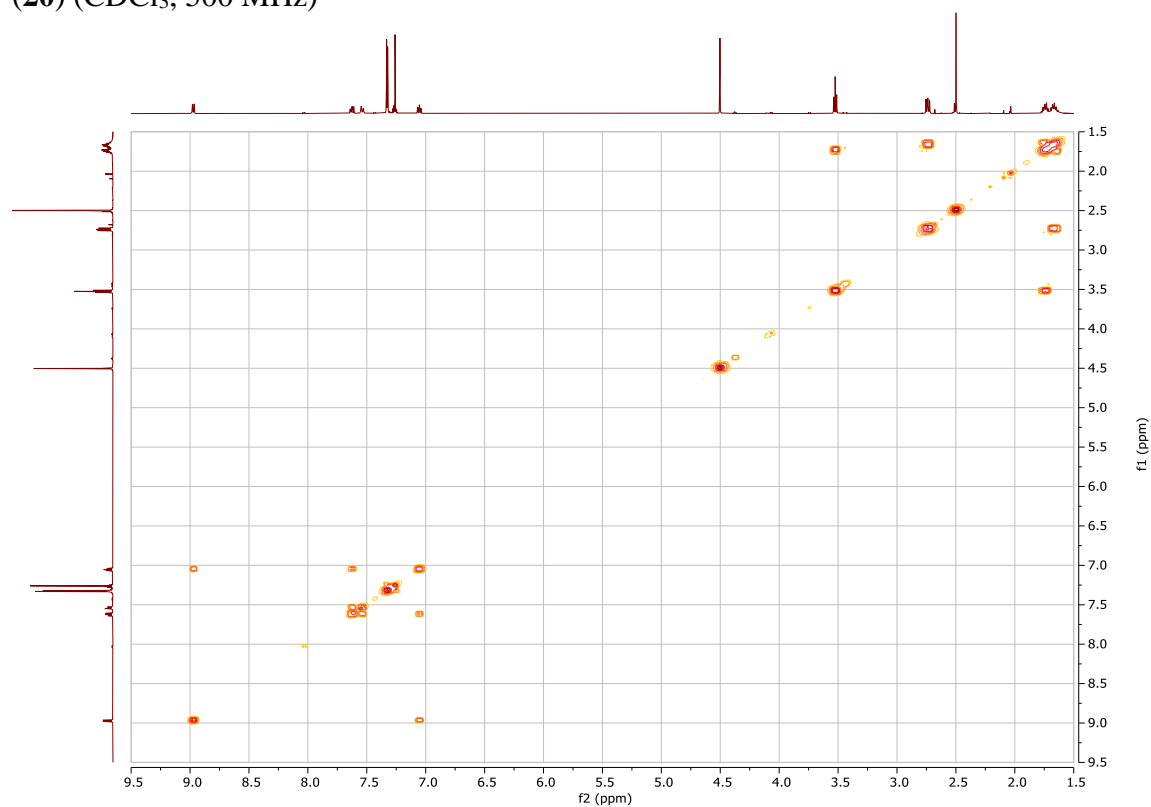
^1H NMR spectrum of 3-(4-(Benzyloxy)butyl)-2-methyl-4*H*-pyrido[1,2- α]pyrimidin-4-one (**20**) (CDCl_3 , 500 MHz)



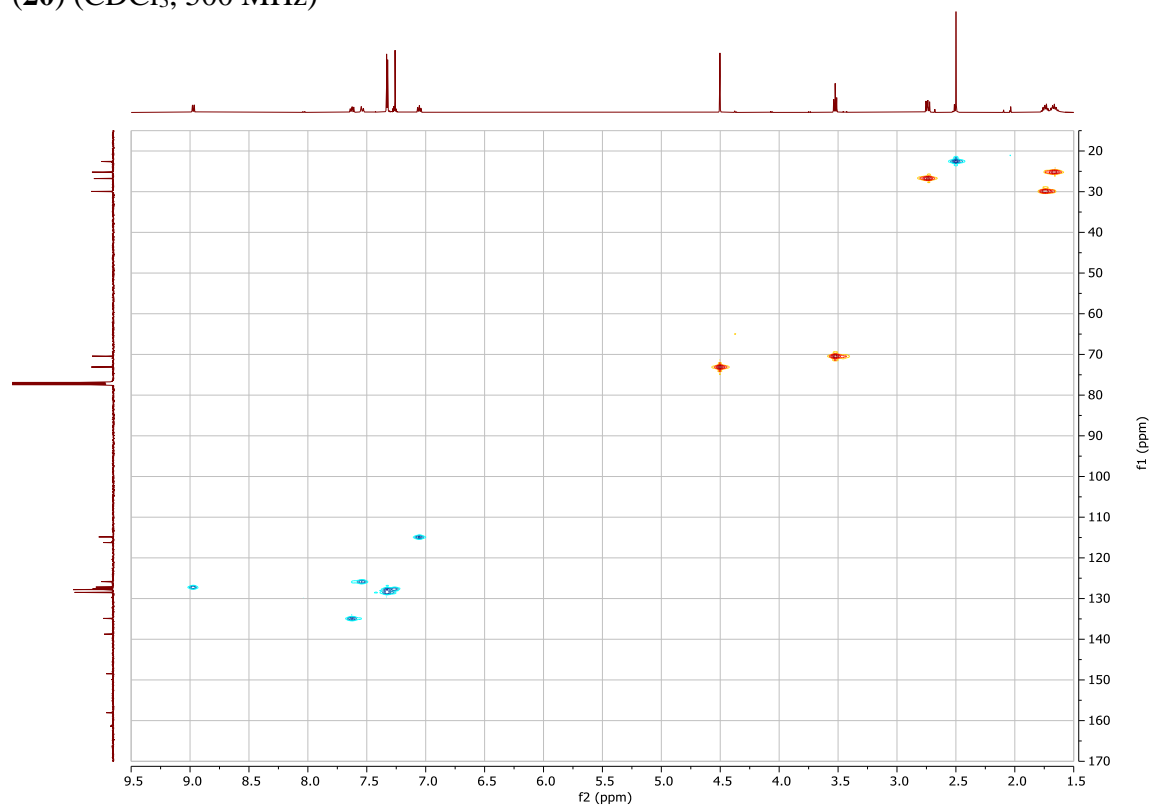
^{13}C NMR spectrum of 3-(4-(Benzyloxy)butyl)-2-methyl-4*H*-pyrido[1,2- α]pyrimidin-4-one (**20**) (CDCl_3 , 126 MHz)



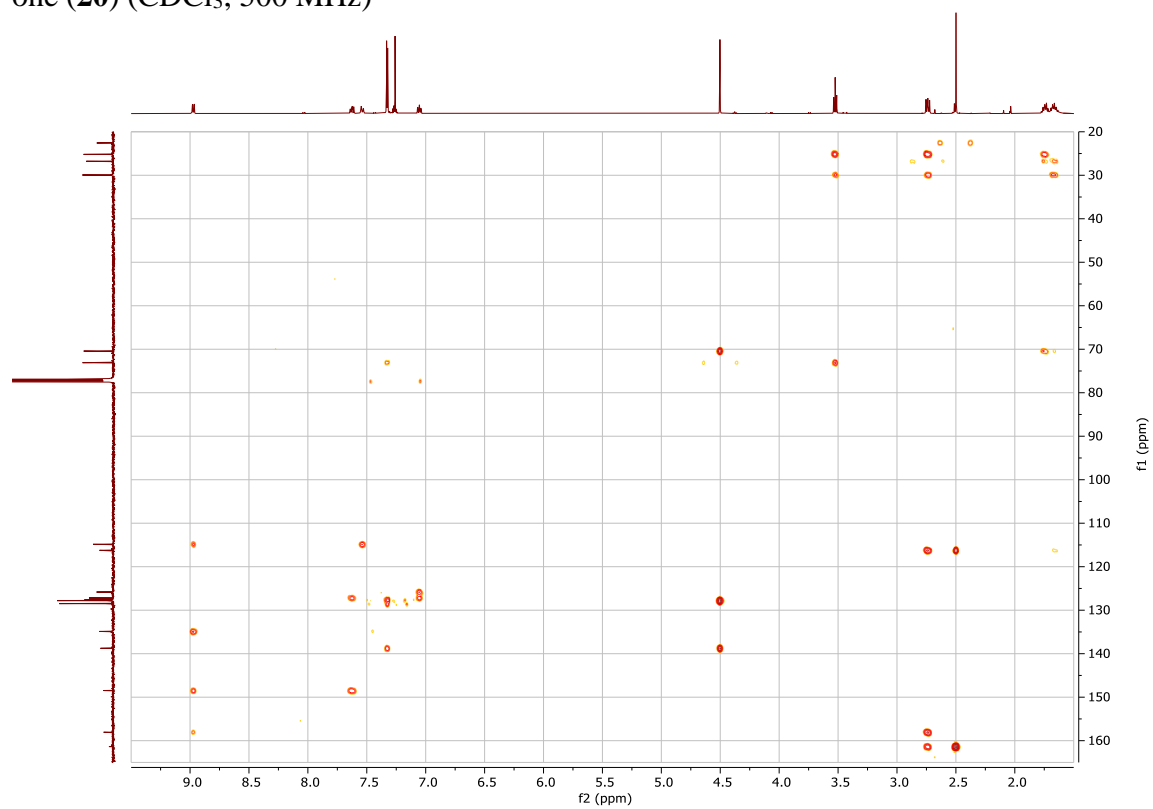
COSY NMR spectrum of 3-(4-(Benzyloxy)butyl)-2-methyl-4*H*-pyrido[1,2-*a*]pyrimidin-4-one (**20**) (CDCl₃, 500 MHz)



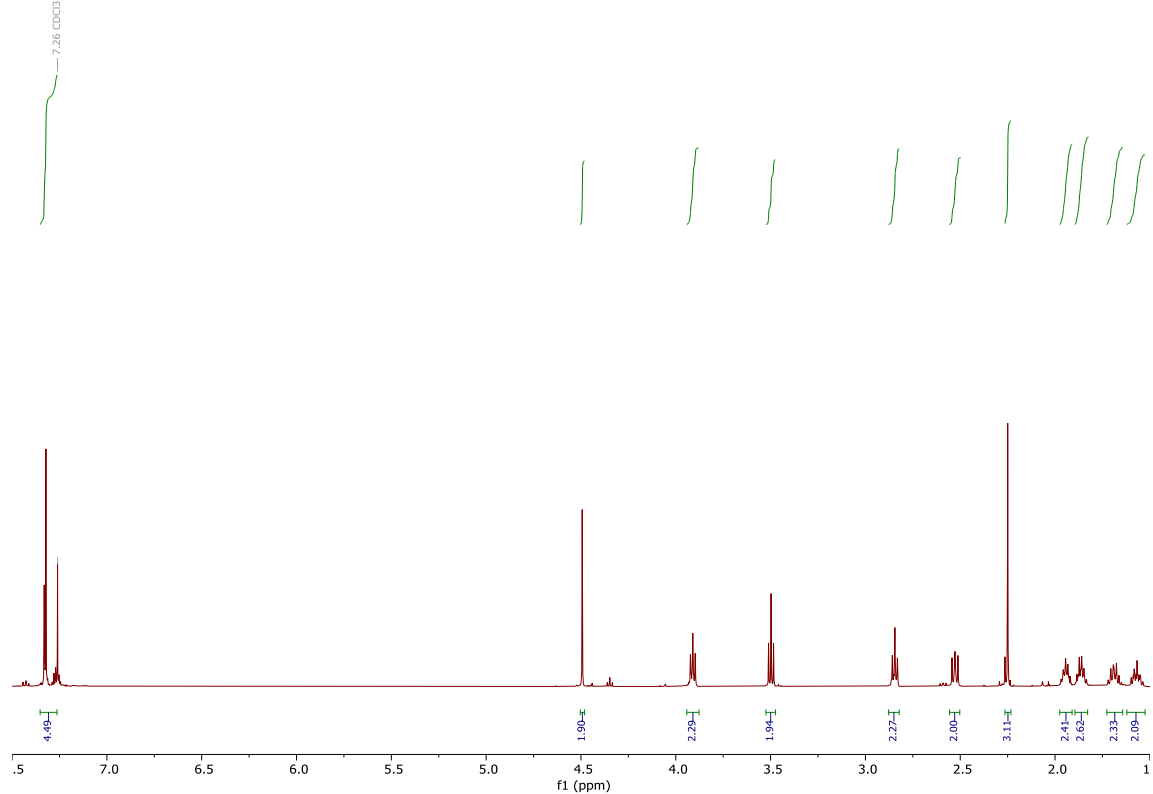
HSQC NMR spectrum of 3-(4-(Benzyloxy)butyl)-2-methyl-4*H*-pyrido[1,2-*a*]pyrimidin-4-one (**20**) (CDCl₃, 500 MHz)



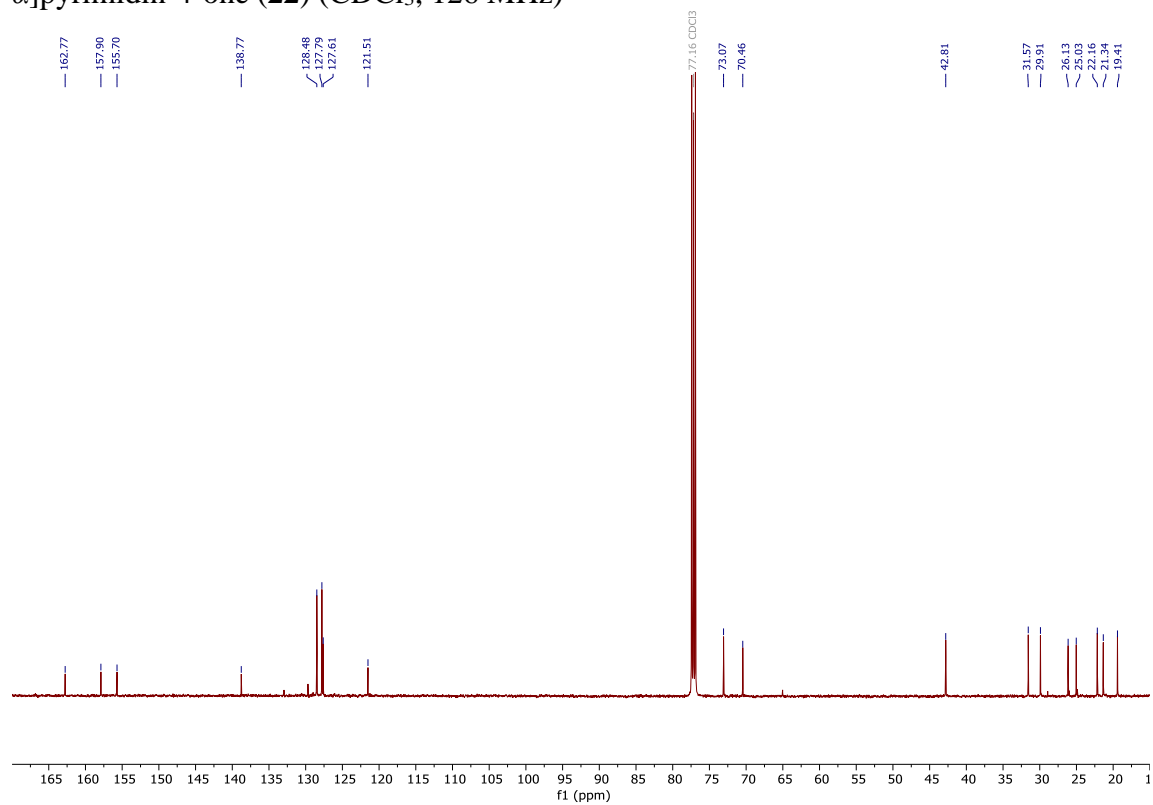
HMBC NMR spectrum of 3-(4-(Benzyloxy)butyl)-2-methyl-4*H*-pyrido[1,2- α]pyrimidin-4-one (**20**) (CDCl₃, 500 MHz)



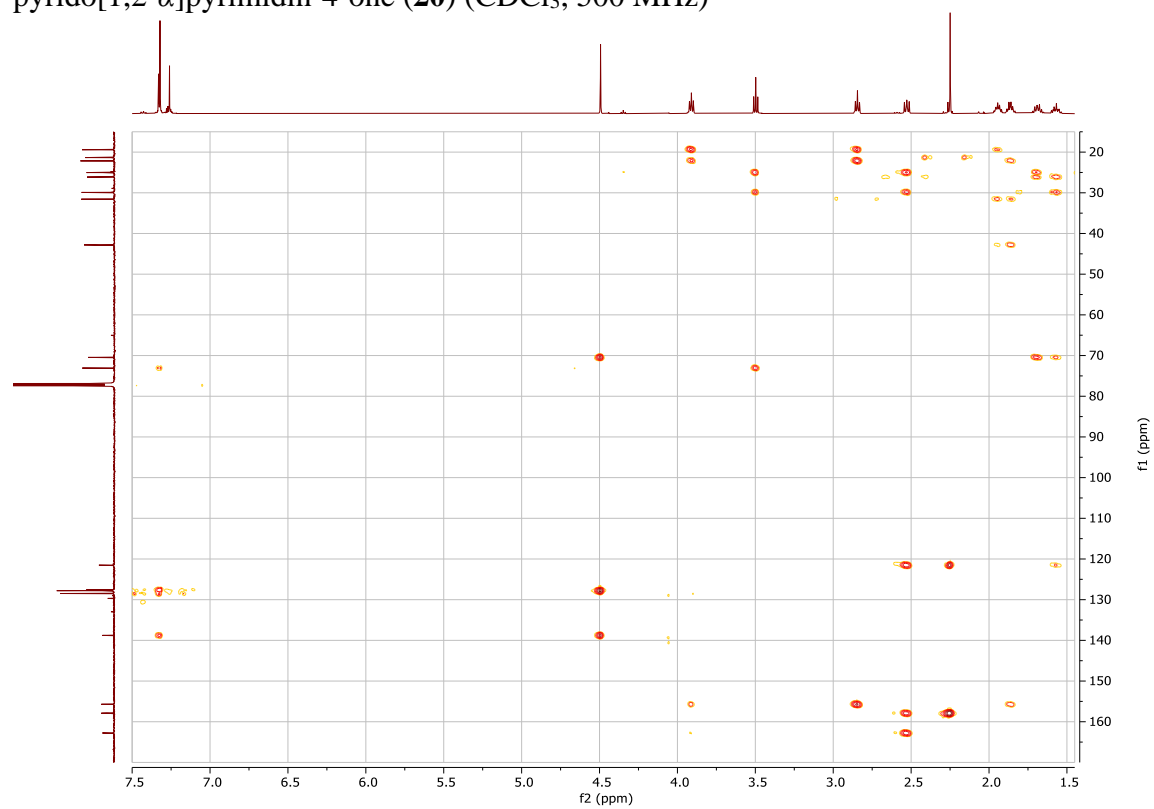
^1H NMR spectrum of 3-(4-(Benzyloxy)butyl)-2-methyl-6,7,8,9-tetrahydro-4*H*-pyrido[1,2- α]pyrimidin-4-one (**22**) (CDCl_3 , 500 MHz)



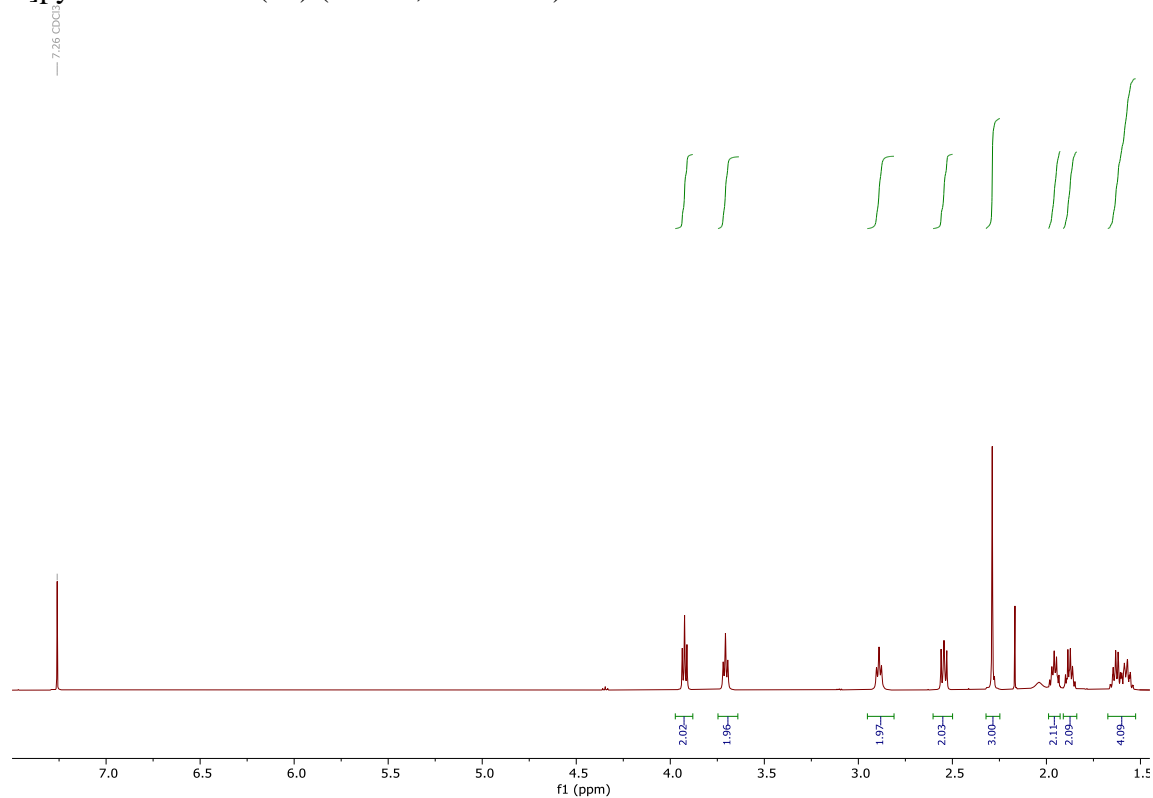
^{13}C NMR spectrum of 3-(4-(Benzyloxy)butyl)-2-methyl-6,7,8,9-tetrahydro-4*H*-pyrido[1,2- α]pyrimidin-4-one (**22**) (CDCl_3 , 126 MHz)



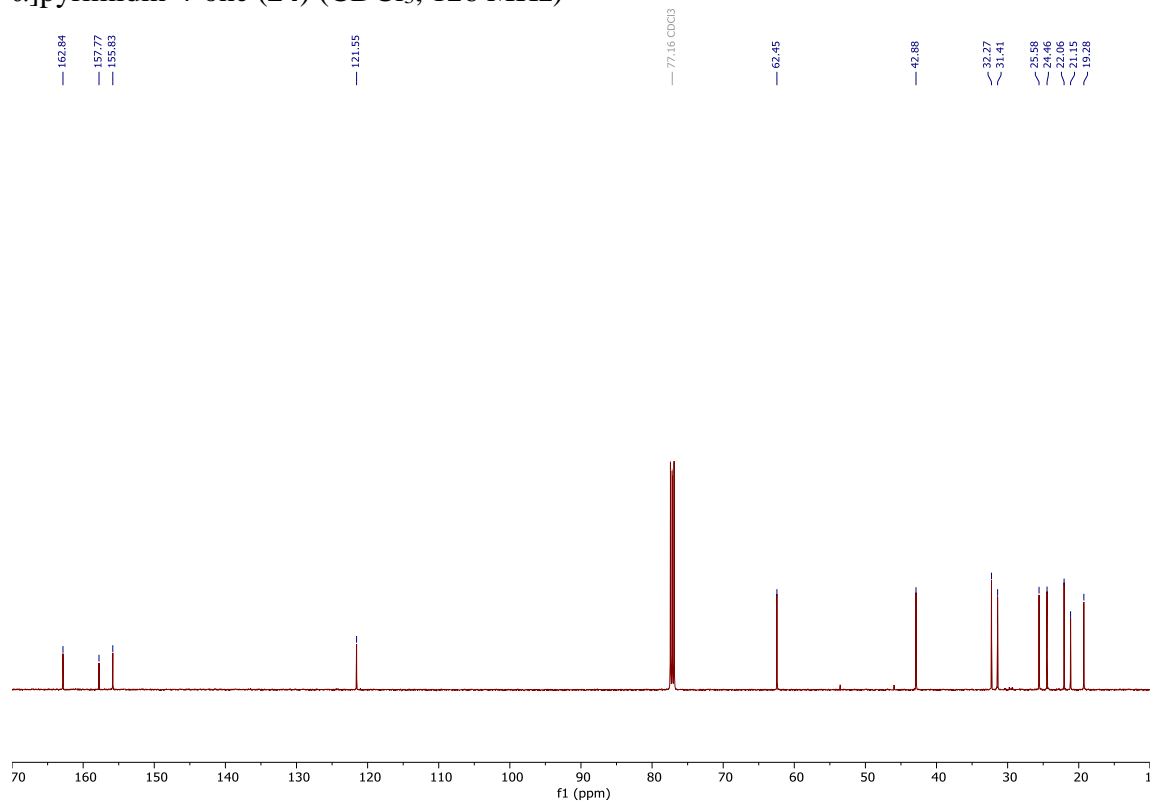
HMBC NMR spectrum of 3-(4-(Benzyloxy)butyl)-2-methyl-6,7,8,9-tetrahydro-4H-pyrido[1,2- α]pyrimidin-4-one (**20**) (CDCl₃, 500 MHz)



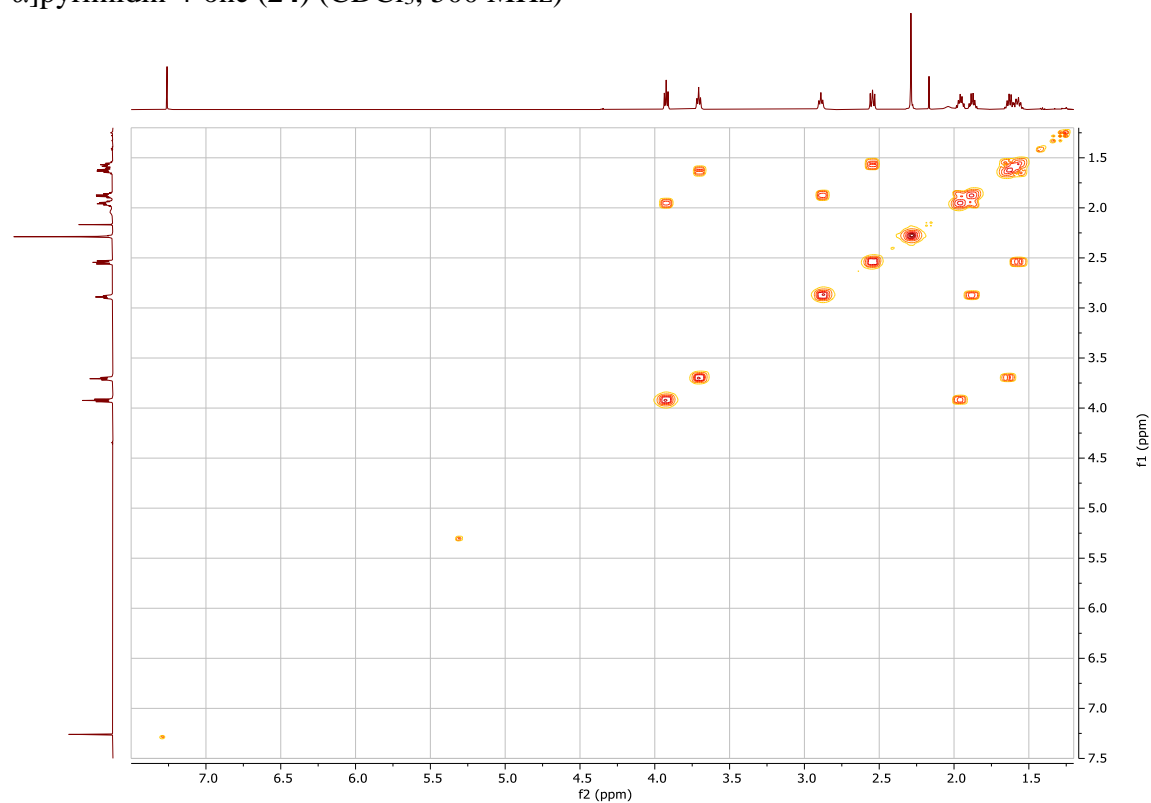
^1H NMR spectrum of 3-(4-Hydroxybutyl)-2-methyl-6,7,8,9-tetrahydro-4*H*-pyrido[1,2- α]pyrimidin-4-one (**24**) (CDCl_3 , 500 MHz)



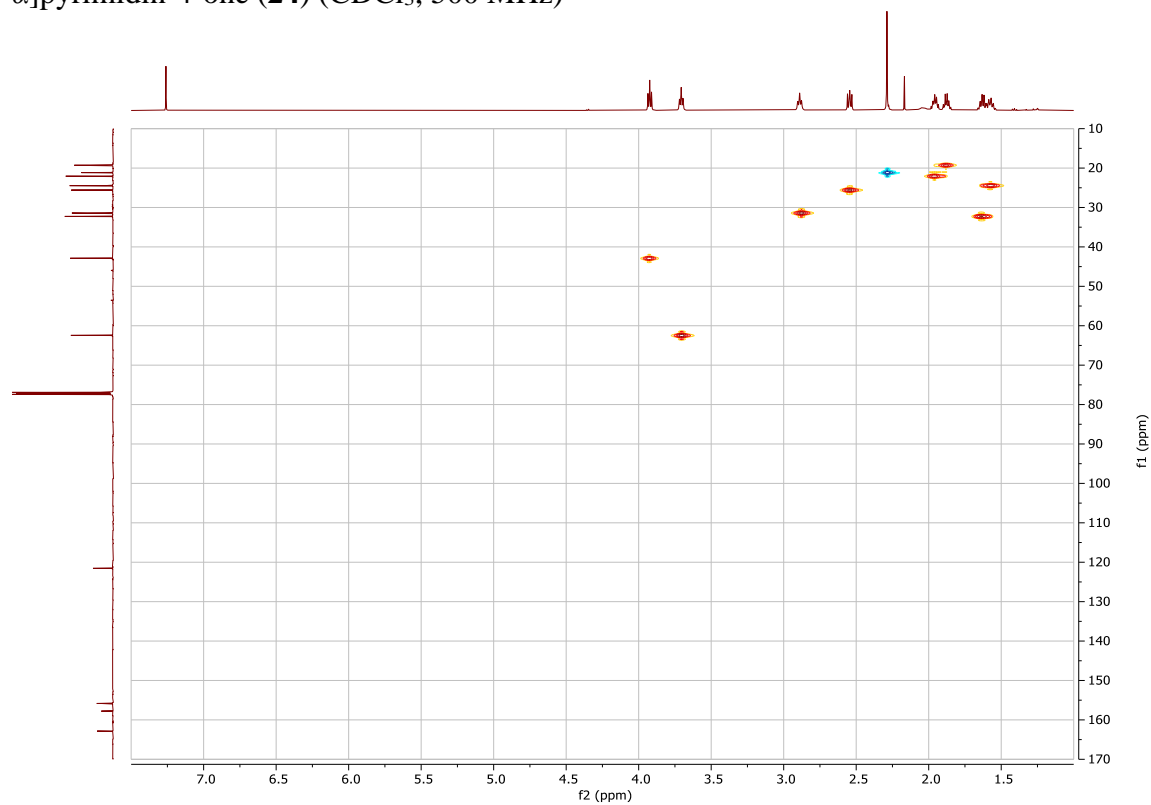
^{13}C NMR spectrum of 3-(4-Hydroxybutyl)-2-methyl-6,7,8,9-tetrahydro-4*H*-pyrido[1,2- α]pyrimidin-4-one (**24**) (CDCl_3 , 126 MHz)



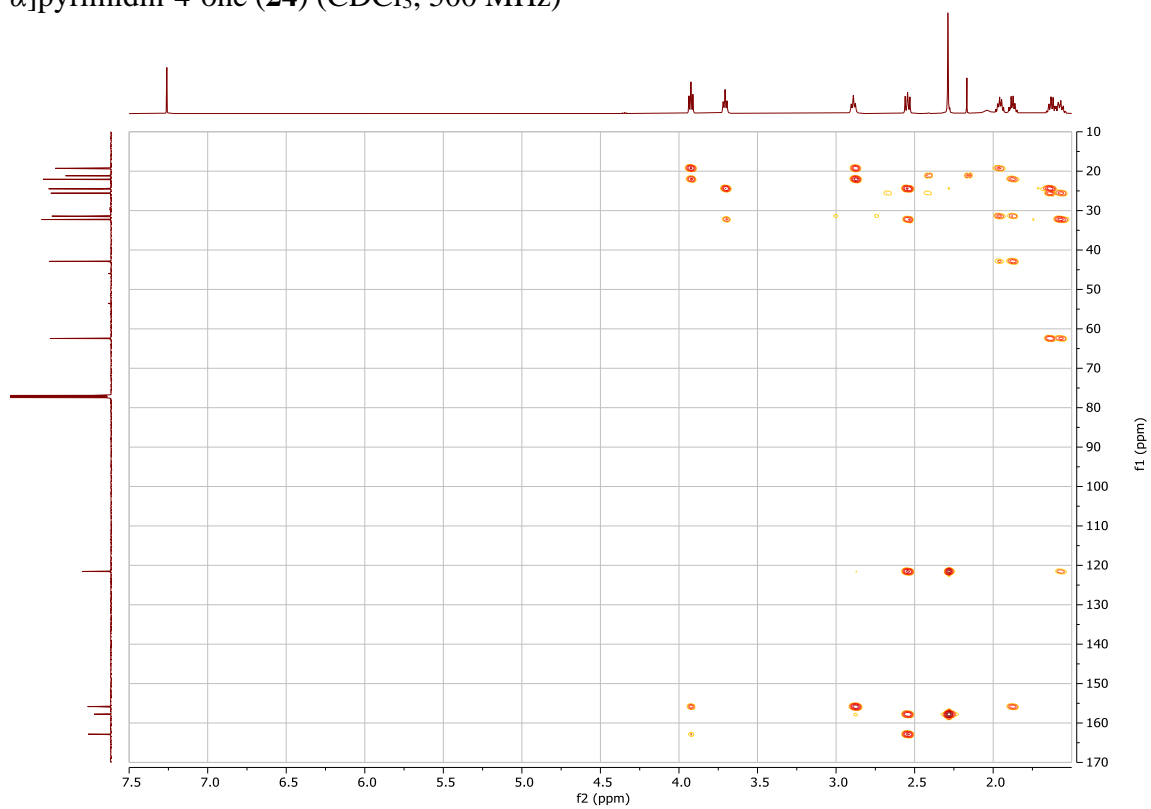
COSY NMR spectrum of 3-(4-Hydroxybutyl)-2-methyl-6,7,8,9-tetrahydro-4*H*-pyrido[1,2- α]pyrimidin-4-one (**24**) (CDCl₃, 500 MHz)



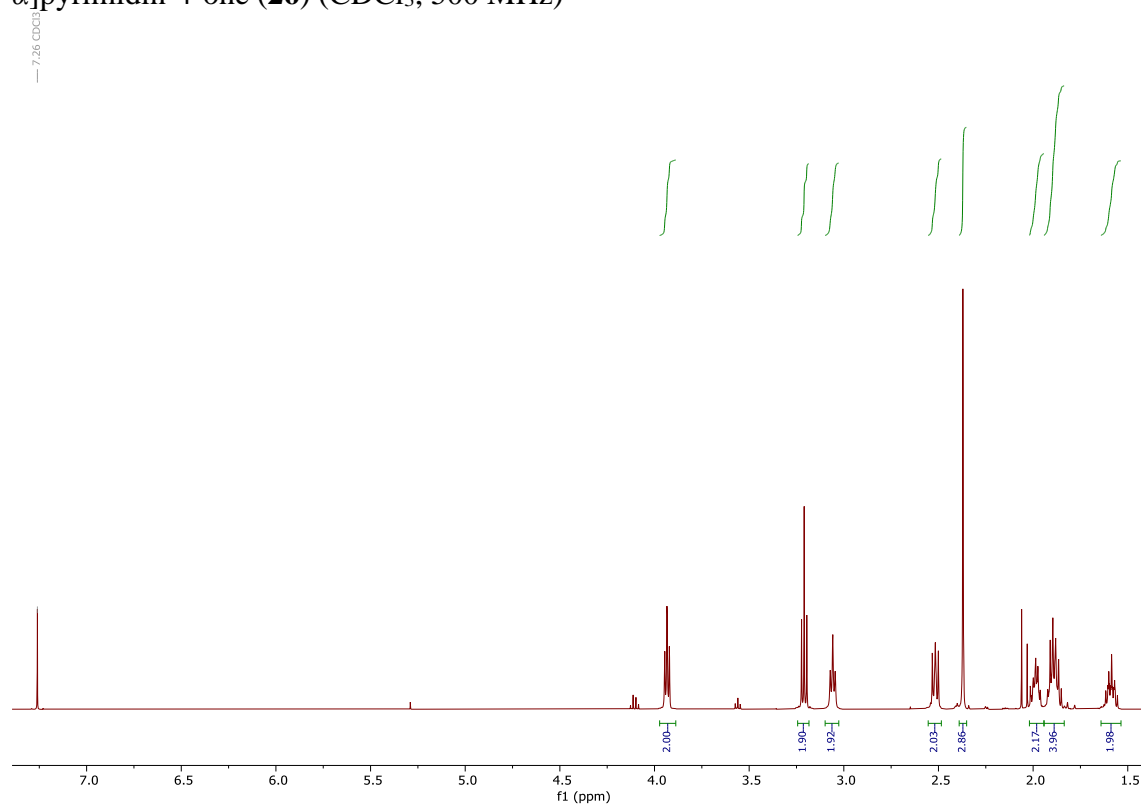
HSQC NMR spectrum of 3-(4-Hydroxybutyl)-2-methyl-6,7,8,9-tetrahydro-4*H*-pyrido[1,2- α]pyrimidin-4-one (**24**) (CDCl₃, 500 MHz)



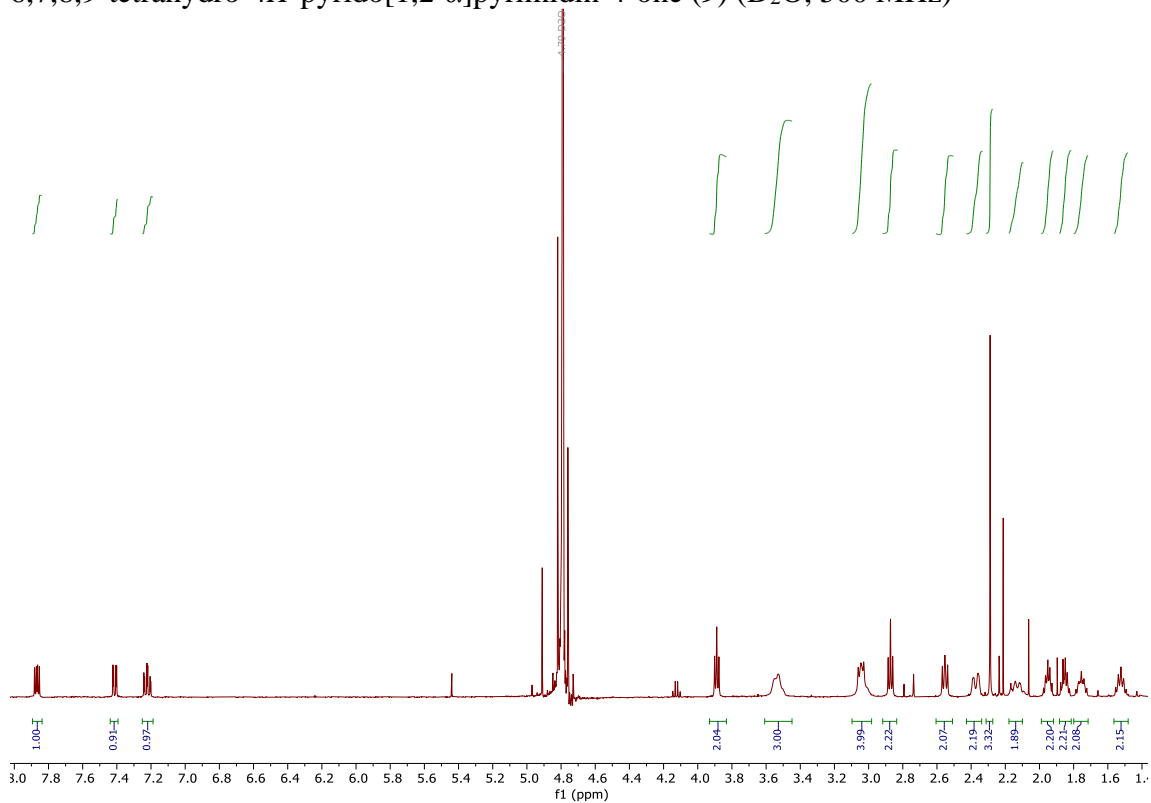
HMBC spectrum of 3-(4-Hydroxybutyl)-2-methyl-6,7,8,9-tetrahydro-4*H*-pyrido[1,2- α]pyrimidin-4-one (**24**) (CDCl₃, 500 MHz)



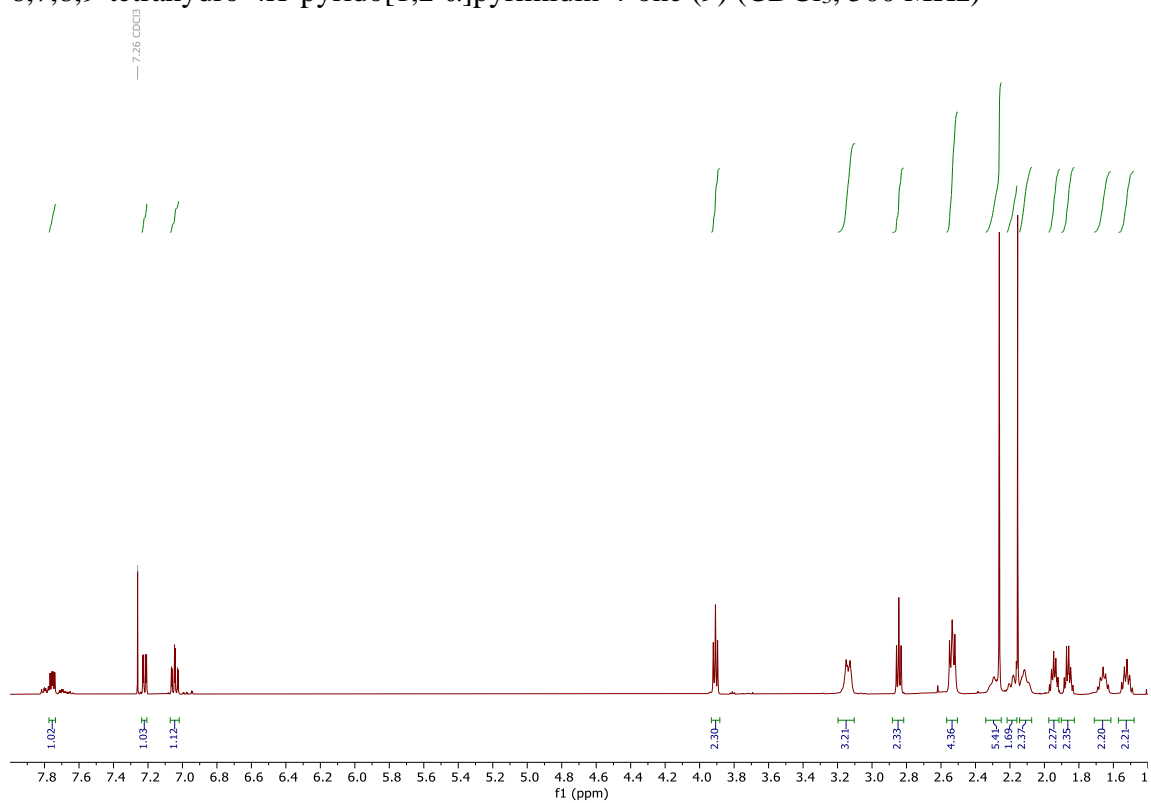
^1H NMR spectrum of 3-(4-Iodobutyl)-2-methyl-6,7,8,9-tetrahydro-4*H*-pyrido[1,2- α]pyrimidin-4-one (**26**) (CDCl_3 , 500 MHz)



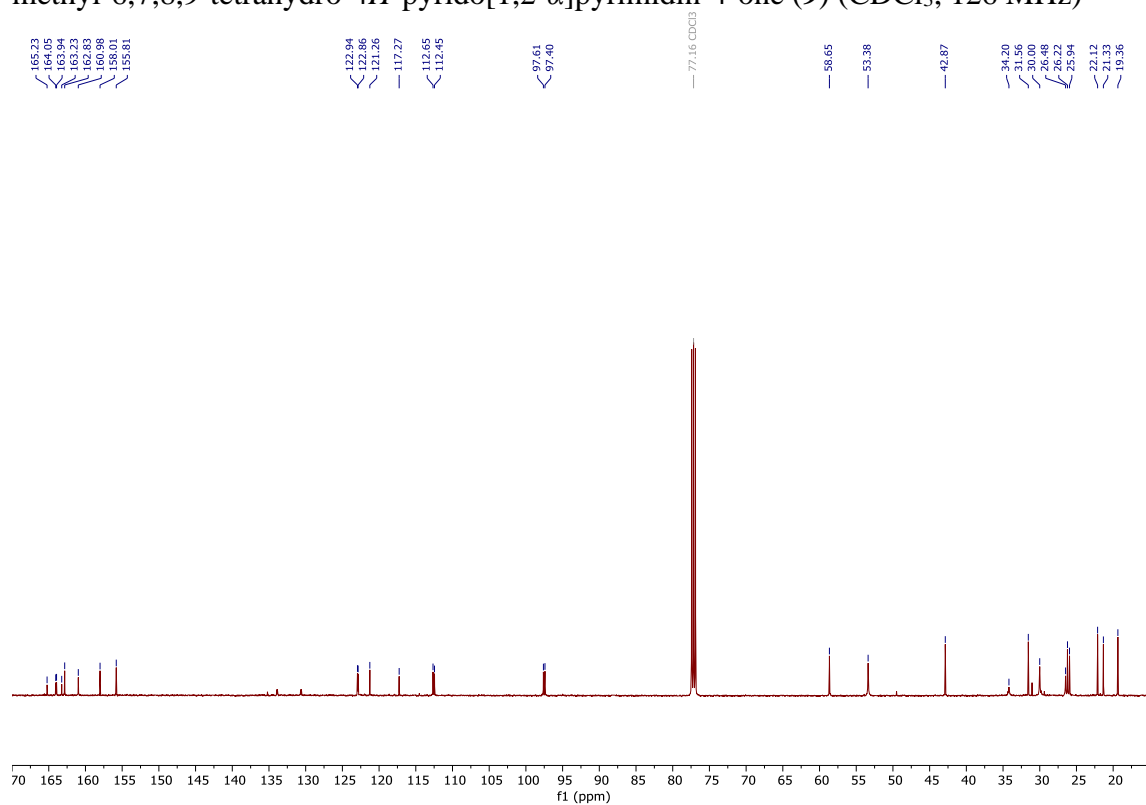
^1H NMR spectrum of 3-(4-(4-(6-Fluorobenzo[*d*]isoxazol-3-yl)piperidin-1-yl)butyl)-2-methyl-6,7,8,9-tetrahydro-4*H*-pyrido[1,2-*a*]pyrimidin-4-one (**9**) (D_2O , 500 MHz)



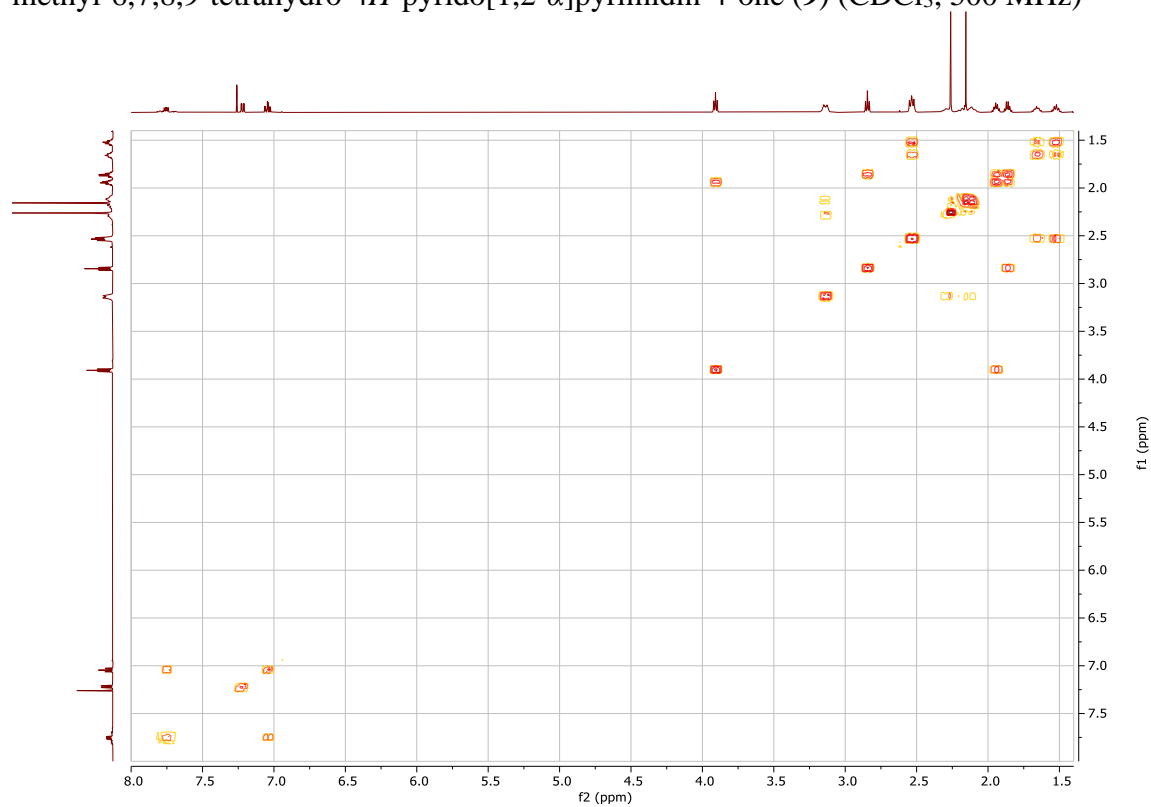
^1H NMR spectrum of 3-(4-(4-(6-Fluorobenzo[*d*]isoxazol-3-yl)piperidin-1-yl)butyl)-2-methyl-6,7,8,9-tetrahydro-4*H*-pyrido[1,2-*a*]pyrimidin-4-one (**9**) (CDCl_3 , 500 MHz)



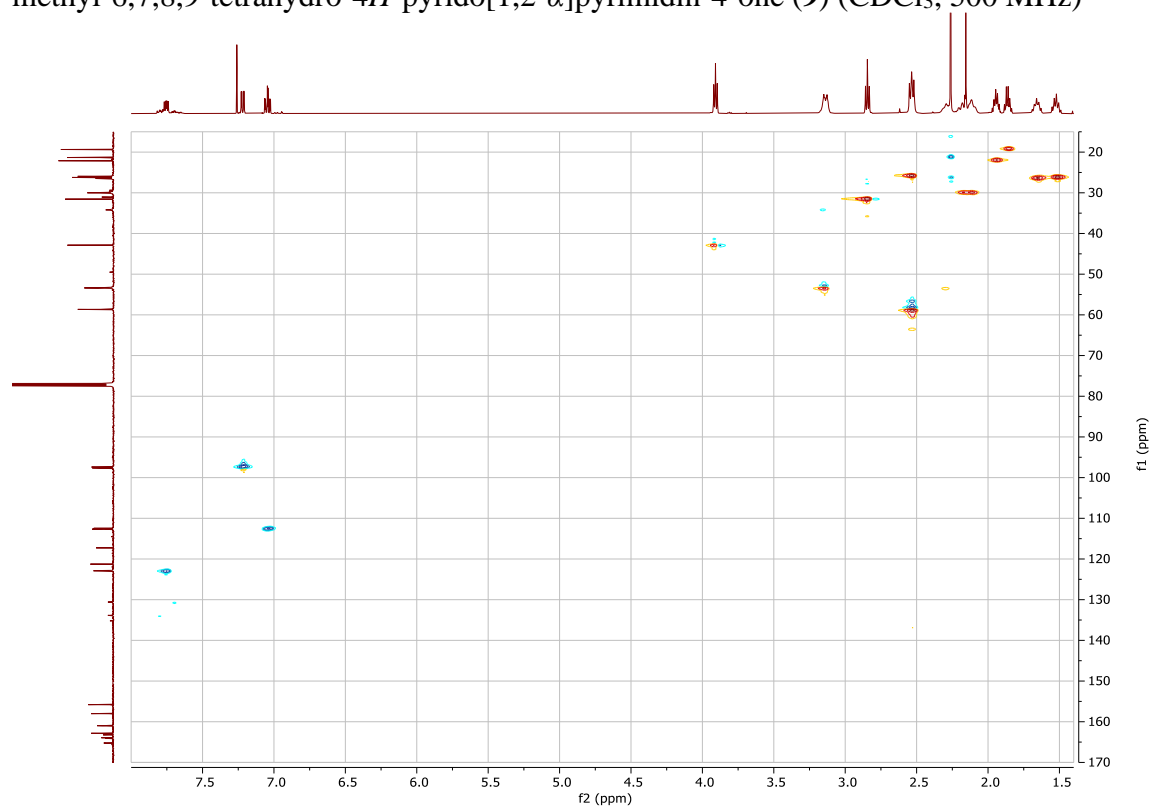
^{13}C NMR spectrum of 3-(4-(4-(6-Fluorobenzo[*d*]isoxazol-3-yl)piperidin-1-yl)butyl)-2-methyl-6,7,8,9-tetrahydro-4*H*-pyrido[1,2- α]pyrimidin-4-one (**9**) (CDCl_3 , 126 MHz)



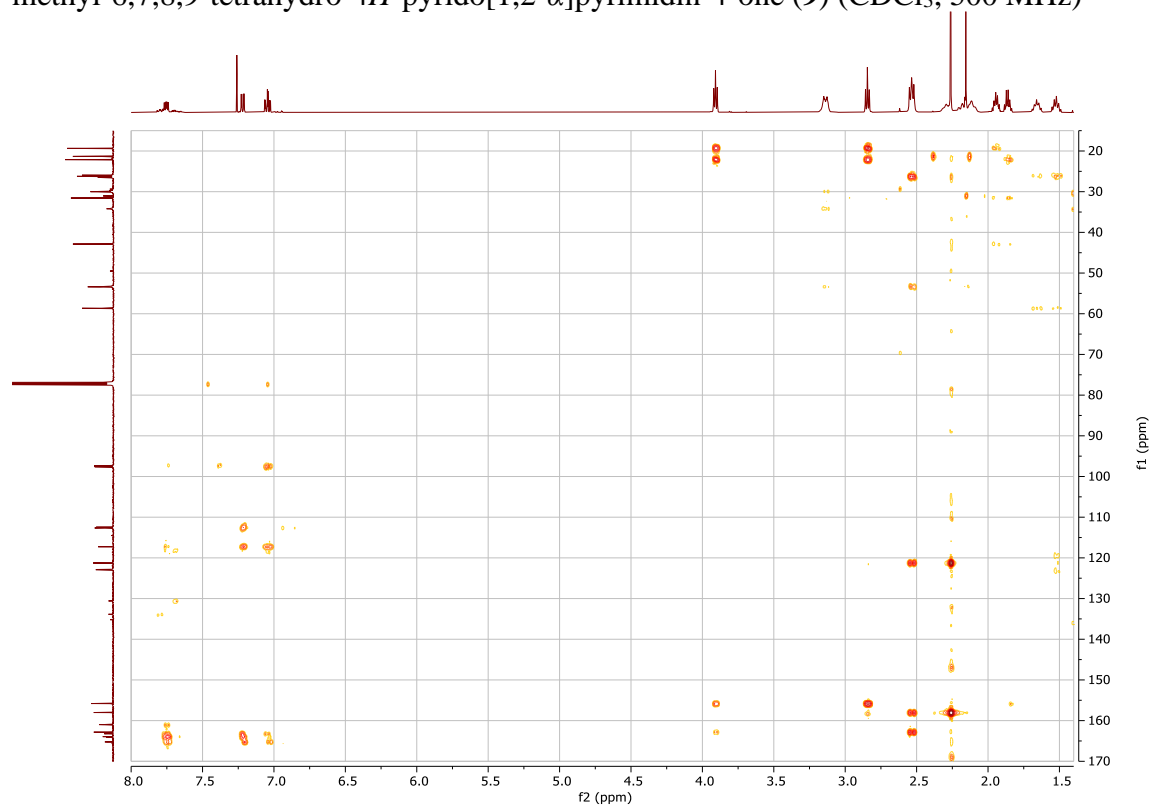
COSY NMR spectrum of 3-(4-(4-(6-Fluorobenzo[*d*]isoxazol-3-yl)piperidin-1-yl)butyl)-2-methyl-6,7,8,9-tetrahydro-4*H*-pyrido[1,2- α]pyrimidin-4-one (**9**) (CDCl_3 , 500 MHz)



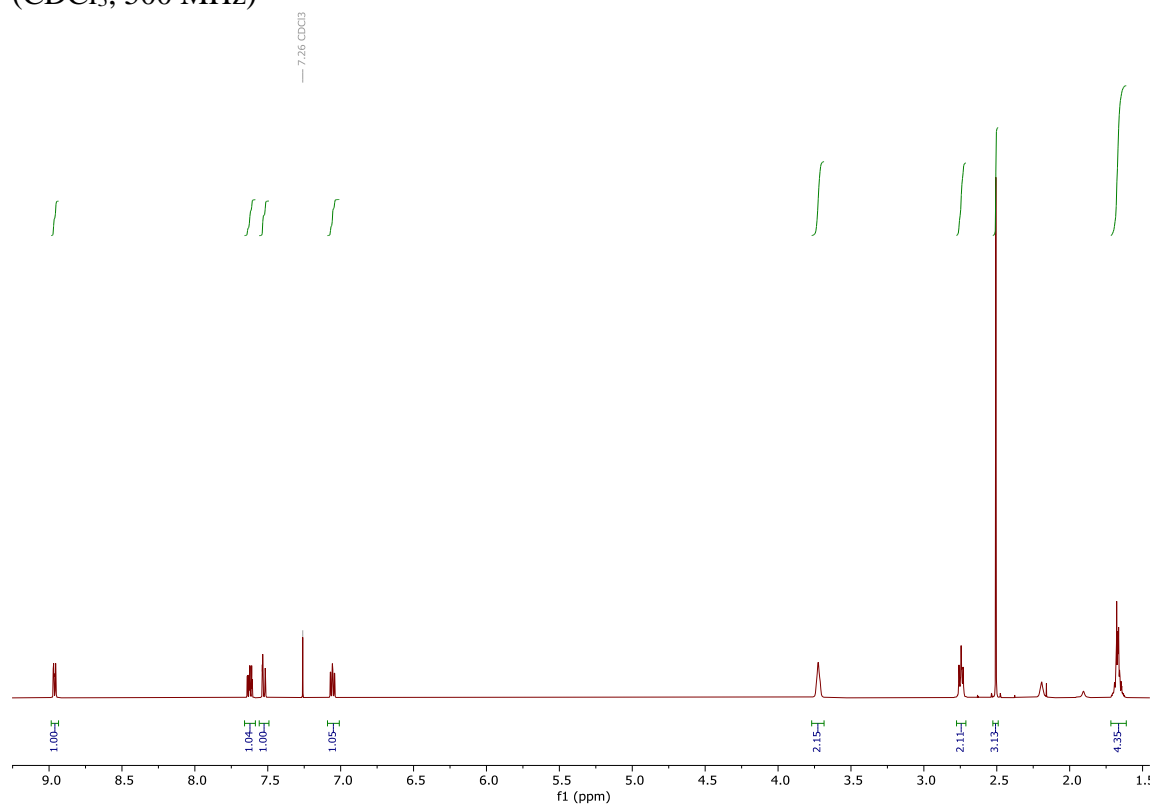
HSQC NMR spectrum of 3-(4-(4-(6-Fluorobenzo[*d*]isoxazol-3-yl)piperidin-1-yl)butyl)-2-methyl-6,7,8,9-tetrahydro-4*H*-pyrido[1,2-*α*]pyrimidin-4-one (**9**) (CDCl₃, 500 MHz)



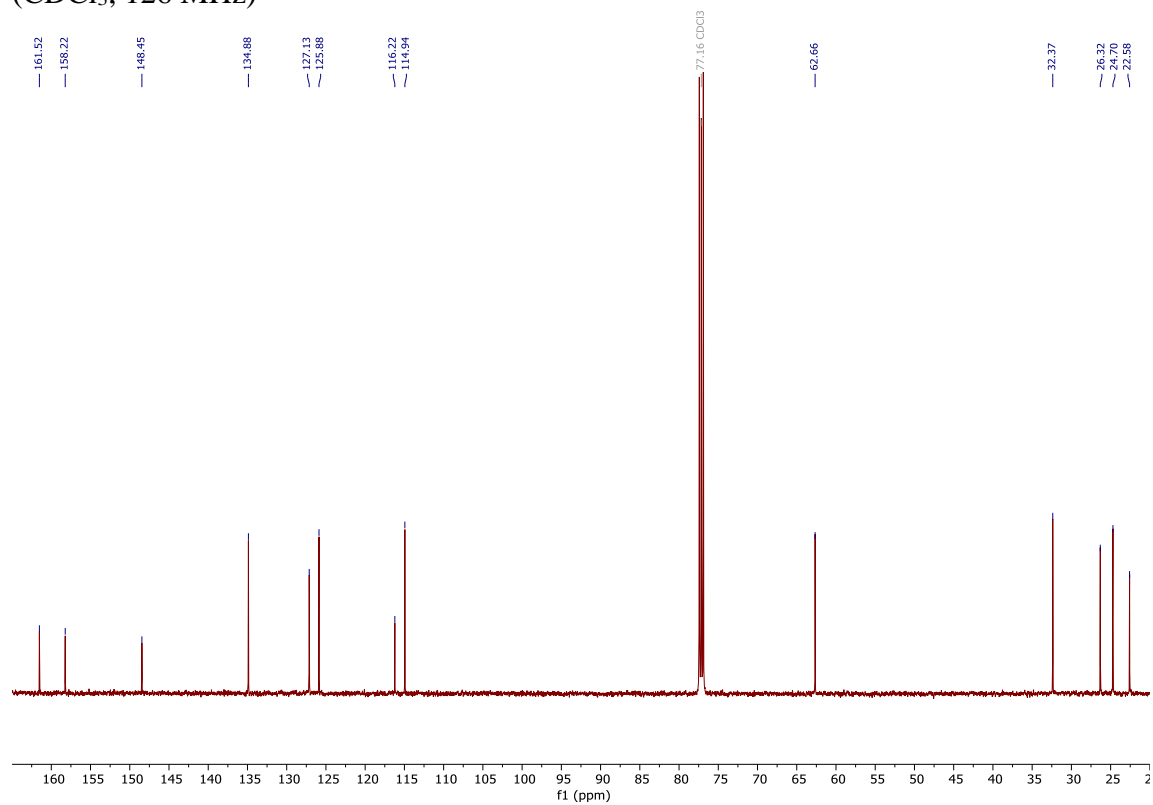
HMBC NMR spectrum of 3-(4-(4-(6-Fluorobenzo[*d*]isoxazol-3-yl)piperidin-1-yl)butyl)-2-methyl-6,7,8,9-tetrahydro-4*H*-pyrido[1,2-*α*]pyrimidin-4-one (**9**) (CDCl₃, 500 MHz)



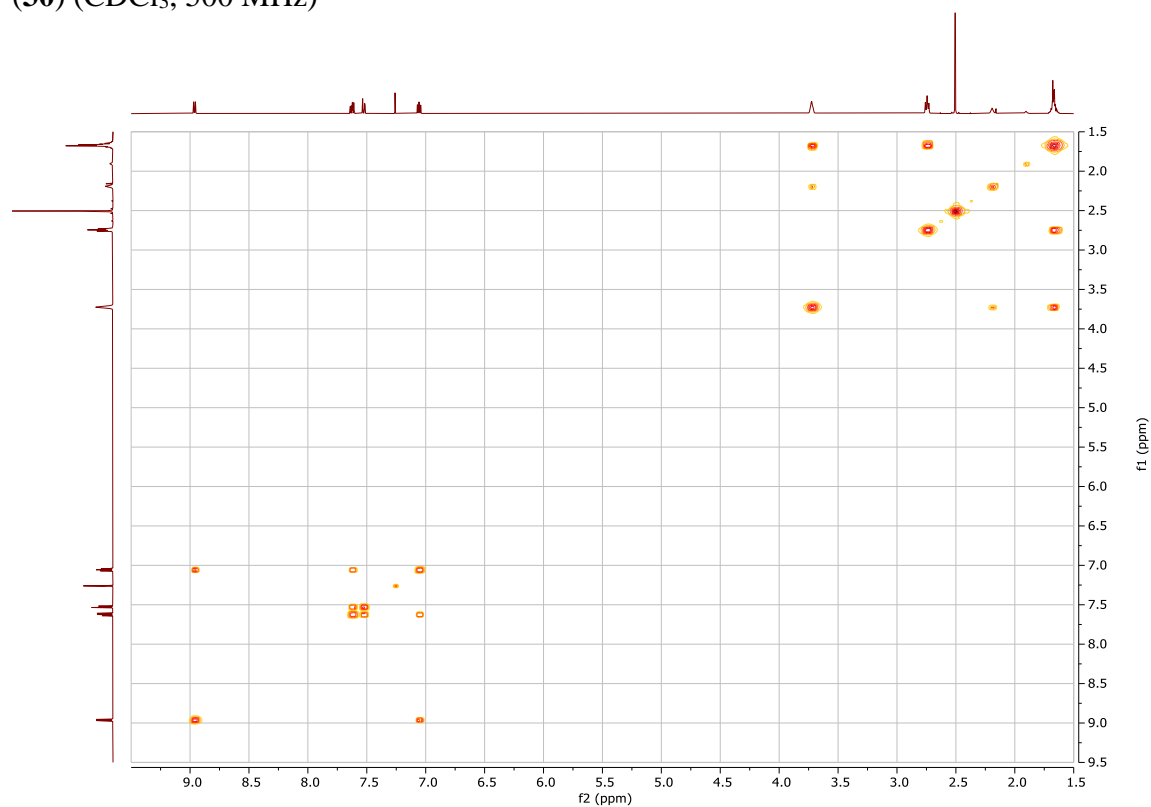
^1H NMR spectrum of 3-(4-Hydroxybutyl)-2-methyl-4*H*-pyrido[1,2- α]pyrimidin-4-one (**30**) (CDCl₃, 500 MHz)



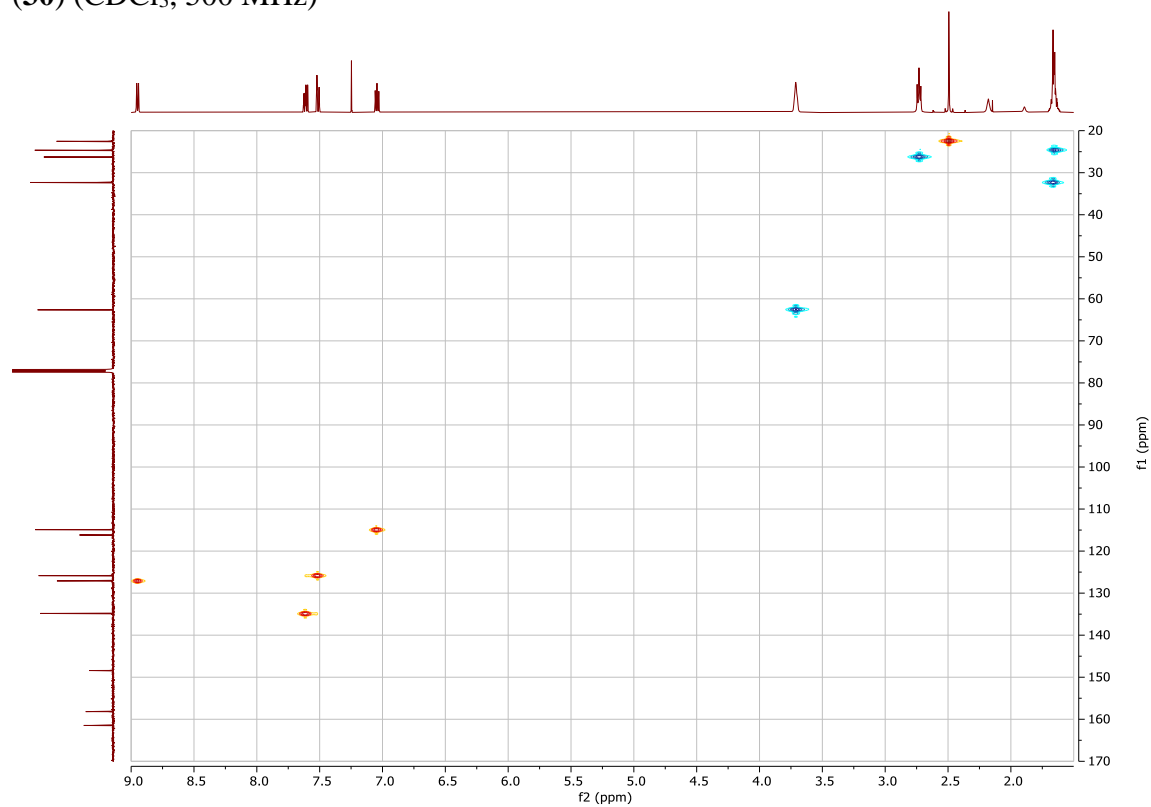
^{13}C NMR spectrum of 3-(4-Hydroxybutyl)-2-methyl-4*H*-pyrido[1,2- α]pyrimidin-4-one (**30**) (CDCl₃, 126 MHz)



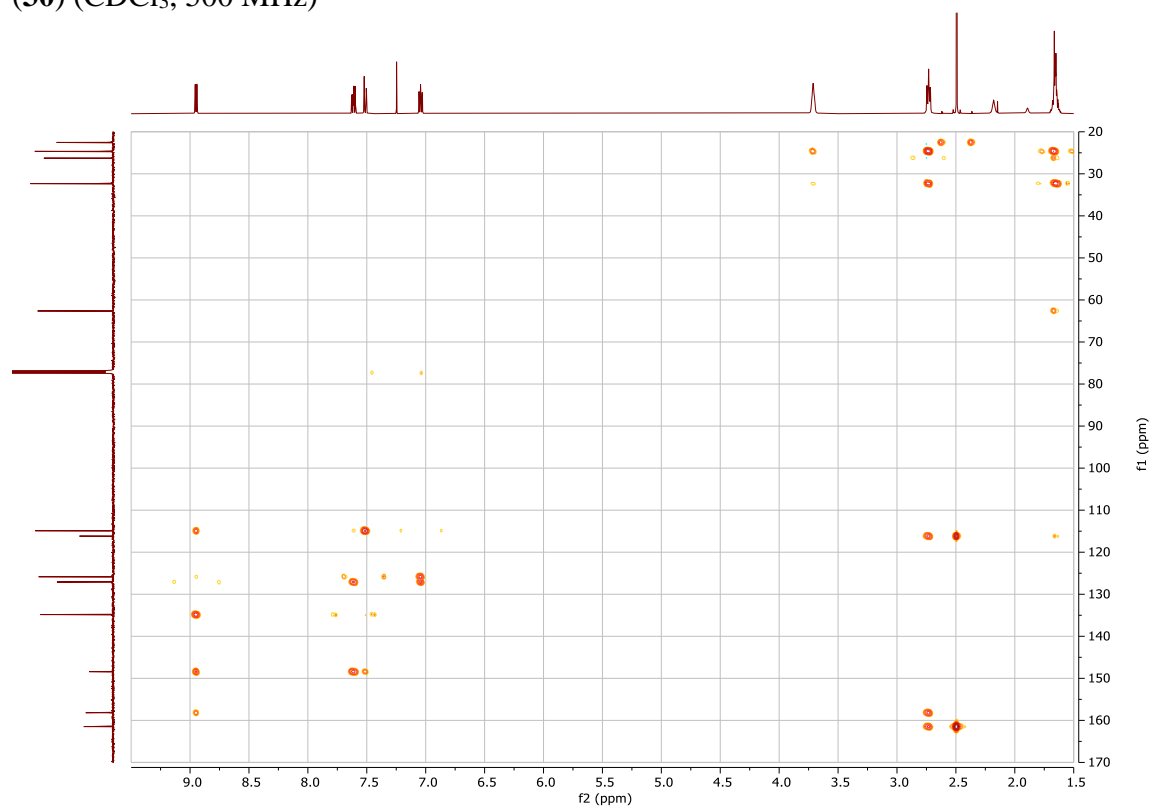
COSY NMR spectrum of 3-(4-Hydroxybutyl)-2-methyl-4*H*-pyrido[1,2-*a*]pyrimidin-4-one (**30**) (CDCl₃, 500 MHz)



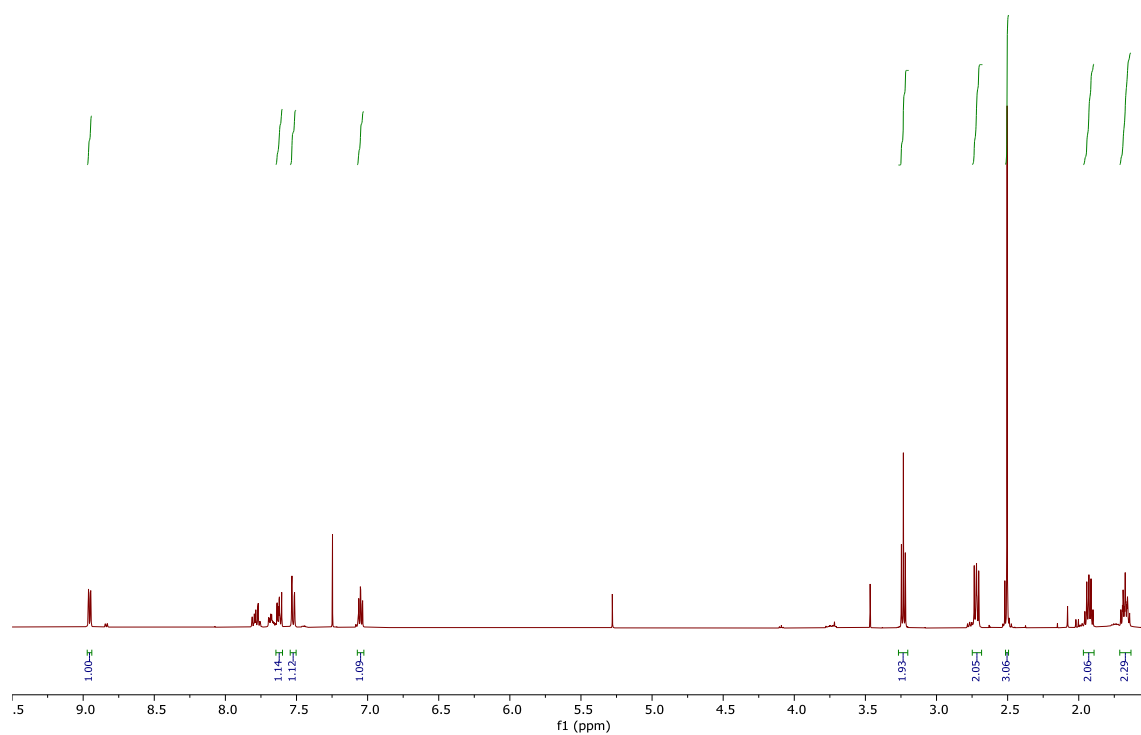
HSQC NMR spectrum of 3-(4-Hydroxybutyl)-2-methyl-4*H*-pyrido[1,2-*a*]pyrimidin-4-one (**30**) (CDCl₃, 500 MHz)



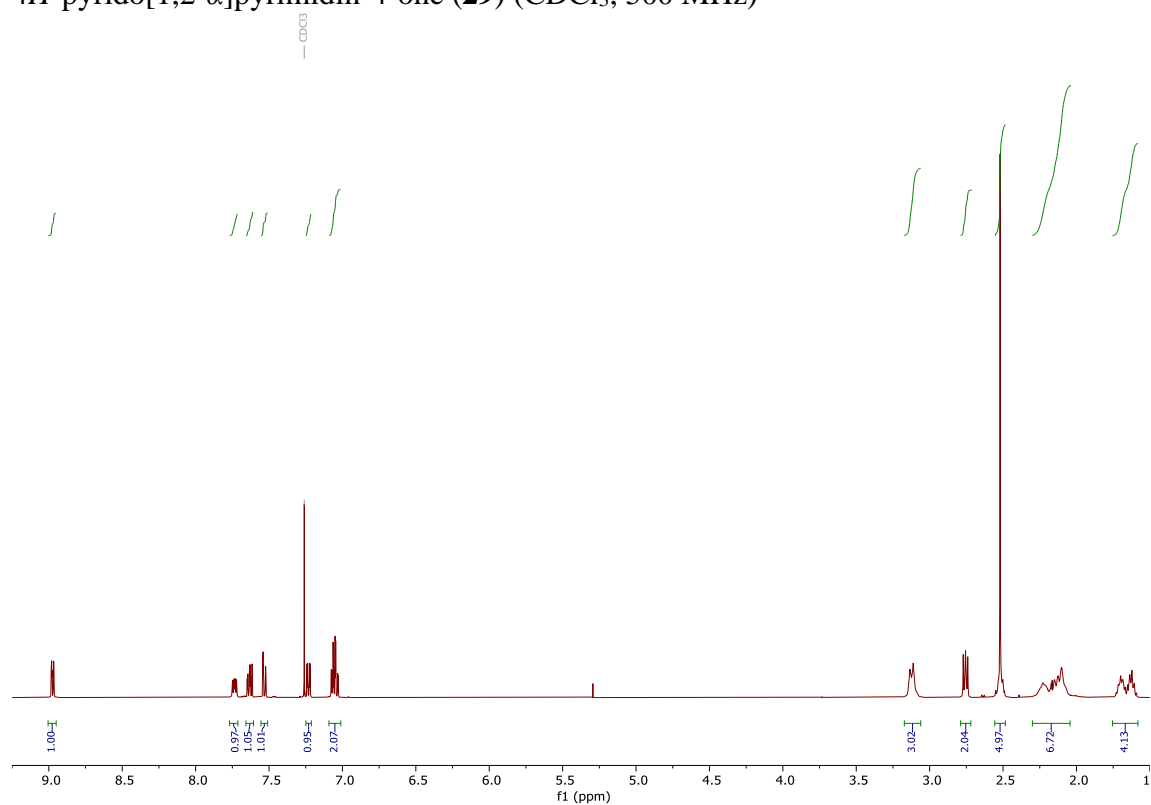
HMBC NMR spectrum of 3-(4-Hydroxybutyl)-2-methyl-4*H*-pyrido[1,2- α]pyrimidin-4-one (**30**) (CDCl₃, 500 MHz)



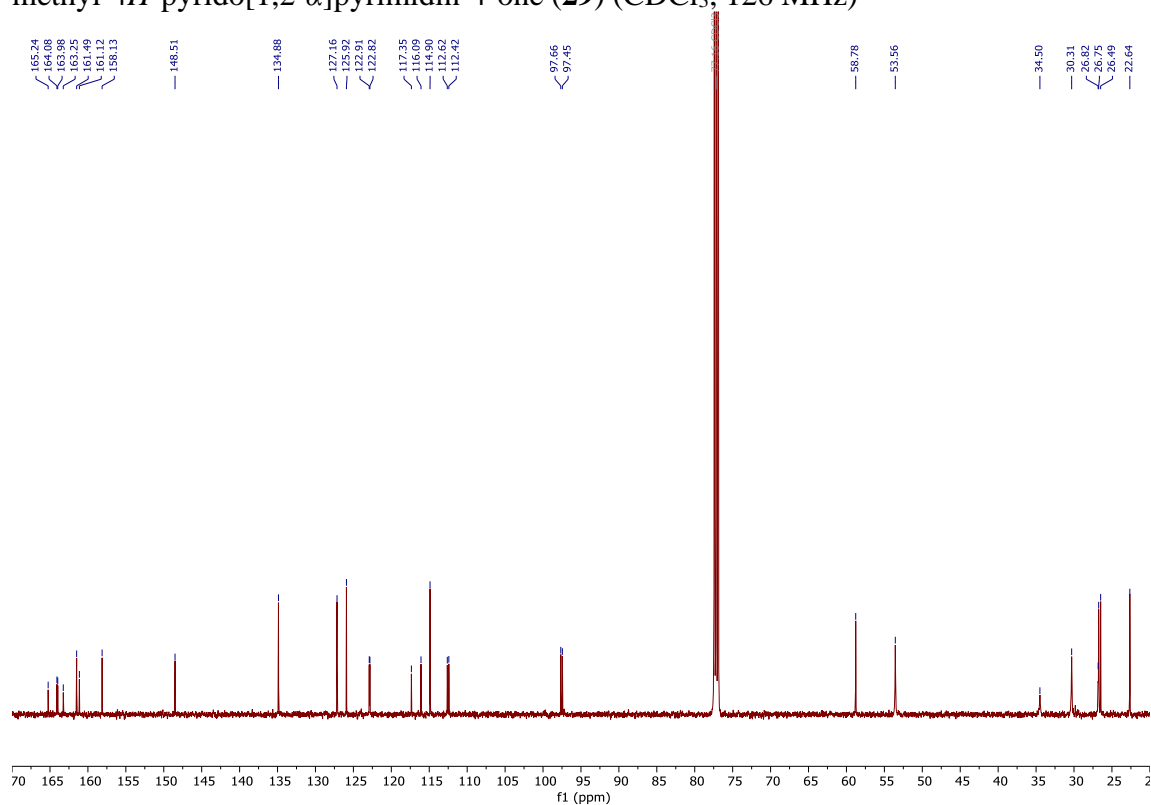
^1H NMR spectrum of 3-(4-Iodobutyl)-2-methyl-4*H*-pyrido[1,2- α]pyrimidin-4-one (**32**)
(CDCl_3 , 500 MHz)



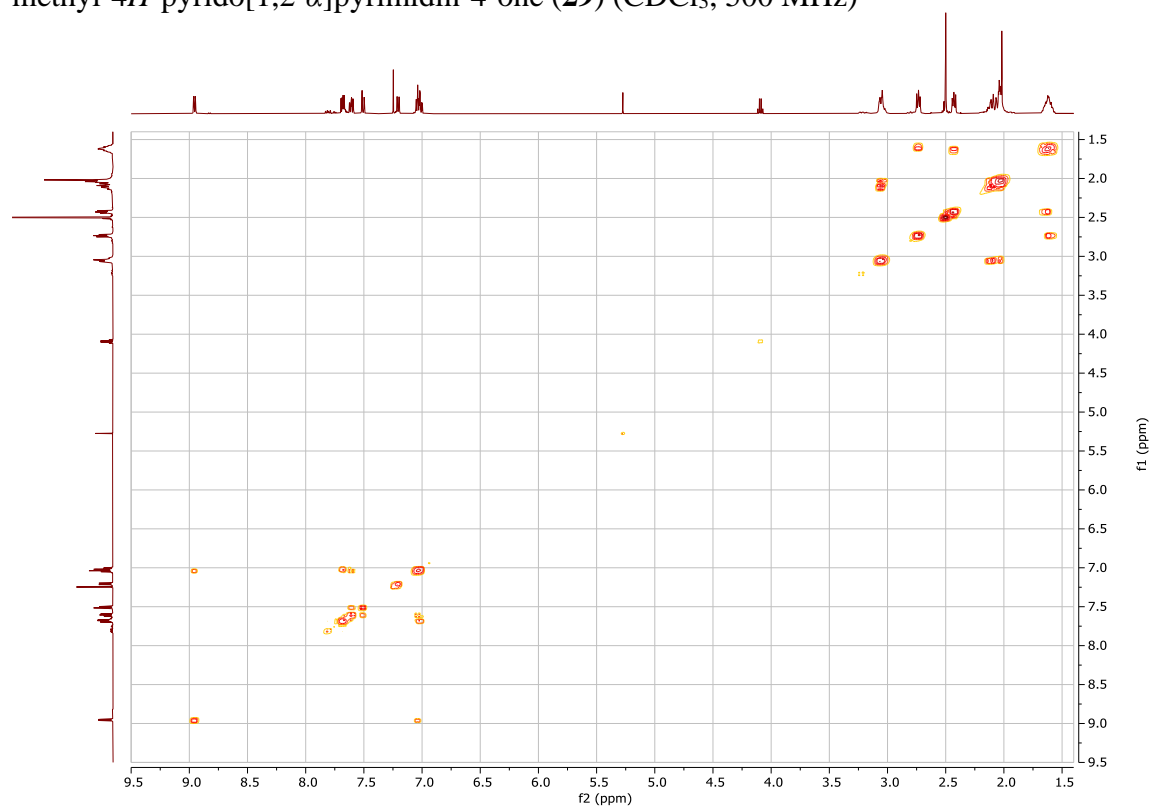
^1H NMR spectrum of 3-(4-(4-(6-Fluorobenzo[*d*]isoxazol-3-yl)piperidin-1-yl)butyl)-2-methyl-4*H*-pyrido[1,2- α]pyrimidin-4-one (**29**) (CDCl_3 , 500 MHz)



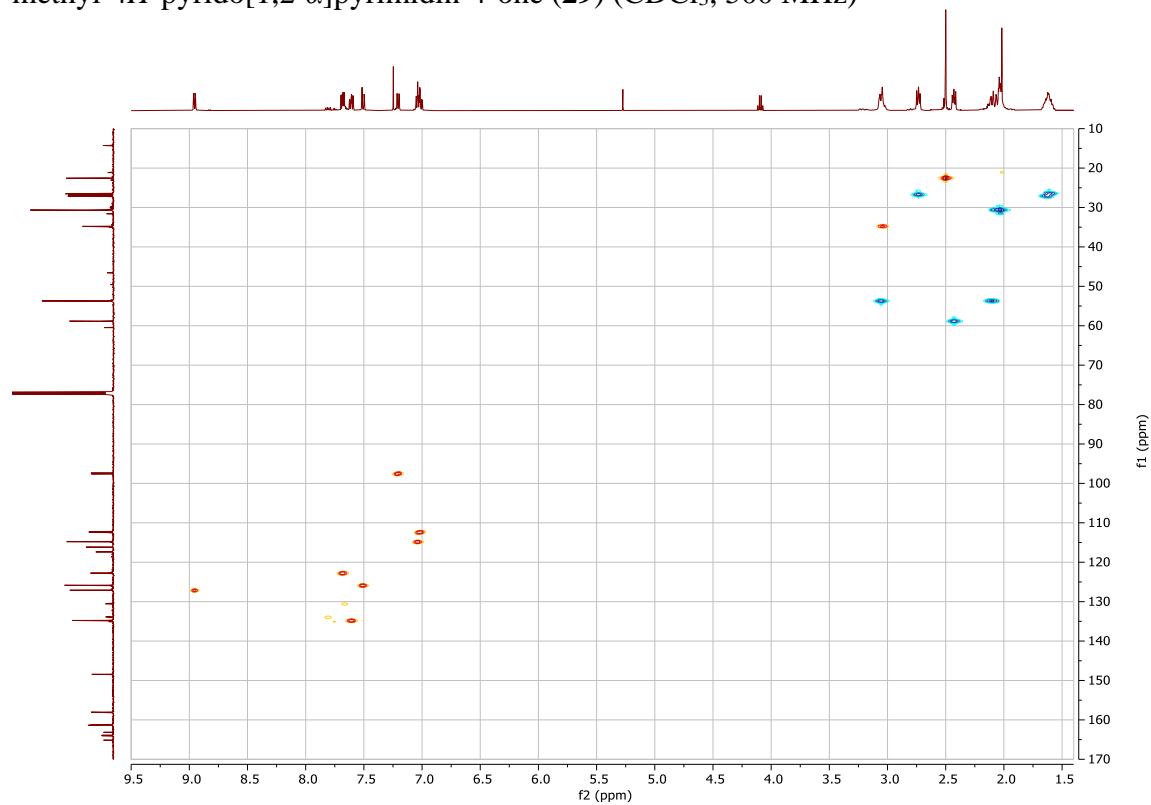
^{13}C NMR spectrum of 3-(4-(4-(6-Fluorobenzo[*d*]isoxazol-3-yl)piperidin-1-yl)butyl)-2-methyl-4*H*-pyrido[1,2- α]pyrimidin-4-one (**29**) (CDCl_3 , 126 MHz)



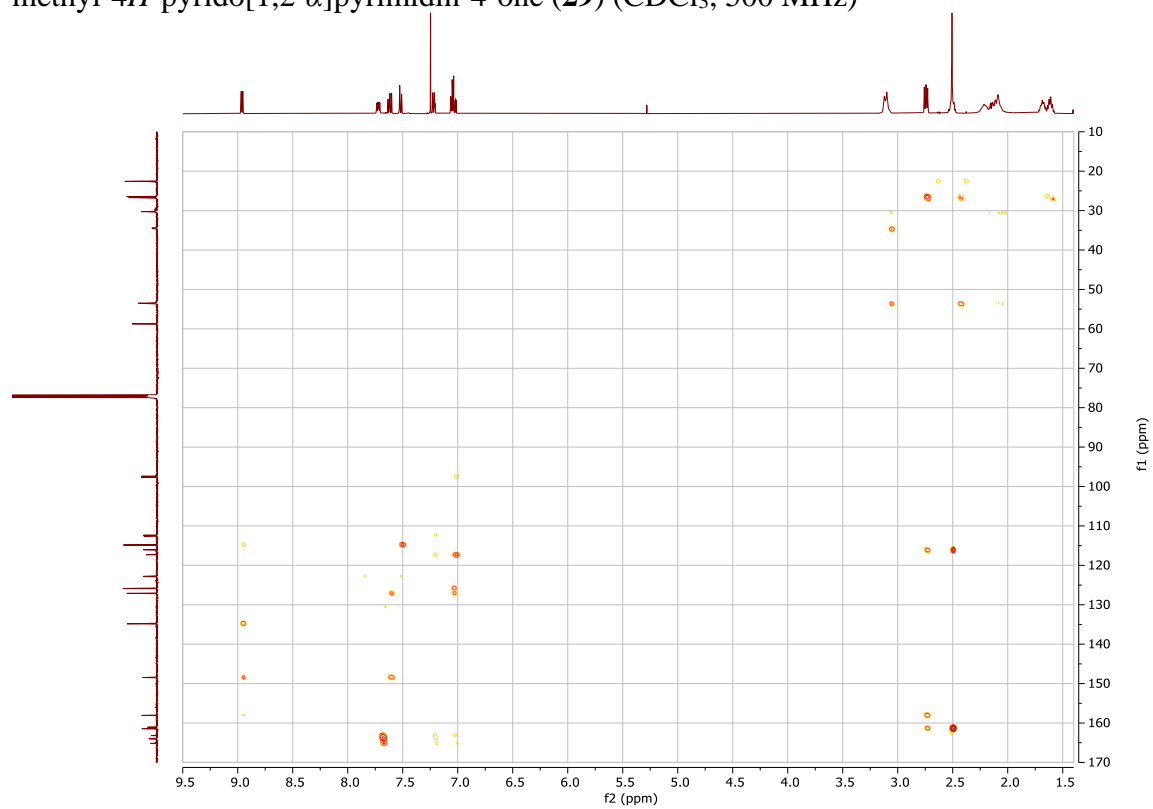
COSY NMR spectrum of 3-(4-(4-(6-Fluorobenzo[d]isoxazol-3-yl)piperidin-1-yl)butyl)-2-methyl-4*H*-pyrido[1,2-*a*]pyrimidin-4-one (**29**) (CDCl₃, 500 MHz)



HSQC NMR spectrum of 3-(4-(4-(6-Fluorobenzo[d]isoxazol-3-yl)piperidin-1-yl)butyl)-2-methyl-4*H*-pyrido[1,2-*a*]pyrimidin-4-one (**29**) (CDCl₃, 500 MHz)



HSQC NMR spectrum of 3-(4-(4-(6-Fluorobenzo[d]isoxazol-3-yl)piperidin-1-yl)butyl)-2-methyl-4*H*-pyrido[1,2-*a*]pyrimidin-4-one (**29**) (CDCl₃, 500 MHz)



6.2 Buffers and Solutions

Cryopreservation Medium

Fetal calf serum **90%**

DMSO **10%**

Lysis Buffer

HEPES **5 mM**

Tween-20 **0.5%**

in dPBS

Complete T cell media (CTCM; 100.1 mL)

Dulbecco's Modified Eagle Medium **86 mL**

Fetal calf serum **10 mL**

β -Mercaptoethanol (55 mM) **0.1 mL**

Non-essential amino acids (10 mM) **1 mL**

L-glutamate (200 mM) **1 mL**

HEPES buffer (1 M) **1 mL**

Penicillin/Streptomycin (100 U/ml/10 mg/ml) **1 mL**

MTT Solution

MTT (in PBS) **5 mg/mL**

Sterile filtered through 0.22 μ M syringe filter

MTT Solubiliser

SDS **10%**

DMF **45%**

dH₂O **45%**

pH to 4.5 with acetic acid

ELISA Capture Buffer

0.1M Na₂HPO₄

pH to 9.0

ELISA Stop Solution

0.18M H₂SO₄

6.3 ELISA Reagents and Concentrations

IL-12 ELISA Reagents

Reagent	Concentration	Diluent	Incubation
Purified rat anti mIL-12 p40/70 (BD Biosciences, CA)	1 µg/mL	0.1 M Na ₂ HPO ₄ , pH 9.0	Overnight 4 °C
Block (FCS)	10%	PBS pH 7.4	2 hours RT
Top standard (rmIL-12p40)	4 ng/mL	PBS + 5% FCS	2 hours RT
Biotin rat anti mIL-12p40 (BD Biosciences, CA)	1 µg/mL	PBS + 5% FCS	1 hour RT
SA-HRP (BD Biosciences, CA)	1:2000	PBS + 5% FCS	1 hour RT

IL-10 ELISA Reagents

Reagent	Concentration	Diluent	Incubation
Purified rat anti mIL-10 (BD Biosciences, CA)	5 µg/mL	0.1 M Na ₂ HPO ₄ , pH 6.0	Overnight 4 °C
Block (FCS)	10%	PBS pH 7.4	2 hours RT
Top standard (rmIL-10)	25 ng/mL	PBS + 10% FCS	2 hours RT
Biotin rat anti-mIL-10 (BD Biosciences, CA)	0.25 µg/mL	PBS + 10% FCS	1 hour RT
SA-HRP (BD Biosciences, CA)	1:1000	PBS + 10% FCS	1 hour RT

7 References

1. Kennis, L. E. J.; Vandenberg, J. 1,2-BenzIsoxazol-3-yl and 1,2-benzIsothiazol-3-yl derivatives. EP 01 96132 A2, 1986.
2. Sajatovic, M.; Subramoniam, M.; Fuller, M. A., Risperidone in the treatment of bipolar mania. *Neuropsychiatr Dis Treat* **2006**, 2 (2), 127-138.
3. Dinnissen, M.; Dietrich, A.; van den Hoofdakker, B. J.; Hoekstra, P. J., Clinical and pharmacokinetic evaluation of risperidone for the management of autism spectrum disorder. *Expert Opinion on Drug Metabolism & Toxicology* **2015**, 11 (1), 111-124.
4. de Oliveira, I. R.; Miranda-Scippa, A. M. A.; de Sena, E. P.; Pereira, E. L. A.; Ribeiro, M. G.; de Castro-e-Silva, E.; Bacaltchuk, J., Risperidone versus haloperidol in the treatment of schizophrenia: a meta-analysis comparing their efficacy and safety. *Journal of Clinical Pharmacy and Therapeutics* **1996**, 21 (5), 349-358.
5. Seeman, P.; Lee, T., Antipsychotic drugs: direct correlation between clinical potency and presynaptic action on dopamine neurons. *Science* **1975**, 188 (4194), 1217-1219.
6. Remington, G.; Kapur, S., D2 and 5-HT2 receptor effects of antipsychotics: bridging basic and clinical findings using PET. *Journal of Clinical Psychiatry* **1999**, 60 Suppl 10, 15-9.
7. Remington, G.; Kapur, S., Atypical antipsychotics: are some more atypical than others? *Psychopharmacology* **2000**, 148 (1), 3-15.
8. Jafari, S.; Fernandez-Enright, F.; Huang, X.-F., Structural contributions of antipsychotic drugs to their therapeutic profiles and metabolic side effects. *Journal of Neurochemistry* **2012**, 120 (3), 371-384.
9. Corena-McLeod, M., Comparative Pharmacology of Risperidone and Paliperidone. *Drugs in R&D* **2015**, 15 (2), 163-174.
10. Wang, S.; Che, T.; Levit, A.; Shoichet, B. K.; Wacker, D.; Roth, B. L., Structure of the D2 dopamine receptor bound to the atypical antipsychotic drug risperidone. *Nature* **2018**, 555, 269.
11. Kimura, K. T.; Asada, H.; Inoue, A.; Kadji, F. M. N.; Im, D.; Mori, C.; Arakawa, T.; Hirata, K.; Nomura, Y.; Nomura, N.; Aoki, J.; Iwata, S.; Shimamura, T., Structures of the 5-HT2A receptor in complex with the antipsychotics risperidone and zotepine. *Nature Structural & Molecular Biology* **2019**, 26 (2), 121-128.
12. Michino, M.; Beuming, T.; Donthamsetti, P.; Newman, A. H.; Javitch, J. A.; Shi, L., What can crystal structures of aminergic receptors tell us about designing subtype-selective ligands? *Pharmacological Reviews* **2015**, 67 (1), 198-213.
13. Marder, S. R.; Meibach, R. C., Risperidone in the treatment of schizophrenia. *American Journal of Psychiatry* **1994**, 151 (6), 825-35.
14. Sampson, S.; Hosalli, P.; Furtado, V. A.; Davis, J. M., Risperidone (depot) for schizophrenia. *Cochrane Database of Systematic Reviews* **2016**, (4).
15. Markowitz, J. S.; Brown, C. S.; Moore, T. R., Atypical Antipsychotics Part I: Pharmacology, Pharmacokinetics, and Efficacy. *Annals of Pharmacotherapy* **1999**, 33 (1), 73-85.
16. Fang, J.; Bourin, M.; Baker, G. B., Metabolism of risperidone to 9-hydroxyrisperidone by human cytochromes P450 2D6 and 3A4. *Naunyn-Schmiedeberg's Archives of Pharmacology* **1999**, 359 (2), 147-51.

17. Yasui-Furukori, N.; Hidestrand, M.; Spina, E.; Facciola, G.; Scordo, M. G.; Tybring, G., Different Enantioselective 9-Hydroxylation of Risperidone by the Two Human CYP2D6 and CYP3A4 Enzymes. *Drug Metabolism and Disposition* **2001**, 29 (10), 1263-1268.
18. Yoo, H.-D.; Lee, S.-N.; Kang, H.-A.; Cho, H.-Y.; Lee, I.-K.; Lee, Y.-B., Influence of ABCB1 genetic polymorphisms on the pharmacokinetics of risperidone in healthy subjects with CYP2D6*10/*10. *Br J Pharmacol* **2011**, 164 (2b), 433-443.
19. Leysen, J. E.; Gommeren, W.; Eens, A.; de Chaffoy de Courcelles, D.; Stoof, J. C.; Janssen, P. A., Biochemical profile of risperidone, a new antipsychotic. *Journal of Pharmacology and Experimental Therapeutics* **1988**, 247 (2), 661-670.
20. Leysen, J. E.; Janssen, P. M.; Gommeren, W.; Wynants, J.; Pauwels, P. J.; Janssen, P. A., In vitro and in vivo receptor binding and effects on monoamine turnover in rat brain regions of the novel antipsychotics risperidone and ocaperidone. *Molecular Pharmacology* **1992**, 41 (3), 494-508.
21. Schotte, A.; Bonaventure, P.; Janssen, P. F.; Leysen, J. E., In vitro receptor binding and in vivo receptor occupancy in rat and guinea pig brain: risperidone compared with antipsychotics hitherto used. *The Japanese Journal of Pharmacology* **1995**, 69 (4), 399-412.
22. Schotte, A.; Janssen, P. F.; Gommeren, W.; Luyten, W. H.; Van Gompel, P.; Lesage, A. S.; De Loore, K.; Leysen, J. E., Risperidone compared with new and reference antipsychotic drugs: in vitro and in vivo receptor binding. *Psychopharmacology (Berl)* **1996**, 124 (1-2), 57-73.
23. Clarke, W. P.; Chavera, T. A.; Silva, M.; Sullivan, L. C.; Berg, K. A., Signalling profile differences: paliperidone versus risperidone. *Br J Pharmacol* **2013**, 170 (3), 532-545.
24. Sullivan, L. C.; Clarke, W. P.; Berg, K. A., Atypical antipsychotics and inverse agonism at 5-HT₂ receptors. *Curr Pharm Des* **2015**, 21 (26), 3732-3738.
25. Strange, P. G., Antipsychotic Drugs: Importance of Dopamine Receptors for Mechanisms of Therapeutic Actions and Side Effects. *Pharmacological Reviews* **2001**, 53 (1), 119-134.
26. Nyberg, S.; Farde, L.; Eriksson, L.; Halldin, C.; Eriksson, B., 5-HT₂ and D₂ dopamine receptor occupancy in the living human brain. *Psychopharmacology* **1993**, 110 (3), 265-272.
27. Nyberg, S.; Eriksson, B.; Oxenstierna, G.; Halldin, C.; Farde, L., Suggested minimal effective dose of risperidone based on PET-measured D₂ and 5-HT_{2A} receptor occupancy in schizophrenic patients. *American Journal of Psychiatry* **1999**, 156 (6), 869-75.
28. Meltzer, H. Y.; Matsubara, S.; Lee, J. C., Classification of typical and atypical antipsychotic drugs on the basis of dopamine D-1, D-2 and serotonin₂ pK_i values. *Journal of Pharmacology and Experimental Therapeutics* **1989**, 251 (1), 238-246.
29. Kusumi, I.; Boku, S.; Takahashi, Y., Psychopharmacology of atypical antipsychotic drugs: From the receptor binding profile to neuroprotection and neurogenesis. *Psychiatry and Clinical Neurosciences* **2015**, 69 (5), 243-258.
30. Haas, M.; Eerdekens, M.; Kushner, S.; Singer, J.; Augustyns, I.; Quiroz, J.; Pandina, G.; Kusumakar, V., Efficacy, safety and tolerability of two risperidone dosing regimens in adolescent schizophrenia: double-blind study. *British Journal of Psychiatry* **2009**, 194 (2), 158-164.
31. Chouinard, G.; Kopala, L.; Labelle, A.; Beauclair, L.; Johnson, S. V.; Singh, K. I., Phase-IV Multicentre Clinical Study of Risperidone in the Treatment of Outpatients with Schizophrenia. *The Canadian Journal of Psychiatry* **1998**, 43 (10), 1018-1025.
32. Smulevich, A. B.; Khanna, S.; Eerdekens, M.; Karcher, K.; Kramer, M.; Grossman, F., Acute and continuation risperidone monotherapy in bipolar mania: a 3-week placebo-controlled trial followed by a 9-week double-blind trial of risperidone and haloperidol. *European Neuropsychopharmacology* **2005**, 15 (1), 75-84.

33. Farde, L.; Nordström, A.-L.; Wiesel, F.-A.; Pauli, S.; Halldin, C.; Sedvall, G., Positron Emission Tomographic Analysis of Central D1 and D2 Dopamine Receptor Occupancy in Patients Treated With Classical Neuroleptics and Clozapine: Relation to Extrapyramidal Side Effects. *JAMA Psychiatry* **1992**, *49* (7), 538-544.
34. Seeman, P., Atypical antipsychotics: mechanism of action. *The Canadian Journal of Psychiatry* **2002**, *47* (1), 27-38.
35. Safer, D. J., A Comparison of Risperidone-Induced Weight Gain Across the Age Span. *Journal of Clinical Psychopharmacology* **2004**, *24* (4), 429-436.
36. Richelson, E.; Souder, T., Binding of antipsychotic drugs to human brain receptors: Focus on newer generation compounds. *Life Sciences* **2000**, *68* (1), 29-39.
37. Song, X.; Fan, X.; Li, X.; Zhang, W.; Gao, J.; Zhao, J.; Harrington, A.; Ziedonis, D.; Lv, L., Changes in pro-inflammatory cytokines and body weight during 6-month risperidone treatment in drug naïve, first-episode schizophrenia. *Psychopharmacology* **2014**, *231* (2), 319-325.
38. Lassmann, H.; van Horssen, J.; Mahad, D., Progressive multiple sclerosis: pathology and pathogenesis. *Nature Reviews Neurology* **2012**, *8*, 647.
39. Wallin, M. T.; Culpepper, W. J.; Nichols, E.; Bhutta, Z. A.; Gebrehiwot, T. T.; Hay, S. I.; Khalil, I. A.; Krohn, K. J.; Liang, X.; Naghavi, M.; Mokdad, A. H.; Nixon, M. R.; Reiner, R. C.; Sartorius, B.; Smith, M.; Topor-Madry, R.; Werdecker, A.; Vos, T.; Feigin, V. L.; Murray, C. J. L., Global, regional, and national burden of multiple sclerosis 1990-2016: a systematic analysis for the Global Burden of Disease Study 2016. *The Lancet Neurology* **2019**, *18* (3), 269-285.
40. Baranzini, S. E.; Oksenberg, J. R., The Genetics of Multiple Sclerosis: From 0 to 200 in 50 Years. *Trends in Genetics* **2017**, *33* (12), 960-970.
41. Brownlee, W. J.; Hardy, T. A.; Fazekas, F.; Miller, D. H., Diagnosis of multiple sclerosis: progress and challenges. *The Lancet* **2017**, *389* (10076), 1336-1346.
42. Polman, C. H.; O'Connor, P. W.; Havrdova, E.; Hutchinson, M.; Kappos, L.; Miller, D. H.; Phillips, J. T.; Lublin, F. D.; Giovannoni, G.; Wajgt, A.; Toal, M.; Lynn, F.; Panzara, M. A.; Sandrock, A. W., A Randomized, Placebo-Controlled Trial of Natalizumab for Relapsing Multiple Sclerosis. *New England Journal of Medicine* **2006**, *354* (9), 899-910.
43. Antonioli, C.; Stankoff, B., Immunological Markers for PML Prediction in MS Patients Treated with Natalizumab. *Front Immunol* **2015**, *5* (668).
44. Yousry, T. A.; Major, E. O.; Ryschkewitsch, C.; Fahle, G.; Fischer, S.; Hou, J.; Curfman, B.; Miszkil, K.; Mueller-Lenke, N.; Sanchez, E.; Barkhof, F.; Radue, E.-W.; Jäger, H. R.; Clifford, D. B., Evaluation of Patients Treated with Natalizumab for Progressive Multifocal Leukoencephalopathy. *New England Journal of Medicine* **2006**, *354* (9), 924-933.
45. Scannevin, R. H.; Chollate, S.; Jung, M.-y.; Shackett, M.; Patel, H.; Bista, P.; Zeng, W.; Ryan, S.; Yamamoto, M.; Lukashev, M.; Rhodes, K. J., Fumarates Promote Cytoprotection of Central Nervous System Cells against Oxidative Stress via the Nuclear Factor (Erythroid-Derived 2)-Like 2 Pathway. *Journal of Pharmacology and Experimental Therapeutics* **2012**, *341* (1), 274-284.
46. Loewe, R.; Holnthoner, W.; Groger, M.; Pillinger, M.; Gruber, F.; Mechtcheriakova, D.; Hofer, E.; Wolff, K.; Petzelbauer, P., Dimethylfumarate inhibits TNF-induced nuclear entry of NF-kappa B/p65 in human endothelial cells. *The Journal of Immunology* **2002**, *168* (9), 4781-7.
47. Mosayebi, G.; Ghazavi, A.; Ghasami, K.; Jand, Y.; Kokhaei, P., Therapeutic Effect of Vitamin D3 in Multiple Sclerosis Patients. *Immunological Investigations* **2011**, *40* (6), 627-639.
48. Soilu-Hänninen, M.; Äivo, J.; Lindström, B.-M.; Elovaara, I.; Sumelahti, M.-L.; Färkkilä, M.; Tienari, P.; Atula, S.; Sarasoja, T.; Herrala, L.; Keskinarkaus, I.; Kruger, J.;

- Kallio, T.; Rocca, M. A.; Filippi, M., A randomised, double blind, placebo controlled trial with vitamin D3 as an add on treatment to interferon β -1b in patients with multiple sclerosis. *Journal of Neurology, Neurosurgery & Psychiatry* **2012**, 83 (5), 565-571.
49. Munger, K. L.; Levin, L. I.; Hollis, B. W.; Howard, N. S.; Ascherio, A., Serum 25-Hydroxyvitamin D Levels and Risk of Multiple Sclerosis. *JAMA* **2006**, 296 (23), 2832-2838.
50. Stein, M. S.; Liu, Y.; Gray, O. M.; Baker, J. E.; Kolbe, S. C.; Ditchfield, M. R.; Egan, G. F.; Mitchell, P. J.; Harrison, L. C.; Butzkueven, H.; Kilpatrick, T. J., A randomized trial of high-dose vitamin D2 in relapsing-remitting multiple sclerosis. *Neurology* **2011**, 77 (17), 1611-1618.
51. Zhang, J.-M.; An, J., Cytokines, inflammation, and pain. *Int Anesthesiol Clin* **2007**, 45 (2), 27-37.
52. Hafler, D. A.; Kent, S. C.; Pietrusewicz, M. J.; Khoury, S. J.; Weiner, H. L.; Fukaura, H., Oral Administration of Myelin Induces Antigen-specific TGF- β 1 Secreting T Cells in Patients with Multiple Sclerosis. *Annals of the New York Academy of Sciences* **1997**, 835 (1), 120-131.
53. Fukaura, H.; Kent, S. C.; Pietrusewicz, M. J.; Khoury, S. J.; Weiner, H. L.; Hafler, D. A., Induction of circulating myelin basic protein and proteolipid protein-specific transforming growth factor-beta1-secreting Th3 T cells by oral administration of myelin in multiple sclerosis patients. *J Clin Invest* **1996**, 98 (1), 70-77.
54. Arango Duque, G.; Descoteaux, A., Macrophage cytokines: involvement in immunity and infectious diseases. *Front Immunol* **2014**, 5, 491-491.
55. Wojdasiewicz, P.; Poniatowski, A., u.; Szukiewicz, D., The Role of Inflammatory and Anti-Inflammatory Cytokines in the Pathogenesis of Osteoarthritis. *Mediators of Inflammation* **2014**, 2014, 19.
56. Dinarello, C. A., Proinflammatory Cytokines. *Chest* **2000**, 118 (2), 503-508.
57. Gee, K.; Guzzo, C.; Che Mat, N. F.; Ma, W.; Kumar, A., The IL-12 family of cytokines in infection, inflammation and autoimmune disorders. *Inflammation & Allergy - Drug Targets* **2009**, 8 (1), 40-52.
58. Hoyer, K. K.; Dooms, H.; Barron, L.; Abbas, A. K., Interleukin-2 in the development and control of inflammatory disease. *Immunological Reviews* **2008**, 226 (1), 19-28.
59. Opal, S. M.; DePalo, V. A., Anti-Inflammatory Cytokines. *Chest* **2000**, 117 (4), 1162-1172.
60. Gold, R.; Linington, C.; Lassmann, H., Understanding pathogenesis and therapy of multiple sclerosis via animal models: 70 years of merits and culprits in experimental autoimmune encephalomyelitis research. *Brain* **2006**, 129 (8), 1953-1971.
61. Constantinescu, C. S.; Farooqi, N.; O'Brien, K.; Gran, B., Experimental autoimmune encephalomyelitis (EAE) as a model for multiple sclerosis (MS). *Br J Pharmacol* **2011**, 164 (4), 1079-1106.
62. Begolka, W. S.; Miller, S. D., Cytokines as intrinsic and exogenous regulators of pathogenesis in experimental autoimmune encephalomyelitis. *Research in Immunology* **1998**, 149 (9), 771-81; discussion 843-4, 855-60.
63. Renno, T.; Taupin, V.; Bourbonnière, L.; Verge, G.; Tran, E.; De Simone, R.; Krakowski, M.; Rodriguez, M.; Peterson, A.; Owens, T., Interferon- γ in Progression to Chronic Demyelination and Neurological Deficit Following Acute EAE. *Molecular and Cellular Neuroscience* **1998**, 12 (6), 376-389.
64. Ferber, I. A.; Brocke, S.; Taylor-Edwards, C.; Ridgway, W.; Dinisco, C.; Steinman, L.; Dalton, D.; Fathman, C. G., Mice with a disrupted IFN-gamma gene are susceptible to the induction of experimental autoimmune encephalomyelitis (EAE). *The Journal of Immunology* **1996**, 156 (1), 5-7.

65. Balashov, K. E.; Comabella, M.; Ohashi, T.; Khoury, S. J.; Weiner, H. L., Defective regulation of IFN γ and IL-12 by endogenous IL-10 in progressive MS. *Neurology* **2000**, 55 (2), 192-198.
66. Kuroda, Y.; Shimamoto, Y., Human tumor necrosis factor- α augments experimental allergic encephalomyelitis in rats. *Journal of Neuroimmunology* **1991**, 34 (2), 159-164.
67. Probert, L.; Akassoglou, K.; Pasparakis, M.; Kontogeorgos, G.; Kollias, G., Spontaneous inflammatory demyelinating disease in transgenic mice showing central nervous system-specific expression of tumor necrosis factor alpha. *Proc Natl Acad Sci U S A* **1995**, 92 (24), 11294-11298.
68. Hofman, F. M.; Hinton, D. R.; Johnson, K.; Merrill, J. E., Tumor necrosis factor identified in multiple sclerosis brain. *The Journal of Experimental Medicine* **1989**, 170 (2), 607-612.
69. Selmaj, K.; Raine, C. S.; Cannella, B.; Brosnan, C. F., Identification of lymphotoxin and tumor necrosis factor in multiple sclerosis lesions. *Journal of Clinical Investigation* **1991**, 87 (3), 949-54.
70. Sharief, M. K.; Hentges, R., Association between Tumor Necrosis Factor- α and Disease Progression in Patients with Multiple Sclerosis. *New England Journal of Medicine* **1991**, 325 (7), 467-472.
71. Smith, T.; Hewson, A. K.; Kingsley, C. I.; Leonard, J. P.; Cuzner, M. L., Interleukin-12 induces relapse in experimental allergic encephalomyelitis in the Lewis rat. *Am J Pathol* **1997**, 150 (6), 1909-1917.
72. Rejdak, K.; Eikelenboom, M. J.; Petzold, A.; Thompson, E. J.; Stelmasiak, Z.; Lazeron, R. H. C.; Barkhof, F.; Polman, C. H.; Uitdehaag, B. M. J.; Giovannoni, G., CSF nitric oxide metabolites are associated with activity and progression of multiple sclerosis. *Neurology* **2004**, 63 (8), 1439-1445.
73. Windhagen, A.; Newcombe, J.; Dangond, F.; Strand, C.; Woodroffe, M. N.; Cuzner, M. L.; Hafler, D. A., Expression of costimulatory molecules B7-1 (CD80), B7-2 (CD86), and interleukin 12 cytokine in multiple sclerosis lesions. *The Journal of Experimental Medicine* **1995**, 182 (6), 1985-1996.
74. Jankovic, S. M., Injectable interferon beta-1b for the treatment of relapsing forms of multiple sclerosis. *J Inflamm Res* **2010**, 3, 25-31.
75. Wang, X.; Chen, M.; Wandinger, K. P.; Williams, G.; Dhib-Jalbut, S., IFN- β -1b Inhibits IL-12 Production in Peripheral Blood Mononuclear Cells in an IL-10-Dependent Mechanism: Relevance to IFN- β -1b Therapeutic Effects in Multiple Sclerosis. *The Journal of Immunology* **2000**, 165 (1), 548-557.
76. Sironi, M.; Breviario, F.; Proserpio, P.; Biondi, A.; Vecchi, A.; Van Damme, J.; Dejana, E.; Mantovani, A., IL-1 stimulates IL-6 production in endothelial cells. *The Journal of Immunology* **1989**, 142 (2), 549-553.
77. Kennedy, M. K.; Torrance, D. S.; Picha, K. S.; Mohler, K. M., Analysis of cytokine mRNA expression in the central nervous system of mice with experimental autoimmune encephalomyelitis reveals that IL-10 mRNA expression correlates with recovery. *The Journal of Immunology* **1992**, 149 (7), 2496-2505.
78. Diab, A.; Zhu, J.; Xiao, B. G.; Mustafa, M.; Link, H., High IL-6 and Low IL-10 in the Central Nervous System Are Associated with Protracted Relapsing EAE in DA Rats. *Journal of Neuropathology & Experimental Neurology* **1997**, 56 (6), 641-650.
79. Frei, K.; Fredrikson, S.; Fontana, A.; Link, H., Interleukin-6 is elevated in plasma in multiple sclerosis. *Journal of Neuroimmunology* **1991**, 31 (2), 147-153.
80. Schönrock, L. M.; Gawlowski, G.; Brück, W., Interleukin-6 expression in human multiple sclerosis lesions. *Neuroscience Letters* **2000**, 294 (1), 45-48.

81. Maimone, D.; Guazzi, G. C.; Annunziata, P., IL-6 detection in multiple sclerosis brain. *Journal of the Neurological Sciences* **1997**, *146* (1), 59-65.
82. Sugino, H.; Futamura, T.; Mitsumoto, Y.; Maeda, K.; Marunaka, Y., Atypical antipsychotics suppress production of proinflammatory cytokines and up-regulate interleukin-10 in lipopolysaccharide-treated mice. *Progress in Neuro-Psychopharmacology and Biological Psychiatry* **2009**, *33* (2), 303-307.
83. MacDowell, K. S.; García-Bueno, B.; Madrigal, J. L. M.; Parellada, M.; Arango, C.; Micó, J. A.; Leza, J. C., Risperidone normalizes increased inflammatory parameters and restores anti-inflammatory pathways in a model of neuroinflammation. *International Journal of Neuropsychopharmacology* **2013**, *16* (1), 121-135.
84. Cazzullo, C. L.; Sacchetti, E.; Galluzzo, A.; Panariello, A.; Adorni, A.; Pegoraro, M.; Bosis, S.; Colombo, F.; Trabattoni, D.; Zagliani, A.; Clerici, M., Cytokine profiles in schizophrenic patients treated with risperidone: a 3-month follow-up study. *Prog Neuropsychopharmacol Biol Psychiatry* **2002**, *26* (1), 33-39.
85. Choi, J. E.; Widjaja, F.; Careaga, M.; Bent, S.; Ashwood, P.; Hendren, R. L., Change in plasma cytokine levels during risperidone treatment in children with autism. *J Child Adolesc Psychopharmacol* **2014**, *24* (10), 586-589.
86. Lu, L. X.; Guo, S. Q.; Chen, W.; Li, Q.; Cheng, J.; Guo, J. H., Effect of clozapine and risperidone on serum cytokine levels in patients with first-episode paranoid schizophrenia. *Di Yi Jun Yi Da Xue Xue Bao = Academic journal of the first medical college of PLA* **2004**, *24* (11), 1251-4.
87. Juncal-Ruiz, M.; Riesco-Dávila, L.; Ortiz-García de la Foz, V.; Martínez-García, O.; Ramírez-Bonilla, M.; Ocejo-Viñals, J. G.; Leza, J. C.; López-Hoyos, M.; Crespo-Facorro, B., Comparison of the anti-inflammatory effect of aripiprazole and risperidone in 75 drug-naïve first episode psychosis individuals: A 3 months randomized study. *Schizophrenia Research* **2018**, *202*, 226-233.
88. Kato, T.; Monji, A.; Hashioka, S.; Kanba, S., Risperidone significantly inhibits interferon- γ -induced microglial activation in vitro. *Schizophrenia Research* **2007**, *92* (1), 108-115.
89. Zhou, P.; Xiang, L.; Zhao, D.; Ren, J.; Qiu, Y.; Li, Y., Synthesis, biological evaluation, and structure activity relationship (SAR) study of pyrrolidine amide derivatives as N-acyl ethanolamine acid amidase (NAAA) inhibitors. *MedChemComm* **2019**, *10* (2), 252-262.
90. Volk, B.; Barkóczy, J.; Hegedus, E.; Udvari, S.; Gacsályi, I.; Mezei, T.; Pallagi, K.; Kompagne, H.; Lévy, G.; Egyed, A.; Hársing, J. L. G.; Spedding, M.; Simig, G., (Phenylpiperazinyl-butyl)oxindoles as Selective 5-HT₇ Receptor Antagonists. *Journal of Medicinal Chemistry* **2008**, *51* (8), 2522-2532.
91. Perrone, R.; Berardi, F.; Colabufo, N. A.; Lacivita, E.; Leopoldo, M.; Tortorella, V., Synthesis and Structure–Affinity Relationships of 1-[ω -(4-Aryl-1-piperazinyl)alkyl]-1-aryl Ketones as 5-HT₇ Receptor Ligands. *Journal of Medicinal Chemistry* **2003**, *46* (4), 646-649.
92. Zajdel, P.; Marciniak, K.; Maślankiewicz, A.; Satała, G.; Duszyńska, B.; Bojarski, A. J.; Partyka, A.; Jastrzębska-Więsek, M.; Wróbel, D.; Wesołowska, A.; Pawłowski, M., Quinoline- and isoquinoline-sulfonamide derivatives of LCAP as potent CNS multi-receptor—5-HT_{1A}/5-HT_{2A}/5-HT₇ and D₂/D₃/D₄—agents: The synthesis and pharmacological evaluation. *Bioorganic & Medicinal Chemistry* **2012**, *20* (4), 1545-1556.
93. Bojarski, A. J.; Duszyńska, B.; Kołaczowski, M.; Kowalski, P.; Kowalska, T., The impact of spacer structure on 5-HT₇ and 5-HT_{1A} receptor affinity in the group of long-chain arylpiperazine ligands. *Bioorg Med Chem Lett* **2004**, *14* (23), 5863-5866.
94. Smid, P.; Coolen, H. K. A. C.; Keizer, H. G.; van Hes, R.; de Moes, J.-P.; den Hartog, A. P.; Stork, B.; Plekkenpol, R. H.; Niemann, L. C.; Stroome, C. N. J.; Tulp, M. T. M.; van

- Stuivenberg, H. H.; McCreary, A. C.; Hesselink, M. B.; Herremans, A. H. J.; Kruse, C. G., Synthesis, Structure–Activity Relationships, and Biological Properties of 1-Heteroaryl-4-[ω-(1H-indol-3-yl)alkyl]piperazines, Novel Potential Antipsychotics Combining Potent Dopamine D2 Receptor Antagonism with Potent Serotonin Reuptake Inhibition. *Journal of Medicinal Chemistry* **2005**, *48* (22), 6855-6869.
95. O'Sullivan, D.; Green, L.; Stone, S.; Zareie, P.; Kharkrang, M.; Fong, D.; Connor, B.; La Flamme, A. C., Treatment with the Antipsychotic Agent, Risperidone, Reduces Disease Severity in Experimental Autoimmune Encephalomyelitis. *PLOS ONE* **2014**, *9* (8), e104430.
96. La Flamme, A. C.; Abernethy, D.; Sim, D.; Phil, M.; Goode, L.; Bourke, D.; Milner, I.; Garrill, T.-M.; Joshi, P.; Watson, E.; Smyth, D.; Lance, S.; Barrett, J.; Conner, B., P031 Crisp: Clozapine and Risperidone for the Treatment of Progressive Multiple Sclerosis. *Multiple Sclerosis Journal* **2018**, *24* (1_suppl), 25.
97. Zareie, P.; Moore, P. W.; Wang, J.; Harvey, J. E.; La Flamme, A. C., Structural modifications to risperidone significantly alter immunomodulatory activity in macrophages: investigations of truncated and unsaturated analogues. *Unpublished work* **2015**.
98. Durrant, B. The Synthesis of Extended Linker Analogues of Risperidone: Towards New Treatments for Multiple Sclerosis. Honours, Victoria University of Wellington, 2015.
99. Shroff, M., Misuse of Drugs (Classification of Fantasy) Order 2001. Health, M. o., Ed. 2001.
100. Radha Krishna, P.; Narasimha Reddy, P. V., Stereoselective total synthesis of (–)-decarestrictine D from l-malic acid. *Tetrahedron Letters* **2006**, *47* (42), 7473-7476.
101. Sudhakar, G.; Kadam, V. D.; Bayya, S.; Pranitha, G.; Jagadeesh, B., Total Synthesis and Stereochemical Revision of Acortatarins A and B. *Organic Letters* **2011**, *13* (20), 5452-5455.
102. Kadam, S. M.; Nayak, S. K.; Banerji, A., Low-valent titanium : A new approach to deprotection of allyl and benzyl groups. *Tetrahedron Letters* **1992**, *33* (35), 5129-5132.
103. Murali, C.; Shashidhar, M. S.; Gopinath, C. S., Hydroxyl group deprotection reactions with Pd(OH)₂/C: a convenient alternative to hydrogenolysis of benzyl ethers and acid hydrolysis of ketals. *Tetrahedron* **2007**, *63* (19), 4149-4155.
104. Bieg, T.; Szeja, W., Removal of O-Benzyl Protective Groups by Catalytic Transfer Hydrogenation. *Synthesis* **1985**, 1985 (01), 76-77.
105. Walker, D.; Hiebert, J. D., 2,3-Dichloro-5,6-dicyanobenzoquinone and Its Reactions. *Chemical Reviews* **1967**, *67* (2), 153-195.
106. Wuts, P., *Greene's Protective Groups in Organic Synthesis: Fifth Edition*. 2014; p 1-1360.
107. Ikemoto, N.; Schreiber, S. L., Total synthesis of (–)-hikizimycin employing the strategy of two-directional chain synthesis. *Journal of the American Chemical Society* **1992**, *114* (7), 2524-2536.
108. Rahim, M. A.; Matsumura, S.; Toshima, K., Deprotection of benzyl ethers using 2,3-dichloro-5,6-dicyano-p-benzoquinone (DDQ) under photoirradiation. *Tetrahedron Letters* **2005**, *46* (43), 7307-7309.
109. Bogie, J. F. J.; Stinissen, P.; Hendriks, J. J. A., Macrophage subsets and microglia in multiple sclerosis. *Acta Neuropathologica* **2014**, *128* (2), 191-213.
110. La Flamme, A. C.; Kharkrang, M.; Stone, S.; Mirmoeini, S.; Chuluundorj, D.; Kyle, R., Type II-Activated Murine Macrophages Produce IL-4. *PLOS ONE* **2012**, *7* (10), e46989.
111. Tierney, J. B.; Kharkrang, M.; La Flamme, A. C., Type II-activated macrophages suppress the development of experimental autoimmune encephalomyelitis. *Immunology & Cell Biology* **2009**, *87* (3), 235-240.
112. Hu, D. X.; Grice, P.; Ley, S. V., Rotamers or Diastereomers? An Overlooked NMR Solution. *The Journal of Organic Chemistry* **2012**, *77* (11), 5198-5202.

113. Sardella, D. J.; Boger, E., ¹H and ¹³C spectra of fluorine-containing polycyclic aromatic hydrocarbons. ¹H-¹⁹F and ¹³C-¹⁹F coupling across bay regions. *Magnetic Resonance in Chemistry* **1989**, 27 (1), 13-20.
114. Lutnaes, B. F.; Luthe, G.; Brinkman, U. A. T.; Johansen, J. E.; Krane, J., Characterization of monofluorinated polycyclic aromatic compounds by ¹H, ¹³C and ¹⁹F NMR spectroscopy. *Magnetic Resonance in Chemistry* **2005**, 43 (7), 588-594.
115. Bouzide, A.; Sauvé, G., Highly selective silver(I) oxide mediated monoprotection of symmetrical diols. *Tetrahedron Letters* **1997**, 38 (34), 5945-5948.
116. Zhou, X.-T.; Carter, R. G., Synthesis of the ABCD and ABCDE ring systems of azaspiracid-1. *Chemical Communications* **2004**, (19), 2138-2140.
117. Muñoz, L.; Bosch, M. P.; Rosell, G.; Guerrero, A., Asymmetric synthesis of (R)- and (S)-4-methyloctanoic acids. A new route to chiral fatty acids with remote stereocenters. *Tetrahedron: Asymmetry* **2009**, 20 (4), 420-424.
118. Hasseroth, J.; Janda, K. D.; Lerner, R. A., Formation of Bridge-Methylated Decalins by Antibody-Catalyzed Tandem Cationic Cyclization. *Journal of the American Chemical Society* **1997**, 119 (26), 5993-5998.
119. Penov Gaši, K. M.; Kuhajda, K. N.; Cvjetičanin, S. M.; Đurendić, E. A.; Medić-Mijačević, L. D.; Pejanović, V. M.; Sakač, M. N., Synthesis of Some Diol Derivatives as Potential Reagents in Steroid Chemistry. *Acta Periodica Technologica* **2003**, (34), 111-118.
120. Grygoriv, G. V.; Lega, D. A.; Zaprutko, L.; Gzella, A. K.; Wieczorek-Dziurla, E.; Chernykh, V. P.; Shemchuk, L. A., Synthesis of novel spiro-condensed 2-amino-4H-pyrans based on 1,2-benzoxathiin-4(3H)-one 2,2-dioxide. *Chemistry of Heterocyclic Compounds* **2019**, 55 (3), 254-260.
121. El-Naggar, M.; Eldehna, W. M.; Almahli, H.; Elgez, A.; Fares, M.; Elaasser, M. M.; Abdel-Aziz, H. A., Novel Thiazolidinone/Thiazolo[3,2-a]Benzimidazolone-Isatin Conjugates as Apoptotic Anti-proliferative Agents Towards Breast Cancer: One-Pot Synthesis and In Vitro Biological Evaluation. *Molecules* **2018**, 23 (6), 1420.
122. Cheng, C.; Xu, J.; Zhu, R.; Xing, L.; Wang, X.; Hu, Y., A highly efficient Pd-C catalytic hydrogenation of pyridine nucleus under mild conditions. *Tetrahedron* **2009**, 65 (41), 8538-8541.
123. Ren, Y.; Wang, Y.; Li, X.; Zhang, Z.; Chi, Q., Selective hydrogenation of quinolines into 1,2,3,4-tetrahydroquinolines over a nitrogen-doped carbon-supported Pd catalyst. *New Journal of Chemistry* **2018**, 42 (20), 16694-16702.
124. Jiang, F.; Wang, H.-J.; Jin, Y.-H.; Zhang, Q.; Wang, Z.-H.; Jia, J.-M.; Liu, F.; Wang, L.; Bao, Q.-C.; Li, D.-D.; You, Q.-D.; Xu, X.-L., Novel Tetrahydropyrido[4,3-d]pyrimidines as Potent Inhibitors of Chaperone Heat Shock Protein 90. *Journal of Medicinal Chemistry* **2016**, 59 (23), 10498-10519.
125. Radhakrishnan, T. V.; Sathe, D. G.; Suryavanshi, C. V. A process for the preparation of anti-psychotic 3- 2- 4-(6-fluoro-1,2-benzisoxazol-3-yl)-1-piperidinyl]ethyl]-6,7,8,9-tetrahydro-2-methyl-4h-pyrido 1,2,-a]pyrimidin-4-one. EP1280804 B1, 2004.
126. Suri, K. A.; Suri, O. P.; Amina, M.; Wakhloo, B. P.; Satti, N. K., Unequivocal total assignment of ¹³C and ¹H NMR spectra of some pyrido[1,2-a]pyrimidine derivatives by 2D-NMR. *Magnetic Resonance in Chemistry* **2003**, 41 (9), 747-749.
127. Kim, D.-m.; Kang, M.-S.; Kim, J. S.; Jeong, J.-H., An efficient synthesis of risperidone via stille reaction: Antipsychotic, 5-HT₂, and dopamine-D₂-antagonist. *Archives of Pharmacal Research* **2005**, 28 (9), 1019-1022.
128. Hirokami, S.; Takahashi, T.; Nagata, M.; Hirai, Y.; Yamazaki, T., Photochemistry of 2,3,6-trialkyl-4-pyrimidinones in liquid ammonia-ether solution. Chemistry of Dewar 4-pyrimidinones. *The Journal of Organic Chemistry* **1981**, 46 (9), 1769-1777.

129. Sajiki, H., Selective inhibition of benzyl ether hydrogenolysis with Pd/C due to the presence of ammonia, pyridine or ammonium acetate. *Tetrahedron Letters* **1995**, 36 (20), 3465-3468.
130. Horita, K.; Yoshioka, T.; Tanaka, T.; Oikawa, Y.; Yonemitsu, O., On the selectivity of deprotection of benzyl, mpbm (4-methoxybenzyl) and dmpbm (3,4-dimethoxybenzyl) protecting groups for hydroxy functions. *Tetrahedron* **1986**, 42 (11), 3021-3028.
131. Oikawa, Y.; Yoshioka, T.; Yonemitsu, O., Specific removal of o-methoxybenzyl protection by DDQ oxidation. *Tetrahedron Letters* **1982**, 23 (8), 885-888.
132. Ikeuchi, K.; Murasawa, K.; Ohara, K.; Yamada, H., p-Methylbenzyl Group: Oxidative Removal and Orthogonal Alcohol Deprotection. *Organic Letters* **2019**, 21 (17), 6638-6642.
133. Shih, T. L.; Fang, Y. C., Expedient Synthesis of New 3,4,6-Trihydroxythiepanes from d-(-)-Quinic Acid. *Synthetic Communications* **2007**, 37 (19), 3337-3349.
134. Hori, H.; Nishida, Y.; Ohnishi, H.; Meguro, H., Regioselective de-O-benzoylation with Lewis acids. *The Journal of Organic Chemistry* **1989**, 54 (6), 1346-1353.
135. Mallampudi, N. A.; Srinivas, B.; Reddy, J. G.; Mohapatra, D. K., Total Synthesis and Structural Revision of Monocillin VII. *Organic Letters* **2019**, 21 (15), 5952-5956.
136. Somaratne, K. K.; McCone, J. A. J.; Brackovic, A.; Rivera, J. L. P.; Fulton, J. R.; Russell, E.; Field, J. J.; Orme, C. L.; Stirrat, H. L.; Riesterer, J.; Teesdale-Spittle, P. H.; Miller, J. H.; Harvey, J. E., Synthesis of Bioactive Side-Chain Analogues of TAN-2483B. *Chemistry – An Asian Journal* **2019**, 14 (8), 1230-1237.
137. Su, Q.; Dakin, L. A.; Panek, J. S., [4 + 2]-Annulations of Chiral Organosilanes: Application to the Total Synthesis of Leucascandrolide A. *The Journal of Organic Chemistry* **2007**, 72 (1), 2-24.
138. West, L. The Isolation of Secondary Metabolites from New Zealand Marine Sponges. Victoria University of Wellington, 2001.
139. Ševčík, J.; Hostinová, E.; Solovicová, A.; Gašperík, J.; Dauter, Z.; Wilson, K. S., Structure of the complex of a yeast glucoamylase with acarbose reveals the presence of a raw starch binding site on the catalytic domain. *The FEBS Journal* **2006**, 273 (10), 2161-2171.
140. Imamura, H.; Fushinobu, S.; Yamamoto, M.; Kumasaka, T.; Jeon, B.-S.; Wakagi, T.; Matsuzawa, H., Crystal Structures of 4- α -Glucanotransferase from *Thermococcus litoralis* and Its Complex with an Inhibitor. *Journal of Biological Chemistry* **2003**, 278 (21), 19378-19386.
141. Haupt, V. J.; Daminelli, S.; Schroeder, M., Drug Promiscuity in PDB: Protein Binding Site Similarity Is Key. *PLOS ONE* **2013**, 8 (6), e65894.
142. Rabasseda, X., Brivudine: a herpes virostatic with rapid antiviral activity and once-daily dosing. *Drugs of Today* **2003**, 39 (5), 359-371.
143. Heinrich, J.-C.; Tuukkanen, A.; Schroeder, M.; Fahrig, T.; Fahrig, R., RP101 (brivudine) binds to heat shock protein HSP27 (HSPB1) and enhances survival in animals and pancreatic cancer patients. *Journal of Cancer Research and Clinical Oncology* **2011**, 137 (9), 1349.
144. Gao, M.; Skolnick, J., Structural space of protein–protein interfaces is degenerate, close to complete, and highly connected. *Proceedings of the National Academy of Sciences* **2010**, 107 (52), 22517-22522.
145. Campbell, S. J.; Gold, N. D.; Jackson, R. M.; Westhead, D. R., Ligand binding: functional site location, similarity and docking. *Current Opinion in Structural Biology* **2003**, 13 (3), 389-395.
146. Laskowski, R. A.; Luscombe, N. M.; Swindells, M. B.; Thornton, J. M., Protein clefts in molecular recognition and function. *Protein Science* **1996**, 5 (12), 2438-52.
147. Gao, M.; Skolnick, J., A comprehensive survey of small-molecule binding pockets in proteins. *PLoS Comput Biol* **2013**, 9 (10), e1003302-e1003302.

148. Fang, Z.; Song, Y. n.; Zhan, P.; Zhang, Q.; Liu, X., Conformational restriction: an effective tactic in 'follow-on'-based drug discovery. *Future Medicinal Chemistry* **2014**, *6* (8), 885-901.
149. Zareie, P. Investigating the mechanism by which the atypical antipsychotic clozapine reduces disease in experimental autoimmune encephalomyelitis. Victoria University of Wellington, 2017.